REPORT NO.
UC SESM 79-3

STRUCTURES AND MATERIALS RESEARCH
DEPARTMENT OF CIVIL ENGINEERING

NONLINEAR GEOMETRIC, MATERIAL AND TIME DEPENDENT ANALYSIS OF REINFORCED AND PRESTRESSED CONCRETE SLABS AND PANELS

BY

J. VAN GREUNEN

Report to
National Science Foundation
NSF Grant ENG 77-00146

OCTOBER 1979

COLLEGE OF ENGINEERING
UNIVERSITY OF CALIFORNIA
BERKELEY CALIFORNIA

Structures and Materials Research
Department of Civil Engineering
Division of Structural Engineering
and Structural Mechanics

NONLINEAR GEOMETRIC, MATERIAL AND TIME DEPENDENT ANALYSIS OF REINFORCED AND PRESTRESSED CONCRETE SLABS AND PANELS

by

Johannes van Greunen

Faculty Investigator: A. C. Scordelis

Prepared under the Sponsorship of
National Science Foundation
Grant ENG 77-00146

College of Engineering
Office of Research Services
University of California
Berkeley, California

October 1979

BIBLIOGRAPHIC DATA SHEET	1. Report No.	2.	3. Recipient's Accession No.

4. Title and Subtitle

NONLINEAR GEOMETRIC, MATERIAL AND TIME DEPENDENT ANALYSIS OF REINFORCED AND PRESTRESSED CONCRETE SLABS AND PANELS

5. Report Date: October 1979

6.

7. Author(s): Johannes Van Greunen

8. Performing Organization Rept No. UC-SESM 79-3

9. Performing Organization Name and Address

Department of Civil Engineering
University of California
Berkeley, California 94720

10. Project/Task/Work Unit No.

11. Contract/Grant No.: ENG 77-00146

12. Sponsoring Organization Name and Address

National Science Foundation
Washington, D. C. 20550

13. Type of Report & Period Covered: Final Report

14.

15. Supplementary Notes

16. Abstracts An efficient numerical procedure for the material and geometric nonlinear analysis of reinforced and prestressed concrete slabs and panels including the time-dependent effects due to load history, temperature history, creep, shrinkage and aging of the concrete and relaxation of prestress is developed. The procedure, based on the finite element method, is capable of predicting the response of these structures throughout their service load history as well as throughout elastic, cracking, inelastic and ultimate load ranges. An updated Lagrangian formulation is employed to take the effects of changing structural geometry on the response of planar structures into account. Slabs or panels having an arbitrary tendon layout with either pretensioned, or bonded or unbonded post-tensioned tendons can be analyzed.

A series of numerical examples are presented to study the validity and applicability of the present method. The results obtained are compared with experimental and/or analytical results obtained by other investigators.

17. Key Words and Document Analysis. 17a. Descriptors

Structural engineering; Reinforced concrete; Prestressed concrete; Post-tensioned; Finite elements; Nonlinear analysis; Material nonlinearities; Geometric nonlinearities; Cracking; Creep; Shrinkage; Temperature; Load History; Slabs; Panels.

17b. Identifiers/Open-Ended Terms

17c. COSATI Field/Group

18. Availability Statement: Release Unlimited

19. Security Class (This Report) UNCLASSIFIED

20. Security Class (This Page) UNCLASSIFIED

21. No. of Pages: 286

22. Price

NONLINEAR GEOMETRIC, MATERIAL AND TIME DEPENDENT ANALYSIS OF REINFORCED AND PRESTRESSED CONCRETE SLABS AND PANELS

Doctor of Philosophy Johannes van Greunen Civil Engineering

A. C. Scordelis
A. C. Scordelis
Chairman of Committee

ABSTRACT

A numerical method of analysis is developed to trace the quasi-static response of reinforced and prestressed concrete slabs and panels under short time and sustained load conditions. Time-dependent effects due to load history, temperature history, creep, shrinkage and aging of concrete and stress relaxation in prestressing steel are incorporated. The load-deflection history of such structures through the elastic, inelastic and ultimate ranges is calculated. The ultimate failure of these structures due to in-plane membrane plus bending effects is then predicted considering local failures in steel and concrete along with the deterioration of the structural stiffness due to progressive cracking.

A finite element tangent stiffness formulation, coupled with a time step integration scheme, is developed to analyze reinforced and prestressed concrete slab and panel structures. Within a time step, an incremental load procedure with an iterative approach to obtain an equilibrium position of the structure for each load increment, is adopted to trace the nonlinear behavior of such structures.

An updated Lagrangian formulation is employed to take the effects of changing structural geometry on the response of structures into account.

The effect of initial stresses is incorporated by the inclusion of the geometric stiffness. By separating the rigid body displacements from the true element deformations, large displacements are allowed, while the theory assuming small strains and rotations is still valid at the element level.

The reinforced concrete section is modeled as a layered system of concrete and "equivalent smeared" steel layers. Perfect bond is assumed to exist between the concrete and bonded steel layers. The stiffness of an element is then obtained by integrating the contribution from all the layers in the section.

Concrete behavior under the biaxial state of stress is represented by a nonlinear constitutive relationship which incorporates tensile cracking at a limiting stress, tensile stiffening between cracks and the strain-softening phenomenon beyond the maximum compressive strength. The effects of the stress history, creep and partial creep recovery, aging, temperature variations and shrinkage are included in the long time deformations in the concrete layers. Creep under a biaxial state of stress and at high stress levels is considered. The steel reinforcement is represented by a bilinear, strain hardening model approximating the Bauschinger effect. The prestressing steel is modeled by a multi-linear stress-strain relationship and the relaxation of stress over time is taken into account. The constitutive relations are based on the assumption of small strains and include unloading paths for stress reversals.

Slabs or panels having an arbitrary tendon layout with either pretensioned, or bonded or unbonded post-tensioned tendons can be analyzed. The tendon layout data is specified and the loading due to prestressing and discretization of the tendons are calculated in the computer program.

Finally, several numerical examples are presented to demonstrate the validity and applicability of the present method of analysis. The numerical results obtained from the analyses are compared to available experimental data and the analytical results obtained by other investigators and good agreement is demonstrated.

ACKNOWLEDGEMENTS

The author wishes to express his sincere gratitude to Prof. A. C. Scordelis who served as thesis supervisor. His constructive suggestions, criticism and encouragement during the course of this study are highly appreciated. Professors S. A. Mahin and A. Chorin are thanked for serving as members of the thesis committee. A special word of thanks is also extended to Joy Kono for her skillful typing of the manuscript.

This research was sponsored by the National Science Foundation Grant No. ENG 77-00146. The financial aid provided by Van Wyk & Louw, Inc., Consulting Civil Engineers and the Council for Scientific and Industrial Research of the Republic of South Africa is also gratefully acknowledged. The Computer Center at the University of California, Berkeley provided the facilities for the numerical work.

Finally (but certainly not least), the love, support and encouragement of family and friends, especially the author's wife, have played a major role in making it possible to complete this study.

TABLE OF CONTENTS

Page

Page

Page

1. INTRODUCTION

1.1 GENERAL REMARKS

In the past few decades reinforced and prestressed concrete have been used for increasingly sophisticated and complex structures such as tall multi-story buildings, nuclear containment vessels, longspan bridges and offshore platforms. The analysis of such structures have been made possible largely by the development of the modern digital computer. However, current design methods rely heavily on linear elastic analyses based on empirically derived material laws assuming homogeneous, isotropic materials. Experimental and field studies on shells, folded plates and other structures have indicated that many of these structures are in fact loaded beyond the range of linear elastic behavior. In addition, long-term effects such as load history, temperature changes, creep, shrinkage and relaxation in prestressing steel may have a significant influence on the behavior of such structures. Due to the complexity of these structures and the nature of the materials involved, it has therefore become necessary to employ highly sophisticated analysis procedures, not only to ensure their safety as far as short time loadings are concerned, but also to guarantee their safety and serviceability over their design life.

The development of an analytical model for reinforced and prestressed concrete structures is complicated by the following factors: nonhomogeneity of the composite material, compounded by the fact that concrete itself is a nonhomogeneous material exhibiting cracking at relatively low stress levels and for which only averaged material parameters can be obtained; the nonlinearity of the stress-strain relationship of

concrete and reinforcing and prestressing steels; changes in geometry of the structure due to progressive cracking under sustained loads and environmental conditions, especially in thin shells, slender arches and similar structures; time-dependent deformation of concrete caused by the long-term effects mentioned above; and finally, the complexity and lack of precise information on bond slip, dowel action of the steel reinforcement and aggregate interlock at cracks make these phenomena extremely difficult to model analytically.

Experiments on microconcrete models can furnish valuable insight into the behavior of prototype structures, but such tests are very expensive and time-consuming, particularly when the time-dependent effects are to be considered. Furthermore, a large number of models must be tested if variations of important parameters are to be investigated. It is therefore essential to develop general methods of analysis to complement and, eventually, to replace most of the physical experiments. The accuracy and reliability of such methods have to be insured by correlation with selected experiments.

Since this study is mainly concerned with slabs and panels, the generally accepted analysis procedures, used for the design of reinforced and prestressed concrete slabs, will be briefly discussed below.

Reinforced concrete slabs

The design procedures for reinforced concrete continuous slab systems as set forth in the ACI Building Code [1] are based on an extensive series of experimental studies carried out at the University of Illinois and the well-established performance record of various slab systems [2, Chapter 13]. The design methods apply to two-way flat slab systems, with

or without beams or drop panels and also waffle slabs. Two design procedures are described:

The direct design procedure [1, 2, Section 13.6] is based on determining a total design moment for a given panel, distributing this moment to the positive and negative moment design sections and then distributing these positive and negative design moments to the column and middle strips.

The equivalent frame method [1, 2, Section 13.7] is based on representing the three-dimensional slab and column system by a series of equivalent two-dimensional frames which can then be analyzed for the design loads. The torsional stiffness of the slab system transverse to the frame being considered is taken into account.

Further details of these methods and the other design considerations can be found in the ACI code [1] and Commentary [2].

Prestressed concrete slabs

For reasons of economy and practical considerations, unbonded tendons have generally been used for prestressed concrete slabs. Recommendations for the design of post-tensioned slabs are not provided in the ACI Code [1]. However, the Commentary on the ACI Code [2] and the design guide of the Post-Tensioning Institute (PTI) [3], both based on the report of ACI-ASCE Committee 423 [4], give guidelines for the design of post-tensioned flat slab systems. An extensive review of all the experimental studies on post-tensioned slabs, which forms the basis for these guidelines, is provided in the PTI-publication [3].

It is recommended [2,3] that the equivalent frame method (also known as the beam method and similar to the method described above for

reinforced concrete slabs) be used for the analysis of prestressed concrete slab systems. When the load-balancing concept [5] is employed, the effect of the prestress on the slab can be easily examined, since it then becomes another set of loads applied to the structure. The proportioning of tendons to column and middle strips is recommended by ACI-ASCE Committee 423 [4], but the PTI-guidelines [3] considers uniform spacing of tendons to be adequate. Further details of the design procedures concerning provisions for shear, seismic design, etc. can be found in these references [3,4].

1.2 REVIEW OF PREVIOUS WORK

The main emphasis of this study is on the application of the finite element method (FEM) to the analysis of reinforced and prestressed concrete slabs. The review of the literature will therefore be limited to investigations concerning these topics. Comprehensive surveys on the application of the FEM to reinforced and prestressed concrete structures in general can be found in papers such as the state-of-the-art review by Scordelis [6] and surveys by Schnobrich [7], Wegner [8] and Scordelis [9].

Reinforced concrete

Studies of reinforced concrete slabs by the FEM have been presented by Jofriet and McNeice [10] and by Bell and Elms [11,12]. They incorporated progressive cracking in triangular or quadrilateral plate bending elements. The changing bending stiffness of the elements, due to cracking normal to the principal moment direction, is accounted for by using a reduced flexural rigidity in forming the element stiffnesses.

Scanlon and Murray [13,14] developed a method of incorporating both cracking and the time-dependent effects of creep and shrinkage in slabs.

They used layered rectangular plate elements, which are assumed to be cracked progressively layer by layer. They assume that cracks propagate only parallel and perpendicular to the orthogonal reinforcement. Similar layered-type solutions, not including creep and shrinkage have been presented to determine the nonlinear behavior of reinforced concrete slabs by Dotroppe et al. [15], Berg et al. [16,17], Backlund [18], Shafer et al. [19] and Wegner et al. [20]. Berg [16] also included the effects of nonlinear geometry in his solution.

More recently Bashur and Darwin [21,22] have presented a solution procedure using rectangular plate bending elements and numerical integration through the thickness of the slab. Kristjansson [23] used a hybrid element to investigate the nonlinear behavior of reinforced concrete slabs caused by both material and geometric effects.

The analysis of reinforced concrete thin shells including cracking is complicated by the fact that the in-plane membrane action and the plate bending action are coupled. Bell and Elms [11,24] made a shell analysis by accounting for progressive cracking in an approximate manner through using reduced flexural and membrane stiffnesses for the elements. These stiffnesses were dependent on the stress level.

Hand et al. [25], using shallow shell parallelogram elements, and Lin and Scordelis [26,27], using triangular shell elements, adopted a different approach from that of Bell and Elms. They used layered finite elements to represent the concrete and steel reinforcement, and progressive cracking through the concrete layers is accurately modeled to include the coupling of the membrane and plate bending action. Kabir [28,29] has extended this approach to include the load history and time dependent effects of creep and shrinkage. Arneson et al. [30,126] have

recently presented an analysis procedure using triangular shell elements, a nonlinear material model based on endochronic theory with numerical integration through the element thickness, and incorporating nonlinear geometric effects.

Prestressed concrete

In the application of the FEM to the analysis of prestressed concrete structures the emphasis has been on the analysis of nuclear reactor vessels. Rashid [31,32] and Wahl and Kasiba [33] made early finite element studies of prestressed concrete reactor structures treated as axisymmetric structures. Further developments in the analysis of reactor vessels using axisymmetric or three-dimensional solid elements were presented by Zienkiewicz et al. [34], Argyris et al. [35] and Connor and Sarne [36].

Kang [37] presented a method for the analysis of reinforced and prestressed concrete frames, including nonlinear material and geometric effects and also accounted for the time-dependent effects of creep shrinkage and temperature. Prestressed concrete slabs have also been studied by Youssef et al. [38] using an elasto-plastic concept to account for cracking in the finite elements.

1.3 OBJECTIVE AND SCOPE

The objective of the present study is to develop an efficient numerical analysis procedure for the material and geometric nonlinear analysis of reinforced and prestressed concrete slabs and panels, including the time-dependent effects due to load history, temperature history, creep, shrinkage and aging of concrete and the relaxation of stress in the prestressing steel. The aim of the analysis is an accurate prediction of

the response of such structures throughout their service load history as well as throughout the elastic, inelastic and ultimate ranges. The collapse of these structures due to in-plane membrane plus bending effects is then predicted considering local failures in steel and concrete along with the deterioration of the structural stiffness due to progressive cracking.

The possibility of shear failure in the slab is not included in the present study. The shear strength of a slab, especially for punching shear may be of significant importance in some instances -- a comprehensive survey of shear in reinforced concrete can be found in ACI special publication SP-42 [39]. The factors influencing the progressive collapse of flat plate structures have also been described by Hawkins and Mitchell [40]. Bond slip, dowel action of reinforcement and aggregate interlock at cracks are also not considered in this study.

A finite element tangent stiffness formulation, coupled with a time step integration scheme, is developed to analyze reinforced and prestressed concrete slab and panel structures. Within a time step, an incremental load procedure with an iterative approach to obtain an equilibrium position of the structure for each load increment, is adopted to trace the nonlinear behavior of such structures.

The reinforced concrete section is modeled as a layered system of concrete and "equivalent smeared" steel layers. Perfect bond is assumed to exist between the concrete and bonded steel layers. The stiffness properties of an element are then obtained by integrating the contribution from all the layers in the section.

Concrete behavior under the biaxial state of stress is represented by a nonlinear constitutive relationship which incorporates tensile

cracking at a limiting stress, tensile stiffening between cracks and the strain-softening phenomenon beyond the maximum compressive strength. The effects of the stress history, creep and partial creep recovery, aging, temperature variations and shrinkage are included in the long time deformations in the concrete layers. Creep under a biaxial state of stress and at high stress levels is considered. The steel reinforcement is represented by a bilinear, strain hardening model approximating the Bauschinger effect. The prestressing steel is modeled by a multilinear stress-strain relationship and the relaxation of stress over time is taken into account. The constitutive relations are based on the assumption of small strains and include unloading paths for stress reversals.

Slabs or panels having an arbitrary tendon layout with either pretensioned, or bonded or unbonded post-tensioned tendons can be analyzed. The tendon layout data is specified and the loading due to prestressing and discretization of the tendons are calculated in the computer program.

An updated Lagrangian formulation is employed to take the effects of changing structural geometry on the response of structures into account. The effect of initial stresses is incorporated by the inclusion of the geometric stiffness. By separating the rigid body displacements from the true element deformations, large displacements are allowed, while the theory assuming small strains and rotations is still valid at the element level.

Finally, several numerical examples are presented to demonstrate the validity and applicability of the present method of analysis. The numerical results obtained from the analyses are compared to available experimental data and the analytical results obtained by other investigators.

2. BASIC RELATIONSHIPS

2.1 GENERAL REMARKS

In this chapter the basic relationships from the theory of elasticity and the equations which are used in the application of the Finite Element Method (FEM) to the solution of structural analysis problems, will be presented. No attempt will be made to present detailed rigorous mathematical derivations of the above mentioned relationships -- these can be found in texts on solid mechanics like that of Fung [41] or on the FEM such as that of Zienkiewicz [42]. The intention is rather to provide some background and to point out the similarities in assumptions that are generally used to derive the equations of classical plate theory and which are also used for the FEM in the analysis of shells.

A general discussion of the possible types of nonlinearities that may be necessary to consider in the analysis of structures is appropriate here -- especially to clarify the terminology which will be used in this study. Nonlinearities may arise from the use of any of the basic equations of elasticity (section 2.3) relating to equilibrium (statics), kinematics (geometry) or constitutive relations.

1. Equilibrium can be considered in the original undeformed position (L) or in the deformed position (NL).

2. The kinematic relationship can be formulated neglecting all higher order terms (L) or including some or all of these terms. (See section 2.3.1.)

3. The constitutive relationship can be taken as linear elastic (L) on the one hand, or any of the typical nonlinear stress-strain relationships (NL) that are generally used, on the other.

The most important different combinations of these effects are shown in Table 2.1 and will be briefly discussed.

	EQUILIBRIUM	KINEMATICS	CONSTITUTIVE RELATIONS	TYPE OF ANALYSIS
1	L	L	L	Linear elastic
2	NL	L	L	Nonlinear small deflection
3	NL	NL	L	Nonlinear large deflection
4	L	L	NL	Nonlinear material
5	NL	L	NL	Nonlinear material and small deflection
6	NL	NL	NL	Nonlinear material and large deflection

TABLE 2.1 CLASSIFICATION OF TYPES OF ANALYSIS

1. Linear elastic analysis

   This is the conventional type of analysis generally used for most problems in which all nonlinearities are ignored.

2. Nonlinear small deflection analysis

   This type of analysis is used when the equilibrium of the structure has to be considered in the deformed position in such cases as for buckling problems, slender arches, etc. Displacements and strains are assumed to remain small.

3. Nonlinear large deflection analysis

   For a structure that exhibits large displacements when loaded, such as certain classes of cables or cable net structures, the kinematic relations become nonlinear and equilibrium has to be considered in the final structural configuration.

4. Nonlinear material analyses

   In certain structures the nonlinear behavior of the material, e.g., concrete, may be the dominant effect that has to be considered.

5. Nonlinear material and small deflection analysis

   This is used when the effect of material nonlinearity has to be included in considering equilibrium for the types of structural problems mentioned under 2.

6. Nonlinear material and large deflection analysis

   In these problems nonlinear effects due to material nonlinearity as well as significant changes in the geometry of the structure, have to be taken into account.

After a discussion of the approaches to the description of motion and deformation and the three basic sets of equations of elasticity, namely those of strain-displacement, constitutive relations and equilibrium, the derivation of an incremental equilibrium equation by the use of the Principle of Virtual Work (P of VW) will be presented. The formulation of the FEM will then be discussed with special reference to the sources of nonlinearity and the way in which these aspects will be handled in this study. In section 2.8 the basic assumptions discussed in this chapter and on which the solution procedure is based, will be summarized.

2.2 DESCRIPTION OF MOTION AND DEFORMATION

There are several ways in which it is possible to describe the motion and deformation of a body. The two classical approaches to the problem are the material and spatial descriptions. Although both methods are due to Euler, the first is generally known as the Lagrangian description while the second is called the Eulerian description.

The material or Lagrangian approach is based on following the path of material particles in a body by referring to some reference configuration. This approach is again subdivided into the Total Lagrangian (TL) and the Updated Lagrangian (UL) approaches. In the TL approach the reference configuration is taken to be the initial undeformed position of the body and all static and kinematic variables are referred to this configuration while any integration or differentiation is also done over the undeformed body. For the UL approach the last position of the body is taken to be the reference configuration. The static and kinematic variables are referred to this configuration, and integration or differentiation is also carried out in this configuration.

The Eulerian or spatial description is frequently used in fluid mechanics. Fixed points in space are observed while material particles flow through them. Displacements are then found by integrating velocities, and any integration or differentiation must be performed over the deformed body.

Another method of great importance for large deflection theory is the convected description. Here the coordinate system remains fixed in the body and deforms with it. All particles therefore retain the same coordinates throughout a deformation, while the metric tensor of the coordinate system changes continuously.

The Lagrangian approach is most generally used in the application of the FEM. Both the TL and UL approaches can be formulated to include all the nonlinear effects due to large displacements and material nonlinearities and lead to the same result [43]. The only advantage of using one approach rather than the other is for reasons of computational efficiency [44]. In this study the Updated Lagrangian approach will be used since it requires less computer memory for storage of variables as it is not necessary to retain the initial undeformed configuration.

2.3 THREE BASIC PRINCIPLES OF ELASTICITY

2.3.1 Strain-displacement relationship

In the mechanics of solids the basic measure of deformation is represented by Green's strain tensor E_{ij} [41] and is given by:

$$E_{ij} = \frac{1}{2}\left(u_{i,j} + u_{j,i} + u_{k,i}u_{k,j}\right) \tag{2.1}$$

where

x_i = rectangular Cartesian coordinate axes, $i = 1,2,3$.

u_i = displacement in i-direction

$$u_{i,j} \equiv \partial u_i / \partial x_j$$

$$u_{k,i}u_{k,j} \equiv \sum_{k=1}^{3} (u_{k,i}u_{k,j}); \quad \text{summation convention used}$$

Equation (2.1) is completely general for a three-dimensional body and refers to the reference configuration. By introducing the Kirchhoff assumptions Eq. (2.1) can be reduced to the usual two-dimensional form of the plate equations. These assumptions are:

1. Normals to the plate middle surface remain normal and straight after deformation.

2. The strain in the thickness direction of the plate can be neglected.

Using the more conventional xyz-coordinates, with the z-direction being the normal to the plate surface, these assumptions allow us to reduce Eq. (2.1) to the following:

$$E_{xx} = u_{,x} + \frac{1}{2}\left(u_{,x}^2 + v_{,x}^2 + w_{,x}^2\right)$$

$$E_{yy} = v_{,y} + \frac{1}{2}\left(u_{,y}^2 + v_{,y}^2 + w_{,y}^2\right) \qquad (2.2)$$

$$E_{xy} = \frac{1}{2}\left(u_{,y} + v_{,x} + u_{,x}u_{,y} + v_{,x}v_{,y} + w_{,x}w_{,y}\right)$$

where

u,v,w = displacements in the x, y and z-directions respectively.

If the gradients of the in-plane displacements are assumed to be of second order magnitude and can therefore be neglected, Eqs. (2.2) become the Von Karman equations, which assume small strains, but include the effect of moderate rotations as represented by the derivatives of the out-of-plane displacement w :

$$\begin{Bmatrix} E_{xx} \\ E_{yy} \\ E_{xy} \end{Bmatrix} = \begin{Bmatrix} u_{,x} + \frac{1}{2}w_{,x}^2 \\ v_{,y} + \frac{1}{2}w_{,y}^2 \\ \frac{1}{2}\left(u_{,y} + v_{,x} + w_{,x}w_{,y}\right) \end{Bmatrix} \qquad (2.3)$$

When all the quadratic strain terms are neglected, Eqs. (2.2) reduce to the usual equations of linear elastic theory for small strains and rotations and in which the engineering strains are given by:

$$\begin{Bmatrix} E_{xx} \\ E_{yy} \\ E_{xy} \end{Bmatrix} = \begin{Bmatrix} \varepsilon_{xx} \\ \varepsilon_{yy} \\ \frac{1}{2}\gamma_{xy} \end{Bmatrix} = \begin{Bmatrix} u_{,x} \\ v_{,y} \\ \frac{1}{2}(u_{,y} + v_{,x}) \end{Bmatrix} \tag{2.4}$$

By defining the nonlinear part of the strain-displacement relationship of Eq. (2.3) as:

$$\underset{\sim}{\eta}^T = \frac{1}{2}\langle w_{,x}^2 \; w_{,y}^2 \; w_{,x} w_{,y} \rangle \tag{2.5}$$

Equation (2.3) can also be written as:

$$\underset{\sim}{E} = \underset{\sim}{\varepsilon} + \underset{\sim}{\eta} \tag{2.6}$$

where

$\underset{\sim}{\varepsilon}$ = engineering strains or linear part of the strain-displacement vector.

2.3.2 Constitutive relationship

The general constitutive relationship is of the form [41]:

$$S_{ij} = C_{ijk\ell} E_{k\ell} \tag{2.7}$$

where

S_{ij} = second Piola-Kirchhoff stress tensor

$E_{k\ell}$ = Green's strain tensor

$C_{ijk\ell}$ = tensor containing elastic moduli.

Because of the symmetry of the stress and strain tensors, $C_{ijk\ell}$ is simplified and the number of independent moduli reduced. For an isotropic elastic material there are only two independent elastic constants. In addition the second Kirchhoff assumption of section 2.3.1 leads to the fact that S_{zz} is negligibly small. As a result of assumption 1 it is also possible to set $E_{yz} = 0$ and $E_{zx} = 0$, which means that the stresses S_{yz} and S_{zx} cannot be determined from the strains, although their existence is required for equilibrium. The conditions $S_{zz} = S_{yz} = S_{zx} = 0$ define a plane stress condition and it is therefore assumed that each horizontal layer of the plate can be considered to be in a state of plane stress. As a result of these assumptions Eq. (2.7) may be reduced to the following form:

$$\begin{Bmatrix} S_{xx} \\ S_{yy} \\ S_{xy} \end{Bmatrix} = \frac{E}{(1-\nu^2)} \begin{bmatrix} 1 & \nu & 0 \\ \nu & 1 & 0 \\ 0 & 0 & (1-\nu)/2 \end{bmatrix} \begin{Bmatrix} E_{xx} \\ E_{yy} \\ 2E_{xy} \end{Bmatrix} \tag{2.8}$$

For linear elastic theory assuming small strains and rotations, there is no difference between the reference and the displaced configurations and the second Piola-Kirchhoff stress tensor $\underset{\sim}{S}$ is equal to the Cauchy or engineering stress $\underset{\sim}{\sigma}$.

2.3.3 Equilibrium

The equilibrium equation can be written as [41] (referring to the reference configuration):

$$\frac{\partial}{\partial x_k}\left(\frac{\partial x_i}{\partial x_j} S_{jk}\right) + \rho P_i = 0 \tag{2.9}$$

where

ρP_i = body force per unit volume of the reference configuration

By substituting Eqs. (2.4) and (2.8) into Eq. (2.9), using the Kirchhoff assumptions and defining stress resultants by integrating the stresses through the thickness of the plate, the classical plate equilibrium equations representing force and moment equilibrium can be obtained. For details of this approach, reference may be made to the work of Murray [45].

For the application of the FEM it is more convenient to use the equilibrium equation (2.9) to establish a Principle of Virtual Work (P of VW). Consider a general body B with surface S which consists of two parts. On one part S_1 the surface tractions T_i are prescribed, while the displacements or boundary conditions are prescribed on the other part, S_2. Then, using Eq. (2.9), these prescribed conditions on the surface and the Green-Gauss divergence theorem the virtual work equation can be written as:

$$\int_V S_{ij}\delta E_{ij}dV - \int_{S_1} T_i\delta u_i dS - \int_V P_i\delta u_i dV = 0 \qquad (2.10)$$

Equation (2.10) is just an equivalent way of stating the equilibrium conditions for the body, but this variational formulation has computational advantages. The volume and surface integrals are taken over the body in the reference configuration. The virtual displacement field $\delta\underset{\sim}{u}$ is any arbitrary kinematically admissible displacement field satisfying the boundary conditions on S_2. Equation (2.10) is also valid for large displacements and is independent of the material properties.

In the application of the FEM the equilibrium in the deformed configuration can be established by calculating the internal resisting forces in the structure due to the deformation and comparing this with the externally applied loads. When the difference, representing the unbalanced forces, is within an acceptable tolerance, equilibrium is assumed to have been achieved.

2.4 INCREMENTAL VIRTUAL WORK EQUATION

In the application of the FEM to the solution of structural problems, the stiffness formulation has proved to be much easier to implement on the computer than the flexibility or force method. To use either the Total or Updated Lagrangian approaches, an incremental equilibrium equation, relating any increment in external loads to the corresponding increment in deformation of the structure, must be established. Such an equation makes the solution of a series of linear problems possible, leading to a stable equilibrium position of the structure in the deformed position.

In this section the stiffness formulation will be developed in general terms by establishing an incremental equilibrium equation. This can be done by using either the principle of minimum potential energy or the P of VW. The P of VW as represented by Eq. (2.10) is more general and is therefore selected here. In this derivation it is assumed that the structure remains elastic and that the strains are small.

Consider a body in an "initial" configuration subject to body forces P_{oi} and surface tractions T_{oi} which are in equilibrium with the internal forces σ_{oij}. If the loads are incremented to

$$P_{1i} = P_{oi} + \Delta P_i \tag{2.11a}$$

and

$$T_{1i} = T_{oi} + \Delta T_i \tag{2.11b}$$

The structure will displace Δu_i and the new internal forces will be:

$$S_{1ij} = \sigma_{oij} + \Delta S_{ij} \tag{2.11c}$$

All variables are referred to the initial configuration, and it is assumed that the displacement is sufficiently small so that the initial stresses σ_{oij} maintain a constant magnitude and the same orientation for subsequent incremental deformations.

From Eqs. (2.1) and (2.6) the displacement increment Δu_i causes a strain increment:

$$\Delta E_{ij} = \frac{1}{2}\left(\Delta u_{i,j} + \Delta u_{j,i} + \Delta u_{k,i} u_{k,j}\right) \tag{2.12}$$

$$= \Delta\varepsilon_{ij} + \Delta\eta_{ij}$$

Taking the variation of ΔE_{ij} the following result is obtained:

$$\delta\Delta E_{ij} = \frac{1}{2}\left(\delta\Delta u_{i,j} + \delta\Delta u_{j,i} + \delta\Delta u_{k,i}\Delta u_{k,j} + \Delta u_{k,i}\delta\Delta u_{k,j}\right) \tag{2.13}$$

$$= \delta\Delta\varepsilon_{ij} + \delta\Delta\eta_{ij}$$

For the initial state $\Delta u_i = 0$, and thus:

$$\delta\Delta E_{ij} = \delta\Delta\varepsilon_{ij} \tag{2.14}$$

For the initial state, by using Eqs. (2.13) and (2.14), Eq. (2.10) becomes:

$$\int_{V_o} \sigma_{oij}\delta\Delta\varepsilon_{ij}dV_o = \int_{S_o} T_{oi}\delta\Delta u_i dS_o + \int_{V_o} P_{oi}\delta\Delta u_i dV_o \qquad (2.15)$$

However, the structure is also in equilibrium in the deformed position and Eq. (2.10) may then be written as:

$$\int_{V_o} S_{1ij}\delta\Delta E_{ij}dV_o = \int_{S_o} T_{1i}\delta\Delta u_i dS_o + \int_{V_o} P_{1i}\delta\Delta u_i dV_o \qquad (2.16)$$

By using Eqs. (2.11), (2.13) and (2.15), Eq. (2.16) may be rewritten as follows:

$$\int_{V_o} \left(\Delta S_{ij}\delta\Delta\varepsilon_{ij} + \sigma_{oij}\delta\Delta\eta_{ij}\right)dV_o = \int_{S_o} \Delta T_i\delta\Delta u_i dS_o + \int_{V_o} \Delta P_i\delta\Delta u_i dV_o \qquad (2.17)$$

where $\Delta S_{ij}\delta\Delta\eta_{ij}$ is considered a higher order term and thus neglected.

Equation (2.17) is the incremental equilibrium equation where the first term represents the usual elastic stiffness. The second term represents the effect of the initial stresses when the body is subjected to an increment in deformation and is designated the geometric stiffness. The terms on the right hand side represent the external load vector.

In the next section it will be shown how Eq. (2.17) is used to obtain an incremental formulation of the FEM.

2.5 FINITE ELEMENT FORMULATION

The FEM has gained universal acceptance and is today the most important and powerful method available for the analysis of structures. Several

texts [42,47] have been written containing details about the method, therefore only a brief description, highlighting the main steps of the method, will be presented here.

The first approximation is the idealization of a structure with an infinite number of degrees of freedom (DOF), by an assemblage of elements joined at and interacting with each other only at selected nodal points. This reduces the infinite number of DOF to a manageable number. The second important approximation is that the elements are deemed to be able to represent the general behavior of the structure between the nodal points. To accomplish this the displacement field $\underset{\sim}{u}$ within an element is approximated by a set of interpolation or shape functions $\underline{N}$, which are chosen to reflect the deformation patterns within an element as accurately as possible, as follows:

$$\underset{\sim}{u} = \underline{N}\,\underset{\sim}{r} \tag{2.18}$$

where

$\underset{\sim}{r}$ = vector of element nodal displacements

The strain-displacement relationship of Eq. (2.3) can be expressed as follows:

$$\underset{\sim}{\varepsilon} = \underline{L}\,\underset{\sim}{u} \tag{2.19}$$

where

$\underline{L}$ = differential operator

Substituting Eq. (2.18) into (2.19) yields:

$$\underset{\sim}{\varepsilon} = \underline{B}\,\underset{\sim}{r} \tag{2.20}$$

where

$\underline{B} = \underline{L}\,\underline{N}$ = strain-displacement matrix

For the case of linear elastic theory as represented by Eq. (2.4) or for a linearized incremental approach, $\underline{L}$ is a linear operator and $\underline{B}$ is independent of $\underset{\sim}{r}$, but in general $\underline{B}$ is a function of $\underset{\sim}{r}$.

The constitutive relationship can be expressed as:

$$\underset{\sim}{\sigma} = \underline{C}(\underset{\sim}{\varepsilon} - \underset{\sim}{\varepsilon}_0) + \underset{\sim}{\sigma}_0 \tag{2.21}$$

where

$\underset{\sim}{\sigma}_0$ = initial stress vector

$\underset{\sim}{\varepsilon}_0$ = initial strain vector

Considering the case of a small displacement from a stress-free initial state, the term representing the geometric stiffness in Eq. (2.17) may be neglected and the incremental equilibrium equation rewritten as follows:

$$\sum_e \int_V \delta\underset{\sim}{\varepsilon}^T \underset{\sim}{\sigma} dV = \sum_e \int_S \delta\underset{\sim}{u}^T \underset{\sim}{T} dS + \sum_e \int_V \delta\underset{\sim}{u}^T \underset{\sim}{P} dV \tag{2.22}$$

where

$\sum_e$ = summation over all elements

V = volume of an element

S = surface of an element

$\underset{\sim}{T}$ = vector of surface tractions

$\underset{\sim}{P}$ = vector of body forces

$\delta\underset{\sim}{u}, \delta\underset{\sim}{\varepsilon}$ = virtual displacement vector and corresponding strain vector

Using Eqs. (2.18), (2.20) and (2.21), Eq. (2.22) may be rewritten as:

$$\delta \underset{\sim}{r}^T \left[\sum_e \int_V \underline{B}^T \underline{C}\, \underline{B}\, dV\, \underset{\sim}{r} - \sum_e \int_V \underline{B}^T \underline{C}\, \underset{\sim}{\varepsilon}_o dV + \sum_e \int_V \underline{B}^T \underset{\sim}{\sigma}_o dV \right]$$

$$= \delta \underset{\sim}{r}^T \left[\sum_e \int_S \underline{N}^T \underline{T}\, dS + \sum_e \int_V \underline{N}^T \underline{P}\, dV \right] \qquad (2.23)$$

where

$\delta \underset{\sim}{r}$ = virtual nodal displacement vector

By recognizing that $\delta \underset{\sim}{r}$ is arbitrary and rearranging terms, Eq. (2.23) reduces to the familiar relationship:

$$\underline{K}\, \underset{\sim}{r} = \underset{\sim}{R} \qquad (2.24)$$

where

$$\underline{K} = \sum_e \int_V \underline{B}^T \underline{C}\, \underline{B}\, dV \qquad (2.25)$$

= elastic stiffness matrix

$$\underset{\sim}{R} = \underset{\sim}{R}_S + \underset{\sim}{R}_B + \underset{\sim}{R}_\varepsilon + \underset{\sim}{R}_\sigma \qquad (2.26)$$

= external load vector

$$\underset{\sim}{R}_S = \sum_e \int_S \underline{N}^T \underline{T}\, dS \qquad (2.27a)$$

= equivalent nodal force vector due to surface tractions

$$\underset{\sim}{R}_B = \sum_e \int_V \underline{N}^T \underline{P}\, dV \qquad (2.27b)$$

= equivalent nodal force vector due to body forces

$$\underset{\sim}{R}_{\epsilon} = \sum_{e} \int_{V} \underline{B}^{T} \underline{C} \, \underset{\sim}{\epsilon}_{o} dV \tag{2.27c}$$

= equivalent nodal force vector due to initial strains

$$\underset{\sim}{R}_{\sigma} = \sum_{e} \int_{V} \underline{B}^{T} \underset{\sim}{\sigma}_{o} dV \tag{2.27d}$$

= equivalent nodal force vector due to initial stresses

The set of equations (2.24) can be solved for the unknown nodal displacements $\underset{\sim}{r}$. Strains and then stresses for all elements can be calculated from Eqs. (2.20) and (2.21).

When the effect of initial stresses is considered, the second term on the left hand side of Eq. (2.17), neglected above and representing the geometric stiffness, must be considered. Expanding $\delta\Delta\eta_{ij}$, this term becomes:

$$\frac{1}{2} \int_{V_o} \sigma_{oij} \left(\delta\Delta u_{k,i} \Delta u_{k,j} + \Delta u_{k,i} \delta\Delta u_{k,j} \right) dV_o$$

Using Eq. (2.18) it can be expressed as:

$$\sum_{e} \frac{1}{2} \int_{V} \sum_{i=1}^{3} \sum_{j=1}^{3} \sigma_{oij} \left(\underline{N}^{T}_{,i} \underline{N}_{,j} + \underline{N}^{T}_{,j} \underline{N}_{,i} \right) dV \, \underset{\sim}{r} \tag{2.28}$$

Defining the geometric stiffness $\underline{K}_{G}$ as:

$$\underline{K}_{G} = \sum_{e} \frac{1}{2} \int_{V} \sum_{i=1}^{3} \sum_{j=1}^{3} \sigma_{oij} \left[\underline{N}^{T}_{,i} \underline{N}_{,j} + \underline{N}^{T}_{,j} \underline{N}_{,i} \right] dV \tag{2.29}$$

Equation (2.24) can then be rewritten as:

$$(\underline{K} + \underline{K}_G)\underset{\sim}{r} = \underset{\sim}{R} \tag{2.30}$$

or

$$\underline{K}_I \underset{\sim}{r} = \underset{\sim}{R}$$

where

$$\underline{K}_I = \underline{K} + \underline{K}_G = \text{incremental stiffness.}$$

In Eq. (2.30) the elastic stiffness contains the incremental material stress-strain relationship, while the geometric stiffness reflects the influence of initial stresses during a subsequent deformation increment.

2.6 INCREMENTAL CONSTITUTIVE RELATIONSHIP

An incremental formulation of the FEM is used in this study to trace the nonlinear behavior of a structure. This means that a linearized or tangent constitutive relationship is adopted for each step or iteration, the set of equations solved for the unknown nodal displacements and the constitutive relations updated. The above process is repeated until convergence has been obtained. An incremental form of the material matrix is therefore needed. From Eq. (2.8), for a isotropic material under plane stress, the incremental constitutive relationship referred to the two principal axes can be written as:

$$\begin{Bmatrix} d\sigma_1 \\ d\sigma_2 \\ d\tau_{12} \end{Bmatrix} = \frac{1}{(1-\nu^2)} \begin{bmatrix} E & \nu E & 0 \\ \nu E & E & 0 \\ 0 & 0 & (1-\nu^2)G \end{bmatrix} \begin{Bmatrix} d\varepsilon_1 \\ d\varepsilon_2 \\ d\gamma_{12} \end{Bmatrix} \tag{2.31}$$

where E = tangent modulus of elasticity

ν = Poisson's ratio

$G = E/2(1+\nu)$ = shear modulus

For an orthotropic material this can be extended to:

$$\begin{Bmatrix} d\sigma_1 \\ d\sigma_2 \\ d\tau_{12} \end{Bmatrix} = \frac{1}{(1-\nu_1\nu_2)} \begin{bmatrix} E_1 & \nu_2 E_2 & 0 \\ \nu_1 E_1 & E_2 & 0 \\ 0 & 0 & (1-\nu_1\nu_2)G' \end{bmatrix} \begin{Bmatrix} d\varepsilon_1 \\ d\varepsilon_2 \\ d\gamma_{12} \end{Bmatrix} \tag{2.32}$$

where 1 and 2 are the othotropic directions

G' = shear modulus for the material under plane stress

For simplicity it is usually assumed that:

$$\nu^2 = \nu_1\nu_2 \tag{2.33}$$

where

ν = effective Poisson's ratio under biaxial stress

For symmetric behavior the following relationship is also generally assumed to be valid:

$$\nu_1 E_1 = \nu_2 E_2 \tag{2.34}$$

These assumptions make it possible to rewrite Eq. (2.31) as follows:

$$\begin{Bmatrix} d\sigma_1 \\ d\sigma_2 \\ d\tau_{12} \end{Bmatrix} = \frac{1}{(1-\nu^2)} \begin{bmatrix} E_1 & \nu\sqrt{E_1E_2} & 0 \\ \nu\sqrt{E_1E_2} & E_2 & 0 \\ 0 & 0 & (1-\nu^2)G' \end{bmatrix} \begin{Bmatrix} d\varepsilon_1 \\ d\varepsilon_2 \\ d\gamma_{12} \end{Bmatrix} \tag{2.35}$$

This equation expresses the incrementally linear constitutive relationship in the two orthotropic material directions under a state of biaxial stress. If the 1-2 coordinate system forms an angle θ with the reference coordinate system x-y, then the constitutive relationship in the x-y coordinate system, after a proper coordinate transformation can be written as:

$$\begin{Bmatrix} d\sigma_{xx} \\ d\sigma_{yy} \\ d\tau_{xy} \end{Bmatrix} = \frac{1}{(1-\nu^2)} \begin{bmatrix} E_1C^2 + E_2S^2 & \nu\sqrt{E_1E_2} & \frac{1}{2}(E_1 - E_2)CS \\ & E_1S^2 + E_2C^2 & \frac{1}{2}(E_1 - E_2)CS \\ \text{symmetric} & & (1-\nu^2)G' \end{bmatrix} \begin{Bmatrix} d\varepsilon_{xx} \\ d\varepsilon_{yy} \\ d\gamma_{xy} \end{Bmatrix} \tag{2.36}$$

where

$$C = \cos\theta$$

$$S = \sin\theta$$

The manner in which these relationships are applied in this study to model the behavior of concrete will be presented in Chapter 3, where the details of the concrete model will be discussed.

2.7 LARGE DEFLECTION PROBLEM

The approach used in this study to solve the problem which incorporates geometric nonlinearities is basically the same as that used by Murray [45,46] in his study of the large deflection analysis of plates by the FEM. The basic assumption made is that a unique structural configuration can be found in which the externally applied loads and the internal resisting forces are in equilibrium. The internal resisting forces are calculated in the displaced configuration, taking any material nonlinearities into account. Although the uniqueness of the solution cannot be

proved mathematically, in the solution of a physical problem, an incremental technique like the one used here, will select a stable equilibrium position which for practical purposes is unquestionably the solution to the physical problem. The manner in which the final configuration is achieved is therefore not important.

Consider a triangular element which forms part of a structure as shown in Fig. 2.1. The global coordinate system XYZ is a fixed rectangular Cartesian coordinate system which is used for the whole structure. A local coordinate system $\bar{x}\bar{y}\bar{z}$ (state 1) is defined for each element. After deformation the displaced local coordinate system is xyz (state 2). The displaced local coordinate system is oriented in such a way that the nodal points of the element after deformation (1",2",3") lie in the xy-plane. The displaced local coordinate system xyz is therefore the same original local system $\bar{x}\bar{y}\bar{z}$ which has undergone rigid body translations and rotations along with the element. (1',2',3' represents the undeformed element in the new local coordinate system.)

The following procedure is then used to compute the equilibrium configuration:

1. Assume that the nodal locations have been specified in the global coordinate system by some approximate method -- usually the last increment in displacements.

2. From these locations establish the displaced local coordinate system for an element in its deformed position. Determine the element deformations with respect to the displaced local coordinate system by eliminating the effect of any rigid body translations and rotations.

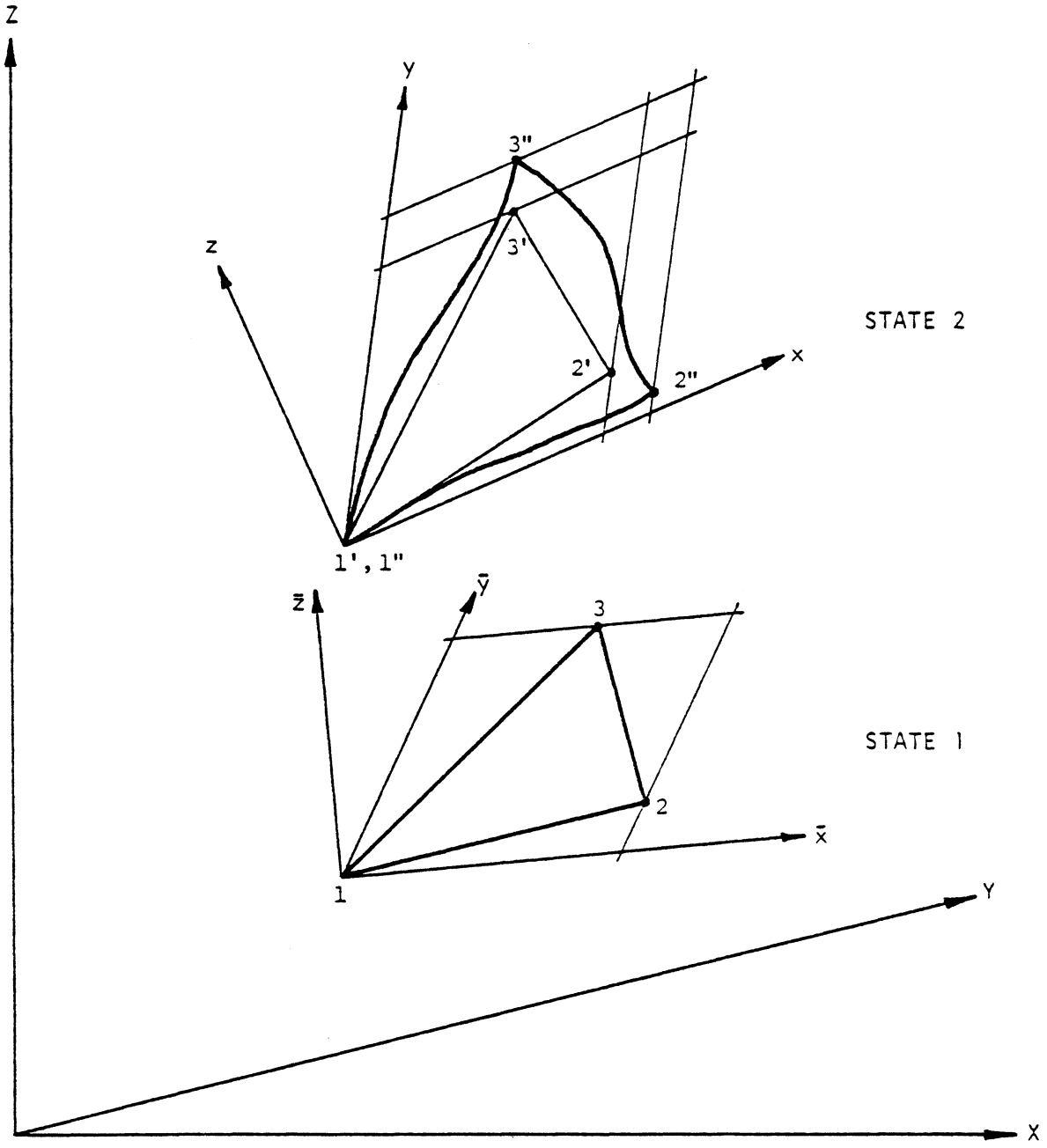

FIG. 2.1 TRIANGULAR ELEMENT BEFORE AND AFTER DEFORMATION

3. Using these deformations and the constitutive relations, determine the element internal resisting force vector and element stiffness in the displaced coordinate system.

4. Transform the element stiffness and internal resisting force vector to the global coordinate system.

5. Repeat steps 2 thru 4 for all the elements and form the structural internal resisting force vector and also assemble a new structural stiffness matrix. The difference between the internal resisting force vector and the external load vector represents an unbalanced force vector for the configuration found in step 1.

6. Analyze the structure for the unbalanced load vector. The increment in nodal displacements gives a new estimate of the nodal locations.

7. Repeat steps 2 thru 6 until equilibrium is achieved within some specified limit.

Although the displacements, displacement gradients and rotations as referred to the initial configuration in the global coordinate system may be large, they can be reduced to arbitrarily small quantities with respect to the displaced local coordinate system by refining the mesh subdivision or using smaller load increments. This is necessary to satisfy the assumption that the engineering strains are second order quantities which allows the use of linear elastic plate theory in the element local coordinate system.

Since the structural stiffness matrix is assembled using the current geometry, the effect of the changes in the structural configuration is included in the analysis.

Because the final structural configuration is based on achieving equilibrium between the external loads and internal forces, the assembled stiffness matrix used to determine the displacement increments for the next iteration need not be exact. The only requirement on the structural stiffness matrix is that the displacement increments determined from it should ultimately lead to an equilibrium configuration. This means that an analysis excluding the geometric stiffness will also yield satisfactory results, although it should in general be included.

A disadvantage of this method is the additional computational effort involved since each iteration requires the complete solution of a small deflection problem. In cases where a reasonable estimate of the stiffness can be obtained, it is possible to avoid a major part of this effort by iterating with the same stiffness matrix as will be discussed in Chapter 5.

2.8 SUMMARY

The basic assumptions which are used for the development of the solution procedure employed in this study will be summarized here.

The Updated Lagrangian formulation will be used in this study. This means that the last equilibrium position (state 1) of the structure is taken to be the reference configuration for the next solution step. The displacement increment obtained from the next solution of the equilibrium equations is taken from this reference configuration (state 1) to the next position (state 2), represented by the updated nodal coordinates. By using the procedure described in section 2.7, through which the effect of large displacements is accounted for by eliminating the rigid body displacements which the element undergoes from state 1 to state 2, the strain-displacement relationship for linear elastic theory can be used in

the element local coordinate system. It should be noted that strains are assumed to be small. Details of this procedure will be presented in section 5.5.

The constitutive models for the materials to be considered in this study, namely concrete, reinforcing and prestressing steel, will be dealt with in detail in Chapter 3.

An incremental formulation of the FEM, based on the P of VW is used in the present study. Details of the specific finite elements used will be presented in section 5.2. The evaluation of the geometric stiffness will be given in section 5.3.

The aim of this study is therefore to develop an analysis procedure for thin reinforced and prestressed concrete slabs and panels subjected to transverse and/or in-plane loads. The analysis procedure will be capable of solving problems of type 6, those including nonlinear material and large deflection effects described in section 2.1, but assuming small strains.

3. MATERIAL MODELS

3.1 GENERAL REMARKS

Although reinforced and prestressed concrete are very complex heterogeneous materials, they are very widely used in the construction of modern structures, and the realistic modeling of their properties therefore remains one of the most difficult and important aspects of any meaningful analysis. Since the mathematical modeling of the properties of these composite materials is such a complicated problem, it is usually endeavored to find models which represent the dominant behavior of the material in such a way that the overall response of actual structures can be modeled analytically.

Reinforcing and prestressing steels on their own can be considered homogeneous materials with fairly well defined properties which can be modeled satisfactorily with simple models. The way in which their stress-strain relationships are idealized will be presented in sections 3.3 and 3.4.

Concrete, on the other hand, is in itself a nonhomogeneous material consisting of aggregate and cement mortar. Due to the nature of the material the only realistic way in which its properties can be defined is through the use of statistical averaging. These average values have proved to be good representations of the macroscopic behavior of concrete over the years. Concrete exhibits a pronounced nonlinear behavior at higher stress levels, and it differs markedly in its response to compression and tension. The low tensile strength and accompanying tensile cracking of concrete at a relatively low stress is one of the major factors causing nonlinear behavior of the reinforced concrete composite.

In addition to the highly nonlinear behavior of concrete, its properties also depend on its age and environmental factors like ambient humidity and temperature. This leads to creep and shrinkage of concrete which can in some cases be of major importance in assessing the behavior of a structure over its lifetime. This is especially true for prestressed concrete, where these factors usually are major causes of prestress loss, or in the case of thin shells, where they can dramatically lower the buckling load. The modeling of concrete in this study will be described in section 3.2.

Although dynamic loadings are not considered in this study, a quasi-static analysis through time is carried out, and this means that unloading and reloading can take place. This will generally not be of major importance, thus load reversals are modeled in a simple fashion as described for each material.

To represent the variation of strain and stress as well as cracking, yielding, etc., through the thickness of a slab, it will be divided into a number of layers. Each layer will be assumed to be in a state of plane stress. The reinforcement is treated as "smeared" layers, with specific orientations, at a specified depth in the cross section while the contribution of each prestressing tendon segment in an element is taken into account separately as discussed in section 4.5.

For reinforcing steel and bonded prestressing tendons, it will be assumed that perfect bond exists between the steel and the concrete. This means that the displacement field within an element can be considered to be continuous. Unbonded prestressed tendons are assumed to be only fixed at their anchors, while the friction forces along their length are taken into account. The iterative way in which unbonded tendons are treated is described in detail in section 4.6.

3.2 CONCRETE

3.2.1 Deformation of concrete

The nonlinear behavior of concrete is best demonstrated by a discussion of its deformation. The complexity of the factors influencing the deformation of concrete has up to date prevented the formulation of a general theory encompassing the results of all experimental investigations. One of the most important assumptions, which makes it possible to study different factors affecting the deformation of concrete separately, is that the deformation or strain can be considered to be the sum of the deformations caused by a limited number of phenomena. The main factors generally considered in addition to stress are aging, creep, shrinkage and thermal deformation -- the last of which is neglected here for simplicity, but will be discussed in section 3.2.8.

In Fig. 3.1 the deformation of a concrete specimen under different loading and environmental conditions are shown. The deformation in Fig. 3.1a is that of the unloaded specimen with the passage of time. This is defined as shrinkage and occurs mainly because of hygral inequilibrium between the specimen and its environment. In Fig. 3.1b the deformation of a specimen subjected to a constant compressive load and maintained in hygral equilibrium is shown. The deformation at time t_o due to the application of the load can be defined as the instantaneous elastic deformation. An increase in deformation is observed with passage of time from t_o to t. Due to the fact that the strength of concrete increases with time, the true instantaneous elastic deformation at time t would be less than at t_o. This difference is the deformation due to aging. The creep can then be defined as the deformation in excess of the true instantaneous deformation at time t.

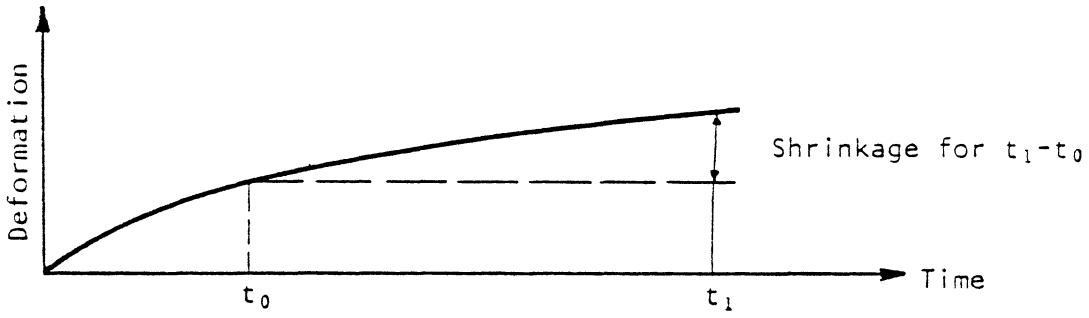

a. SHRINKAGE OF AN UNLOADED SPECIMEN

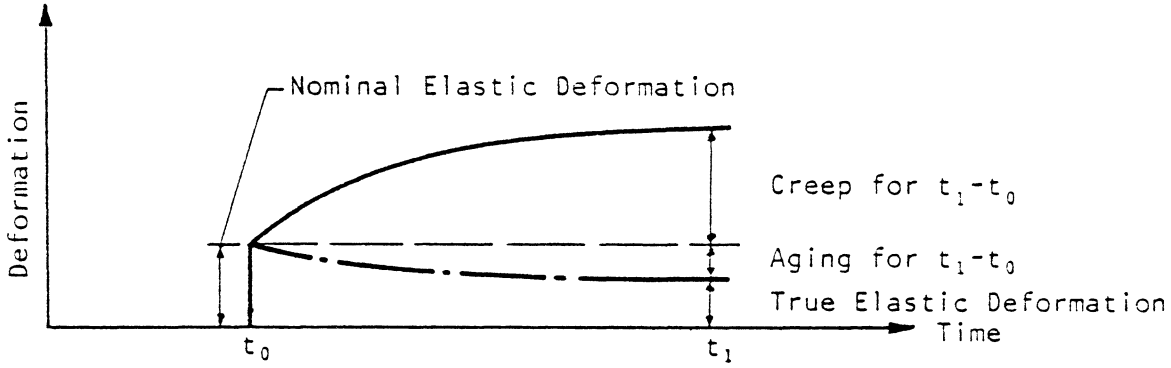

b. CREEP OF A LOADED SPECIMEN IN HYGRAL EQUILIBRIUM WITH THE AMBIENT MEDIUM

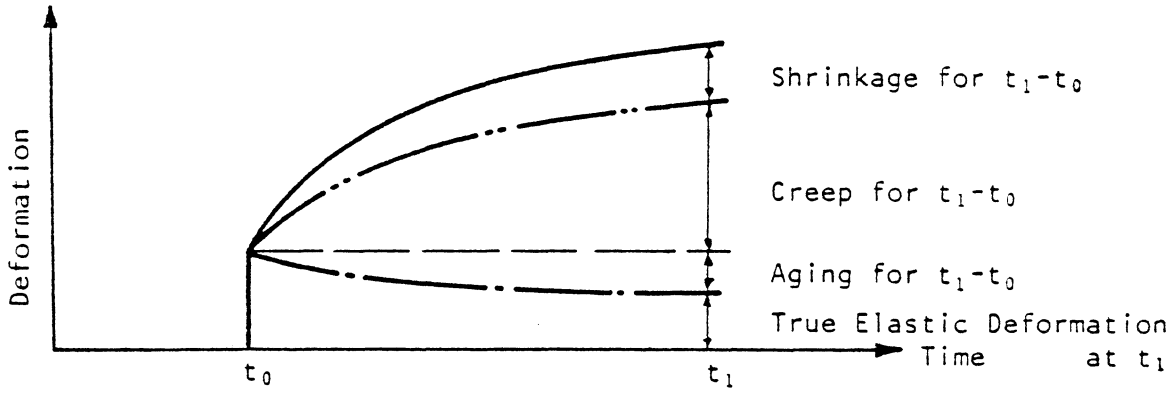

c. CHANGE OF DEFORMATION OF A LOADED AND DRYING SPECIMEN

FIG. 3.1 DEFORMATION COMPONENTS OF CONCRETE

The different components of the deformation of concrete is shown in Fig. 3.1c. This simplified approach is of course not completely accurate, since creep and shrinkage are known to be interdependent phenomena, for example, but this is an assumption that is generally accepted.

3.2.2 Concrete under biaxial stress

From experimental investigations it has been established that under a state of biaxial stress the behavior of concrete is significantly different from that observed under uniaxial stress. It has recently been recognized that many of the earlier investigations may not be completely reliable because of the experimental techniques used [48]. One of the most comprehensive and dependable studies was done by Kupfer et al. [49], and some of their results are presented here to illustrate the behavior of concrete under biaxial stress.

In Fig. 3.2 it can be seen that the maximum compressive strength increases under biaxial compression -- values of up to 27% higher than the uniaxial strength being obtained. The concrete ductility at maximum compressive strength also increases.

Another important factor is that the stiffness of the concrete in a principal direction increases in the presence of compression in the other principal direction. This increase in stiffness is mainly ascribed to the confinement of potential microcracking because of the biaxial stress state.

In Figs. 3.3 to 3.5 stress-strain curves for specimens tested at different constant principal stress ratios are shown. Nine ratios, which cover the whole range of compression-compression, compression-tension and tension-tension, were used. Failure modes for the various stress ratios

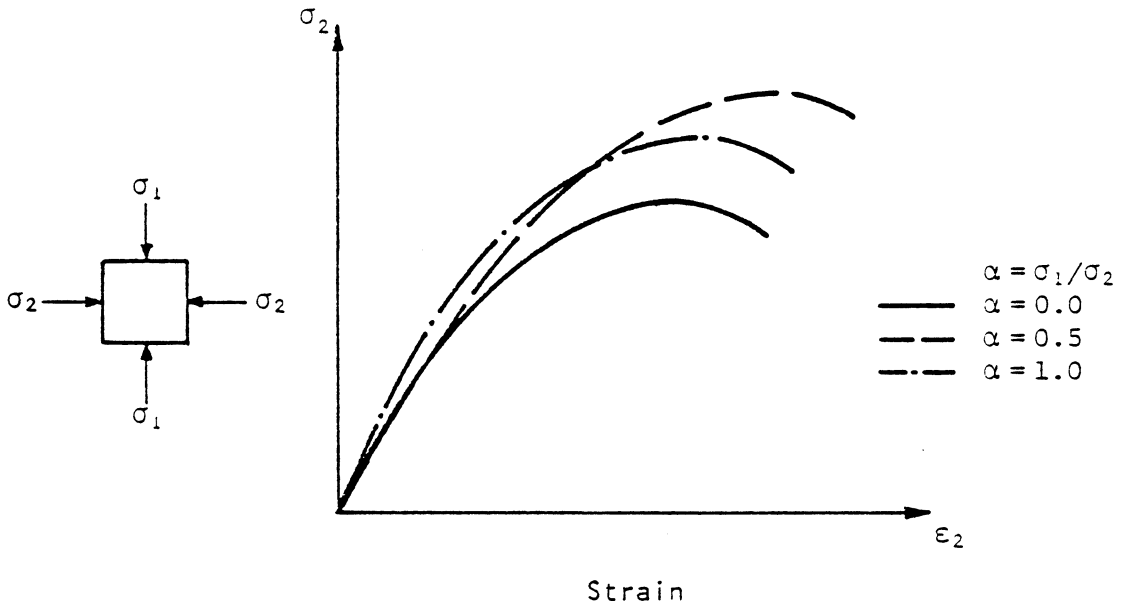

FIG. 3.2 STRESS-STRAIN RELATIONSHIPS OF CONCRETE UNDER BIAXIAL COMPRESSION

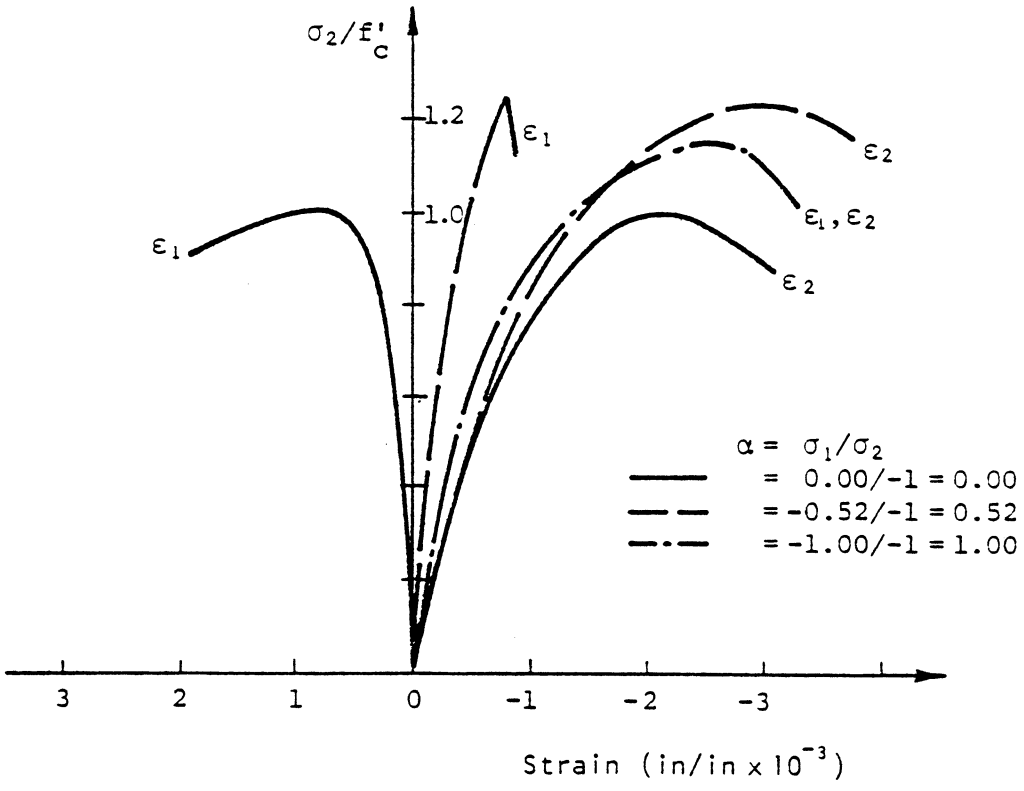

FIG. 3.3 EXPERIMENTAL STRESS-STRAIN CURVES FOR BIAXIAL COMPRESSION [49]

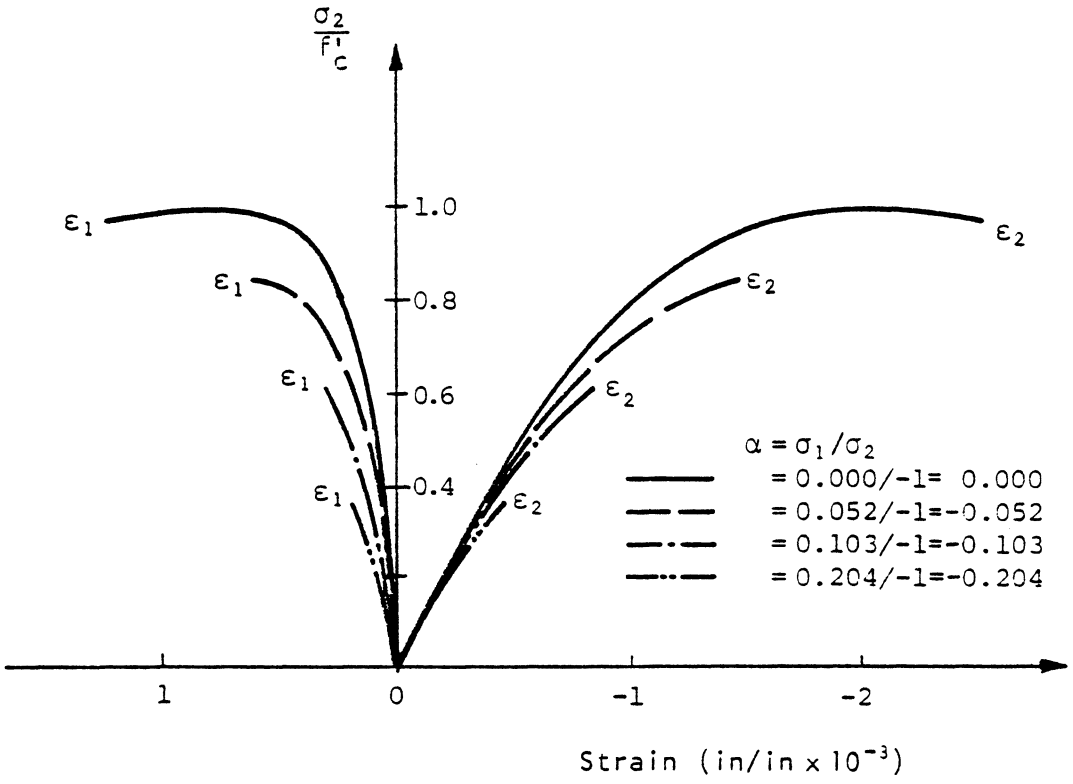

FIG. 3.4 EXPERIMENTAL STRESS-STRAIN CURVES FOR BIAXIAL TENSION-COMPRESSION [49]

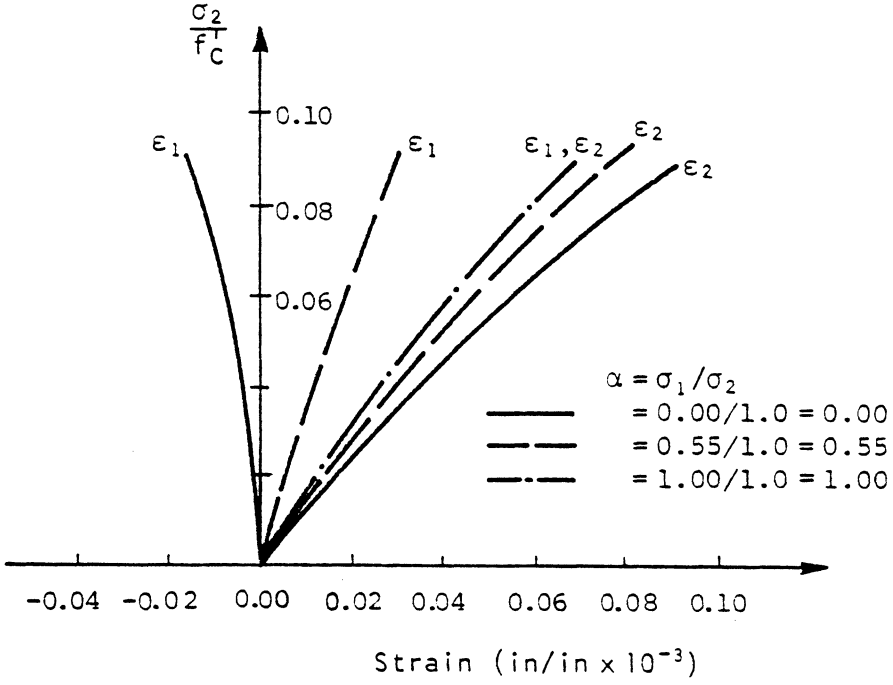

FIG. 3.5 EXPERIMENTAL STRESS-STRAIN CURVES FOR BIAXIAL TENSION [49]

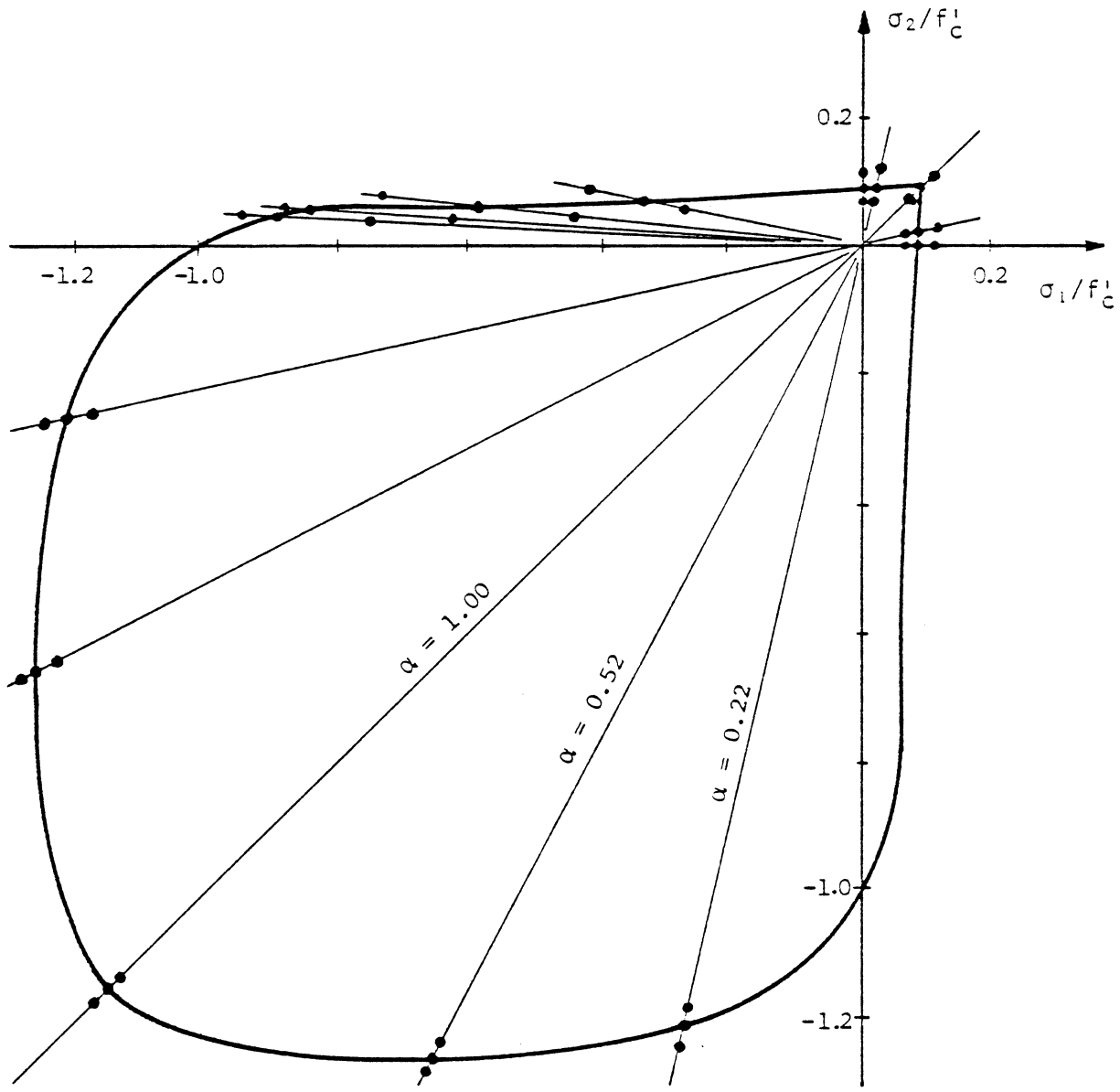

$\alpha = \sigma_1/\sigma_2$ Compression = - Tension = +
• = Experimental Points

FIG. 3.6 EXPERIMENTAL BIAXIAL STRENGTH ENVELOPE [49]

were recorded and in Fig. 3.6 the biaxial strength envelope obtained by Kupfer et al. [49] is shown.

3.2.3 Review of analytical models

The pronounced nonlinear behavior of concrete discussed in the previous sections, the increased need for a comprehensive model to characterize the constitutive relationship of concrete for use in increasingly sophisticated analyses of concrete structures utilizing the finite element method, has brought about an intensive research effort in the past few years, resulting in the proposal of a large number of constitutive models. No agreement on a constitutive relationship for the inelastic response under one, two or three-dimensional stress states for short time loading has been reached at the present. Excellent reviews and extensive references are given in papers by Argyris et al. [35], Scordelis [50] and Aoyama et al. [51].

Most analytical models attempt to derive constitutive relationships for one, two or three-dimensional stress states in terms of one or more values obtained from a simple uniaxial test or a triaxial cell test. In many cases everything is defined in terms of one measured property, the uniaxial compressive strength of the concrete f'_c. In other cases, where measured uniaxial stress-strain data are available for the material, one or more additional factors such as the initial tangent modulus of elasticity E_o, the tensile strength f'_t, the strain at compressive strength ε_c or Poisson's ratio ν may be considered. It is important to note that even this simple uniaxial curve for a given concrete is subject to considerable variations depending on environmental conditions, rate of loading and cyclic loading.

The more important of these constitutive models for short time loading will be discussed using the following broad categorization: (1) nonlinear elasticity, (2) plasticity and (3) endochronic theory.

1. Nonlinear elasticity

These models generally utilize a hypo-elastic formulation which characterizes the material to be path-dependent and stress reversible. An attempt is made to find an incremental stress-strain relationship for the mathematical model. In the simplest approach to two or three-dimensional models an isotropic formulation is used while an orthotropic formulation is employed to obtain a more sophisticated model.

a) Models based on an isotropic formulation.

Nilson [52] transformed the biaxial stresses to uniaxial stresses and then used Saenz's [53] equation in compression and a linear relationship for tension. Franklin [54] also transformed the biaxial stresses to uniaxial but used a multilinear stress-strain curve for the concrete. The failure envelope he used is indicated in Fig. 3.7.

Kupfer and Gerstle [55] proposed a more sophisticated isotropic model employing secant shear and bulk moduli derived from experimental results based on the use of octahedral stresses and strains. Unloading is not taken into account and at high stress levels the correlation with experimental data is not good.

Romstad et al. [56] proposed a multilinear model with four stages of behavior prior to failure in compression at a stress equal to the uniaxial strength. The strain space is divided into regions of equal damage for which values of E and ν can be estimated by using uniaxial test results.

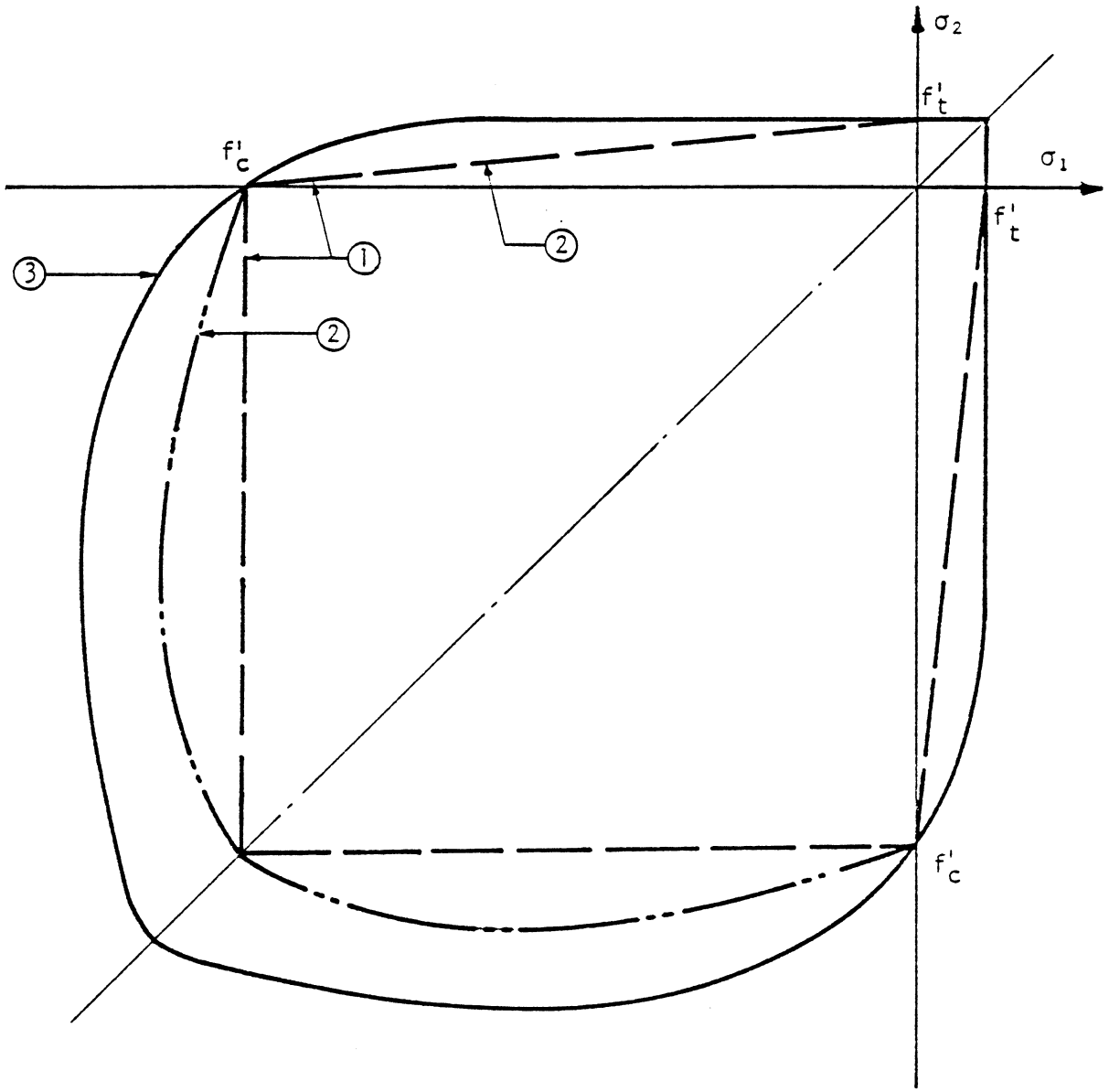

① — — FRANKLIN [54]

② —·—·— LIN [26]

③ ——— KABIR [28] (Darwin et al. [59], Kupfer et al. [55])

FIG. 3.7 FAILURE ENVELOPES

A problem with these models is that they assume concrete to be an isotropic material while in Fig. 3.3 it can be seen that concrete exhibits stress-induced orthotropic behavior under a state of biaxial stress.

b) Models based on an orthotropic formulation:

Liu, Nilson and Slate [58] proposed a model based on their tests [57] in which concrete is assumed to be an orthotropic material under biaxial loading. For compression they proposed a constitutve relationship of the form:

$$\sigma_i = \frac{\varepsilon_i E_o}{(1 - \nu\alpha)\left[1 + \left(\frac{1}{1-\nu\alpha}\frac{E_o}{E_s} - 2\right)\frac{\varepsilon_i}{\varepsilon_p} + \left(\frac{\varepsilon_i}{\varepsilon_p}\right)^2\right]} \qquad (3.1)$$

where

σ_i, ε_i = stress and strain in principal direction i.

σ_p, ε_p = maximum biaxial compression stress and corresponding strain.

ν = Poisson's ratio.

E_o = initial tangent modulus for uniaxial loading.

$E_s = \frac{\sigma_p}{\varepsilon_p}$ = secant modulus at maximum stress.

$\alpha = \frac{\sigma_1}{\sigma_2}$ = stress ratio, $\sigma_1 \geqslant \sigma_2$

For the case of uniaxial stress ($\alpha = 0$) Eq. (3.1) reduces to Saenz's [53] equation. Equation (3.1) does not allow for load reversal, however, and is valid for compression only.

Darwin and Pecknold [59,60,61] have extended the model of Liu et al. [58] to incorporate cyclic loading and strain softening in compression. For biaxial compression they proposed a family of curves

which depends on the stress ratio α which they called the "equivalent uniaxial" stress-strain curves. Their procedure provides a way of separating the Poisson effect from the cumulative strain and permits a convenient representation of concrete as an incrementally linear orthotropic material for biaxial stress states. Details of this model, which was also used by Kabir [28], will be presented in section 3.2.4.

2. Plasticity

These models are based on the classical elasto-plastic theory incorporating the flow theory of plasticity. The constitutive model is based on three assumptions [35]: (1) the shape of an initial yield surface, (2) the evolution of subsequent loading surfaces and (3) the formulation of an appropriate hardening rule. The following investigators have utilized models based on this theory.

Lin [26], in his study of slabs and shells, idealized the concrete as a perfectly elastic-plastic material and used the von Mises yield criterion which results in the failure envelope also indicated in Fig. 3.7

Argyris et al. [35] reported on the use of the models of Liu et al. [58], Kupfer et al. [55] and also a model based on the theory of hardening elastic-plastic solids in their paper on the finite element analysis of prestressed concrete reactor vessels. They obtained good correlation with experimental results using all three models. The comparison favours the simpler formulations such as variable bulk and shear moduli or elastic-plastic models. They also state that these models were obviously formulated by fitting the experimental data obtained from homogeneous stress states and proportional monotonic loading. Therefore the extension of

these simple models to more complex structures subjected to non-proportional and non-monotonic loading caused by nonlinear behavior does not follow directly.

Chen and Chen [62,63] applied the principles of plasticity to propose a model assuming concrete to be an isotropic, homogeneous, linear elasto-plastic, strain hardening and fracturing material. The initial discontinuous surface, loading surfaces and failure surface are developed, and the elasto-plastic incremental stress-strain relationships for plane stress are derived in matrix form.

3. Endochronic theory

Bazant et al. [64,65] have extended the application of endochronic theory, which was originally proposed by Valanis [66] for metals, to concrete. The basis of the formulation is the use of a scalar parameter, called intrinsic time, which expresses the distortion that the material has undergone and is a function of the deviatoric strain increments. The model permits the representation of inelastic dilatancy, hydrostatic pressure sensitivity, strain softening at high stress levels and cyclic straining. Good agreement has been achieved in comparisons with experimental studies [65].

In their recent state-of-the-art summary of testing and analytical models for uniaxial cyclic loading and multi-axial loading of concrete Aoyama and Noguchi [51] present a comprehensive review of the various analytical models that have been proposed for concrete under biaxial stress. They report that Noguchi [66] compared a model based on the theory of plasticity and using Drucker-Prager's yield criterion, which has been used by many investigators, and four other models with the test

results of Kupfer et al. [49] and Nelissen [68]. Noguchi concluded that the plasticity model could not represent the behavior of the concrete adequately, especially at higher stress levels, and that the orthotropic model of Darwin et al. [59] gives the best results in both principal directions for the models that he considered.

In his study of the nonlinear material behavior of slabs, panels and shells, Kabir [28] used the model proposed by Darwin et al. [59] with some modifications. Although simpler models have been used with good results and despite the fact that the concrete model seems to have little influence on the calculated behavior, especially near ultimate [69,28], the Darwin model seems to represent a significant improvement over those models used by Nilson [52], Franklin [54] and Lin [26] without a major increase in computational effort. The Darwin model is therefore adopted in this study following a procedure similar to that used by Kabir [28]. Details of the model are presented in the next section.

3.2.4 Concrete model for the present study

The analytical model used to represent the behavior of concrete under biaxial stress in this study is the same as the one used by Kabir [28] and the model will be discussed in detail in this section.

From the experimental results shown in Fig. 3.3, section 3.2.2, it can be seen that concrete behaves as an orthotropic material in the two principal stress directions, and this is the assumption made for this concrete model. Equation (2.35), derived in section 2.6 will therefore be used, assuming that the orthogonal axes 1 and 2 are the principal stress directions.

No experimental data are available regarding the value of the shear modulus G'. It has been demonstrated [59] that the following value of G' does not show bias with respect to any particular direction as far as shear stiffness is concerned:

$$G' = \frac{1}{4(1-\nu^2)}\left(E_1 + E_2 - 2\nu\sqrt{E_1 E_2}\right) \tag{3.2}$$

Equation (2.35) can thus be rewritten as:

$$\begin{Bmatrix} d\sigma_1 \\ d\sigma_2 \\ d\tau_{12} \end{Bmatrix} = \frac{1}{(1-\nu^2)} \begin{bmatrix} E_1 & \nu\sqrt{E_1 E_2} & 0 \\ \nu\sqrt{E_1 E_2} & E_2 & 0 \\ 0 & 0 & \frac{1}{4}\left(E_1 + E_2 - 2\nu\sqrt{E_1 E_2}\right) \end{bmatrix} \begin{Bmatrix} d\varepsilon_1 \\ d\varepsilon_2 \\ d\gamma_{12} \end{Bmatrix} \tag{3.3}$$

The concrete material properties that are needed for any iteration in the solution procedure are the orthotropic tangent moduli E_1 and E_2 and the effective Poisson's ratio ν. The value of ν is obtained from experiments, while the way in which the moduli E_1 and E_2 are obtained will be described below in detail.

The value of Poisson's ratio ν varies from 0.15 to 0.2 below the elastic limit [49]. At a stress level higher than 80% of the ultimate stress an increase in value is observed. In this study, however, a constant value of ν will be assumed for all stress levels, since the influence of ν is relatively small and this is considered to be a reasonable approximation for the cases to be studied.

In general the moduli E_1 and E_2 would be the tangent moduli from uniaxial tests in the orthotropic directions. This means that Eq. (3.3) is based on the assumption that any increase in effective stiffness in either direction resulting from compressive stress in the other direction

is due to the Poisson effect alone. Experimental studies [49] on concrete, however, indicate that a considerably greater increase in stiffness is obtained for a state of biaxial stress than can be explained by the Poisson effect alone. The main cause of this seems to be the confinement of potential microcracking in the presence of biaxial compression. The use of Eq. (3.3) would therefore only be appropriate at low stress levels when the confinement of the microcracking is not yet a significant factor.

If this additional increase in stiffness is to be accounted for, it is clear that E_1 and E_2 cannot simply be obtained from uniaxial stress-strain curves. If Poisson's effect is removed from experimental biaxial stress-strain curves in compression a family of stress-strain curves can be constructed. These curves would include the effect of the microcrack confinement and values of E_1 and E_2 can be obtained from them for use in Eq. (3.3). Darwin et al. [59] proposed the use of such a procedure and called this family of curves the "equivalent uniaxial" stress-strain curves.

A typical equivalent uniaxial stress-strain curve is shown in Fig. 3.8. The constitutive relationship for the compression part of the curve is given by [59]:

$$\sigma_i = \frac{E_o \, \varepsilon_{iu}}{1 + \left(\frac{E_o}{E_s} - 2\right)\left(\frac{\varepsilon_{iu}}{\varepsilon_{ic}}\right) + \left(\frac{\varepsilon_{iu}}{\varepsilon_{ic}}\right)^2} \tag{3.4}$$

where

ε_{iu} = equivalent uniaxial strain in the principal stress direction i .

$\sigma_{ic}, \varepsilon_{ic}$ = maximum compressive stress and corresponding strain in principal direction i obtained from the biaxial failure envelope of Kupfer and Gerstle [55].

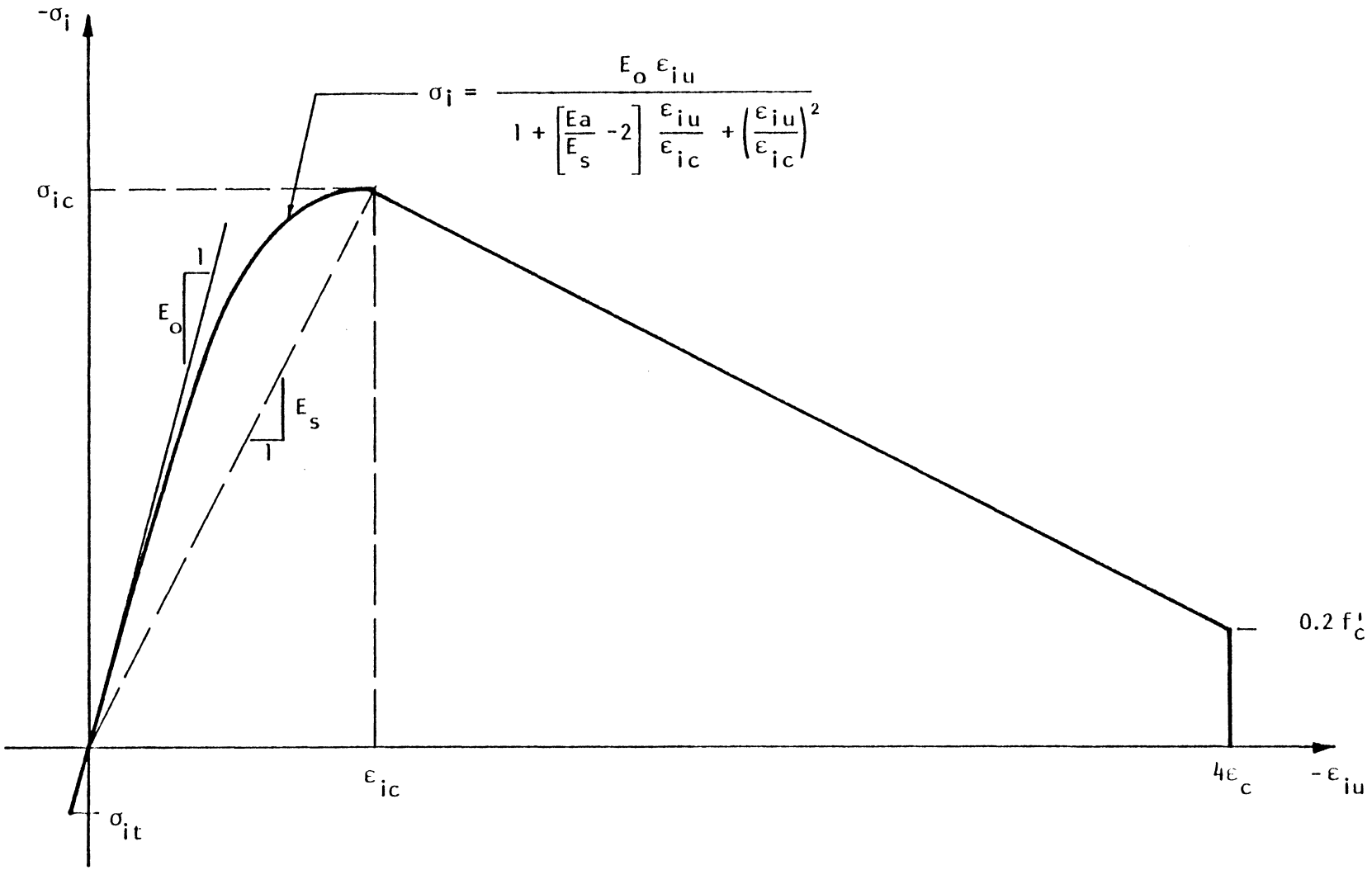

FIG. 3.8 EQUIVALENT UNIAXIAL STRESS-STRAIN MODEL FOR CONCRETE PROPOSED BY DARWIN ET AL. [59]

E_o = initial uniaxial tangent modulus.

$E_s = \sigma_{ic}/\varepsilon_{ic}$ = secant modulus.

For tension the relationship is:

$$\sigma_i = E_o \varepsilon_{iu} \quad \text{for} \quad \sigma_i \leq \sigma_{it} \tag{3.5}$$

where

σ_{it} = tensile strength of the concrete in the principal stress direction.

The model will be presented by illustrating how the equivalent uniaxial stress-strain curves are constructed, and subsequently the stress-strain curve after peak stress and the way in which stress reversals are handled will be discussed.

a) Equivalent uniaxial stress-strain curves

The equivalent uniaxial strain ε_{iu} is the strain obtained when only Poisson's effect is removed from the biaxial strains. This means that the influence of the microcrack confinement will be retained. The following illustration will show how ε_{iu} can be obtained from experimental data.

For concrete under biaxial compression at a stress state of σ_1, σ_2 in the principal directions, assuming proportional loading and that the material behaves piecewise linearly in an increment, the stress-strain relationship is:

$$d\varepsilon_2 = \frac{d\sigma_2}{E_2} - \frac{\nu\, d\sigma_1}{E_1} \tag{3.6}$$

where E_1, E_2 are the tangent moduli.

Rearranging Eq. (3.6) leads to:

$$d\sigma_2 = E_2 \frac{d\varepsilon_2}{1 - \nu\alpha n} = E_2 \, d\varepsilon_{2u} \tag{3.7}$$

where

$\alpha = \sigma_1/\sigma_2$ = biaxial stress ratio

$n = E_2/E_1$ = modular ratio

$d\varepsilon_{2u} = d\varepsilon_2/(1-\nu\alpha n)$ = equivalent uniaxial strain in direction 2.

Thus the slope E_2 of the stress-strain curve represented by Eq. (3.7) does not contain Poisson's effect which is removed by the introduction of $d\varepsilon_{2u}$. The microcrack confinement does influence the experimentally obtained values of $d\varepsilon_2$, thus also $d\varepsilon_{2u}$, and therefore the value of E_2 will include this effect and can be used in Eq. (3.3).

The total equivalent uniaxial strain at any point is obtained by summing for all increments up to that point:

$$\varepsilon_{iu} = \sum d\varepsilon_{iu} = \sum \frac{d\varepsilon_i}{(1 - \nu\alpha n)} = \sum \frac{d\sigma_i}{E_i} \tag{3.8}$$

By differentiating Eqs. (3.4) and (3.5) the slopes of the equivalent uniaxial stress-strain curves are obtained. For compression at a point $(\sigma_i, \varepsilon_{iu})$ it is:

$$E_i = \frac{\partial\sigma_i}{\partial\varepsilon_{iu}} = \frac{E_o(1 - q^2)}{\left[1 + \left(\frac{E_o}{E_s} - 2\right)q + q^2\right]} \tag{3.9}$$

where

$$q = \varepsilon_{iu}/\varepsilon_{ic}$$

For tension the slope is E_o, the initial slope.

A typical equivalent uniaxial stress-strain curve for a biaxial stress ratio $\alpha = \sigma_1/\sigma_2$ is shown in Fig. 3.8. The point of maximum compressive stress $(\sigma_{ic},\varepsilon_{ic})$ under biaxial loading is a function of the principal stress ratio α, the uniaxial compressive strength f'_c and the strain at peak uniaxial stress ε_c. The values of the maximum stresses in the two principal directions, σ_{1c} and σ_{2c} are obtained from the modified biaxial strength envelope of Kupfer and Gerstle [55] which is shown in Fig. 3.9. It is assumed that the maximum tensile stress that the concrete can withstand is the uniaxial tensile strength f'_t.

The biaxial strength envelope of Fig. 3.9 is divided into four regions which depends on the stress state as represented by the stress ratio α. Compressive stresses are always assumed to be negative with tensile stresses positive and the principal directions chosen such that $\sigma_1 \geqslant \sigma_2$ algebraically.

The four regions of the strength envelope with the accompanying equations for the maximum stresses σ_{ic} and corresponding equivalent uniaxial strains ε_{ic} are summarized as follows:

1. For σ_1 = compression, σ_2 = compression. $0 \leqslant \alpha \leqslant 1$

$$\sigma_{2c} = \frac{1 + 3.65\,\alpha}{(1+\alpha)^2} f'_c \tag{3.10a}$$

$$\sigma_{1c} = \alpha\,\sigma_{2c} \tag{3.10b}$$

$$\varepsilon_{2c} = \varepsilon_c[3p_2 - 2] \tag{3.11a}$$

$$\varepsilon_{1c} = \varepsilon_c\left[-1.6p_1^3 + 2.25p_1^2 + 0.35p_1\right] \tag{3.11b}$$

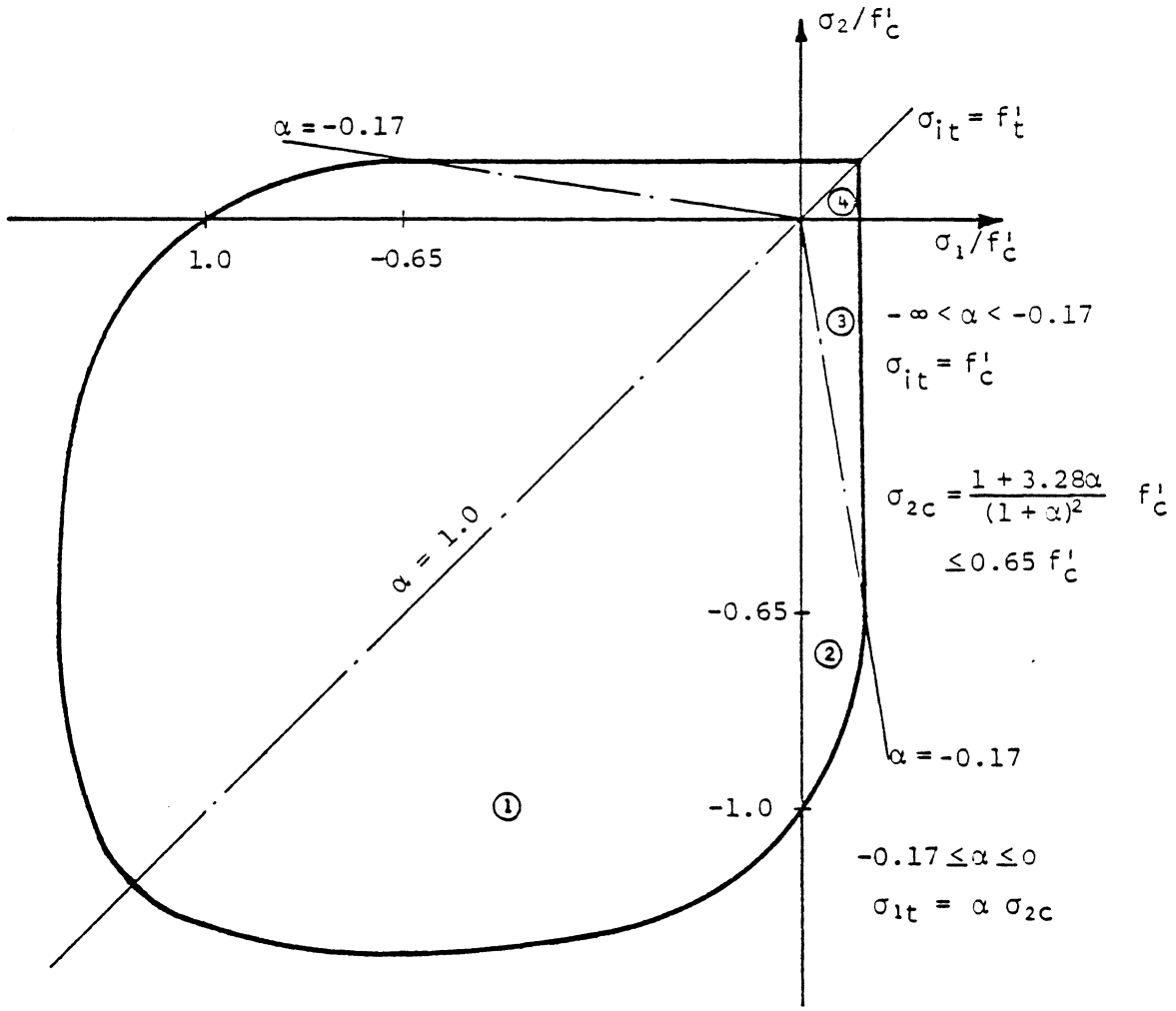

$$\sigma_{2c} = \frac{1 + 3.65\alpha}{(1+\alpha)^2} f'_c$$

$$\sigma_{1c} = \alpha \sigma_{2c}$$

$$\alpha = \sigma_1 / \sigma_2$$

Compression = -
Tension = +

FIG. 3.9 BIAXIAL STRENGTH ENVELOPE USED IN THE PRESENT STUDY

where $p_1 = \sigma_{1c}/f'_c$ and $p_2 = \sigma_{2c}/f'_c$.

Equation (3.10) is based on the Kupfer and Gerstle [55] biaxial strength envelope, while Darwin et al. [59] proposed Eq. (3.11) based on experimental observations of strains corresponding to peak stresses under biaxial compression. Concrete is assumed to yield beyond the maximum compressive stress when a further increase in strain causes a decrease in stress and failure due to crushing occurs at a specified ultimate strain. Concrete behavior beyond yielding will be discussed in more detail in subsection 3.2.4.b.

2. For σ_1 = tension, σ_2 = compression. $-0.17 \leqslant \alpha \leqslant 0$

$$\sigma_{2c} = \frac{1 + 3.28\alpha}{(1+\alpha)^2} f'_c \tag{3.12a}$$

$$\sigma_{1t} = \alpha\, \sigma_{2c} \tag{3.12b}$$

$$\varepsilon_{2c} = \varepsilon_c\left[4.42 - 8.38p_2 + 7.54p_2^2 - 2.58p_2^3\right] \tag{3.13a}$$

where

$$p_2 = \sigma_{2c}/f'_c$$

$$\varepsilon_{1t} = \sigma_{1t}/E_o \tag{3.13b}$$

Darwin et al. [59] suggested Eq. (3.12) while Eq. (3.13) is given by Rajagopal [70]. Failure in this zone is assumed to occur due to the yielding and crushing of concrete in the compression direction.

3. For σ_1 = tension, σ_2 = compression. $-\infty < \alpha < -0.17$

$$\sigma_{2c} = 0.65\, f'_c \tag{3.14a}$$

$$\sigma_{1t} = f'_t \tag{3.14b}$$

$$\varepsilon_{2c} = \varepsilon_c\left[4.42 - 8.38p_2 + 7.54p_2^2 - 2.58p_2^3\right] \tag{3.15a}$$

where

$$p_2 = \sigma_{2c}/f'_c \leqslant 0.65$$

$$\varepsilon_{1t} = \sigma_{1t}/E_o \tag{3.15b}$$

Failure in this zone is assumed to occur due to cracking in the tension direction.

4. For σ_1 = tension, σ_2 = tension. $1 < \alpha < \infty$

$$\sigma_{1t} = \sigma_{2t} = f'_t \tag{3.16}$$

$$\varepsilon_{1t} = \varepsilon_{2t} = f'_t/E_o \tag{3.17}$$

For biaxial tension, the uniaxial tensile strength, f'_t is chosen as the tension cut-off point beyond which cracking is assumed to occur.

Five material properties of concrete are needed for the construction of the equivalent uniaxial stress-strain curves. These are (1) uniaxial initial tangent modulus, E_o ; (2) uniaxial compressive strength, f'_c; (3) strain corresponding to uniaxial compressive strength, ε_c ; (4) uniaxial tensile strength, f'_t ; and (5) Poisson's ratio, ν .

All five parameters may be obtained from uniaxial load tests on concrete and used. Another option, based on recommendations by different ACI committees, is also used in the present study in cases where experimental data are not available.

ACI Committee 209 [71] suggests the following expressions for the initial tangent modulus, the uniaxial compressive and tensile strengths

at any time t :

$$E_o(t) = 33.0\ w^{1.5}\ \sqrt{f'_c(t)} \tag{3.18}$$

where

t = time in days after casting

$E_o(t)$ = initial uniaxial tangent modulus in psi at time t,

$f'_c(t)$ = uniaxial compressive strength in psi at time t.

$$f'_c(t) = \frac{t}{4.0 + 0.85t}\ f'_c(28) \tag{3.19}$$

where

$f'_c(28)$ = 28 day uniaxial compressive strength in psi

$$f'_t(t) = 0.65\sqrt{w\ f'_c(t)} \tag{3.20}$$

where

$f'_t(t)$ = tensile strength in psi
(represented by the modulus of rupture)

Hognestad [72] suggested the following relationship for the strain corresponding to peak uniaxial compressive stress:

$$\varepsilon_c(t) = 2\ f'_c(t)/E_o(t) \tag{3.21}$$

where

$\varepsilon_c(t)$ = strain corresponding to peak stress $f'_c(t)$
at t days after casting

The value of Poisson's ratio is assumed to be independent of age and stress level in the present study although at a stress level higher than 0.8 f'_c, significant increase in this value has been observed [49]. Generally, Poisson's ratio for concrete is taken to be 0.15 in this study.

b) Stress-strain curve beyond maximum compressive strength.

The existence of the falling branch, or part of the stress-strain curve beyond maximum compressive strength, of concrete has long been established. There is also general agreement that an envelope curve, coinciding with the stress-strain curve obtained from monotonic loading, can be defined [51].

Aoyama and Noguchi [51] give a comprehensive summary of a number of envelope curves that have been proposed. Darwin et al. [59] based the curve for the falling branch of their model on the envelope curves obtained from uniaxial cyclic loading tests by Karsan and Jirsa [73] due to a lack of experimental data on cyclic loading under biaxial stress (Fig. 3.8).

Beyond the maximum compressive strength, the stress in the concrete decreases with an increase in strain and this leads to a negative tangent modulus. This may cause numerical problems when used in the constitutive equation (3.3). The following procedure is adopted in this study to avoid this problem: When a calculated principal stress $\sigma_i^{n'}$ exceeds the value of σ_{ic}, as shown in Fig. 3.10, "yielding" is assumed to have occurred. The stress drops to σ_i^n and the elastic moduli are set to zero for the next iteration. The constitutive relationship after yielding becomes:

$$\underset{\sim}{d\sigma} = \underline{0}\ \underset{\sim}{d\varepsilon} \tag{3.22}$$

It should be noted here that an "unconstrained flow rule" is assumed for the unloading part of this model once yielding has started. This implies that after the first yielding, subsequent unloading will take place along the path determined by the current stresses corresponding to the current total strains. Lin [26] used both the unconstrained flow rule and the normality flow rule with a Von Mises yield criterion

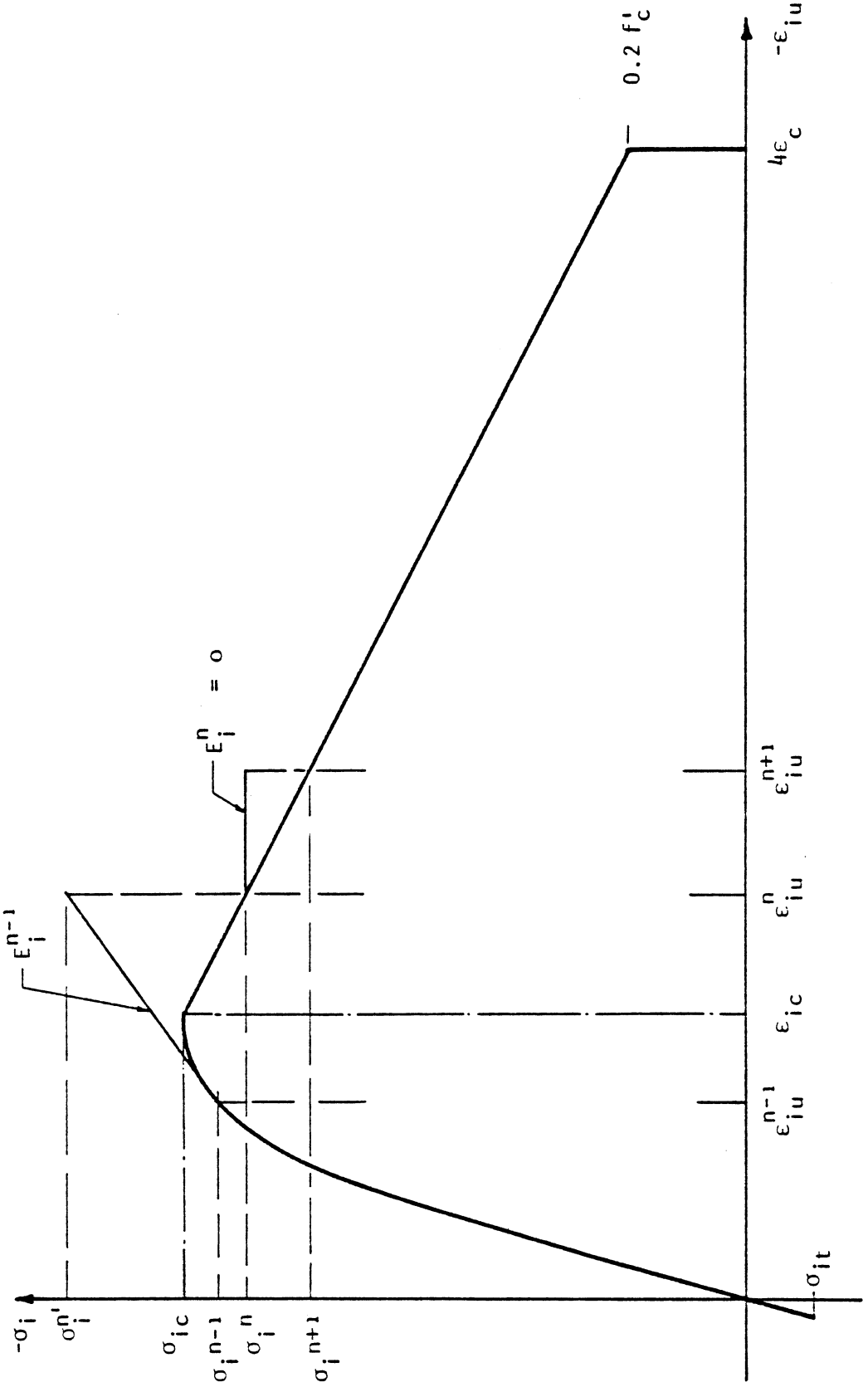

FIG 3.10 UNLOADING BEYOND COMPRESSIVE STRENGTH

and found that the flow rule used has little influence on the behavior of reinforced concrete slabs and shells. In view of this result, and since the unconstrained flow rule is much simpler to formulate, this approach will also be used in the present study.

c) Unloading

Unloading or stress reversal is possible during the time-dependent analysis due to the effects of creep and shrinkage or loading history and must therefore be taken into account.

In their proposed model Darwin et al. [59] included complete loading, unloading and reloading curves for use in the analysis of structures subjected to cyclic loading. In the present study cyclic loading is not considered and a simpler load reversal model is therefore adopted. Darwin et al. [59] proposed the use of the initial tangent modulus E_o for unloading before the maximum compressive stress has been reached. Beyond this point the unloading and reloading paths are modeled in a more complex fashion which will not be described here. For this study it is assumed that all unloading takes place with initial modulus E_o. This simple model is chosen here as a first approximation due to the fact that unloading is not considered to be of major importance for the type of applications foreseen for this model and to avoid excessive computational effort.

The equivalent uniaxial stress-strain curve shown in Fig. 3.11 is made up of four parts:

1. Compressive loading up to σ_{ic} along AB. Unloading on this part occurs with slope E_o, e.g. along PA' (and then along A'F'G', similar to AFG). Reloading will take place along A'P and then continue along PB.

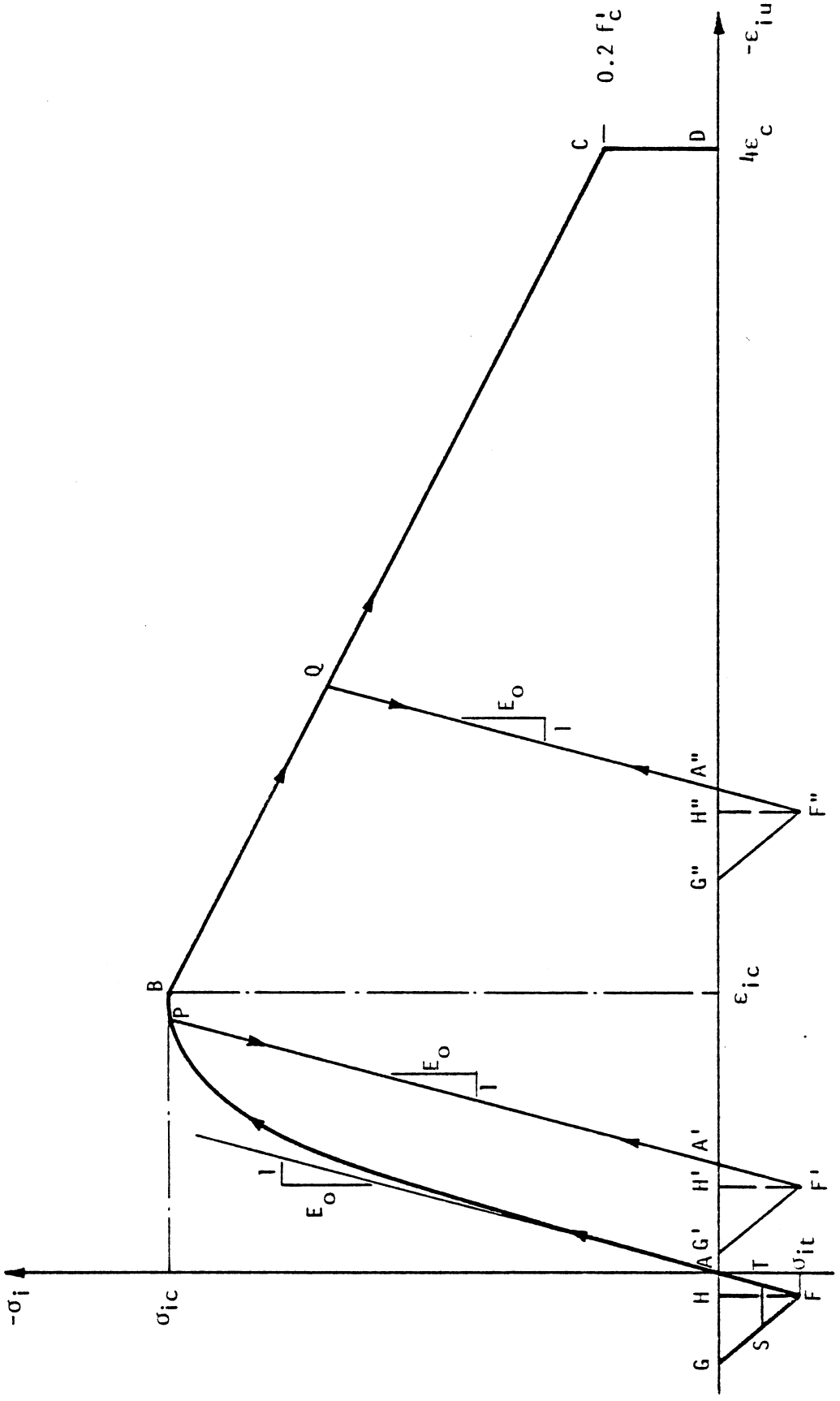

FIG. 3.11 MODEL FOR LOAD REVERSALS

2. Compressive stress reduction after yield along BCD. Unloading occurs along QA" with slope E_o similar to PA'. The strain increment determines whether unloading path QC or QA" will be followed at point Q.

3. Tensile loading up to tensile strength σ_{it} along AF. Unloading takes place along FA with slope E_o .

4. Tensile unloading after tensile strength has been exceeded occurs along FG or FH depending on which tension stiffening model is used -- see section 3.2.5. For the gradually unloading model, unloading proceeds along FG and at G the stress reduces to zero. At G reloading will follow GA and then AB. At a point S between F and G, reloading follows ST and then TAB. For the increased steel modulus model, the concrete stress drops to zero from F to H and any reloading takes place along HA and then AB.

3.2.5 Cracking and tension stiffening

The low tensile strength of concrete, which is generally only about one tenth of its compressive strength, is one of its most important properties. Concrete behaves as a linear elastic brittle material in tension, and this is a major factor causing the nonlinear behavior of reinforced concrete structures.

When a principal stress exceeds the uniaxial tensile strength of concrete, it is assumed that a crack is formed perpendicular to this principal direction. The modulus of elasticity in this principal direction is set to zero and a cracked shear constant β is introduced. If this occurs in direction 1 for example, the constitutive relationship in Eq. (2.35) reduces to:

$$\begin{Bmatrix} d\sigma_1 \\ d\sigma_2 \\ d\tau_{12} \end{Bmatrix} = \begin{bmatrix} 0 & 0 & 0 \\ 0 & \dfrac{E_2}{(1-\nu^2)} & 0 \\ 0 & 0 & \beta G' \end{bmatrix} \begin{Bmatrix} d\varepsilon_1 \\ d\varepsilon_2 \\ d\gamma_{12} \end{Bmatrix} \qquad (3.23)$$

The determination of an effective shear modulus depends on the effects of dowel action and aggregate interlock across the crack. The cracked shear constant was introduced by Lin [26] to provide a way of estimating the effective shear modulus after cracking. He has found that the solution is insensitive to the value of β $(0.0 \leqslant \beta \leqslant 1.0)$, but that numerical stability may become a problem if $\beta = 0$.

After the concrete has cracked in one direction, any additional tensile cracking is restricted to a direction orthogonal to the first crack. When cracks in both directions have occurred, the effective shear modulus is the only nonzero term left in the material matrix.

The cracking in the concrete is further complicated by the presence of the reinforcing steel. The basic mechanism is illustrated in Fig. 3.12 for a reinforced concrete element under uniaxial tension. When the concrete reaches its tensile strength, primary cracks will form. At these primary cracks the stress in the concrete drops to zero while the steel has to carry the full load. The concrete between the cracks is still capable of carrying some tensile stresses due to the bond between the concrete and the steel. This is called the tension stiffening effect. As the load increases secondary cracks will form with the result that the portion of the load carried by the concrete, and thus the average stress in the concrete, will decrease. Finally, after the smallest crack spacing has occurred, the bond between the steel and the concrete will deteriorate completely and the steel will carry all the load.

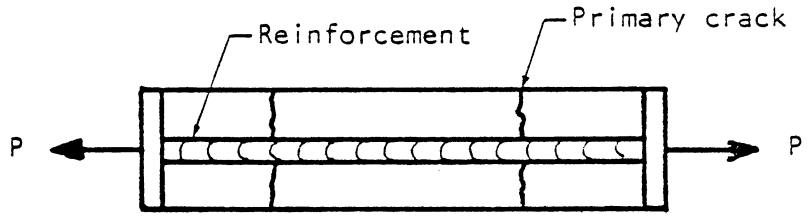

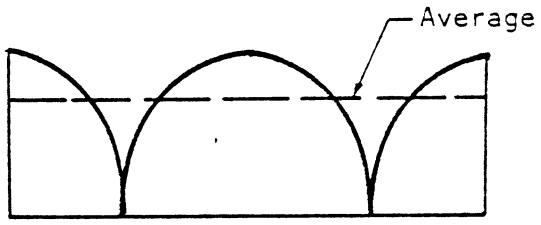

STRESS IN CONCRETE

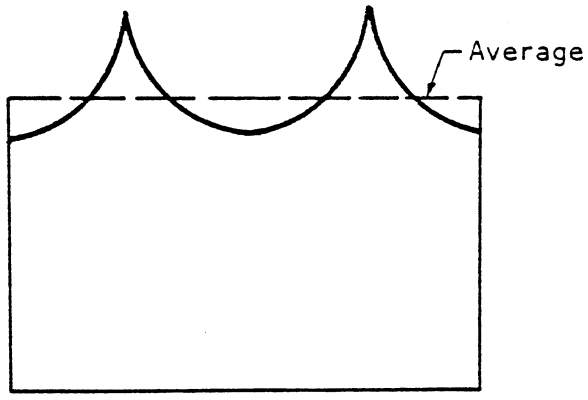

STRESS IN REINFORCEMENT

FIG. 3.12 STRESS DISTRIBUTION IN A CRACKED REINFORCED CONCRETE ELEMENT

There are basically two ways of incorporating the tension stiffening effect. The first is to assume unloading in the concrete and to attempt to estimate the remaining average tensile stress in the concrete. This has been done in different ways by Scanlon [13] and Lin [26] as shown in Fig. 3.13. The second possibility is to ignore the concrete after cracking and use an increased stiffness for the reinforcing steel. Gilbert and Warner [74] investigated both possibilities and found that modeling the tension stiffening by using an increased stiffness for the reinforcing steel was the simplest and computationally most efficient way. Among other models they used to estimate the tensile stress in the concrete, one similar to the approach of Scanlon [13] gave good results, but would be much more cumbersome to implement.

The approach by which the stiffness of the steel, after cracking of the concrete, is increased, is incorporated in this study. The stress-strain diagram of the reinforcing steel is modified as shown in Fig. 3.13c after the surrounding concrete has cracked. The additional stress in the steel accounts for the total internal tensile force carried by the concrete between cracks, but is conveniently lumped at the level of the steel and oriented in the same direction.

As an alternative the model adopted by Lin [26], but employing a linear unloading curve [28], will also be included in the present study. For this model the modulus of the concrete is assumed to be zero after cracking, but the stress-strain relationship follows the unloading branch of the curve.

It should be noted that the steel and concrete stresses obtained from Lin's model are estimates of the average stresses in the concrete and the

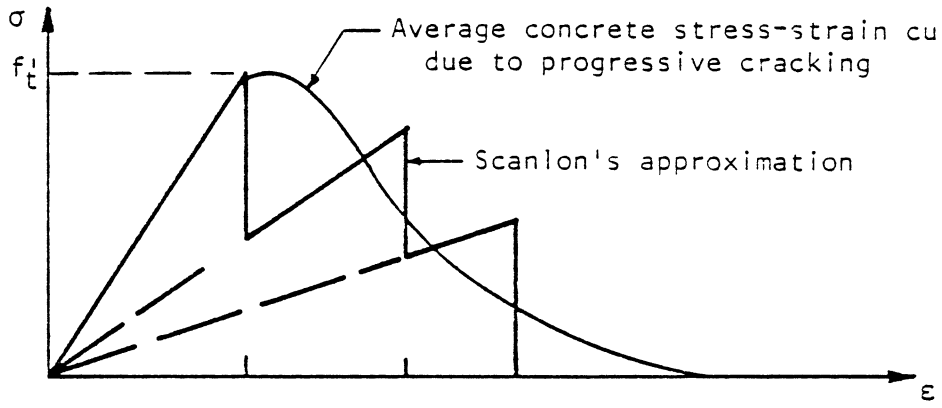

a. SCANLON'S STEPPED MODEL

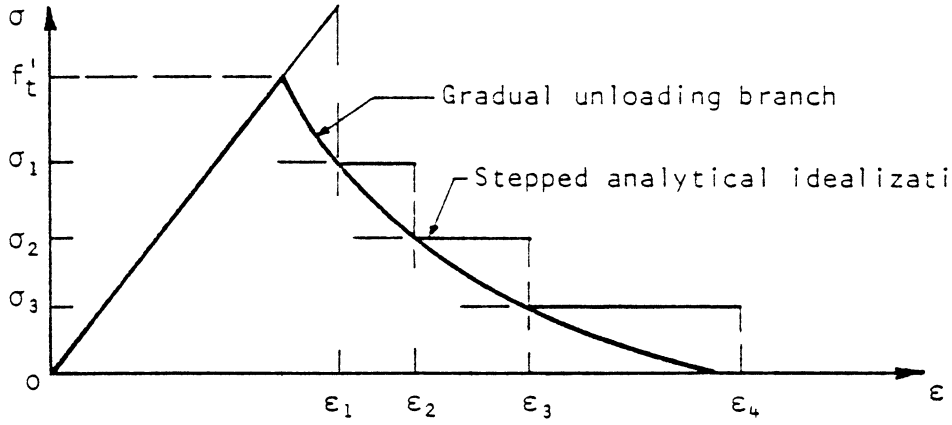

b. LIN'S GRADUALLY UNLOADING MODEL

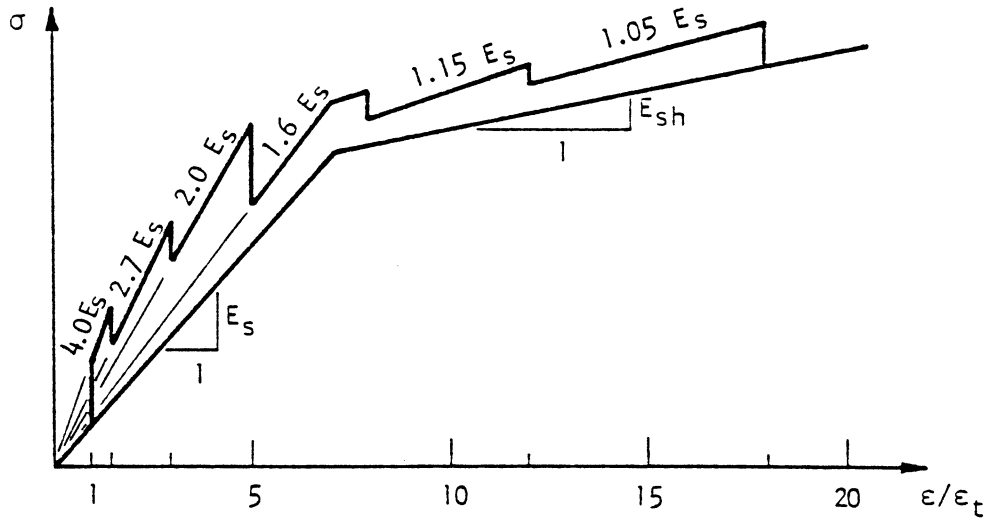

c. MODIFIED STRESS-STRAIN DIAGRAM FOR REINFORCING STEEL

FIG. 3.13 MODELS TO ACCOUNT FOR TENSION STIFFENING IN CONCRETE AFTER CRACKING

steel (Fig. 3.12). The steel stress at the actual crack is therefore always underestimated while the concrete stress is overestimated, since it should be zero. In the alternative approach of increasing the steel stiffness, the concrete and steel stresses are again estimated over an element. The steel stress should be a reasonably good estimate of the maximum steel stress at a crack while the concrete stress, which is zero at a crack, is exact.

3.2.6 Shrinkage

Shrinkage of concrete has been defined in section 3.2.1 as the volume change which occurs with time, independent of any applied loads. Shrinkage causes cracking in concrete structures which is very difficult to prevent in some cases. In order to try and predict whether cracking caused by shrinkage will occur, and how best to adapt a design to prevent it from happening, it is necessary to understand the mechanism of shrinkage and the factors influencing it.

Shrinkage is ascribed to two main factors: Loss of water on drying and volume changes due to carbonation. Carbonation shrinkage is caused by a chemical reaction between calcium hydroxide, a hydrated cement mineral, and atmospheric carbon dioxide in the presence of water to form calcium carbonate. This part of shrinkage is generally not separated from drying shrinkage and most experimental data on drying shrinkage includes this effect.

Drying shrinkage occurs due to the loss of water from the concrete to the surrounding unsaturated air. The free water held in the capillaries is lost first -- this causes practically no shrinkage. During further drying, shrinkage starts with the loss of absorbed water. The process of

moisture diffusion from the interior of the concrete to the surface is very slow and complex. The surface dries more rapidly than the interior and this causes nonuniform distribution of shrinkage through the volume of the specimen, termed differential shrinkage. In general, however, uniform shrinkage is considered to be an adequate approximation for the purpose of most analysis and design problems concerning panels, slabs and shells.

The factors which influence shrinkage are generally taken to be the water-cement ratio, the relative humidity, size of the member and aggregate content. Shrinkage increases with the increase in water-cement ratio, while it decreases for any increase in the ambient relative humidity, the size of the member and the aggregate content.

The shrinkage strain at any time t can be found from experimental curves when they are available or from the recommendations by ACI Committee 209 [71] based on studies by Branson et al. [75].

ACI Committee 209 recommends the use of the following formula for the calculation of the shrinkage strain at any time t :

$$\varepsilon_{sh}(t) = K_s K_h K_H \frac{(t - t_o)^e}{f + (t - t_o)^e} \varepsilon_{shu} \tag{3.25}$$

where

$\varepsilon_{sh}(t)$ = shrinkage strain at time t

ε_{shu} = ultimate shrinkage strain as determined for local conditions

t_o = time from which shrinkage starts

f,e = constants, determined from experiments

K_s = correction factor for slump of the concrete mix

K_h = correction factor for the size of the concrete member

K_H = correction factor for relative humitity

The ranges for e, f and ε_{shu} for normal or lightweight concrete and for moist or steam curing have been found to be:

$$e = 0.9 \text{ to } 1.10$$

$$f = 20 \text{ to } 130$$

$$\varepsilon_{shu} = 415 \times 10^{-6} \text{ to } 1070 \times 10^{-6} \text{ in/in}$$

The following standard equations for predicting shrinkage strain are recommended by ACI Committee 209 [71]:

For concrete moist cured for 7 days:

$$\varepsilon_{sh}(t) = K_s K_h K_H \frac{(t-7)}{35 + (t-7)} 800 \times 10^{-6} \qquad (3.26)$$

For concrete steam cured for 3 days:

$$\varepsilon_{sh}(t) = K_s K_h K_H \frac{(t-3)}{55 + (t-3)} 730 \times 10^{-6} \qquad (3.27)$$

The correction factors are provided to take into account any variation in field conditions that may exist for different cases and are also shown graphically in Fig. 3.14.

Slump correction factor K_s :

$$K_s = 0.89 + 0.041s \qquad (3.28)$$

where

s = slump in inches.

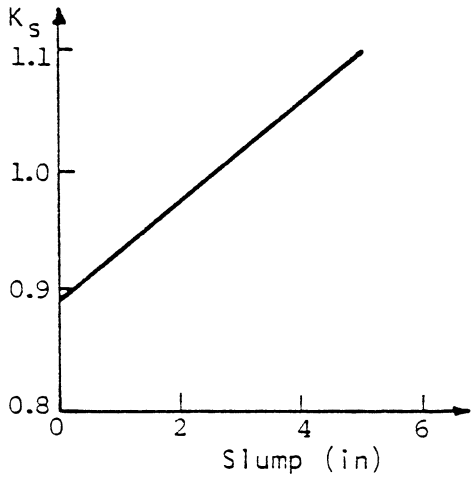

a. SLUMP CORRECTION

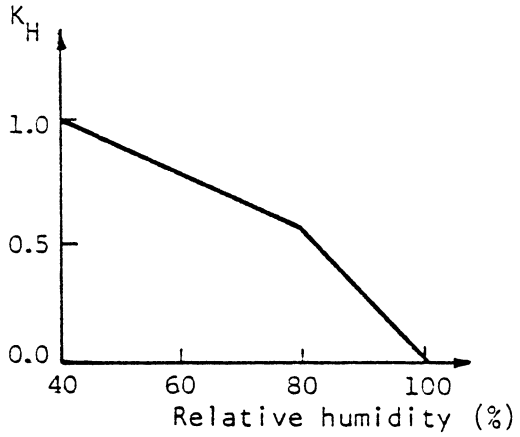

b. HUMIDITY CORRECTION

c. THICKNESS CORRECTION

FIG. 3.14 SHRINKAGE CORRECTION FACTORS

Size correction factor K_h :

The curve as shown in Fig. 3.14.b.

Humidity correction factor K_H :

$$K_H = 1.4 - 0.01\,H \qquad 40 \leq H \leq 80$$
$$K_H = 3.0 - 0.03\,H \qquad 80 \leq H \leq 100 \tag{3.29}$$

where

H = percent relative ambient humidity

ACI Committee 209 [71] also gives values for correction factors for cement content, percent fines by weight and air content, but indicates that they can normally be neglected since they tend to offset each other.

3.2.7 Creep

Creep of concrete has been defined in section 3.2.1 as the deformation in excess of the true instantaneous elastic deformation at any time t after loading. Creep affects the serviceability of reinforced concrete structures and is one of the major causes of prestress loss in prestressed concrete. A thorough understanding of the phenomenon of creep, leading to an ability to model it analytically is essential in order to be able to investigate the behavior of these structures over their expected design life.

Several theories have been proposed to explain the mechanism of creep, but no theory has been able to explain all the observed behavior regarding creep of concrete. These theories can be broadly classified as: mechanical deformation theory [76], plastic theories [77], viscous flow theories [78] and a theory based on the seepage of gel water [79].

A great number of factors influence the creep of concrete. The most important factors have been identified as [80]: Creep deformation is inversely proportional to concrete strength, the age of the concrete at loading, the volume and modulus of elasticity of the aggregate, the relative ambient humidity and the thickness of the specimen. For a temperature range between 0°F and 180°F creep deformation is directly proportional to the temperature. Creep deformation is also directly proportional to the imposed stress -- the relationship is linear up to a level of approximately 0.35 f'_c, above this it is nonlinear. (See Fig. 3.15.) Finally, the deformation due to creep is directly proportional to the duration of the applied stress in an asymptotic manner; initially deformation increases rapidly, but then tends towards an asymptotic value.

The quantititative determination of these factors is a statistical problem as the experimental results are inherently random variables with a coefficient of variation of the order of 15 to 20 percent at best [71]. Up to the present time, however, the solutions found in the creep literature are all deterministic in nature. Moreover, they only try to establish correlations between the analytical models and laboratory specimens. The correspondence between laboratory and field conditions are not yet well established. These would put limitations on the accuracy of the quantitative measures of the factors affecting creep of concrete, and this should be kept in mind whenever some values are given to creep coefficients.

a) Analytical methods

Any realistic analytical method should take the above mentioned effects into account. An additional important factor for the implementation of any method is the storage of the stress history. Efforts have thus been directed towards finding a method which

minimizes the number of variables which contains the stress and creep history, but still gives good agreement with experimental results.

The different analytical models for the representation of creep can be divided into approximate methods, a differential formulation and an integral formulation. Approximate methods like the effective modulus and rate of creep methods have been developed as simplified design tools and do not take the stress history and aging into account. The differential formulation has been used [125], but difficulties associated with the experimental determination of coefficients and numerical problems with implementation, has restricted its use. The integral formulation has thus far been the most promising, and an efficient model has been developed by Kabir [28] based on the work of Zienkiewicz and Watson [81]. More complete reviews of the various analytical models that have been proposed are given by Kabir [28] and Kang [37].

The model developed by Kabir [28] will also be used in the present study and will be presented in section 3.2.7.d. The basic development of the integral formulation will be presented below.

For a linear visco-elastic, aging material under uniaxial stress the constitutive relationship is given by Volterra [82] as:

$$\varepsilon(t) = \int_{-\infty}^{t} \bar{C}(\tau, t-\tau) \frac{\partial \sigma(\tau)}{\partial \tau} d\tau \qquad (3.30)$$

where

$\varepsilon(t)$ = strain at time t

$\bar{C}(\tau, t-\tau)$ = specific compliance at time t

τ = time of initial application of load

The solution of Eq. (3.30) depends on the form of the kernel function $\bar{C}(\tau,t-\tau)$ which is generally known as the specific compliance function. This can generally be written as:

$$\bar{C}(\tau,t-\tau) = \frac{1}{E(\tau)} + C(\tau,t-\tau) \tag{3.31}$$

where

$\frac{1}{E(\tau)}$ = instantaneous compliance function

$C(\tau,t-\tau)$ = creep compliance function

This results in the following equation for the creep strain:

$$\varepsilon^c(t) = \int_0^t C(\tau,t-\tau)\,\frac{\partial\sigma(\tau)}{\partial\tau}\,d\tau \tag{3.32}$$

The key to the solution of Eq. (3.32) is the form of the creep compliance function. The criteria which are generally used to select an expression for the creep compliance function are: The function should fit the experimental compliance surface accurately, taking into account the factors influencing creep mentioned above. The unknown coefficients of the function should be easy to evaluate. The function should also be of such a form that the numerical evaluation of Eq. (3.32) does not require excessive computational effort.

A number of different creep compliance functions proposed by various researchers are given by Kabir [28]. The function used by Kabir is in the form of a Dirichlet series as follows:

$$C(\tau,t-\tau,T) = \sum_{i=1}^{m} \alpha_i(\tau)\left[1 - e^{-\lambda_i\phi(T)(t-\tau)}\right] \tag{3.33}$$

where $\alpha_i(\tau)$ = scale factor depending on loading age τ

λ_i = constants determining the shape of the logarithmically decaying creep curve

$\phi(T)$ = temperature shift function

T = temperature

The method of Kabir is similar to one proposed by Bazant and Wu [83] in which the stress history is also contained in a set of variables they called the hidden state variables $\underset{\sim}{A}_{in}$. The way in which these hidden state variables are calculated will be shown in section 3.3.7.d.

The advantages of Kabir's method are the following: It takes into account three very important factors influencing creep -- age at loading, duration of loading and temperature variations. Since the stress history is stored in the hidden state variables, it is computationally very efficient, requiring a minimum of computer storage. When experimental data are available, accurate creep parameters can be readily determined. On the other hand, the use of the ACI Committee 209 recommendations [71] makes it possible to carry out a creep analysis for cases where experimental data are not available, by making realistic assumptions about expected field conditions.

b) Creep under biaxial stress

Experimentally it has been ascertained that lateral creep strains occur in uniaxial creep tests. The ratio of lateral creep strain to the creep strain in the direction of the applied stress is called the creep Poisson's ratio, analogous to the elastic case. Recent experimental studies have shown the creep Poisson's ratio to have a range of values from 0.16 to 0.25 and thus being very close to the elastic one in value.

Gopalakrishnan et al. [84] have found that the creep Poisson's ratio under a multiaxial stress state is a function of the relative magnitudes of the principal stresses and that it is also less than the uniaxial one. As was done by Kabir [28] it will be assumed that the creep Poisson's ratio is the same as the elastic Poisson's ratio, also under states of biaxial stress. The relationship between the creep strain and a stress increment can therefore be written as:

$$\begin{Bmatrix} \Delta\varepsilon_x^c(t) \\ \Delta\varepsilon_y^c(t) \\ \Delta\gamma_{xy}^c(t) \end{Bmatrix} = \begin{bmatrix} 1 & -\nu_c & 0 \\ -\nu_c & 1 & 0 \\ 0 & 0 & 2(1+\nu_c) \end{bmatrix} C(\tau, t-\tau, T) \begin{Bmatrix} \Delta\sigma_x(t) \\ \Delta\sigma_y(t) \\ \Delta\tau_{xy}(t) \end{Bmatrix} \qquad (3.34)$$

The total creep strain vector from the initial age of loading t_1 to observation time t_n will then be given by:

$$\begin{Bmatrix} \varepsilon_x^c(t_n) \\ \varepsilon_y^c(t_n) \\ \gamma_{xy}^c(t_n) \end{Bmatrix} = \underline{D}_o^{-1} \sum_{i=1}^{n} C\left(t_i, t_n - t_i, T_i\right) \begin{Bmatrix} \Delta\sigma_x(t_i) \\ \Delta\sigma_y(t_i) \\ \Delta\tau_{xy}(t_i) \end{Bmatrix} \qquad (3.35)$$

where

$$\underline{D}_o^{-1} = \begin{bmatrix} 1 & -\nu_c & 0 \\ -\nu_c & 1 & 0 \\ 0 & 0 & 2(1+\nu_c) \end{bmatrix}$$

c) Creep under high stress levels:

From experimental studies it has been established that creep is linearly proportional to stress up to a level of 0.35 f_c'. Beyond this

stress level a deviation from linearity is observed as shown in Fig. 3.15. To account for this nonlinear effect Becker and Bresler [85] suggested the use of an effective stress to calculate the creep strains as follows:

$$\sigma_{eff} = \sigma \quad \text{for} \quad \sigma/f'_c \leq 0.35$$
$$\sigma_{eff} = 2.33\,\sigma - 0.465\,f'_c \quad \text{for} \quad 0.35 \leq \sigma/f'_c \leq 1.0 \tag{3.36}$$

This is an empirical equation based on experimental data, particularly that of Roll [86].

Experimentally it has also been established [86] that the relationship between creep recovery after removal of the loading and the stress level is linear as shown in Fig. 3.16. This indicates that when the creep recovery is calculated, the actual stress, rather than the effective stress, should be used.

d) Analytical model for creep of concrete to be used in this study

The model proposed by Kabir [28] will be used and the following description is generally taken from his work [28].

An incremental method is chosen for the creep strain calculation which will facilitate a step-by-step solution in the time domain. A number of assumptions have to be made in order to develop the creep model. These assumptions are:

1. Each component of strain is composed of strains produced by different effects. These effects are broadly classified into two groups - stress originated and nonstress originated. The stress originated strain is known as compliance; instantaneous and creep strains are examples of compliance. Thermal and shrinkage strains are examples of nonstress originated strains. The consequence of this assumption is that the different

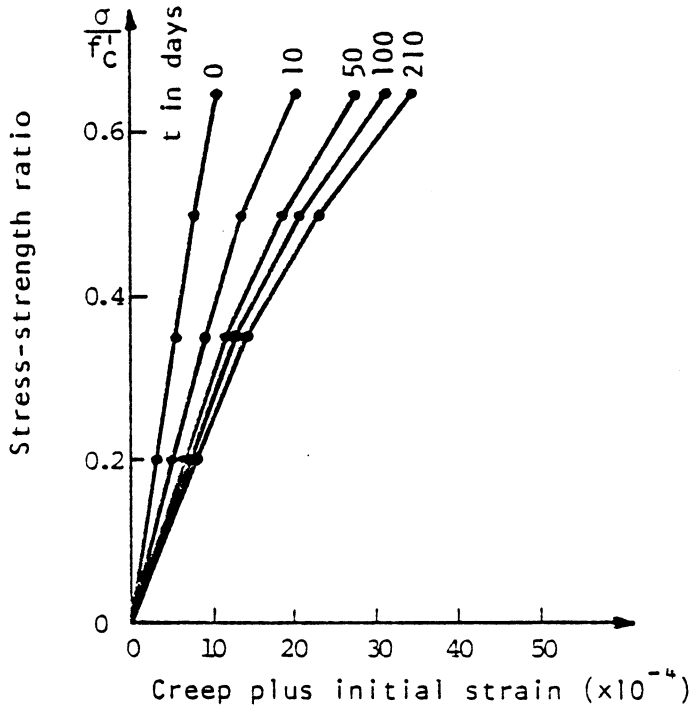

FIG. 3.15 EFFECT OF STRESS-STRENGTH RATIO ON CREEP AT HIGH STRESSES

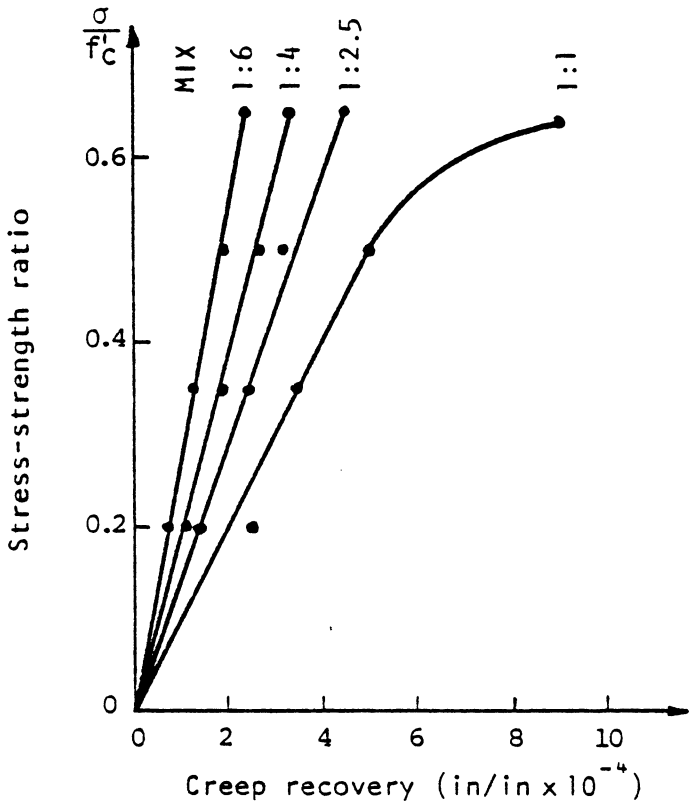

FIG. 3.16 STRESS-LEVEL VS. TOTAL TIME-DEPENDENT RECOVERY WITH MIX AS A PARAMETER

strain components can be calculated separately and added together. This makes the whole computational process easier.

2. The principle of superposition is assumed to be valid for creep strains. This principle asserts that the strain at a given time is the sum of the strains caused by the loads applied immediately for their respective durations of time. The assumption implicit in this principle is that there is no coupling between the single response behavior from individual load input.

3. The time-dependent response for uncracked concrete is the same in tension and in compression.

4. Concrete is assumed to be a thermorheologically simple material [87]. Such a material is defined as one which obeys the time-shift principle for the temperature variation as illustrated in Fig. 3.17. Let T_o be the fixed reference temperature and T a constant temperature such that $T > T_o$. The specific creep vs. logarithmic time curves at temperatures T_o and T are identical in shape, but a distance $\psi(T)$ apart horizontally. This relationship can be written as:

$$c_T(\ln t) = c_{T_o}(\ln t + \psi(T)) \tag{3.37}$$

where c_T, c_{T_o} are the specific creep curves for temperatures T and T_o respectively.

Since both sides of the equation represent the same curve, taking the exponential of the arguments on both sides yields:

$$c_T(t) = c_{T_o}\left(t\, e^{\psi(T)}\right) = c_{T_o}\left(t\, \phi(T)\right) \tag{3.38}$$

where

$\phi(T) = e^{\psi(T)}$ is called the temperature shift function

The specific creep for any temperature T is then obtained by replacing the time t by $t\phi(T)$ in the specific creep curve for the reference temperature T_o. The validity of this time-shift principle for concrete was demonstrated by Mukaddam and Bresler [87] using temperature dependent creep data from various investigators.

These assumptions are implicit in Eq. (3.35) which may now be rewritten as:

$$\underline{D}_o\varepsilon_n^c = \Delta\sigma_1\, C\left(t_1, t_n - t_1, T_1\right) + \Delta\sigma_2\, C\left(t_2, t_n - t_2, T_2\right) + \ldots + \ldots + \Delta\sigma_{n-1}\, C\left(t_{n-1}, t_n - t_{n-1}, T_{n-1}\right) \tag{3.39}$$

where

$$\varepsilon_n^c = \langle \varepsilon_x^c(t_n)\ \varepsilon_y^c(t_n)\ \gamma_{xy}^c(t_n) \rangle^T$$

$$\Delta\sigma_i = \langle \Delta\sigma_x(t_i)\ \Delta\sigma_y(t_i)\ \Delta\sigma_{xy}(t_i) \rangle^T$$

and

t_1 = age at initial loading

t_n = final observation time

T_i = temperature at age t_i

Similarly for time t_{n+1}, the following may be written:

$$D_o\varepsilon_{n+1}^c = \Delta\sigma_1\, C\left(t_1, t_{n+1} - t_1, T_1\right) + \Delta\sigma_2\left(t_2, t_{n+1} - t_2, T_2\right) + \ldots + \Delta\sigma_n\, C\left(t_n, t_{n+1} - t_n, T_n\right) \tag{3.40}$$

The increment in the creep strain for the time step $\Delta t_n = t_{n+1} - t_n$ can then be expressed as:

$$\Delta\varepsilon_n^c = \varepsilon_{n+1}^c - \varepsilon_n^c \tag{3.41}$$

Equation (3.41) is graphically represented in Fig. 3.18. It is clear from this figure that one assumption inherent in the summation

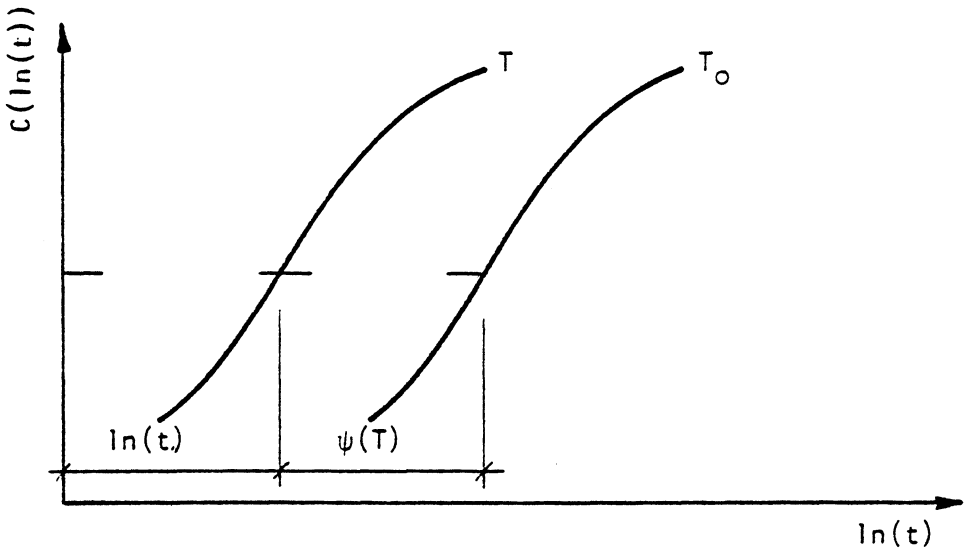

FIG. 3.17 SPECIFIC CREEP CURVES

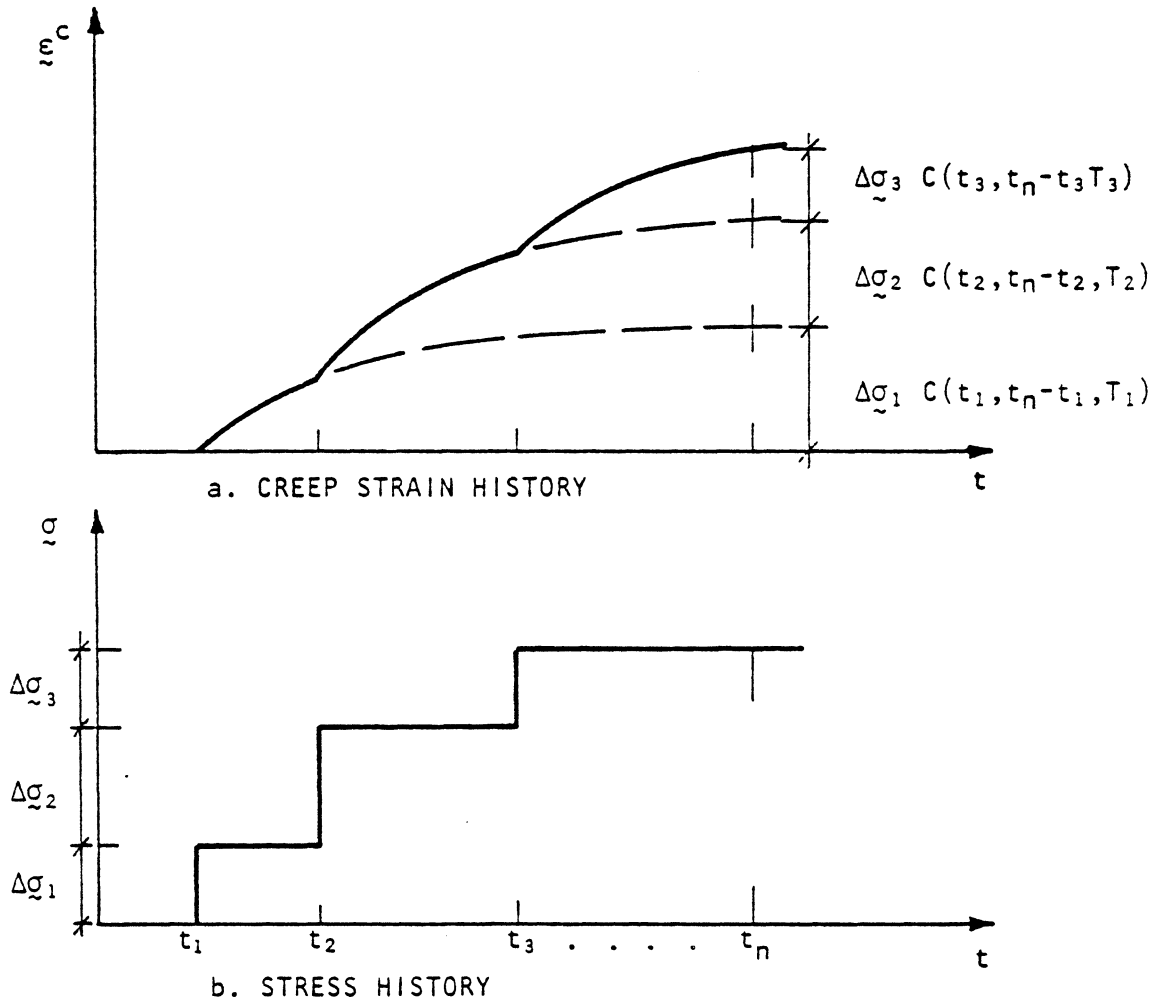

FIG. 3.18 SUPERPOSITION OF CREEP STRAINS

expression is that stress changes occur in steps and no stress change occurs during a time step. This is obviously not true, but in most load cases, if the time step sizes are chosen properly, the constant-step stresses will represent the load history quite accurately.

It is also evident from Eqs. (3.39) and (3.40) that the calculation of creep increment during time step Δt_n in going from t_n to t_{n+1} necessitates knowledge of all previous stress increments $\Delta\underset{\sim}{\sigma}_1$, $\Delta\underset{\sim}{\sigma}_2$, $\Delta\underset{\sim}{\sigma}_3 \ldots \Delta\underset{\sim}{\sigma}_{n-1}$ as well as the most current stress increment, $\Delta\underset{\sim}{\sigma}_n$. This requires a large storage capacity for even a moderately complex structural system and in fact the storage requirement, apart from being extremely large, may also become very unwieldy.

It has been found [81,85,88] that certain types of mathematical approximations for the creep compliance function, $C(\tau,t-\tau,T)$, while representing the experimental data accurately, overcome the necessity of storing all the stress increments of the previous time steps. A similar function in the form of a Dirichlet series is proposed in the present study for the creep compliance function:

$$C(\tau,t-\tau,T) = \sum_{i=1}^{m} \alpha_i(\tau) \left[1 - e^{-\lambda_i \phi(T)(t-\tau)}\right] \qquad (3.42)$$

where

$\alpha_i(\tau)$ = scale factor dependent on age at loading τ

λ_i = exponential constants determining the shape of the logarithmically decaying creep curve

$\phi(T)$ = shift function dependent on temperature T

Substituting the value of $C(\ )$ from Eq. (3.42) into Eq. (3.39), yields:

$$
\begin{aligned}
\underline{D}_0\hat{\varepsilon}^c_n = {} & \Delta\hat{\sigma}_1 \sum_{i=1}^{m} \alpha_i(t_1)\left[1 - e^{-\lambda_i\phi(T_1)(t_n-t_1)}\right] \\
& + \Delta\hat{\sigma}_2 \sum_{i=1}^{m} \alpha_i(t_2)\left[1 - e^{-\lambda_i\phi(T_2)(t_n-t_2)}\right] \\
& +\ldots \\
& + \Delta\hat{\sigma}_{n-1} \sum_{i=1}^{m} \alpha_i(t_{n-1})\left[1 - e^{-\lambda_i\phi(T_{n-1})(t_n-t_{n-1})}\right]
\end{aligned}
\tag{3.43}
$$

Equation (3.43) may be rearranged as:

$$
\begin{aligned}
\underline{D}_0\hat{\varepsilon}^c_n = {} & \Delta\hat{\sigma}_1 \sum_{i=1}^{m} \alpha_{i1}\left[1 - e^{-\lambda_i\phi_1\Delta t_1 - \lambda_i\phi_2 t_2 \ldots - \lambda_i\phi_{n-1}\Delta t_{n-1}}\right] \\
& + \Delta\hat{\sigma}_2 \sum_{i=1}^{m} \alpha_{i2}\left[1 - e^{-\lambda_i\phi_2\Delta t_2 \ldots - \lambda_i\phi_{n-1}\Delta t_{n-1}}\right] \\
& +\ldots \\
& + \Delta\hat{\sigma}_{n-1} \sum_{i=1}^{m} \alpha_{in-1}\left[1 - e^{-\lambda_i\phi_{n-1}\Delta t_{n-1}}\right]
\end{aligned}
\tag{3.44}
$$

where

$$\alpha_{ii} = \alpha_i(t_i)$$

$$\phi_i = \phi(T_i)$$

$$\Delta t_i = t_{i+1} - t_i$$

Similarly, Eq. (3.40) may be written as:

$$
\begin{aligned}
\underline{D}_0\hat{\varepsilon}^c_{n+1} = {} & \Delta\hat{\sigma}_1 \sum_{i=1}^{m} \alpha_{i1}\left[1 - e^{-\lambda_i\phi_1\Delta t_1 - \lambda_i\phi_2\Delta t_2 \ldots - \lambda_i\phi_n\Delta t_n}\right] \\
& + \Delta\hat{\sigma}_2 \sum_{i=1}^{m} \alpha_{i2}\left[1 - e^{-\lambda_i\phi_2\Delta t_2 - \lambda_i\phi_3\Delta t_3 \ldots - \lambda_i\phi_n\Delta t_n}\right] \\
& +\ldots \\
& + \Delta\hat{\sigma}_n \sum_{i=1}^{m} \alpha_{in}\left[1 - e^{-\lambda_i\phi_n\Delta t_n}\right]
\end{aligned}
\tag{3.45}
$$

Substituting values from Eqs. (3.44) and (3.45) into Eq. (3.41), the following is obtained:

$$\begin{aligned}
\underline{D}_o \Delta \underset{\wedge}{\varepsilon}^c_n &= \underline{D}_o \underset{\wedge}{\varepsilon}^c_{n+1} - \underline{D}_o \underset{\wedge}{\varepsilon}^c_n \\
&= \Delta \underset{\wedge}{\sigma}_1 \sum_{i=1}^{m} \alpha_{i1} e^{-\lambda_i \phi_1 \Delta t_1 \ldots -\lambda_i \phi_{n-1} \Delta t_{n-1}} \left[1 - e^{-\lambda_i \phi_n \Delta t_n}\right] \\
&\quad + \Delta \underset{\wedge}{\sigma}_2 \sum_{i=1}^{m} \alpha_{i2} e^{-\lambda_i \phi_2 \Delta t_2 \ldots -\lambda_i \phi_{n-1} \Delta t_{n-1}} \left[1 - e^{-\lambda_i \phi_n \Delta t_n}\right] \\
&\quad + \ldots \\
&\quad + \Delta \underset{\wedge}{\sigma}_{n-1} \sum_{i=1}^{m} \alpha_{in-1} e^{-\lambda_i \phi_{n-1} \Delta t_{n-1}} \left[1 - e^{-\lambda_i \phi_n \Delta t_n}\right] \\
&\quad + \Delta \underset{\wedge}{\sigma}_n \sum_{i=1}^{m} \alpha_{in} \left[1 - e^{-\lambda_i \phi_n \Delta t_n}\right]
\end{aligned} \tag{3.46}$$

or,

$$\underline{D}_o \Delta \underset{\wedge}{\varepsilon}^c_n = \sum_{i=1}^{m} \underset{\wedge}{A}_{in} \left[1 - e^{-\lambda_i \phi_n \Delta t_n}\right] \tag{3.47}$$

where

$$\underset{\wedge}{A}_{in} = \underset{\wedge}{A}_{in-1} e^{-\lambda_i \phi_{n-1} \Delta t_{n-1}} + \Delta \underset{\wedge}{\sigma}_n \alpha_{in} \tag{3.48}$$

$$\underset{\wedge}{A}_{i1} = \Delta \underset{\wedge}{\sigma}_1 \alpha_{i1} \tag{3.49}$$

Therefore the relationships necessary for calculating an increment of creep strain for any time step Δt_n, in going from t_n to t_{n+1}, are:

$$\underline{D}_o \Delta \underset{\wedge}{\varepsilon}^c_n = \sum_{i=1}^{m} \underset{\wedge}{A}_{in} \left[1 - e^{-\lambda_i \phi_n \Delta t_n}\right] \tag{3.50a}$$

$$\underset{\wedge}{A}_{in} = \underset{\wedge}{A}_{in-1} e^{-\lambda_i \phi_{n-1} \Delta t_{n-1}} + \Delta \underset{\wedge}{\sigma}_n \alpha_{in} \tag{3.50b}$$

$$\underset{\sim}{A}_{i1} = \Delta\underset{\sim}{\sigma}_1 \alpha_{i1} \tag{3.50c}$$

The above Eqs. (3.50) does not require the storage of all previous stress histories in order to calculate the creep strain increment as is necessary in the case of Eq. (3.41). Rather, the stress history is stored in the vector $\underset{\sim}{A}_{in}$, also called the hidden state variables [83], which can be calculated as a progressive sum by the use of Eq. (3.50) knowing the stress change $\Delta\underset{\sim}{\sigma}_n$ at the current time t_n. This formulation reduces the computation and storage time considerably, making time-dependent analysis of reasonably large structural problems possible.

e) Determination of creep compliance coefficients

The key to the formulation of creep strain computation algorithm in the previous sub-section is the assumption of a creep compliance function according to Eq. (3.42) as follows:

$$C(\tau, t-\tau, T) = \sum_{i=1}^{m} \alpha_i(\tau) \left[1 - e^{-\lambda_i \phi(T)(t-\tau)}\right]$$

Before proceeding with the creep analysis of any particular concrete structure, four sets of quantities have to be evaluated -- (1) m, (2) $\alpha_i(\tau)$, (3) λ_i and (4) $\phi(T)$. Two methods may be used to calculate the above quantities. For the first method experimental creep data of the concrete must be available while the second method is based on the recommendations of ACI Committee 209 [71] as developed by Branson [75].

1. Experimental creep data analysis:

In this method creep data are obtained for some particular concrete. $C(\tau, t-\tau, T)$ values must be available for different τ and T

for a range of $t-\tau$. Then, the following procedure is followed:

(i) m and λ_i, $i = 1,m$ are chosen on a trial basis.

(ii) A particular age τ_o and temperature T_o are chosen.

(iii) Various times $t_j, j=1,2,\ldots,n$ are chosen such that $t_j \geq \tau_o$.

(iv) Values of $C(\tau_o, t_j-\tau_o, T_o)$ are found at $j = 1,2,\ldots,n$ points.

(v) Then, the simultaneous equations are set up:

$$\begin{bmatrix} 1-e^{-\lambda_1(t_1-\tau_o)} & 1-e^{-\lambda_2(t_1-\tau_o)} & \ldots & 1-e^{-\lambda_m(t_1-\tau_o)} \\ & & & \\ 1-e^{-\lambda_1(t_n-\tau_o)} & 1-e^{-\lambda_2(t_n-\tau_o)} & \ldots & 1-e^{-\lambda_m(t_n-\tau_o)} \end{bmatrix}_{nxm} \begin{Bmatrix} \alpha_1(\tau_o) \\ \alpha_2(\tau_o) \\ \vdots \\ \alpha_m(\tau_o) \end{Bmatrix}_{mx1} = \begin{Bmatrix} C(\tau_o, t_1-\tau_o, T_o) \\ C(\tau_o, t_2-\tau_o, T_o) \\ \vdots \\ C(\tau_o, t_n-\tau_o, T_o) \end{Bmatrix}_{nx1} \tag{3.51}$$

or

$$\underline{A}_{nxm}\, \underset{\sim}{a}_{mx1} = \underset{\sim}{B}_{nx1} \quad n>m \tag{3.52}$$

The least squares method is applied to solve the overdeterminate system of equations of Eq. (3.52) to give the values of $\underset{\sim}{a}$:

$$\underline{A}^T_{mxn}\, \underline{A}_{nxm}\, \underset{\sim}{a}_{mx1} = \underline{A}^T_{mxn}\, \underset{\sim}{B}_{nx1} \tag{3.53}$$

or

$$(\underline{A}^T\underline{A})_{mxm}\, \underset{\sim}{a}_{mx1} = (\underline{A}^T\underset{\sim}{B})_{mx1}$$

or

$$\underset{\sim}{a}_{mx1} = (\underline{A}^T\underline{A})^{-1}_{mxm}\, (\underline{A}^T\underset{\sim}{B})_{mx1} \tag{3.54}$$

(vi) Choose a different m and/or λ_i and go through steps (ii)-(v).

(vii) Optimum m's and λ's are chosen based on the following criteria:

a. least squares errors are minimized.

b. $\alpha_i(\tau)$ for which the ultimate creep strain is about 4/3 of the 1-year creep strain.

c. the contributions of all $\alpha_i(1 - e^{-\lambda_i(t-\tau)})$ terms are nearly equal.

(viii) Now choose a different age τ_1 and go through steps (iii) - (v) to determine a new set of $\alpha_i(\tau_1)$. This is continued to give sets of $\alpha_i(\tau)$ for different ages. The in-between ages can be determined by linear interpolation.

(ix) The temperature shift function $\phi(T)$ can be obtained by constructing specific creep vs. logarithmic time creep curves for different temperatures as shown in Fig. 3.17. The function $\psi(T)$ $(\phi(T) = e^{\psi(T)})$ can then be approximated by a polynomial expression. (A polynomial function of order four can be used in the computer program.)

2. ACI Committee 209 [71] recommendations:

ACI Committee 209 [71] has proposed the following expression for the prediction of creep deformation:

$$C_t = K_s K_H K_h K_\tau \frac{(t-\tau)^{0.60}}{10 + (t-\tau)^{0.60}} C_u \qquad (3.55)$$

where,

C_t = creep coefficient = $\frac{\text{creep strain at any time, t}}{\text{initial instantaneous strain}}$

C_u = ultimate creep coefficient to be determined from experimental data

= $\frac{\text{creep strain at infinite time after loading}}{\text{initial strain at time of loading}}$

= 2.35 for standard conditions

K_s = slump correction factor

= 0.81 + 0.07 s

K_H = humidity correction factor

= 1.27 - 0.0067 H, $H \geqslant 40$

H = relative humidity

K_h = size correction factor

= 1.0 - 0.0167 (sz - 6.0), $sz > 6.0$

= 1.0, $sz \leqslant 6.0$

K_τ = age at loading correction factor

= $1.25\ \tau^{-0.118}$ for moist cured concrete for 7 days

s = slump in inches

sz = minimum size of member in inches

t = observation time in days

τ = age at loading in days

Standard Conditions for Creep:

(1) slump = 2.7 inches

(2) ambient relative humidity = 40% or less

(3) minimum thickness = 6 inches or less

(4) loading age = 7 days for moist cured concrete

For the standard conditions, all the correction factors are 1.0.

Using Eq. (3.55) for standard conditions, creep data are generated for 15 loading ages -- 7, 10, 14, 21, 28, 40, 60, 80, 91, 100, 120, 180, 270, 365, 400 days. Using $\lambda_1 = 0.1$, $\lambda_2 = 0.01$ and $\lambda_3 = 0.001$, the coefficients α_i of the Eq. (3.42)

$$C(\tau,t-\tau) = \sum_{i=1}^{3} \alpha_i(\tau) \left[1 - e^{-\lambda_i(t-\tau)}\right]$$

are determined by the least squares method as described for the first method. These α_i's are stored as data in the computer subroutine. Values of α_i for any age at loading in between these loading ages are obtained by linear interpolation in the computer program.

The following are values of the coefficients $\alpha_i(\tau_o)$ obtained by the least squares method for standard conditions and $\tau_o = 28$ days, $f'_c = 4000$ psi and $T_o = 68°F$:

$$\alpha_1 = 2.02565 \times 10^{-7}$$

$$\alpha_2 = 1.85702 \times 10^{-7}$$

$$\alpha_3 = 1.37290 \times 10^{-7}$$

For other loading ages and conditions that differ from standard the $\alpha_i(\tau)$ can be modified by multiplication with the correction factors of Eq. (3.55). These α_i values are then used in Eq. (3.42) to calculate the creep compliance.

The temperature shift function $\phi(T)$ can be obtained by plotting specific creep vs. logarithmic time curves for different temperatures as

shown in Fig. 3.17. Then the function $\psi(T)$ can be approximated by a polynomial.

To show the validity of his model Kabir [28] compared creep curves calculated with his model to those obtained experimentally. The curves generated by fitting the experimental data (method one) give excellent results -- the maximum discrepancy is less than 2%. The curves generated by using the ACI Committee 209 Recommendations [71] give a satisfactory correlation with a discrepancy of less than 5%. In another example Kabir compared curves obtained from his model with experimental and theoretical curves of Selna [90] for a concrete prism subjected to different stress histories. Kabir's model shows satisfactory correspondence with the experimental results and compares favorably with the other theoretical methods as regards both accuracy and computational effort.

3.2.8 Deformation caused by temperature changes

Concrete structures are subjected to temperature changes during their service lifetime due to changes in environmental conditions and also artificial heating or cooling. Substantial stresses can be induced by temperature changes in statically indeterminate structures. This can cause damage to such structures and impair their serviceability. It would therefore be desirable to incorporate temperature effects in the analysis of these structures.

Uniaxial temperature strain ε_T may be expressed as follows:

$$\varepsilon_T = \int_{T_0}^{T} \alpha(T)\, dT \qquad (3.56)$$

where T_o = initial temperature

T = current temperature

$\alpha(T)$ = coefficient of thermal expansion

The coefficient of thermal expansion may be temperature dependent, but has been shown to be almost constant below 600°F [91]. Its magnitude depends on the concrete mix and its hygral state at the time of the temperature change. For this study α is assumed to be constant for all temperature levels and ages of the concrete. Equation (3.56) can then be simplified as follows:

$$\varepsilon_T = \alpha(T - T_o) = \alpha\Delta T \tag{3.57}$$

The temperature strain for both orthogonal directions is assumed to be the same and equal to the uniaxial temperature strain of Eq. (3.57). The temperature strains are also treated as initial strains in a procedure discussed in detail in section 5.7.

The creep of concrete is also influenced by temperature as discussed in detail in section 3.2.7.

3.3 REINFORCING STEEL

To model the constitutive relationship of the reinforcing steel the same simple bilinear model, which was used by Kabir [28] and Kang [37], will be used in this study. As shown in Fig. 3.19 the following parameters are needed to determine the stress-strain curve:

E_s = initial modulus of elasticity

E_{sh} = modulus of strain hardening portion

f_y = yield stress

ε_{us} = ultimate strain

This means that the reinforcing steel can exhibit strain hardening with a Bauschinger-type effect or be taken to be perfectly elastic-plastic.

The coefficient of thermal expansion of the reinforcing steel is taken to be $6.5 \times 10^{-6}/°F$ in the computer program.

Four different material states can be identified from Fig. 3.19.

1. Loading in primary tension or compression along AB or AF with modulus E_s .

2. Loading after yielding takes place along BD or FG with modulus E_{sh} .

3. Unloading always takes place along a curve with slope equal to the initial slope. Thus at point C, for example, load reversal will take place along CH with modulus E_s and then HFG with modulus E_{sh} . Reloading along HC will go up to C and then along CD.

4. Failure is assumed to have occurred when the total strain in the reinforcing steel exceeds ε_{us} .

If 1 is an axis parallel to the longitudinal axis of the reinforcing steel with an axis 2 orthogonal to it, the incremental stress-strain relationship can be written as:

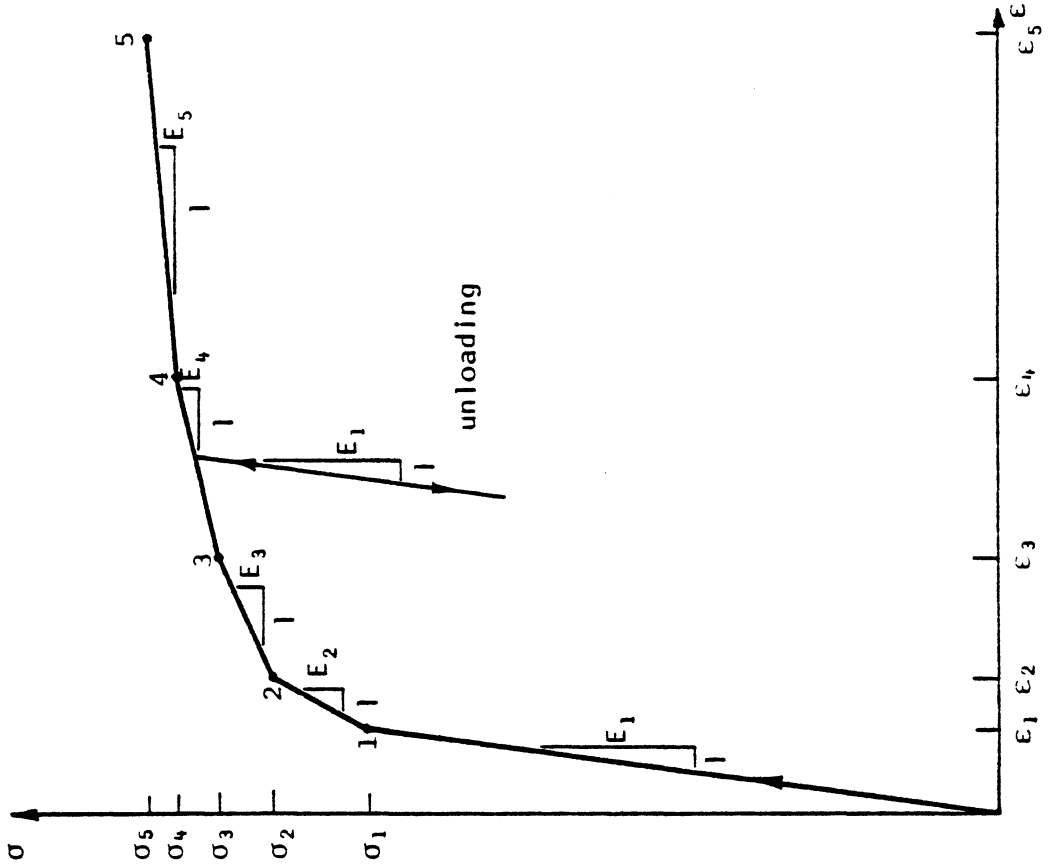

FIG. 3.19 STRESS-STRAIN CURVE FOR REINFORCING STEEL

FIG. 3.20 STRESS-STRAIN CURVE FOR PRESTRESSING STEEL

$$\begin{Bmatrix} d\sigma_1 \\ d\sigma_2 \\ d\tau_{12} \end{Bmatrix} = \begin{bmatrix} E_{sc} & 0 & 0 \\ 0 & 0 & 0 \\ 0 & 0 & 0 \end{bmatrix} \begin{Bmatrix} d\varepsilon_1 \\ d\varepsilon_2 \\ d\gamma_{12} \end{Bmatrix} \tag{3.58}$$

where

E_{sc} = current modulus of elasticity of the steel which is determined as described above.

The relationship of Eq. (3.58) must then be transformed to the x,y-coordinate system in the same manner as Eq. (2.36) in section 2.5.

3.4 PRESTRESSING STEEL

The shape of the stress-strain curve of prestressing steel differs from that of reinforcing steel in that no definite yield plateau or point can be identified. Up to a stress of about two thirds of its tensile strength, the curve is linear. Yielding then develops gradually, and in the inelastic range the curve continues to rise smoothly up to the tensile strength. Because of this a simple bilinear curve would not be an adequate approximation. In this study a multilinear curve, similar to the approach used by Kang [37], is therefore proposed as shown in Fig. 3.20.

It is assumed that the prestressing steel will never be in compression and thus the compression branch of the curve is not considered. Any unloading is assumed to take place along a curve with a slope equal to the initial modulus, for example AB as shown in Fig. 3.20. Reloading along AB will again take place up to A and then continue along A4.

For unbonded tendons any strain caused by a temperature change is taken into account while bonded tendons are treated the same as reinforcing steel.

An important property of prestressing steel is relaxation of the stress in the steel with time. This and all other losses affecting the stress in the prestressing steel will be discussed in detail in Chapter 4.

4. PRESTRESSING

4.1 GENERAL REMARKS

Prestressed concrete has become one of the major structural building materials and is widely used all over the world. An in-depth treatment of the subject will not be presented here, but can be found in texts like those of Lin [5], Nilson [92] and others.

The method of applying prestress to concrete structures can be divided into two main categories. In pretensioning the tendons are tensioned between fixed abutments before the concrete is placed. After the concrete has hardened the stress is transferred to the concrete -- usually just by the bond action between the tendons and the concrete near the member ends. Post-tensioning refers to the method where the tendons are stressed against the hardened concrete and then anchored against it by some mechanical device. In post-tensioned systems a further distinction is made between bonded and unbonded tendons. Bonded tendons are grouted after completion of the stressing operation and then form an integral part of the structure. Unbonded tendons are generally just protected against corrosion and are therefore only tied to the structure at anchorage points (except for the presence of frictional forces along the length of the tendon).

In addition to the concentrated forces applied to the structure at the anchorages, varying the position of the tendon with respect to the neutral axis of a member produces out-of-plane forces which can be utilized to balance applied loads -- a concept developed by Lin [5].

Since the structure derives its tensile strength from the presence of the prestressing tendons, any change in the stresses in the tendons affect the load-carrying ability of the structure directly. It is

therefore essential to calculate changes in the tendon stresses as accurately as possible to ensure the soundness of the structure over its lifetime. Thus, a very important aspect of prestressed concrete that has to be considered is the factors which cause a loss of tendon stress -- these will be presented in section 4.2.

In subsequent sections the modeling of the tendons and the interaction of the tendons with the structure will be discussed in detail.

4.2 LOSSES

Due to the interaction between the tendon and the concrete member and the properties of the materials, a number of different factors which cause a loss of prestress can be identified. These are: losses due to friction along the tendon, losses which occur when a tendon is anchored, relaxation of the stress in the steel with time and the effect of instantaneous and time-dependent deformation of the concrete due to load and temperature history, creep and shrinkage.

4.2.1 Friction loss along the tendon

Due to the curvature of tendons, they are subjected to normal forces which are proportional to the curvature and the force in the tendon. When the tendon is stressed, the friction between the duct and the tendon prevents it from moving freely. This means that the force in the tendon away from the anchor is reduced by an amount corresponding to the magnitude of the friction forces generated by the movement of the tendon.

The curvature can be separated into two components: curvature due to the intentional variation of the tendon position and also the unavoidable small deviations from the actual path, called wobble.

The following well-known equation [5,92] is used to calculate the force at any point in the tendon:

$$P = P_o \, e^{-(\mu\theta + kx)} \tag{4.1}$$

P_o = force in tendon at $x = 0$.

P = force in tendon at x .

μ = curvature friction coefficient.

θ = angle change in tendon over distance x .

k = wobble friction coefficient.

If P_o is replaced by a unit force, a tendon force coefficient can be defined as:

$$f = e^{-(\mu\theta + kx)} \tag{4.2}$$

The use of the tendon force coefficient is illustrated in Fig. 4.1. When stressing from both anchors the variations of tendon force coefficients f^A and f^B as shown in Fig. 4.1 are obtained. At the element boundaries f^A and f^B are compared and the higher value defined as the controlling tendon force coefficient f^C . The controlling tendon force coefficients for each element are then taken as the average of the controlling values at the boundaries of each element as shown. If one of the anchor forces is higher than the other, that curve will move up and change the values of f_i^C accordingly. The force in the tendon in an element i for the case shown will be given by:

$$P_i = P_A \, f_i^C \; ; \quad (P_A = P_B)$$

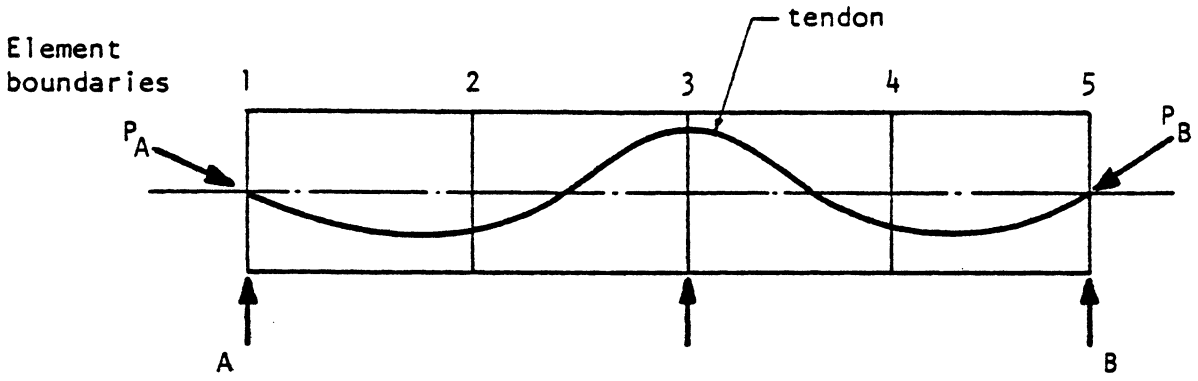

ELEVATION OF TENDON

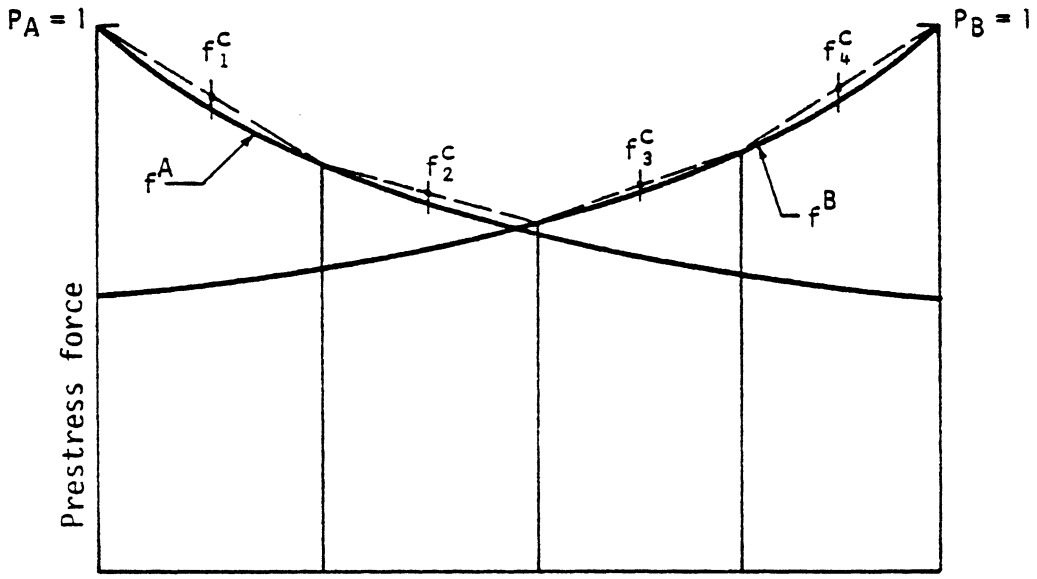

Element No.	1	2	3	4
Controlling anchor	A	A	B	B

FIG. 4.1 TENDON FORCE COEFFICIENTS

The tendon force coefficients are used in section 4.6 for the calculation of the extension ratio R_e for unbonded tendons.

4.2.2 Anchor slip

This occurs when the tendon is anchored after completion of the stressing operation and depends on the prestressing system used. This slip causes the actual force in the tendon to be lower than the final jacking force as shown in Fig. 4.2.a. When there is friction along the tendon, the force P_2 and the length L_a over which the anchor slip takes place are unknown. Huang [93] proposes a method of solving this problem by using the fact that the area under the curve represents the elongation of the tendon. When the tendon curvature varies as shown in Fig. 4.2.b, the solution of sets of equations becomes necessary. An iterative method of solving this problem is proposed in the present study.

From Eq. (4.1) and Fig. 4.2 the following equation containing the unknown length L_a can be obtained -- details of its derivation are presented in Appendix A1.

$$L_a = \frac{2\,\Delta_s A_s E_s}{P_o\left(1 - e^{-2qL_a}\right)} \tag{4.3}$$

where

Δ_s = anchor slip

A_s = tendon area

E_s = modulus of elasticity of the tendon

$q = \mu a + k$ Eq. (A.1), Appendix A1.

By iterating with Newton's method on Eq. (4.3) (details of the iteration scheme can be found in Appendix A1) the length L_a can be calculated also for cases like the one shown in Fig. 4.2.b. The force in

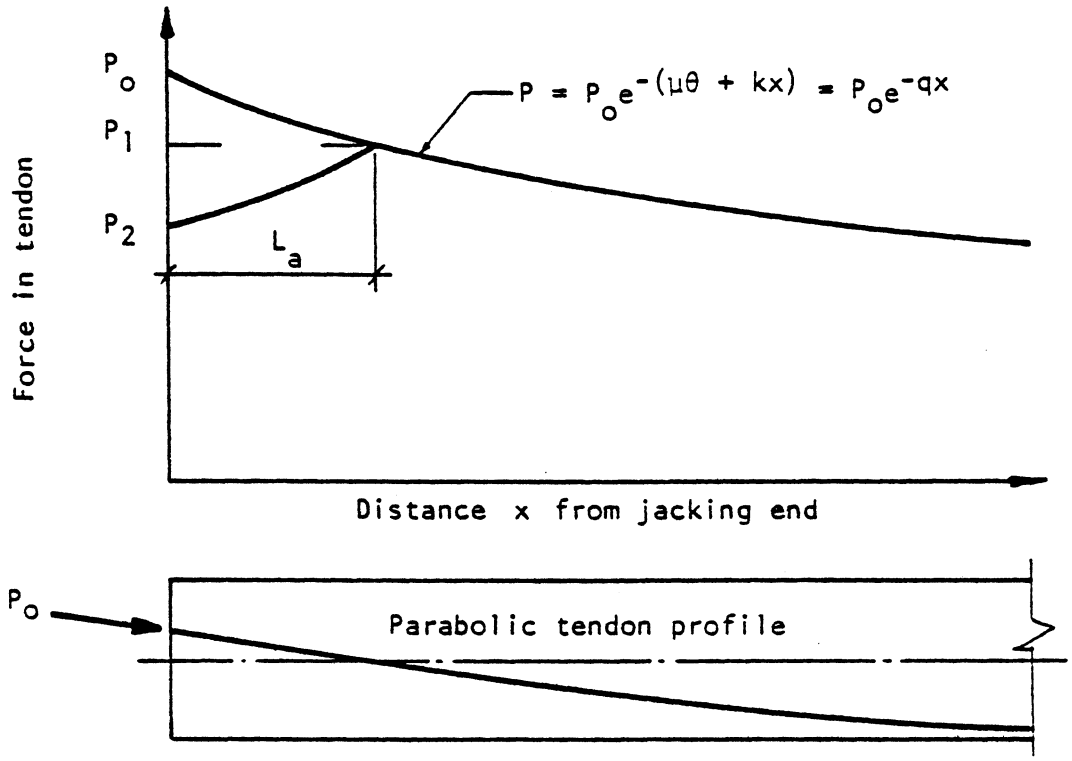

a. GENERAL CASE WITH CONSTANT q

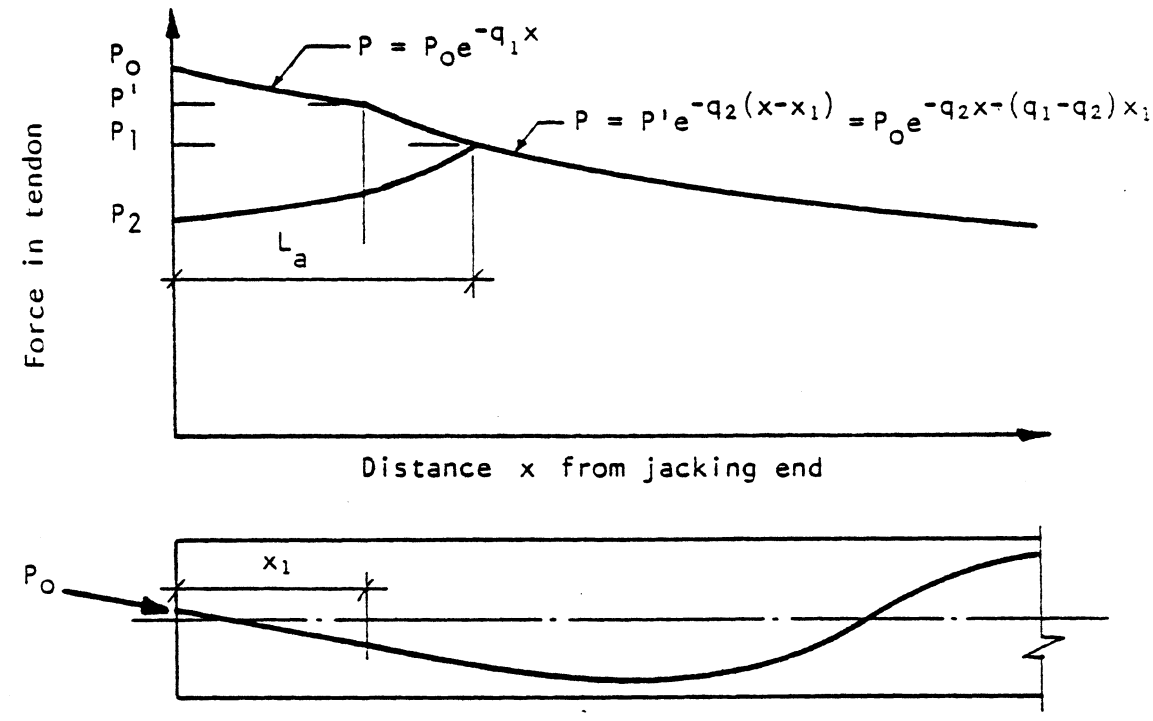

b. CASE WITH VARIABLE q

FIG. 4.2 PRESTRESS VARIATION BEFORE AND AFTER ANCHORING

the tendon for $x \leq L_a$ is then calculated as:

$$P = P_o \, e^{-q(2L_a - x)} \tag{4.4}$$

4.2.3 Relaxation in the prestressing steel

Relaxation is a phenomenon similar to creep and is defined as the decrease in stress under constant strain with the passing of time. The following equation for the calculation of the stress relaxation in prestressing steel was proposed by Mugura et al. [94] after a comprehensive analysis of a large number of experimental studies on different prestressing steels:

$$\frac{f_s}{f_{si}} = 1. - \frac{\log t}{c}\left[\frac{f_{si}}{f_{sy}} - .55\right] \tag{4.5}$$

for $f_{si}/f_{sy} > .55$

where f_s = steel stress at time t

f_{si} = initial steel stress

f_{sy} = .1% offset yield stress

c = constant = 10. for ordinary prestressing steel

t = time in hours after stressing

The procedure used to calculate the relaxation of the steel in this study is set out in section 4.8.

4.2.4 Change in prestress caused by concrete deformation

The deformation of the structure is caused by the application of loads, stressing of tendons, temperature changes and the creep and shrinkage of the concrete with time.

The deformation of the structure due to the applied loads is obtained from the solution of the equilibrium equations. The deformation of the tendon and the stress changes it produces are then calculated as described in section 4.7. Due to the iterative nature of the solution process, the forces caused by the changes in the prestressing tendon stresses are again applied to the structure and the procedure repeated until convergence has been achieved.

At transfer in post-tensioning, it may be necessary to consider a deviation from the straightforward solution process described above for the following reason: When a number of tendons are stressed and anchored in sequence, the elastic shortening of the concrete due to the stressing of subsequent tendons causes a loss of prestress in those tendons already stressed. This produces an overall loss of prestress equivalent to approximately one half of the total elastic shortening of the concrete. To allow for this case an option is provided in the computer program to neglect some fraction of the tendon deformation in the state determination after the application of a prestress loading to the structure, i.e., at transfer.

4.3 MODELING THE TENDONS

In this section the manner in which an arbitrary tendon layout is modeled will be described. The assumptions and approximations which are necessary to obtain a workable mathematical model will also be discussed. The emphasis in this study is on flat slabs, but due to the fact that the effects of large displacements are also incorporated, which means that the resultant structure becomes a shallow shell, a more general approach is required.

Pretensioning is seldom used in slab construction, but is included here for completeness. The emphasis in the following discussion is therefore on post-tensioning.

The tendon layout is specified on the global XY-plane which is taken to be the plan view. (The relation between the global and local coordinate systems is explained in section 5.5.) The tendon anchors must lie on element boundaries. The layout in the global X and Y-coordinates is used to tie the tendon to all the elements it spans. After the intersection of the tendon with the boundaries of each element has been established, all subsequent calculations are performed in the local coordinate system of each element. (In the case of a flat slab lying in the global XY-plane, which coincides with the local $\bar{x}\bar{y}$-plane, it would make no difference for the initial configuration.

Tendons are divided into two groups: Slab tendons are straight in plan and can have a profile in a plane perpendicular to the plane of the element (i.e., a plane containing the local $\bar{z}$-axis). Panel tendons can have a profile in plan view and only lie at the slab middepth (i.e., on the reference or local $\bar{x}\bar{y}$-plane). Subject to these restrictions, tendons can be on a line of nodes or element boundaries, or follow any path across the elements.

The tendon profile can be made up of any combination of straight and parabolic portions. Straight tendons may have harp points, but it is assumed that no concentrated angle changes occur in tendons containing parabolic sections -- their profile is assumed to be a smooth continuous curve. The eccentricities of the tendons at the element boundaries are calculated accurately in the computer program and are assumed to be in the local $\bar{z}$-direction for each element.

Tendons can be stressed from one or both ends and must have a constant cross section. It is assumed that all the tendons are stressed to the specified jacking forces at the same time. At transfer all post-tensioned tendons are treated as unbonded. Pretensioned tendons are always taken to be bonded. After transfer, i.e., after the time step at which the prestress loading is applied, bonded tendons are assumed to have been grouted and thus completely bonded to the concrete.

The following assumptions are made in the modeling of the tendons:

a) Geometry: It is assumed that a tendon can be approximated by a series of straight sections between element boundaries. For normal structural discretization, the errors introduced are not significant.

b) Losses: The losses are taken into account as described in section 4.2. For unbonded tendons it is assumed that any change in tendon length causes a change in tendon force which is the same at both anchors and that its distribution over the tendon length varies due to friction. This is used in section 4.7 for the state determination. For pretensioned tendons the effect of creep and shrinkage before transfer is ignored.

c) Force in a tendon segment: The force acting in a tendon segment is assumed to be the average of the tendon forces which are calculated at the element boundaries. The interaction between the tendon and the element is also assumed to take place only at these element boundaries. This is the same method used by Kang [37] in a study of one-dimensional beam or column members. Van Zyl [95], in his study of box girder bridges, also assumed a constant tendon force in each element, but applied the forces exerted by the tendon on the structure at a point halfway between the element ends. Both of these methods were investigated, and they give

similar results, but due to the simplicity and smaller storage requirements necessary for the method used by Kang, it was selected. The calculation of the force vector due to prestress is presented in section 4.4.

d) Tendon stiffness contribution: Unbonded tendons are assumed to have a negligible stiffness, while the manner in which the stiffness of bonded tendons is calculated is discussed in section 4.5.

e) Bond: Pretensioned tendons and post-tensioned bonded tendons after transfer are assumed to be perfectly bonded to the concrete, which means that the displacement field within an element is taken to be continuous.

f) Material properties: The stress-strain curve of the prestressing steel is modeled by a multi-linear curve as discussed in section 3.4. The other properties are taken to remain constant throughout the analysis.

4.4 LOAD VECTOR DUE TO PRESTRESS

To model the effect of a tendon on a structure analytically, the equivalent load concept [5] will be used. This means that the tendon is replaced by a set of loads which corresponds to the actual loading imposed by the tendon on the concrete structure. As a result of the assumptions indicated in section 4.3, the load vector due to prestress is calculated as follows:

Consider a triangular shell element in the local $\bar{x}\bar{y}$-plane with a tendon segment in it as shown in Fig. 4.3. The calculated tendon forces at i and j are P_i and P_j respectively, but it is assumed that an average force P is acting in the tendon segment.

$$P = (P_i + P_j)/2 \tag{4.6}$$

Since the tendon is assumed to be straight between element boundaries, the slope angle α can be calculated as:

$$\alpha = \tan^{-1}\left((e_j - e_i)/\ell\right) \tag{4.7}$$

The out-of-plane and in-plane forces due to the tendon then are:

$$\begin{aligned} P_v &= P \sin \alpha \\ P_H &= P \cos \alpha \end{aligned} \tag{4.8a}$$

The x- and y-components of P_H are then given by:

$$\begin{aligned} P_x &= P_H \cos \phi \\ P_y &= P_H \sin \phi \end{aligned} \tag{4.8b}$$

The moments about the x- and y-axes caused by the eccentricity of the force P at point i, for example, are then:

$$\begin{aligned} M_{xi} &= -P_y e_i \\ M_{yi} &= P_x e_i \end{aligned} \tag{4.8c}$$

These forces which are acting at points i and j are then transferred to the nodes on either side of them in proportion to the distance from that node. The complete load vector for an element due to one tendon segment is given in Appendix A.2.

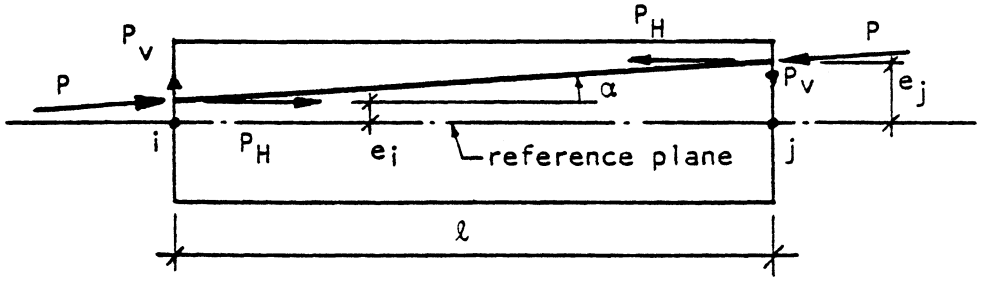

a. ELEVATION : SECTION AA

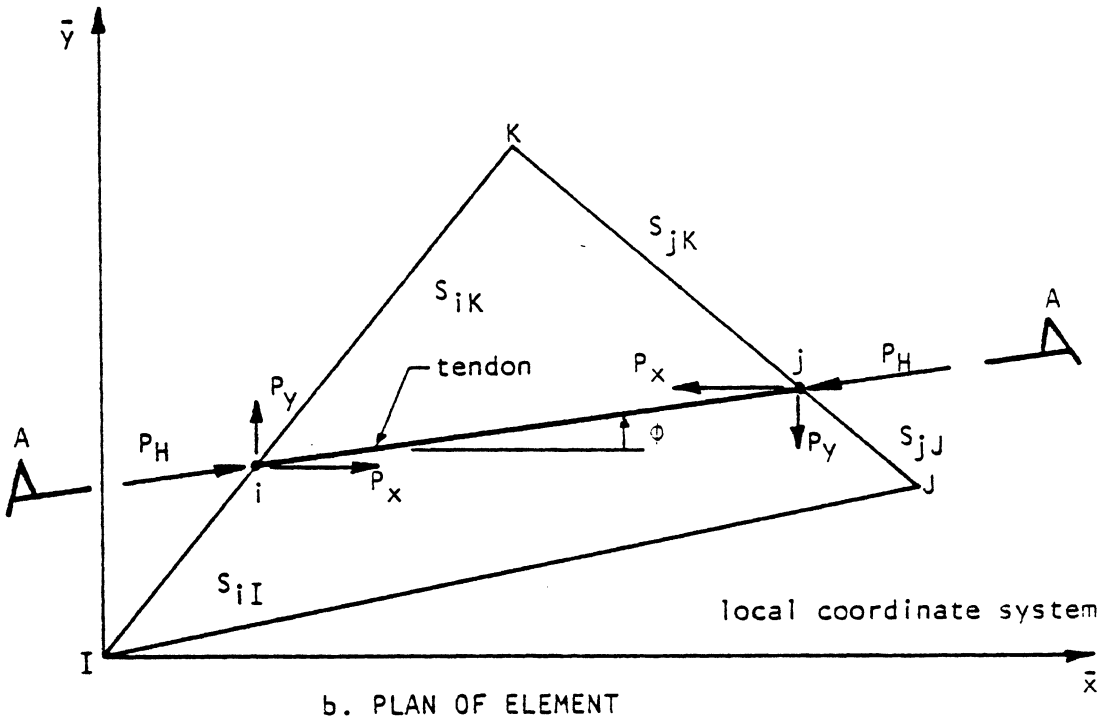

b. PLAN OF ELEMENT

FIG. 4.3 EQUIVALENT LOADS DUE TO PRESTRESS

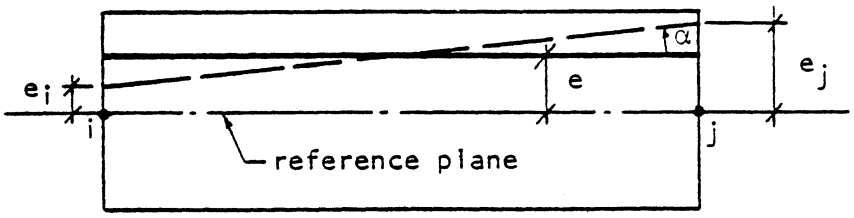

ELEVATION

FIG. 4.4 IDEALIZATION OF TENDON SEGMENT TO CALCULATE TENDON STIFFNESS

4.5 TENDON STIFFNESS CONTRIBUTION

Bonded tendons, which form an integral part of the structure, contributes towards its stiffness and are incorporated in this study as described below. The stiffness of unbonded tendons is ignored.

Bonded tendon segments can usually be located anywhere in an element and therefore have a stiffness contribution to all the degrees of freedom of the shell element. Ideally the stiffness of a tendon segment should therefore be incorporated by treating it as a uniaxial truss bar. However, since the tendon segment ends are generally not on nodes, the displacement field assumed for the tendon segment must also be compatible with that assumed for the element.

In this study the tendon segment in an element is therefore modeled as a straight bar at a distance equal to the average eccentricity from the reference surface (Fig. 4.4) and converted to an "equivalent smeared" layer as will be described below. The out-of-plane stiffness contribution of the tendon segment is neglected for the following reasons: Compared to the concrete stiffness the tendon stiffness is small and since the angle α (Fig. 4.4), which the tendon makes with the reference plane, is usually also small, the out-of-plane stiffness of the tendon will be of second order magnitude. To incorporate this contribution will also require a substantial additional computational effort, which is not deemed to be worth the effort.

The tendon segment is converted to an "equivalent smeared" layer as follows: The volume of the tendon segment in the element is divided by the element area A_e to give an equivalent layer thickness:

$$t_p = A_s \ell_t / A_e \tag{4.9}$$

where ℓ_t = tendon length

The stiffness of this equivalent layer of prestressing steel of thickness t_p, located at a distance e from the reference surface, is then incorporated in the same manner as a layer of reinforcing steel, as described in section 3.3.

4.6 EXTENSION RATIO FOR UNBONDED TENDONS

For bonded tendons the deformation field of the tendon is the same as that of the concrete and the strain, and therefore stress change, in a segment can be calculated directly.

In the case of unbonded tendons, however, the tendon is assumed to be fixed to the concrete only at the anchorages, although there is some interaction between the tendon and the concrete due to friction. The effect of a change in length of a tendon segment in one element is therefore not only restricted to that segment, but affects the tendon over its whole length.

Kang [37] presented a method in which an equivalent force at the anchors can be calculated by an iterative method. Van Zyl [95] proposed the use of an average extension factor which makes it possible to calculate the change in force, resulting from a change in tendon length, directly. In this study the basic idea of the average extension factor will be used, but due to the fact that a multilinear stress-strain curve is used for the prestressing steel, some modification is necessary. The use of an extension ratio is therefore proposed.

Van Zyl [95] defined the average extension factor as the prestressing force which must be applied at both anchors of a tendon to produce a

unit extension of the tendon including the effect of friction along the tendon. If a unit force is applied at both anchors, the tendon force in element i will be f_i^C as defined in section 4.2.1 (the larger of f_i^A or f_i^B, depending on which anchor is controlling -- see Fig. 4.1). The elongation of the tendon segment of length ℓ_i in element i will be:

$$\Delta L_i = \frac{\ell_i}{E_s A_s} f_i^C \tag{4.10}$$

where

E_s = modulus of elasticity of the prestressing steel

A_s = tendon area

The total elongation of the tendon is:

$$\Delta L = \sum_i^n \left(\frac{\ell_i}{E_s A_s} f_i^C \right) \tag{4.11}$$

where

n = number of segments in the tendon

The average extension factor is:

$$A_{ef} = E_s A_s / \sum_i^n \left(\ell_i f_i^C \right) \tag{4.12}$$

The change in force at the anchors in a tendon due to an extension of ΔL, is then given by:

$$\Delta P_o = \Delta L \, A_{ef}$$

and the force in each tendon segment is then adjusted by $\Delta P_o f_i^C$.

The extension ratio R_e, which is used in this study, can be defined as the ratio between the extension of a frictionless tendon and that of a

tendon including the effect of friction due to a unit force applied at both anchors and is given by:

$$R_e = L/\sum_i^n \left(\ell_i f_i^c\right); \quad R_e \geqslant 1 \tag{4.13}$$

where

L = length of the whole tendon

If friction is neglected, R_e is equal to one, but otherwise it will be greater than one. The change in anchor force due to a tendon extension ΔL is calculated as:

$$\Delta P_o = A_s E_{sc} R_e \, \Delta L/L \tag{4.14}$$

where

E_{sc} = current modulus of elasticity of the prestressing steel

The use of R_e will be illustrated in section 4.7.

4.7 STATE DETERMINATION FOR THE TENDONS

For each element the local nodal displacement increments $\Delta \underset{\sim}{r}_\ell$ are calculated by a transformation from the global displacement increments as discussed in section 5.4. For each tendon segment in an element the translations u, v and w of its ends are calculated by using the interpolation functions. The extension ΔL_i of a tendon segment is obtained by subtracting the old length from the new length. The stress change for bonded and unbonded tendons is then calculated as follows:

4.7.1 Bonded tendons

Since the displacement field of the tendon is the same as that of the concrete, the incremental and total strain in each tendon segment is

calculated and the stress change established from the stress-strain curve for the prestressing steel.

4.7.2 Unbonded tendons

The following iterative procedure is used to find the stress change in each tendon segment due to the fact that any change in tendon length affects the whole tendon.

The extensions of all the tendon segments of a tendon is summed to find ΔL for the tendon:

$$\Delta L = \sum_{i}^{n} \Delta L_i \tag{4.15}$$

and the average strain increment for the tendon then is:

$$\Delta\varepsilon = \Delta L/L \tag{4.16}$$

Using the extension ratio R_e defined in section 4.6 (Eq. (4.13)) and an average modulus of elasticity E_{SA}, the change in anchor force due to this strain increment is calculated as:

$$P_o = A_s E_{SA} R_e \tag{4.17}$$

For loading $(\Delta\varepsilon > 0)$, the average modulus of elasticity will be the initial modulus of the prestressing steel or the last value from a previous state determination as will be shown below (Eq. (4.22)). In the case of unloading $(\Delta\varepsilon < 0)$, the initial modulus is used.

The force change in a tendon segment due to ΔP_o is given by:

$$\Delta P'_{i,r} = \Delta P_o \alpha_r f_i^c \tag{4.18}$$

where r = iteration number

α_r = modification factor defined in Eq. (4.21)

Another value for the force change in each tendon segment can be calculated by using the current modulus of elasticity for that segment:

$$\Delta P_{i,r} = A_s E_{sc,i} R_e \Delta\varepsilon f_i^c \beta_{i,r-1} \alpha_r \tag{4.19}$$

where

$\beta_{i,r}$ = magnification factor

This $\Delta P_{i,r}$ will be the same or smaller than $\Delta P'_{i,r}$ and this is the reason for the magnification factor $\beta_{i,r}$. $\beta_{i,o}$ is set to one at the start of the iterations and is then calculated as follows:

$$\beta = \frac{\Delta P'_{i,r}}{\Delta P_{i,r}} ; \quad \beta \geqslant 1$$

and then

$$\beta_{i,r} = \beta_{i,r-1} + (\beta - 1)\gamma; \quad \beta_{i,r} \geqslant 1 \tag{4.20}$$

where

γ = an overestimation factor to speed up convergence, taken = 2

The modification factor α_r is then calculated as:

$$\alpha_r = n/\sum_{i}^{n} \beta_{i,r}; \quad \alpha_r \leqslant 1 \tag{4.21}$$

where

n = number of elements

For $\alpha_r < 1$, $\Delta P'_{i,r}$, $\Delta P_{i,r}$ and $\beta_{i,r}$ are recalculated from Eqs. (4.18), (4.19) and (4.20) respectively and the process repeated until α_r

is constant. When $\alpha_1 = 1$ the segments are all on the same section of the stress-strain curve and no iteration is necessary. After convergence, the force in each tendon segment is adjusted according to Eq. (4.19). When $\alpha_r < 1$ the value of the average modulus of elasticity to be used in the next state determination is calculated as:

$$E_{SA} = E_{SA}\,\alpha_f \tag{4.22}$$

where

$$\alpha_f = \alpha_r \quad \text{at convergence}$$

The iterative procedure can be summarized as follows:

1. Calculate ΔL, $\Delta\varepsilon$, determine E_{SA} and calculate ΔP_o from Eq. (4.17).
2. Calculate $\Delta P'_{i,r}$, $\Delta P_{i,r}$, $\beta_{i,r}$ and α_r using Eqs. (4.18) through (4.21).
3. If $\alpha_r < 1$ and until α_r approximately constant, repeat step 2. For $\alpha_r = 1$, or at convergence, go on to step 4.
4. Use Eq. (4.19) and adjust the tendon force in each segment accordingly. Calculate a new value of E_{SA} if necessary.

4.8 CALCULATION OF STRESS RELAXATION

Equation (4.5) presented in section 4.2.3 was developed assuming that the strain remains constant and that the only stress applied is the initial prestress. Since creep and shrinkage for example, cause additional losses with time, this assumption is not valid for any comprehensive analysis of a structure. To incorporate any additional variations in prestress in the calculation of the relaxation, Hernandez and Gamble

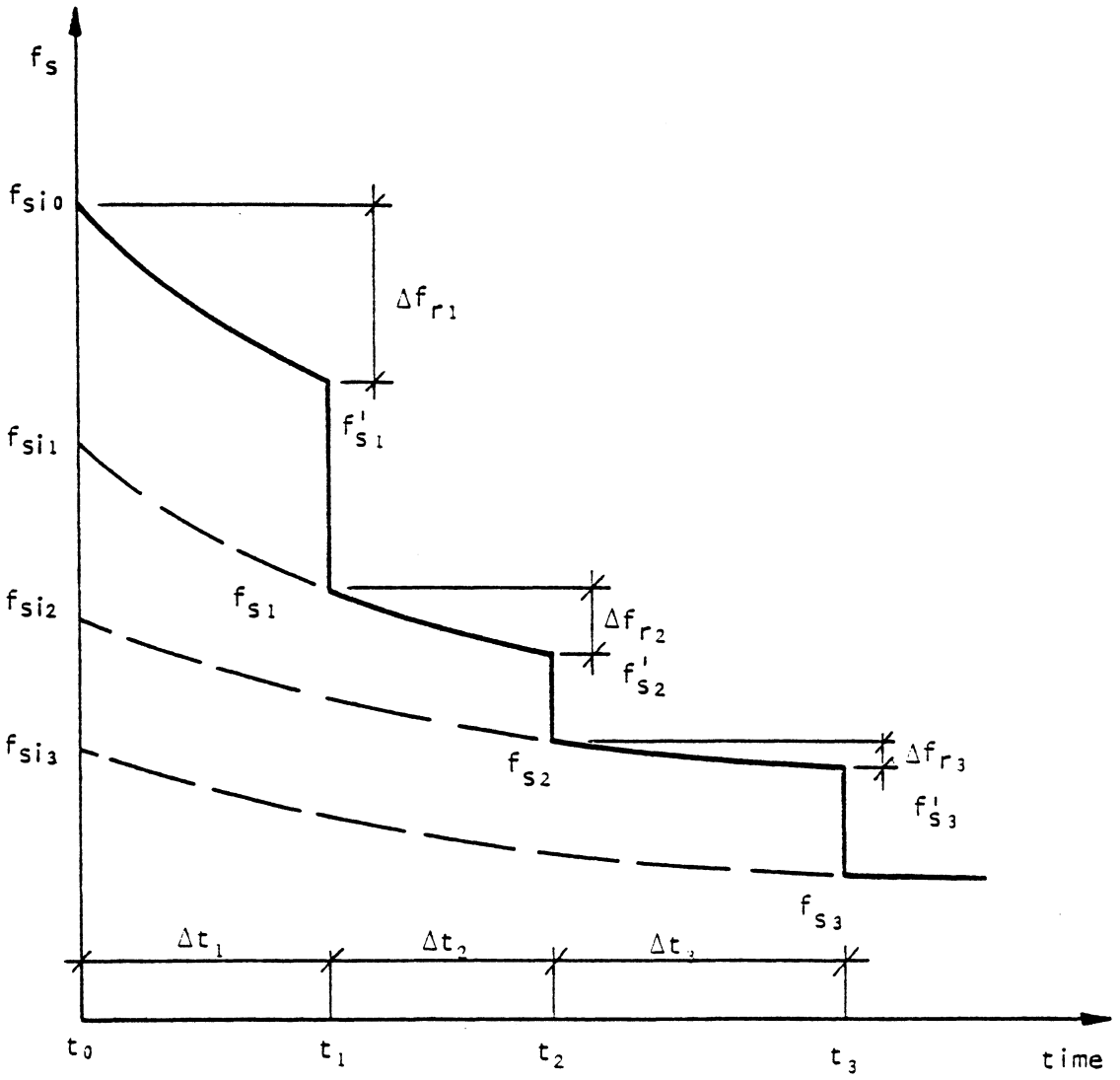

FIG. 4.5 STRESS RELAXATION IN PRESTRESSING STEEL

[96] suggested the following procedure which was also used by Kang [37] and van Zyl [95]. Ghali et al. [97] used a similar procedure, but based on the relaxation curve recommended by the CEB-FIP [98].

Referring to Fig. 4.5, it is assumed that the other losses occur at the end of the time steps. The initial prestress f_{sio}, applied at time t_o, therefore relaxes to f'_{s1} during time interval Δt_1:

$$\Delta f_{r1} = f_{sio} - f'_{s1}$$

At time t_1 additional losses of prestress cause the stress to drop to f_{s1}. To calculate the stress relaxation Δf_{r2} during time interval Δt_2, Eq. (4.5) is used to calculate a fictitious initial prestress f_{si1} which would have relaxed to f_{s1} during Δt_1. The stress f'_{s2} is then calculated, using f_{si1} as the initial prestress and then:

$$\Delta f_{r2} = f_{s1} - f'_{s2}$$

By repeating this procedure for subsequent time steps the total stress relaxation at time t_n can be obtained by summation:

$$f_{rn} = \sum_{i=1}^{n} \Delta f_{ri} \qquad (4.23)$$

where

n = number of time steps

4.9 SUMMARY

A summary is presented of the steps and calculations as described in this chapter pertaining to the analysis of a structure with prestressing. The emphasis is on the prestressing and in Chapter 5 it will be shown how this fits into the overall analysis procedure.

1. Read in the structural data, material properties and tendon geometry and data of the problem to be analyzed.

2. Calculate the tendon profile and the force variation along it. Calculate the position, length and force in the tendon segments of each element. Also compute R_e for unbonded tendons.

3. Calculate the element load vectors due to prestress.

4. Read the load control card for the time and form the structural load vector for the number of load steps specified.

5. Form the element and structural stiffness matrices. Add in the stiffness of tendons which are bonded at that time.

6. Solve the equilibrium equations.

7. State determination: Calculate the strain increments for all the tendon segments in each element and the accompanying force changes as set out in section 4.7. Update the tendon forces, calculate the internal stress resultants and form the unbalanced load vector.

8. Check whether convergence has been achieved. If not, repeat steps 5 thru 8 until convergence is obtained, then go on to step 9.

9. Repeat steps 5 thru 8 for the other load steps of this time.

10. If a time-dependent analysis is to be done, calculate the relaxation of the steel, the concrete strains due to temperature change, creep and shrinkage and form the load vector due to these effects.

11. Repeat steps 5 thru 8 for all the load steps specified for the time-dependent analysis.

12. Repeat steps 4 thru 11 for all further times.

5. METHOD OF ANALYSIS AND COMPUTER PROGRAM

This chapter deals with the overall method of analysis used in this study and the manner in which it has been implemented in a computer program for the analysis of thin reinforced and prestressed concrete structures, with the emphasis on slabs and panels, by the FEM.

The following topics will be discussed: The solution techniques used to solve the nonlinear problem. The different finite elements used will be described in detail. The solution algorithm,with emphasis on those special procedures developed in this study, will be outlined. Finally a brief description of the computer program will be presented.

5.1 SOLUTION OF THE NONLINEAR PROBLEM

The solution techniques used in the solution of the set of incremental equilibrium equations

$$\underset{\sim}{K}\,\Delta\underset{\sim}{r} = \Delta\underset{\sim}{R} \tag{5.1}$$

when nonlinearities are involved, will be discussed here. The nonlinearity may be caused by a nonlinear constitutive relationship (material nonlinearity) or a nonlinear strain-displacement relationship (geometric nonlinearity). The following three methods are generally used:

5.1.1 Incremental load method (Cauchy-Euler)

a) Without equilibrium corrections

The load vector $\Delta\underset{\sim}{R}$ is subdivided into a number of increments. Using the tangent stiffness at the beginning of each load increment, Eq. (5.1) is solved for the displacement increment due to each load increment. The total displacement due to $\Delta\underset{\sim}{R}$ is then found by a summation of all

the displacement increments. This may lead to a deviation from the true path as shown in Fig. 5.1.a.

b) With equilibrium corrections

The same procedure as outlined in 1.a is followed, except that equilibrium is checked after each increment. Any unbalanced loads are then added to the next load increment. The result is a better approximation of the true load-deflection path as shown in Fig. 5.1.b.

5.1.2 Iterative method (Newton-Raphson)

The load is applied in one step and a series of iterations performed by applying the unbalanced forces until equilibrium is achieved to the desired degree. The manner in which the stiffness matrix is selected leads to the following three classifications:

a) Constant or initial stiffness

The initial stiffness is used each time to solve for the displacement increment as is shown in Fig. 5.2.a. This means that $\underline{K}$ has to be assembled and triangularized only once which is computationally advantageous, but usually more iterations are also required to obtain convergence.

b) Tangent stiffness

A new tangent stiffness is formed after each increment and used to solve for the next displacement increment as can be seen in Fig. 5.2.b. This leads to the most rapid convergence, but means the complete solution of a set of equations for each iteration.

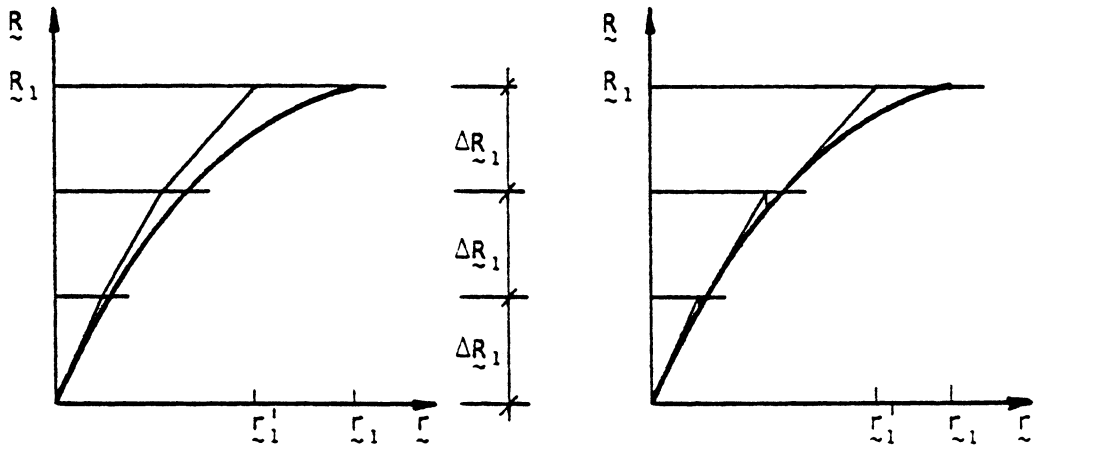

a. WITHOUT EQUILIBRIUM CORRECTIONS b. WITH EQUILIBRIUM CORRECTIONS

FIG. 5.1 INCREMENTAL LOAD METHOD

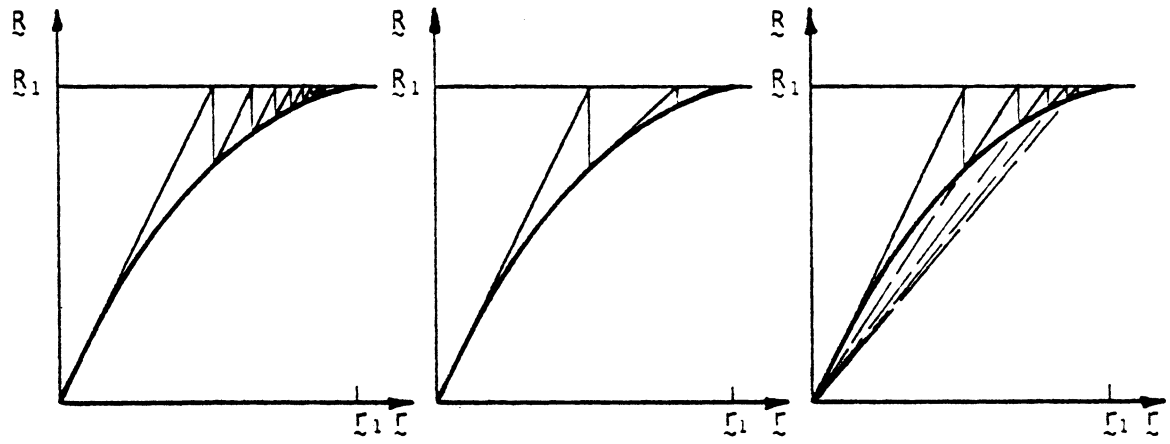

a. CONSTANT STIFFNESS b. TANGENT STIFFNESS c. SECANT STIFFNESS

FIG. 5.2 ITERATIVE METHOD

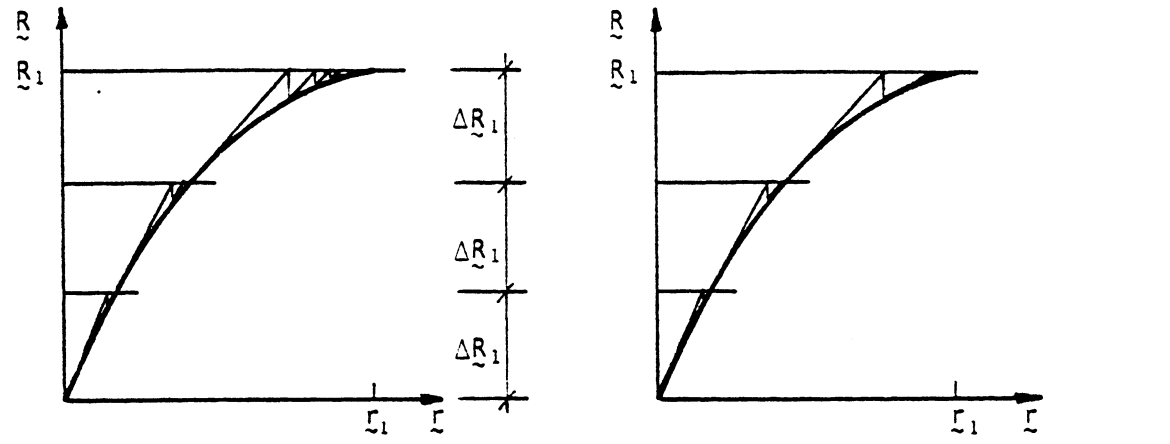

a. CONSTANT STIFFNESS IN LOAD STEPS b. TANGENT STIFFNESS IN LOAD STEPS

FIG. 5.3 COMBINED METHODS

c) Secant stiffness

An attempt is made to find an average stiffness which satisfies the load-displacement relationship as shown in Fig. 5.2.c. This method may lead to instability when geometric nonlinearities are involved and is therefore restricted to problems with material nonlinearity only.

5.1.3 Combined method

Methods 1 and 2 can be combined in a variety of ways to try and find a computationally efficient solution scheme for any given problem. Usually the load vector is divided into steps and constant or tangent stiffness iterations performed in each step as shown in Fig. 5.3. In the present study an option is provided for the analyst to select a combined method best suited for the problem at hand.

5.2 FINITE ELEMENTS USED IN THIS STUDY

5.2.1 General

In the present study four finite elements are used in the computer program. Major factors considered in choosing the elements are the accuracy of the elements regarding both displacements and stresses which are obtained from an assembled model, the numerical efficiency of the elements with regard to the computational effort needed to form the element stiffness matrices and the ability of the elements to allow the accurate modeling of the geometry of various structures that may be considered.

The emphasis in this study is on flat slabs and panels, but when such a structure is analyzed for large deflections, the resulting structure becomes a shallow shell. The effect of membrane forces developed because of the large out-of-plane deflections is one of the most important

phenomena that has to be accounted for in such an analysis. A considerable effort has thus been made to find an efficient and accurate shell element.

Since the application of the FEM to the analysis of shells, three approaches to the finite element representation of thin shells have emerged [99]: (1) with flat elements, (2) using three-dimensional solid elements and (3) by means of curved thin shell elements.

Curved thin shell elements

The curved thin shell elements have been developed for use in the aerospace industry where very thin metal shells are extremely important structural elements and therefore have to be modeled very accurately. Because of the specialized nature of these elements and their large number of DOF, such a representation was not considered for this study.

Three-dimensional solid elements

Three-dimensional solid elements cannot be applied directly to thin shell analysis -- they have to be modified in a way analogous to the assumptions made for classical shell theory. Two elements which fall into this category were considered and will be discussed briefly. The first is a sixteen node isoparametric shell element developed by Dovey [100] and the second is the bilinear degenerated shell element developed by Kanoknukulchai [101].

(i) Sixteen-node isoparametric shell element

This solid shell element was developed by Dovey [100] from the twenty-node isoparametric solid brick element by eliminating the nodes on the middle surface. The element has forty-eight DOF, six per pair of nodes (one node on each face), and by defining a relative DOF in the

thickness direction this is reduced to five DOF per pair of nodes and overcomes the problem of sensitivity when dealing with thin shells. The displacement, and thus the geometric shape functions, are linear in the thickness direction and quadratic in the two in-plane directions. This makes an accurate representation of the geometry of a curved shell possible. Incompatible modes and reduced integration are used to improve the element behavior.

Although both displacements and stresses obtained from the element are good, the disadvantages associated with using it are the following: The assembled global stiffness matrix has more equations and also a greater bandwidth than is the case for an equivalent mesh of flat elements -- this increases the time needed for equation solving considerably. To model the cracking of the reinforced concrete and to discretize the prestressing tendons fairly accurately a reasonably fine mesh is considered to be more desirable. This element would therefore be uneconomical in this respect as well and it was therefore not used in this study.

(ii) Bilinear Degenerated Shell (BDS) element

This is a four-node isoparametric quadrilateral shell element developed by Kanoknukulchai [101] from an eight-node isoparametric solid brick element. The element has twenty-four DOF (six per node) and by enclosing the midsurface of the element with four straight sides it forms a hyperbolic paraboloid which makes it possible to represent the geometry of an arbitrary shell. The usual Kirchhoff assumptions are relaxed, and the rotations θ_x and θ_y of a normal to the midsurface are taken to be independent variables. By using selectively reduced numerical integration on the shear terms for the evaluation of the stiffness matrix, very good results have been obtained [101,102].

The problem associated with the rotation about a normal to the element plane is overcome by adding a so-called "torsional" stiffness at the element level in such a way that a constraint is added between this rotation and the in-plane rotation of the midsurface. This has no adverse effect on the general functioning of the element and good results were obtained for shallow shells [101].

The only disadvantage associated with this element is a rank deficiency of the element stiffness matrix due to the presence of additional zero energy modes over and above the rigid body modes. This problem stems from the reduced integration used in evaluating the element stiffness matrix. Generally, however, the boundary conditions render the global stiffness matrix positive definite [103].

Although the BDS-element performs very well, the problem concerning the rank deficiency of the stiffness matrix mentioned above, affects the solution of a plate on point supports so seriously that it prohibits the use of the element in a general structural analysis program at present.

Flat elements

Either a quadrilateral or a triangular flat element can be used. The disadvantages associated with a flat quadrilateral element are the difficulty to model an arbitrary shell surface and that in an analysis including nonlinear geometric effects, the four corner nodes do not stay on a common plane. The conforming quadrilateral element developed by Clough and Felippa [104] avoids these problems since it is formulated by assembling four flat triangular elements. For the modeling of the material and geometric nonlinearities and for a better discretization of the prestressing tendons, a simpler model was considered to be more convenient.

Since this quadrilateral element was, in any event, assembled from triangular elements, it was decided to choose a flat triangular shell element as the finite element for this study.

Due to the Kirchhoff assumptions presented in Chapter 2, the bending and membrane actions can be separated for a linear analysis. To model plane stress problems the constant strain triangle (CST) was one of the first elements developed. It is also used to model the membrane behavior in this study and will be discussed in more detail in section 5.2.3.

The two triangular plate bending elements considered were the LCCT9 (nine DOF linear curvature compatible triangle) developed by Felippa [104] and the synthetic triangular element developed by Irons and Razzaque [105,106]. The latter element performs considerably better than the LCCT9 [104] and seems to be the most efficient triangular plate bending element, using a displacement formulation, developed up to the present. The Irons-Razzaque element is selected as the plate bending element for this study -- details will be presented in section 5.2.4.

The flat triangular shell element selected for this study therefore consists of the nine DOF Irons-Razzaque triangular plate bending element combined with a CST for the membrane action. This element was also used by Arnesen et al. [30] for their study on the nonlinear analysis of reinforced concrete.

The flat triangular shell element used in this study has the following advantages:

1. Ease with which an arbitrary geometrical layout can be modeled.

2. In regions of steep stress or moment gradients, the mesh can easily be refined.

3. The element stiffness matrix is simple and inexpensive to calculate.

4. The assembled structural stiffness matrix has the minimum bandwidth for a particular nodal and element layout.

5. Nonlinear geometric analysis is simplified since the three corner nodes always define a plane.

The disadvantages of using this flat triangular shell element are as follows:

1. The CST cannot model a stress gradient and thus gives poor results in areas of high stress gradients, unless a very fine mesh is used.

2. The fact that the rotation about the normal to the element plane has not been included may cause problems -- the way in which it can be taken care of is discussed in section 5.2.3.

3. "Discontinuity" bending moments, which are not present in a continuously curved actual shell, are generated.

5.2.2 Triangular shell element

The triangular shell element employed in this study is formed by combining the 9 DOF Irons-Razzaque plate bending triangle [106] with the CST as the membrane element to obtain a flat triangular element with 5 DOF at each node as is shown in Fig. 5.4.

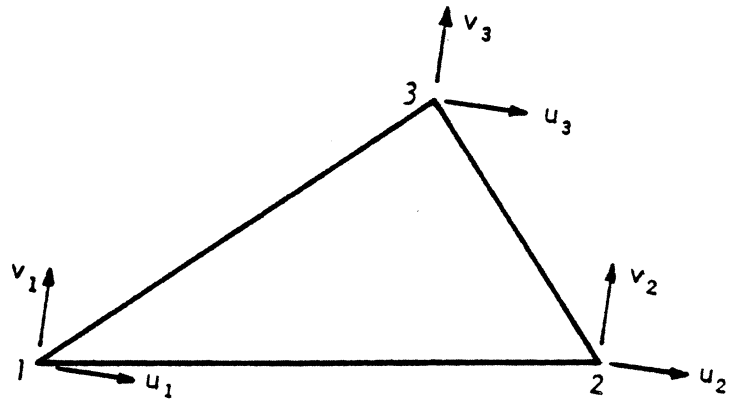

a. CONSTANT STRAIN TRIANGLE

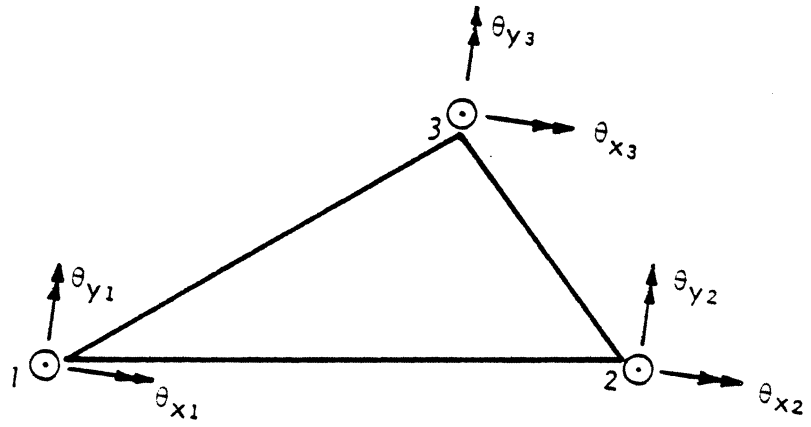

b. IRONS-RAZZAQUE PLATE BENDING TRIANGLE

FIG. 5.4 TRIANGULAR SHELL ELEMENT

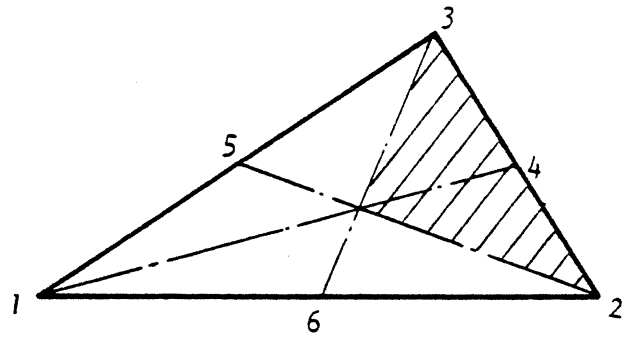

FIG. 5.5 AREA OF TRIANGULAR ELEMENT REPRESENTED BY AN INTEGRATION POINT

By using the Kirchhoff assumptions presented in section 2.2.1 the problem is simplified and the displacements at any point within an element can be expressed as follows.

$$\begin{aligned} u(x,y,z) &= u_o(x,y) + z\,\theta_y \\ v(x,y,z) &= v_o(x,y) - z\,\theta_x \\ w(x,y,z) &= w_o(x,y) \end{aligned} \tag{5.2}$$

where

x,y,z = the local element coordinate system

u,v,w = displacements in the x,y,z-directions

u_o,v_o,w_o = displacements of the element reference surface

θ_x,θ_y = rotations about the x- and y-axes (See Fig. 5.4.)

The assumption that normals remains normal to the reference surface after deformation also results in the following relationships:

$$\begin{aligned} \theta_x &= \partial w/\partial y \\ \theta_y &= -\,\partial w/\partial x \end{aligned} \tag{5.3}$$

Substituting Eq. (5.3) into (5.2) yields:

$$\begin{aligned} u &= u_o - z\,w_{,x} \\ v &= v_o - z\,w_{,y} \\ w &= w_o \end{aligned} \tag{5.4}$$

Choosing two different sets of shape functions for the bending displacements (w,θ_x,θ_y) and the in-plane displacements (u,v), analogous to Eq. (2.18), u_o, v_o and w_o can be expressed in the following way:

$$u_o = \underline{N}_m\,(x,y)\;\underset{\sim}{u}$$
$$v_o = \underline{N}_m\,(x,y)\;\underset{\sim}{v} \qquad (5.5)$$
$$w_o = \underline{N}_b\,(x,y)\;\underset{\sim}{w}$$

where

$\underline{N}_m$ = shape functions for in-plane displacements

$\underline{N}_b$ = shape function for bending displacements

and the vectors of nodal displacements are

$$\underset{\sim}{u}^T = \langle u_1\ u_2\ u_3 \rangle$$
$$\underset{\sim}{v}^T = \langle v_1\ v_2\ v_3 \rangle \qquad (5.6)$$
$$\underset{\sim}{w}^T = \langle w_1\ w_2\ w_3\ \theta_{x1}\ \theta_{x2}\ \theta_{x3}\ \theta_{y1}\ \theta_{y2}\ \theta_{y3} \rangle$$

The strain-displacement relationship is given by Eq. (2.4) (See sections 2.7 and 2.8) and combining it with Eq. (5.4) results in:

$$\underset{\sim}{\varepsilon} = \begin{Bmatrix} u_{,x} \\ v_{,z} \\ u_{,y} + v_{,x} \end{Bmatrix} = \begin{Bmatrix} u_{o,x} \\ v_{o,y} \\ u_{o,y} + v_{o,x} \end{Bmatrix} - z \begin{Bmatrix} w_{,xx} \\ w_{,yy} \\ 2w_{,xy} \end{Bmatrix} \qquad (5.7)$$

$$= \underset{\sim}{\varepsilon}_o - z\,\underset{\sim}{\chi}$$

where

$\underset{\sim}{\varepsilon}_o$ = in-plane strain vector at the reference surface

$\underset{\sim}{\chi}$ = curvature vector at the reference surface

By using Eq. (5.5) $\underset{\sim}{\varepsilon}_o$ and $\underset{\sim}{\chi}$ can be expressed as follows:

$$\underset{\sim}{\varepsilon}_o = \begin{bmatrix} \underline{N}_{m,x} & 0 \\ 0 & \underline{N}_{m,y} \\ \underline{N}_{m,y} & \underline{N}_{m,x} \end{bmatrix} \begin{Bmatrix} \underset{\sim}{u} \\ \underset{\sim}{v} \end{Bmatrix} = \underline{B}_m \, \underset{\sim}{r}_m \tag{5.8}$$

$$\underset{\sim}{\chi} = \begin{Bmatrix} \underline{N}_{b,xx} \\ \underline{N}_{b,yy} \\ 2\underline{N}_{b,xy} \end{Bmatrix} \underset{\sim}{w} = \underline{B}_b \, \underset{\sim}{r}_b \tag{5.9}$$

where

$$\underset{\sim}{r}_m^T = \langle \underset{\sim}{u}^T \; \underset{\sim}{v}^T \rangle$$

$$\underset{\sim}{r}_b = \underset{\sim}{w}$$

Equation (5.7) can now be rewritten by using Eqs. (5.8) and (5.9) as follows:

$$\underset{\sim}{\varepsilon} = \underline{B}_m \, \underset{\sim}{r}_m - z \, \underline{B}_b \, \underset{\sim}{r}_b = \underline{B} \, \underset{\sim}{r} \tag{5.10}$$

where

$$\underset{\sim}{r}^T = \langle \underset{\sim}{r}_m^T \; \underset{\sim}{r}_b^T \rangle$$

From Eq. (2.25) the element stiffness is calculated as:

$$\underline{K} = \int_V \underline{B}^T \underline{D} \, \underline{B} \, dV = \begin{bmatrix} \underline{K}_{mm} & \underline{K}_{mb} \\ \underline{K}_{bm} & \underline{K}_{bb} \end{bmatrix} \tag{5.11}$$

where

$\underline{K}_{mm}$ = membrane stiffness matrix

$$= \int_V \underline{B}_m \, \underline{C} \, \underline{B}_m \, dV$$

$$= \int_A \underline{B}_m^T \left[\int_h \underline{C} \, dz \right] \underline{B}_m \, dA \tag{5.12}$$

$$= \int_A \underline{B}_m^T \, \underline{D}_{mm} \, \underline{B}_m \, dA$$

$$\underline{K}_{bb} = \text{bending stiffness matrix}$$

$$= \int_V z^2 \, \underline{B}_b^T \, \underline{C} \, \underline{B}_b \, dV$$

$$= \int_A \underline{B}_b^T \left[\int_h z^2 \, \underline{C} \, dz \right] \underline{B}_b \, dA \qquad (5.13)$$

$$= \int_A \underline{B}_b^T \, \underline{D}_{bb} \, \underline{B}_b \, dA$$

$$\underline{K}_{bm} = \underline{K}_{mb}^T = \text{coupling stiffness matrix}$$

$$= \int_V - z \, \underline{B}_b^T \, \underline{C} \, \underline{B}_m \, dV$$

$$= \int_A \underline{B}_b^T \left[\int_h - z \, \underline{C} \, dz \right] \underline{B}_m \, dA \qquad (5.14)$$

$$= \int_A \underline{B}_b^T \, \underline{D}_{bm} \, \underline{B}_m \, dA$$

where

$\underline{D}$ = material matrices

A = triangular element area

h = element thickness

In the calculation of the stiffness matrix the components that have to be evaluated are the following: The strain-displacement matrices $\underline{B}_m$ and $\underline{B}_b$, which depend on the shape functions and are a function of the x & y-coordinates. The material matrices $\underline{D}_{mm}$, $\underline{D}_{bb}$ and $\underline{D}_{bm}$ which reflect the material constitutive relations. The stiffness matrix is generally evaluated by numerical integration. The matrices $\underline{B}_b$ and $\underline{B}_m$ will be discussed in more detail in sections 5.2.3 and 5.2.4.

To evaluate the material matrices, the reinforced concrete composite section is assumed to be made up of a system of concrete layers and "equivalent smeared" steel layers as illustrated in Fig. 5.6. The reinforcing steel is converted to a uniform layer with an equivalent thickness determined by:

$$t_s = A_s/b \tag{5.15}$$

where

A_s = area of one reinforcing bar

b = spacing of the bars

Due to the Kirchhoff assumption of normals to the reference surface remaining normal and straight, compatibility between adjacant layers of concrete and steel is maintained. Every layer is thus taken to be in a state of plane stress and it is assumed that no bond slip occurs between the steel and the concrete. The material matrix for each layer depends on its state of deformation according to the procedure detailed in Chapter 3. The material matrices for the element are obtained by summing the contribution of each layer in the following way:

$$\underline{D}_{mm} = \int_h \underline{C}\, dz = \sum_{i=1}^{c} \left(z_{i+1}-z_i\right) \underline{C}_{ci} + \sum_{j=1}^{s} \underline{C}_{sj}\, t_{sj} \tag{5.16}$$

$$\underline{D}_{bm} = \int_h - z\, \underline{C}\, dz = - \sum_{i=1}^{c} \frac{1}{2}\left(z_{i+1}^2 - z_i^2\right) \underline{C}_{ci} - \sum_{j=1}^{s} z_j\, \underline{C}_{sj}\, t_{sj} \tag{5.17}$$

$$\underline{D}_{bb} = \int_h z^2\, \underline{C}\, dz = \sum_{i=1}^{c} \frac{1}{3}\left(z_{i+1}^3 - z_i^3\right) \underline{C}_{ci} + \sum_{j=1}^{s} z_j^2\, \underline{C}_{sj}\, t_{sj} \tag{5.18}$$

where $\underline{C}_{ci}$ = material matrix for concrete layer i (Eq. 3.4))

$\underline{C}_{sj}$ = material matrix for steel layer j (Eq. (3.54))

c,s = number of concrete and steel layers

z_i, z_j = z-coordinates as shown in Fig. 5.6

t_{sj} = equivalent steel layer thicknesses

It should be noted that the sixth DOF, the rotation θ_z around the local z-axis, is not considered as a DOF in the above formulation. For a flat plate the global stiffness associated with this DOF will be zero, thus it must be constrained through the boundary conditions. In a shell this stiffness, for a number of nearly co-planar elements framing into a node, may be close to zero or negative. To prevent numerical problems in the solution of the equilibrium equations, a fictitious rotational stiffness about a normal to the shell surface at the node, may be provided by the use of a boundary element (section 5.2.5). It is suggested that the value of this rotational stiffness be taken to be about 10% of the bending stiffness of the shell [28]. This assures positive definiteness and also avoids ill-conditioning of the structural stiffness matrix. The latter problem could occur if a very large rotational stiffness is assigned to the boundary element and it contributes to more than one global DOF which produces large off-diagonal terms.

During the nonlinear analysis of flat plates Murray [45] ignored this DOF and obtained good results. For the analysis of slabs in the present study this DOF is also constrained through the boundary conditions. The discussion above therefore only concerns the analysis of shell-type structures.

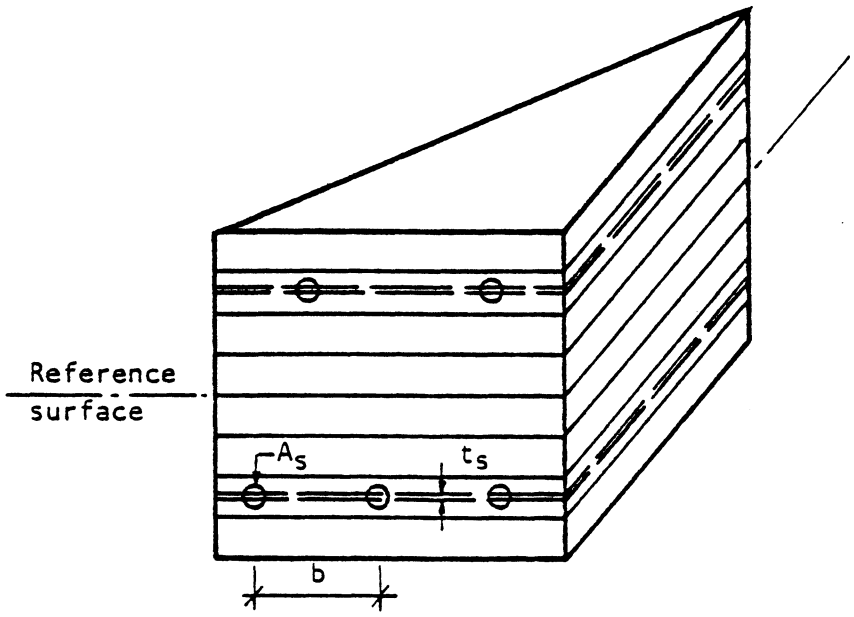

CONCRETE AND "EQUIVALENT SMEARED" STEEL LAYERS

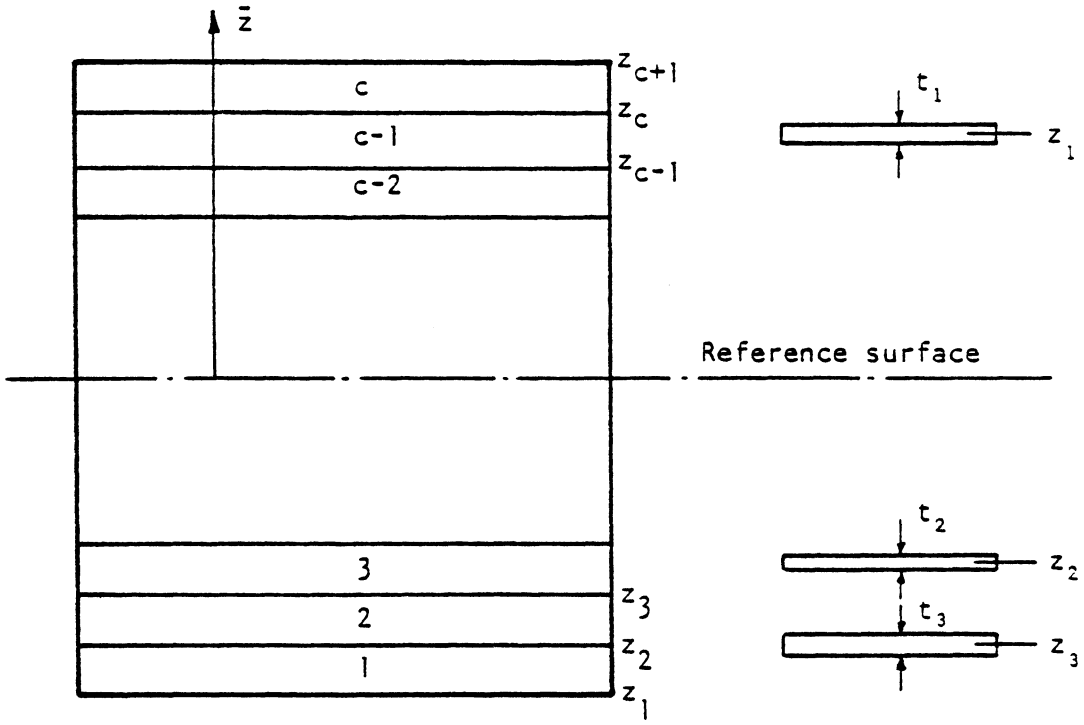

CONCRETE LAYERS STEEL LAYERS

FIG. 5.6 LAYER SYSTEM OF A TRIANGULAR ELEMENT

The shell element used in this study has good bending capability, but the inability of the CST to capture high stress gradients is its most severe shortcoming. For reinforced and prestressed concrete slabs the out-of-plane deflections are generally restricted to a maximum of about half the plate thickness at ultimate loads -- the membrane action should therefore not become a dominant factor. The advantages of the flat triangular element were discussed in section 5.2.1.

5.2.3 Triangular membrane element

The element used in this study is the well known CST with two DOF at each node, six per element. This type of element is used in plane stress analysis and it is used here to represent the membrane or in-plane action of a slab or panel.

Triangular coordinates are usually employed to express the variation of the shape functions over the element and details of this is available in any textbook on finite elements, for example that of Zienkiewicz [42]. The stiffness matrix is calculated from Eq. (5.12), while the material matrix for the layered composite material model used for reinforced concrete in this study can be found from Eq. (5.16).

For plane stress systems only in-plane forces are assumed to exist in the membrane element. Therefore a restriction is placed on the choice of the layer system -- the element properties must be symmetric about the reference surface. Generally the variation in material properties through the thickness can be ignored for thin concrete members and only one concrete layer may be used.

5.2.4 Triangular plate bending element

This element may be used for the analysis of flat slabs where the transverse bending of the slabs is the predominant load-carrying mechanism and no significant membrane forces are developed. This element is used to provide the plate bending part of the shell element as described in section 5.2.2 and more details of its formulation will be provided here.

Two triangular plate bending elements were developed by Irons and Razzaque [105,106] by employing derivative smoothing. The first element has twelve DOF (the transverse displacement and two rotational DOF at each corner node and the relative rotation of the midside normals), while the second has nine DOF (obtained by enforcing a linear variation of the normal slope along the element edges and thus leaving only the three DOF at each of the corner nodes). The shape functions $\underline{N}_b$ of the 'conforming displacement triangle' are given by Zienkiewicz [42] as consisting of the complete cubic polynomial terms and two additional independent rational functions (needed to ensure slope conformity). The second derivatives $\underline{N}_{b,ii}$ $(i = x,y)$, which are needed to evaluate $\underline{B}_b$ from Eq. (5.9), have singularities at the corners and a very high order of numerical integration is therefore necessary to obtain convergence. In an effort to find more economical but converging elements, Irons and Razzaque [106] substituted the true derivatives $\underline{N}_{b,ii}$ by pseudo-derivatives $\underline{N}^*_{b,ii}$, where $\underline{N}^*_{b,ii}$ are the least squares linear polynomial version of $\underline{N}_{b,ii}$. These smoothed second derivatives now only contain linear polynomial terms and the stiffness matrix (Eq. (5.13)) can thus be integrated by the three-point integration rule (the three midsides with equal weight).

The two elements converge for any mesh pattern and perform better than corresponding displacement elements. Details of the theory can be

found in references [105] and [107]. These elements are shown to compare favorably with other elements (specifically the HCT [108] or LCCT9 [104] triangle and the nonconforming triangle of Zienkiewicz [109] for various standard problems [106]). From a comparison of stiffness coefficients it was established that these synthetic elements, obtained with a displacement formulation, exactly simulate the hybrid elements developed by Allwood [110] and Allman [111].

In this study the nine DOF Irons-Razzaque element is used -- the shape functions and their derivatives are obtained from the subroutine SFGR provided in reference [106]. Employing this subroutine to calculate the strain-displacement matrix $\underline{B}_b$ and obtaining the material matrix $\underline{D}_{bb}$ from Eq. (5.18) the element stiffness matrix is evaluated from Eq. (5.13) by numerical integration.

The composite section is modeled as for the shell element where every layer is assumed to be in a state of plane stress. However, each layer will be in a different state of deformation and stress because of the variation of strain through the thickness due to bending. This will result in local failures in those layers where the stress or strain state has exceeded the failure criteria specified. Thus the layered system can trace the progressive cracking in reinforced concrete or the softening of the concrete at high compressive stress levels with the associated deterioration in stiffness.

It should be noted that the strains and stresses are evaluated at the integration points of the element -- thus at the midpoint of the sides of each triangular layer. The state at an integration point can be considered to represent the average state in the corresponding part of the triangle. When cracking is indicated at integration point 4, for

example, the whole shaded portion of the element is assumed to be cracked as shown in Fig. 5.5. (See p. 129.)

5.2.5 Boundary element

This element can be used for three purposes -- to limit nodal displacements or rotations to prescribed values, to compute support reactions, or to provide linear-elastic supports for nodes. The element was developed by Wilson [112].

The boundary element is defined by a single directed axis through the nodal point to which it is attached. It can be assigned a linear elastic extensional stiffness along the axis or a linear elastic rotational stiffness about the axis. The element stiffnesses are added directly to the structural stiffness matrix and thus have no effect on its size.

The forces in the boundary elements have to be included in the calculation of the internal resisting load vector as described in section 5.4.

5.3 EVALUATION OF THE GEOMETRIC STIFFNESS

Murray [45], in his study of the large deflection of plates, developed an expression for the "complete" geometric stiffness for the two-dimensional theory used to analyze shells, as is presented in Chapter 2. The "complete" geometric stiffness is derived from Eq. (2.29) and involves the in-plane, bending and shear stress resultants and thus also both the in-plane and bending shape functions. From a practical point of view, however, it is not necessary to evaluate this "complete" geometric stiffness since most of the terms are of higher order and can be neglected [45]. The most significant term reflects the effect of the in-plane

membrane stress resultants on the bending behavior. The geometric stiffness is therefore reduced to a matrix related only to the DOF represented by the displacement vector $\underset{\sim}{r}_b$ as follows.

$$\underset{\sim}{K}'_G = \int_A \sum_{\alpha=x,y} \sum_{\beta=x,y} \left[\underset{\sim}{N}_{b,\alpha} \; \underset{\sim}{N}_{\alpha\beta} \; \underset{\sim}{N}^T_{b,\beta} \right] dA \tag{5.19}$$

where

$\underset{\sim}{N}_b$ = shape function for bending deflections (Eq. (5.5))

$\underset{\sim}{N}_{\alpha\beta}$ = vector of membrane stress resultants

A = element area

When assembling the structural stiffness matrix zero submatrices are added to $\underset{\sim}{K}'_G$ to form the structural geometric stiffness $\underset{\sim}{K}_G$ and the incremental structural stiffness matrix is then given by Eq. (2.30) as:

$$\underset{\sim}{K}_I = \underset{\sim}{K} + \underset{\sim}{K}_G$$

As was pointed out in section 2.7, the geometric stiffness is not essential to perform an analysis, but its use generally speeds up convergence, and it is therefore advantageous to include it in any analysis in which geometric nonlinearities are to be considered.

5.4 GENERAL SOLUTION ALGORITHM

To trace the nonlinear and time-dependent behavior of reinforced and prestressed concrete structures due to material and geometric nonlinearities and the effects of time-dependent phenomena like creep and shrinkage of concrete, an incremental formulation of the FEM, coupled with a step-by-step integration scheme through the time domain, is employed in this

study. For each time step, an incremental load procedure combined with constant or tangent stiffness iterations in each load step, is used to find the load-displacement path of a structure based on equilibrium considerations.

The time period over which the response history of the structure is to be traced is divided into n time steps: $\Delta t_1, \Delta t_2, \ldots, \Delta t_n$ as shown in Fig. 5.7. Any changes in external loads are assumed to occur only at the beginning or end of the time steps, i.e., at times $t_1, t_2, \ldots, t_{n+1}$. During a time step the external loads are therefore assumed to remain constant. The external loads applied at a particular time, may be sub-divided into a number of equal load steps to obtain a more detailed load-deflection path. Consider for example $\underset{\sim}{R}_1$, the external load vector applied at time t_1 as shown in Fig. 5.7. It is divided into three load steps of $\Delta\underset{\sim}{R}_1$. The structure is then analyzed for each load step by an iterative approach and the increments calculated in the field variables (displacements, strains, stresses) are added to the previous totals to evaluate the current state in the structure. After all the load increments from the applied loads have been dealt with, the analysis for the effects of creep, shrinkage, temperature and relaxation from the current time to the next, i.e., for time step Δt_1 at time t_1, for example, are carried out. It is again possible to divide the time-dependent load vector into a number of equal load steps. A procedure similar to the one described above for externally applied loads is then utilized to find the equilibrium position of the structure at the beginning of the next time step (time t_2).

An algorithm, outlining the basic steps of the method of analysis can be summarized as follows:

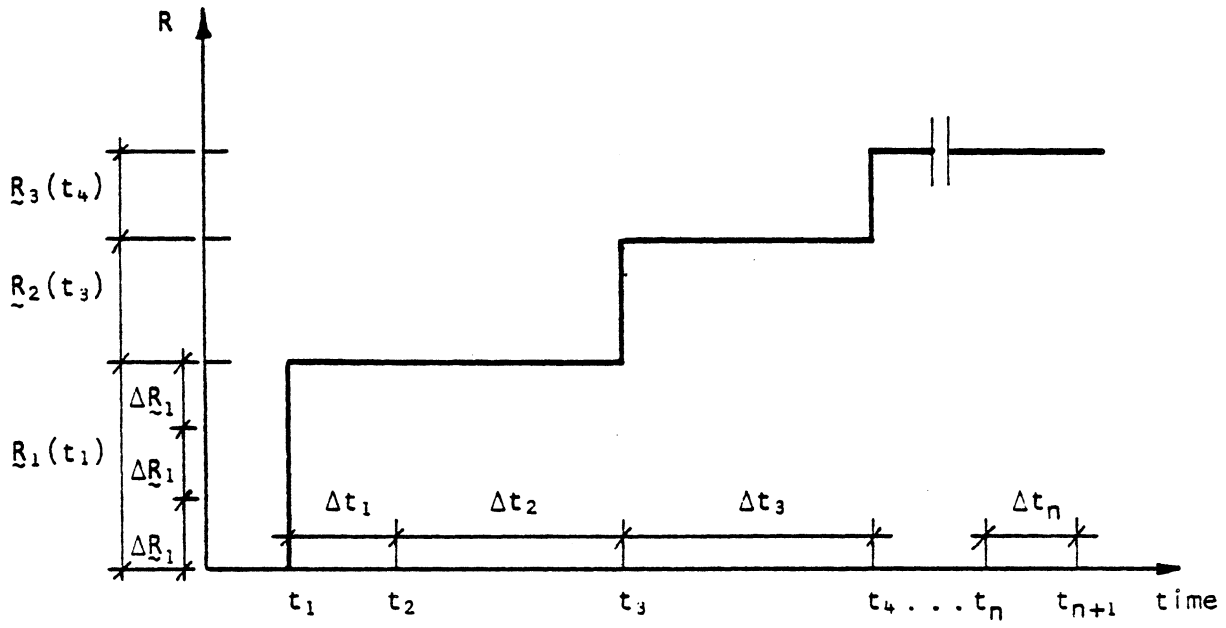

a. EXTERNAL LOAD HISTORY

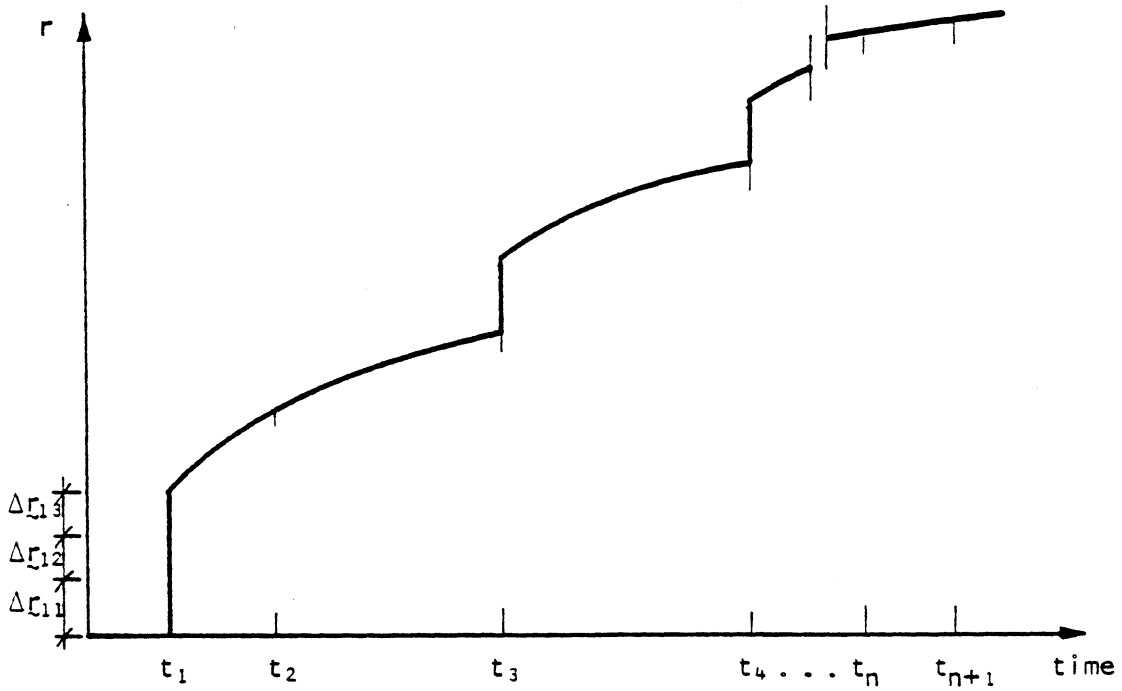

b. DISPLACEMENT HISTORY

FIG. 5.7 SCHEMATIC RESPONSE HISTORY OF A STRUCTURE DUE TO EXTERNAL LOADS, CREEP AND SHRINKAGE EFFECTS

1. Read the control parameters specifying the problem size, convergence criteria and the type of analysis to be performed.

2. Specify the structure geometry, material properties, element particulars and prestressing tendon data (if applicable). Form the element load vectors.

3. Read the load control card for the current time t_i and time step Δt_i $(\Delta t_i = t_{i+1} - t_i)$. Form the applied load vector $\underset{\sim}{R}_i$ and the load step vector $\Delta\underset{\sim}{R}_i$ for time t_i.

4. Increment the current total external load vector $\underset{\sim}{R}_E^j$ and form the structural load vector $\Delta\underset{\sim}{R}^j$ for this iteration:

$$\underset{\sim}{R}_E^j = \underset{\sim}{R}_E^{j-1} + \Delta\underset{\sim}{R}_i \tag{5.20}$$

$$\Delta\underset{\sim}{R}^j = \underset{\sim}{R}_u^{j-1} + \Delta\underset{\sim}{R}_i \tag{5.21}$$

where

j = iteration number

$j = 0$ means the last value from the previous load step

$\underset{\sim}{R}_u^{j-1}$ = unbalanced load vector

$\underset{\sim}{R}_E$ is incremented only for external loads and $\underset{\sim}{R}_E^0 = \underset{\sim}{R}_u^0 = \underset{\sim}{0}$ at the start of the problem.

5. Form the element stiffness matrices, assemble the structural stiffness matrix $\underset{\sim}{K}^j$ and triangularize it. This step may be omitted through the use of a control parameter for iterations other than the first of each load step.

6. Solve the set of equations

$$\underset{\sim}{K}^j \, \Delta\underset{\sim}{r}^j = \Delta\underset{\sim}{R}^j \tag{5.22}$$

by back substitution to find the displacement increment $\Delta\underset{\sim}{r}^j$. Check convergence if the displacement norm is used and calculate current total deflections:

$$\underset{\sim}{r}^j = \underset{\sim}{r}^{j-1} + \Delta\underset{\sim}{r}^j \tag{5.23}$$

7. For each element calculate the local deflection increment and the corresponding strain and stress increments. Update the material matrix, calculate current total strains and stresses, and calculate the element resisting forces based on the current state.

8. Transform all the element resisting forces to the global coordinate system and assemble the current structural internal resisting force vector $\underset{\sim}{R}_I^j$. The unbalanced force vector is given by:

$$\underset{\sim}{R}_U^j = \underset{\sim}{R}_E^j - \underset{\sim}{R}_I^j \tag{5.24}$$

Check the force convergence if the force norm is used.

9. If convergence has not been obtained, go back to step 5 and repeat steps 5 thru 8 until convergence is achieved or the maximum number of iterations allowed is reached. If the equilibrium state has been found, continue to step 10, or if the solution diverges, stop the calculations.

10. If this is not the last load step for the current time, go back to step 4 and repeat steps 4 thru 9. When it is the last load step,

continue to step 11 if external loads were considered and to step 13 in the case of time-dependent loads. When the time-dependent analysis is omitted, continue to step 13.

11. Calculate the material properties at the end of the time step, i.e., for time t_{i+1} . For each element the creep, shrinkage and temperature strains are calculated and equivalent nodal loads calculated by treating these strains as initial strains.

12. Assemble the structural time-dependent load vector $\underset{\sim}{R}_{Ti}$ and calculate the load step vector $\Delta\underset{\sim}{R}_{Ti}$. Go to step 4 and repeat steps 4 thru 9.

13. If time t_i is the last time the solution is terminated, otherwise go back to step 3 and continue the analysis for the next time step.

Most of the steps in the algorithm are standard procedures used in any computer program employing the FEM, but a few of the complex aspects that deal with the procedures developed and used in this study, will be discussed in more detail. The treatment of the prestressing is dealt with in Chapter 4, while the calculation of the local displacement increments for large deflections and the state determination in the concrete layers mentioned in step 7 will be discussed in sections 5.5 and 5.6 respectively. The manner in which the time-dependent load vector is calculated (step 11) will be presented in section 5.7.

5.5 NONLINEAR GEOMETRY -- CALCULATION OF LOCAL DISPLACEMENTS

As described in Chapter 2 an Updated Lagrangian approach is used in this study. This means that the last configuration of the structure is assumed to be the reference configuration for any subsequent deformation. When large deflections are taken into account, a displaced position for the structure must be established in this configuration. In order to evaluate the element resisting forces in the displaced configuration, it is necessary to evaluate the element deformations in the displaced element local coordinate system, since nodal displacements and rotations are assumed to be small with respect to the local coordinate system.

To describe the procedure used to find the element deformations in the displaced local coordinate system, consider a typical triangular element, shown in Fig. 5.8 and the displacements it has undergone in going from state 1 to state 2. The displaced local coordinate system (xyz) of state 2 is found by passing a plane through the new locations (1",2",3") of the nodes. The local coordinate system ($\bar{x}\bar{y}\bar{z}$) of state 1 has therefore just undergone rigid body translations and rotations, and so has the undeformed element represented in the displaced coordinate system by nodes (1',2',3').

In the computer program three possibilities of establishing the relationship between the element local coordinate systems and the global coordinate system are provided as shown in Fig. 5.9. The first option is to let the local $\bar{x}$-axis coincide with the direction of vector $\underset{\sim}{IJ}$ (Fig. 5.9). During the analysis this relationship is maintained, thus providing a consistent reference plane for the element throughout the analysis. In the other two options the angle between the global X-axis and the projection of either the local $\bar{x}$-axis or the local $\bar{y}$-axis on the global XY-plane

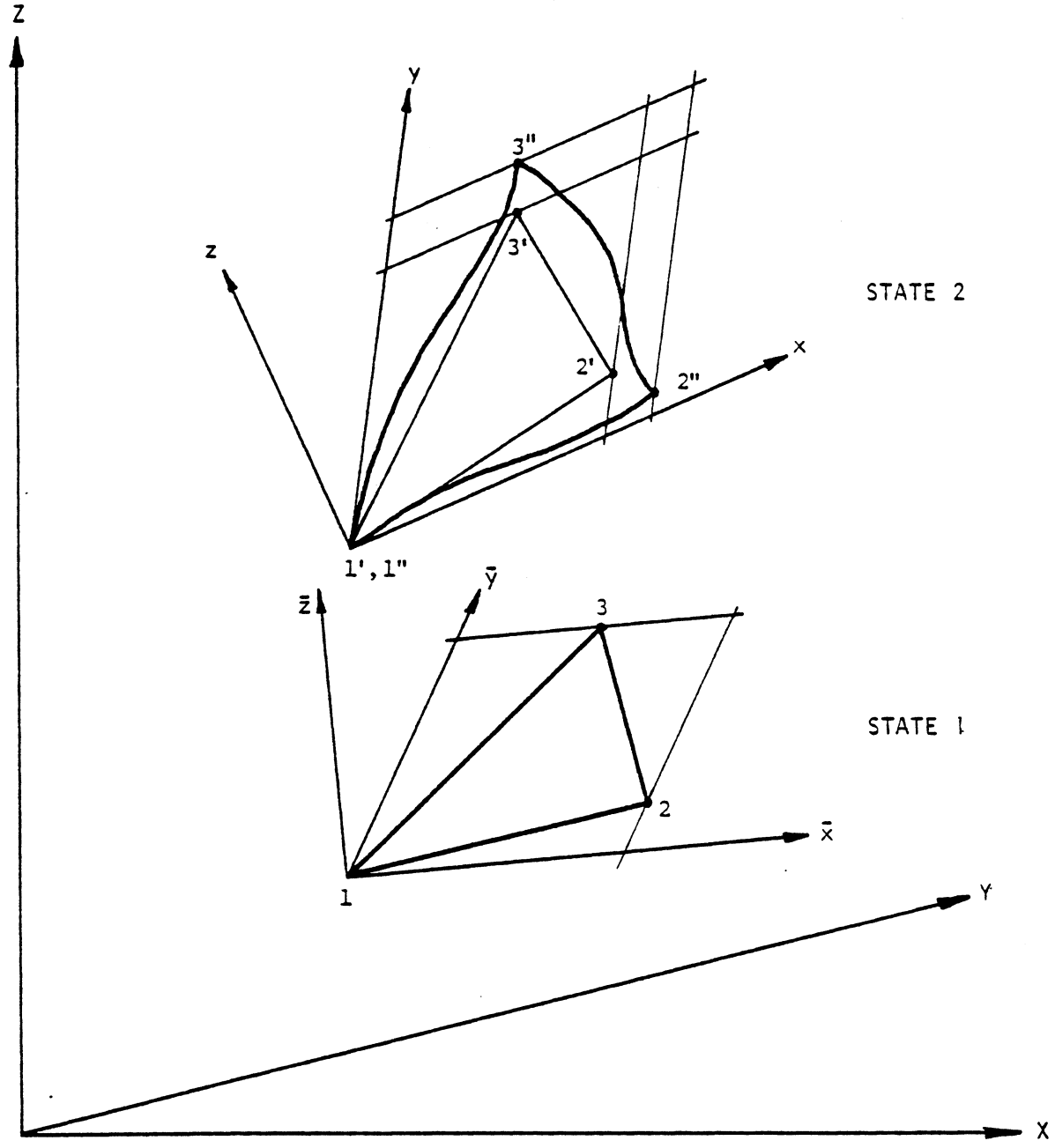

FIG. 5.8 TRIANGULAR ELEMENT BEFORE AND AFTER DEFORMATION

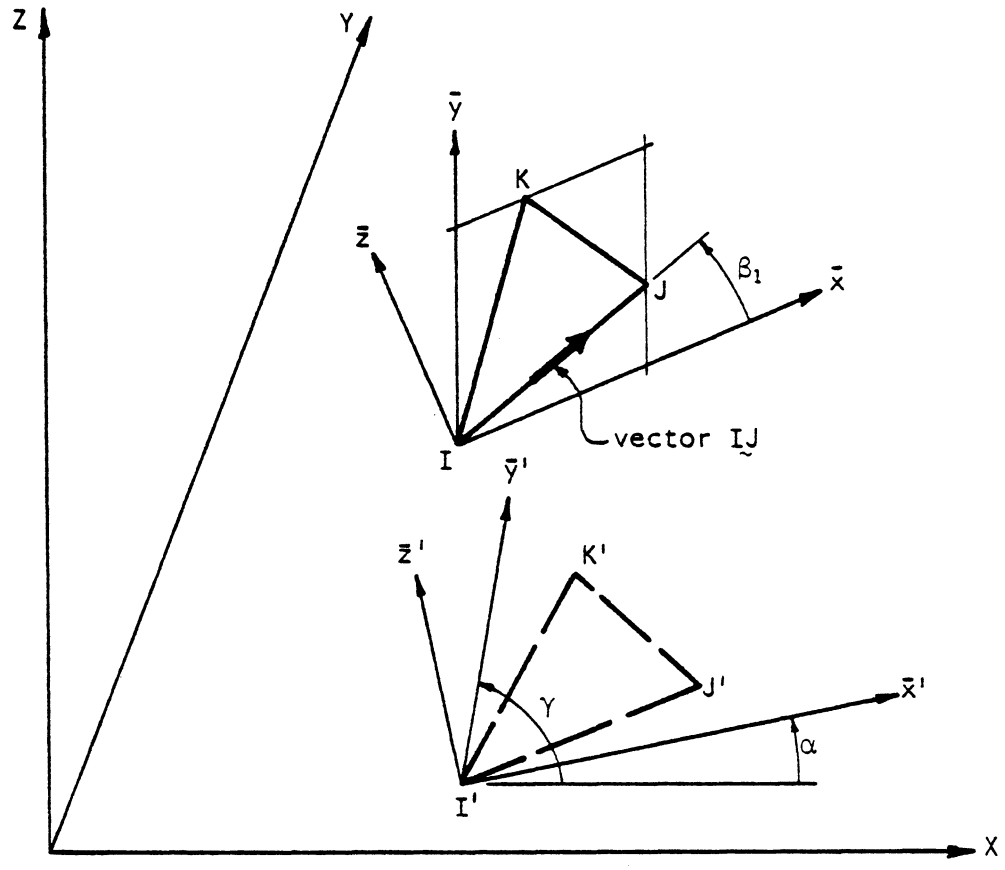

XYZ = Global coordinate system

$\bar{x}\bar{y}\bar{z}$ = Local element coordinate system

ΔIJK = Element with nodes IJK

ΔI'J'K' = ΔIJK projected on global XY plane

$\bar{x}'\bar{y}'\bar{z}'$ = Projection of $\bar{x}\bar{y}\bar{z}$ on XY plane

CASE 1 : LOCO = 0 $\bar{x}$ coincides with IJ

CASE 2 : LOCO = 1 $\bar{x}$ is defined by specifying α

CASE 3 : LOCO = 2 $\bar{y}$ is defined by specifying γ

FIG. 5.9 DEFINITION OF LOCAL ELEMENT COORDINATE SYSTEM

is specified. For these two cases the initial angle β_1 between the local $\bar{x}$-axis and the vector $\underset{\sim}{IJ}$ in the local coordinate system is calculated (See Fig. 5.9). In any subsequent configuration of the element, the angle between the local x'-axis and vector $\underset{\sim}{IJ}$ is kept constant at β_1 and this relationship is used to establish the local coordinate system in the new configuration.

The local in-plane and bending displacements are found in the following manner, using a procedure similar to that employed by Horrigmoe [113] in his finite element study on the stability of free-form shells.

In-plane displacements

From the updated global coordinates of the element nodes in state 2, and the transformation between the coordinate systems, the local coordinates $\underset{\sim}{x}^2$ of the deformed element can be calculated in state 2. The current total membrane displacements $\underset{\sim}{r}_\ell^2$ of the element is then found by taking the difference between the local coordinates in state 2 and the local coordinates $\underset{\sim}{x}^0$ of the undeformed element.

$$\underset{\sim}{r}_\ell^2 = \underset{\sim}{x}^2 - \underset{\sim}{x}^0$$

The local membrane displacement increment $\Delta\underset{\sim}{r}_\ell^2$, going from state 1 to state 2, is then obtained by deducting the previous total membrane displacement of state 1, $\underset{\sim}{r}_\ell^1$, from the current total:

$$\Delta\underset{\sim}{r}_\ell^2 = \underset{\sim}{r}_\ell^2 - \underset{\sim}{r}_\ell^1 \qquad (5.25)$$

Bending displacements

Since the new local coordinate system is taken as a plane through the updated nodal positions, the transverse displacements at the corner

nodes are zero. The bending deformation of the element is therefore obtained from the rotational displacement increments only. These have to be adjusted for the rigid body rotations that the element goes through in moving from state 1 to state 2. Since finite rotations cannot be arbitrarily transformed between coordinate systems, great care must be exercised when they have to be added or subtracted. The reference coordinate system used in this case is the local coordinate system of state 1. (The superscript will be used to show to which local coordinate system the variables are referred to.)

The rotational displacement increment $\Delta \underset{\sim}{r}_r$ in the global coordinate system, obtained from the solution of the equilibrium equations, is transformed to the local coordinate system of state 1:

$$\Delta \underset{\sim}{\theta}^1_{\ell r} = \underline{T}_1 \, \Delta \underset{\sim}{r}_r$$

where

$\Delta \underset{\sim}{\theta}^1_{\ell r}$ = uncorrected rotational increment from state 1 to state 2, referred to state 1

$\underline{T}_1$ = orthogonal transformation matrix relating the global and local 1 coordinate systems

The rigid body rotations β_x and β_y, that the element undergoes from state 1 to state 2, referred to state 1 is obtained by calculating the angles through which the local $\bar{y}_1$-axis and the local $\bar{x}_1$-axis, respectively, have rotated. The true rotational displacement increment $\Delta \underset{\sim}{\theta}^1_{\ell}$ is then found as:

$$\Delta \underset{\sim}{\theta}^1_{\ell} = \Delta \underset{\sim}{\theta}^1_{\ell r} - \underset{\sim}{\beta} \tag{5.26}$$

The new total rotational displacement for the element in state 2, but referred to state 1, is calculated as:

$$\underset{\sim}{\theta}^{1}_{\ell 2} = \underset{\sim}{\theta}^{1}_{\ell 1} + \Delta\underset{\sim}{\theta}^{1}_{\ell} \tag{5.27}$$

where

$\underset{\sim}{\theta}^{1}_{\ell 1}$ = previous total rotational deformation in state 1

Then the total rotational displacement in state 2, referred to state 2, can be obtained by a transformation:

$$\underset{\sim}{\theta}^{2}_{\ell 2} = \underset{=}{T}_{21}\ \underset{\sim}{\theta}^{1}_{\ell 2}$$

where

$\underset{=}{T}_{21}$ = transformation matrix relating local coordinate systems 1 and 2

Since the total rotational displacement of state 1 moves with the element to state 2, the rotational displacement increment in state 2 is found as:

$$\Delta\underset{\sim}{\theta}^{2}_{\ell} = \underset{\sim}{\theta}^{2}_{\ell 2} - \underset{\sim}{\theta}^{1}_{\ell 1} \tag{5.28}$$

The strain and stress state in the element is calculated by using the local element displacements in the displaced local coordinate system as obtained from Eqs. (5.25) and (5.28). The rest of the analysis is then performed as described in section 5.4.

5.6 STATE DETERMINATION IN THE CONCRETE LAYERS

The material behavior of concrete is characterized by a nonlinear constitutive relationship for a state of biaxial stress as described in Chapter 3. The model incorporates tensile cracking, tension stiffening after cracking, the stress-induced orthotropic behavior of concrete under biaxial stress, strain softening at high stress levels and stress reversals.

The state determination procedure is similar to that used by Kabir [28] -- the main difference being the way the unbalanced load vector is calculated.

As described in section 5.4 an incremental load procedure combined with equilibrium iterations is employed to trace the nonlinear response of the structure. For each iteration a linear stress-strain relationship is assumed, the displacement increment calculated, the strain and stress state determined and the material matrix updated. The following steps are used to estimate the actual state of strain and stress in concrete layer k of an element for iteration j :

1. The vector of displacement increments $\Delta \underset{\sim}{r}^j$ is obtained by solving the equilibrium equations as described in section 5.4. The vector of local displacement increments $\Delta \underset{\sim}{r}_\ell^j$ for the element is calculated.

2. The strain increment in concrete layer k of the element is then obtained as:

$$\Delta \underset{\sim}{\varepsilon}_k^j = \underline{B}_k \, \Delta \underset{\sim}{r}_\ell^k \tag{5.29}$$

where

$\underline{B}_k$ = current strain displacement matrix for layer k

The current total strain vector then is:

$$\underset{\sim}{\varepsilon}_k^j = \underset{\sim}{\varepsilon}_k^{j-1} + \Delta \underset{\sim}{\varepsilon}_k^j \tag{5.30}$$

3. Approximate stress increments in the layer are then calculated as:

$$\Delta \underset{\sim}{\bar{\sigma}}_k^j = \underline{C}_k^{j-1} \, \Delta \underset{\sim}{\varepsilon}_k^j \tag{5.31}$$

where $\underset{\sim}{C}_k^{j-1}$ = linearized plane stress orthotropic material matrix from the previous iteration (Eq. (2.36))

The stress increments are only approximate because of the linearized material matrix. The current total approximate stresses are then calculated as:

$$\bar{\underset{\sim}{\sigma}}_k^j = \underset{\sim}{\sigma}_k^{j-1} + \Delta\bar{\underset{\sim}{\sigma}}_k^j \tag{5.32}$$

4. From the total approximate stresses the approximate principal stresses $\bar{\sigma}_{1k}^j$ and $\bar{\sigma}_{2k}^j$ are calculated. Because of the linearized constitutive relationship these are estimates of the principal stresses and 1 and 2 are the approximate principal directions.

5. The increments in the equivalent uniaxial strains are then calculated from Eq. (3.8) as:

$$\begin{aligned} \Delta\varepsilon_{1uk}^j &= \left(\bar{\sigma}_{1k}^j - \sigma_{1k}^{j-1}\right)/E_1^{j-1} \\ \Delta\varepsilon_{2uk}^j &= \left(\bar{\sigma}_{2k}^j - \sigma_{2k}^{j-1}\right)/E_2^{j-1} \end{aligned} \tag{5.33}$$

where

$\sigma_{1k}^{j-1}, \sigma_{2k}^{j-1}$ = principal stresses from the previous iteration

E_1^{j-1}, E_2^{j-1} = tangent moduli from the previous iteration

The total equivalent uniaxial strains are then obtained as follows.

$$\begin{aligned} \varepsilon_{1uk}^j &= \varepsilon_{1uk}^{j-1} + \Delta\varepsilon_{1uk}^j \\ \varepsilon_{2uk}^j &= \varepsilon_{2uk}^{j-1} + \Delta\varepsilon_{2uk}^j \end{aligned} \tag{5.34}$$

where

$\varepsilon_{1uk}^{j-1}, \varepsilon_{2uk}^{j-1}$ = total equivalent uniaxial strains from the previous iteration

6. Determine the biaxial stress ratio:

$$\alpha_k^j = \bar{\sigma}_{1k}^j \; / \; \bar{\sigma}_{2k}^j \tag{5.35}$$

Using α_k^j and the concrete properties E_o, f'_c, f'_t and ε_c the equivalent uniaxial curve C_k^j can be drawn (section 3.2.4) as shown in Fig. 5.10.

7. The principal stresses σ_{1k}^j and σ_{2k}^j corresponding to ε_{1uk}^j and ε_{2uk}^j are calculated from Eqs. (3.4) and (3.5) as shown in Fig. 5.10. The material matrix is also updated to reflect the new tangent moduli. The current total stress vector $\underset{\sim}{\sigma}_k^j$ is obtained by transforming the principal stresses to the element axes.

8. The vector of internal resisting forces for each element is now obtained from Eq. (2.27d) by:

$$\underset{\sim}{R}_{Ie} = \sum_{k=1}^{c} \int_{V_k} \underset{\sim}{B}_k^T \, \underset{\sim}{\sigma}_k^j \, dV \tag{5.36}$$

where

V_k = volume of the layer

$\sum_{k=1}^{c}$ = sum over the concrete layers

All the element vectors are transformed to the global coordinate system and the structural vector of internal resisting forces assembled.

The unbalanced force vector can now be calculated and the solution procedure continued as described in section 5.4.

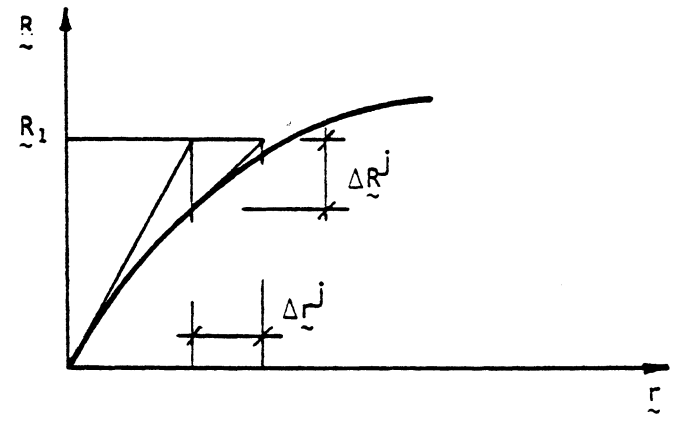

a. LOAD-DEFLECTION CURVE

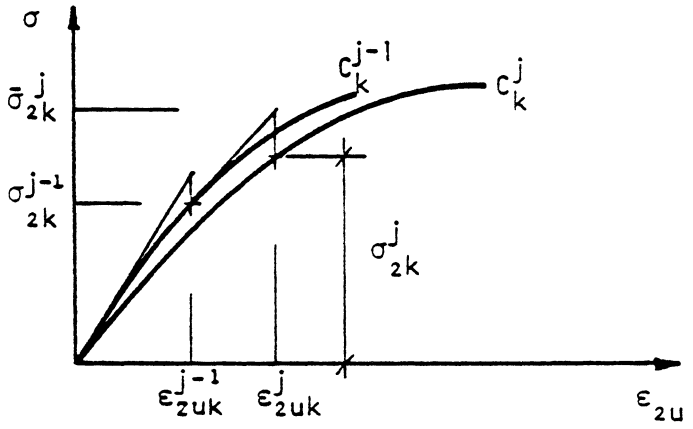

b. EQUIVALENT UNIAXIAL STRESS-STRAIN CURVE--
PRINCIPAL DIRECTION 2

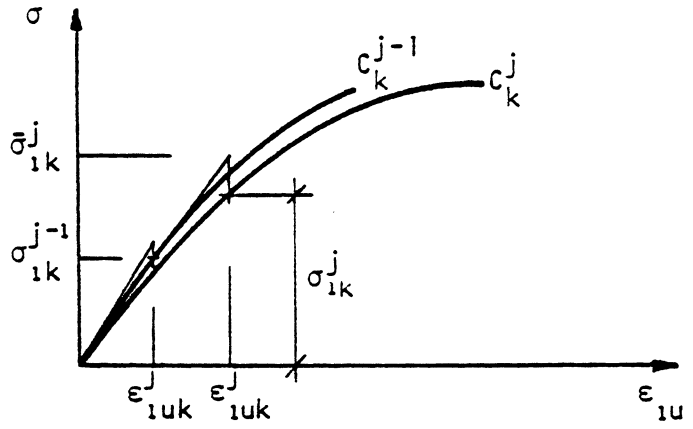

c. EQUIVALENT UNIAXIAL STRESS-STRAIN CURVE--
PRINCIPAL DIRECTION 1

FIG. 5.10 STATE DETERMINATION IN A CONCRETE LAYER

5.7 SOLUTION PROCEDURE FOR TIME-DEPENDENT EFFECTS

A step-by-step integration scheme in the time domain is employed to analyze the effects of time-dependent phenomena such as creep, shrinkage in concrete, relaxation of the prestressing steel and temperature changes on the behavior of reinforced and prestressed concrete structures. The nonlinear response of the structure is traced over a time period by dividing it into a number of smaller time steps. An initial strain approach as described by Zienkiewicz [42] and also used by Kabir [28] is adopted to determine the response of the structure due to the time-dependent strain increments occurring during a time step. This procedure is presented below for time step Δt_i ($\Delta t_i = t_{i+1} - t_i$, Fig. 5.7).

1. It is assumed that all external loads are applied at time t_i and then kept constant for time step Δt_i. The current total values of the field variables in all the elements are found from the analysis of the structure for these loads. The creep, shrinkage and relaxation laws are specified with the material properties.

2. By assuming that the stress state, determined in step 1, remains constant for the time step, calculate the strain increments due to creep, shrinkage and temperature changes occurring in each concrete layer -- details of the procedure can be found in Chapter 3. This results in the following for concrete layer k :

$$\Delta\underset{\sim}{\varepsilon}_{ok} = \Delta\underset{\sim}{\varepsilon}_k^c + \Delta\underset{\sim}{\varepsilon}_k^s + \Delta\underset{\sim}{\varepsilon}_k^T \tag{5.37}$$

where

$\Delta\underset{\sim}{\varepsilon}_k^c, \Delta\underset{\sim}{\varepsilon}_k^s, \Delta\underset{\sim}{\varepsilon}_k^T$ = vectors of the creep, shrinkage and temperature strain increments in layer k for time step Δt_i

$\Delta\underset{\sim}{\varepsilon}_{ok}$ = vector of initial strain increments, similar to $\underset{\sim}{\varepsilon}_o$ in Eq. (2.21)

3. By using Eq. (2.27c) the equivalent nodal forces produced by the initial strain increment can be calculated as:

$$\underset{\sim}{R}_{\varepsilon e} = \sum_{k=1}^{c} \int_A \underline{B}_k^T \underline{D}_k \, \Delta\underset{\sim}{\varepsilon}_{ok} \, dA \qquad (5.38)$$

where

$\underline{D}_k$ = material matrix for the concrete layer at time t_{i+1}

These element load vectors are then transformed to the global coordinate system and the structural load vector $\underset{\sim}{R}_{\varepsilon i}$ due to the time-dependent strains assembled.

4. When prestressing is involved, the force changes in the tendon segments in each element, due to the relaxation of the prestressing steel, are calculated as indicated in section 4.8. A structural load vector $\underset{\sim}{R}_{pi}$ is assembled from all the element load vectors.

5. The structural time-dependent load vector is then given by:

$$\underset{\sim}{R}_{Ti} = \underset{\sim}{R}_{\varepsilon i} + \underset{\sim}{R}_{pi} \qquad (5.39)$$

and the structure analyzed as described in section 5.4. The element stiffness matrices are formed using the concrete material properties at time t_{i+1}.

6. From the displacement increment $\Delta\underset{\sim}{r}^j$, the local displacement increment for the element and the corresponding strain increment $\Delta\underset{\sim}{\varepsilon}_k^j$ in concrete layer k, is calculated in the usual way.

7. The vector of stress increments in the concrete layer is calculated from Eq. (2.21), for the first iteration only, as follows:

$$\Delta\underset{\sim}{\sigma}_k^1 = \underline{C}_k\left(\Delta\underset{\sim}{\varepsilon}_k^1 - \Delta\underset{\sim}{\varepsilon}_{ok}\right) \tag{5.40}$$

For all subsequent iterations, since the initial strains have been accounted for, this becomes:

$$\Delta\underset{\sim}{\sigma}_k^j = \underline{C}_k\ \Delta\underset{\sim}{\varepsilon}_k^j, \quad j \neq 1$$

8. The current total values of all the field variables are then calculated, convergence checked and the solution completed for time step Δt_i as described in section 5.4.

At time t_{i+1} an equilibrium position for the structure, due to the applied load history and including the effect of the time-dependent behavior of the concrete and the prestressing steel up to time t_{i+1}, is therefore found.

5.8 CONVERGENCE CRITERIA

For the iterative technique employed in this study to trace the non-linear behavior of a structure as described in section 5.4, convergence criteria are used to determine whether an equilibrium structural configuration has been achieved. The convergence criteria are set such that iterations are terminated when the change in the state of the structure for an iteration is deemed to be so small that additional iterations would not improve the solution significantly. The major reason for doing this is to avoid unnecessary calculations and thus keep the analysis cost down.

To determine whether the solution is close enough to the equilibrium position, two measures can be used. The first is the amount by which equilibrium is violated, reflected in the magnitude of the unbalanced load vector and called the force norm. The second possibility is to assess the accuracy of the total displacement vector. This can be done by looking at the magnitude of the last displacement increment and is called the displacement norm.

Both these convergence criteria are used in the present study and each is based on the maximum norm of a vector as follows.

Displacement norm

From the vector of nodal displacement increments for iteration j, $\Delta \underset{\sim}{r}^j$, the maximum absolute values of any translational displacement or rotation increments are determined.

$$\begin{aligned} \Delta d &= \max |\Delta \underset{\sim}{r}_d^j| \\ \Delta \theta &= \max |\Delta \underset{\sim}{r}_r^j| \end{aligned} \tag{5.41}$$

where

Δd = maximum translational displacement increment (absolute value)

$\Delta \theta$ = maximum rotation increment (absolute value)

$\Delta \underset{\sim}{r}_d^j$ = vector of translational displacement increments only

$\Delta \underset{\sim}{r}_r^j$ = vector of rotation increments only

For convergence the following is required:

$$\begin{aligned} \Delta d &\leqslant t_d \\ \Delta \theta &\leqslant t_r \end{aligned} \tag{5.42}$$

where t_d = convergence tolerance for translational displacements

t_r = convergence tolerance for rotations

Two ways of specifying the convergence tolerances are provided in the computer program. In the first case absolute values must be specified. For the second option the tolerances are specified to be a fraction of the maximum components of the vector of displacement increments obtained for the first iteration of a load step.

To be able to prevent overshoot, which can lead to instability during nonlinear geometric analysis (for tension stiffening or snap-through problems), an upper limit is set on the displacement increments. This is used in the following way:

$$f = \max\left(\Delta d/V_d,\ \Delta\theta/V_r\right) \tag{5.43}$$

where

f = ratio of displacement increment to upper limit

V_d = upper limit on translational displacements

V_r = upper limit on rotations.

When $f > 1$ the vector of displacement increments are divided by f -- this means that the maximum displacement increment equals the upper limit.

$$\Delta\underset{\sim}{r}^{js} = \Delta\underset{\sim}{r}^{j}/f \tag{5.44}$$

The scaled-down displacement increment vector $\Delta\underset{\sim}{r}^{js}$ is then used to determine the state in the elements.

Force norm

Here a procedure similar to the one used above for displacement convergence is employed. When the second option of specifying the convergence tolerances is used, the tolerances are calculated as a fraction of the maximum components of the applied load vector for the load step. In the case of the force norm the solution is terminated when the upper limits are exceeded, since it is assumed that the solution then diverges.

In addition to the convergence tolerances described above, a ceiling is put on the number of iterations allowed for each load step in case the convergence tolerances have been set too stringently.

5.9 COMPUTER PROGRAM

A computer program has been developed to carry out the analysis of structures utilizing the method which has been described in this study. The program is used to trace the load-deformation response of thin reinforced and prestressed concrete structures, particularly slabs and panels, through the elastic, inelastic and up to the ultimate ranges. The nonlinear stress-strain relationship and cracking of concrete can be modeled. The response of the structure under short-term or sustained loads, during which time-dependent effects such as creep, shrinkage and temperature history could be important, can be simulated. The stress and strain states in the different materials at any stage of the response history are also determined.

The program is coded in FORTRAN IV language and has been tested on the CDC 6400 computer of the University of California, Berkeley computer center. An overlay structure is employed for the program and the blank common dynamically dimensioned within the program to fit the memory

requirements of the problem under consideration. This makes the efficient use of the available central memory capacity of the computer possible and thus minimizes computer expenses.

The overlay structure of the program is shown in Fig. 5.11. The main program NOPARC (NOnlinear analysis of Prestressed And Reinforced Concrete structures) with the accompanying subroutines, called the root, stays in memory while the six links of the primary level are called in the sequence indicated in Fig. 5.12, where a flow diagram of the logical structure of NOPARC is presented. The program is structured such that additional elements could be added easily, if desired. The equation solving is done by Gaussian elimination and the equation solver adapted to solve symmetric banded matrices by triangularization and then back substitution in two separate operations. The functions of each of the links will be described briefly:

Main program: NOPARC

It controls the overall solution procedure by calling the primary links. The subroutines accompanying it in the root are called by more than one of the links, for example MLONG resets the central memory field length to the amount required in each link.

Link 1: PINPUT

All the data for the problem, except for the loads, is read and some preliminary calculations performed. The prestressing tendon layout is reduced to find the tendon segments associated with each element.

Link 2: PLOAD

The load control card and externally applied loads are read. The external load and load step vectors for the time is formed.

Link 3: ELSTIF

This primary link calls secondary links -- each secondary link containing the subroutines to form the element stiffness matrix and the element load vectors for a specific type of element.

Link 4: FORMK

The structural stiffness matrix is assembled.

Link 5: ESOLVE

The equilibrium equations are solved by triangularizing the structural stiffness matrix and then back substituting to find the displacement increment due to the load vector.

Link 6: STATE

In this link the strain and stress state in the structure is determined, the unbalanced load vector calculated, convergence checked, the time-dependent load vector calculated and the results of the analysis output as specified by the control parameters.

A detailed description of the input and output for the program is presented in Appendix B.

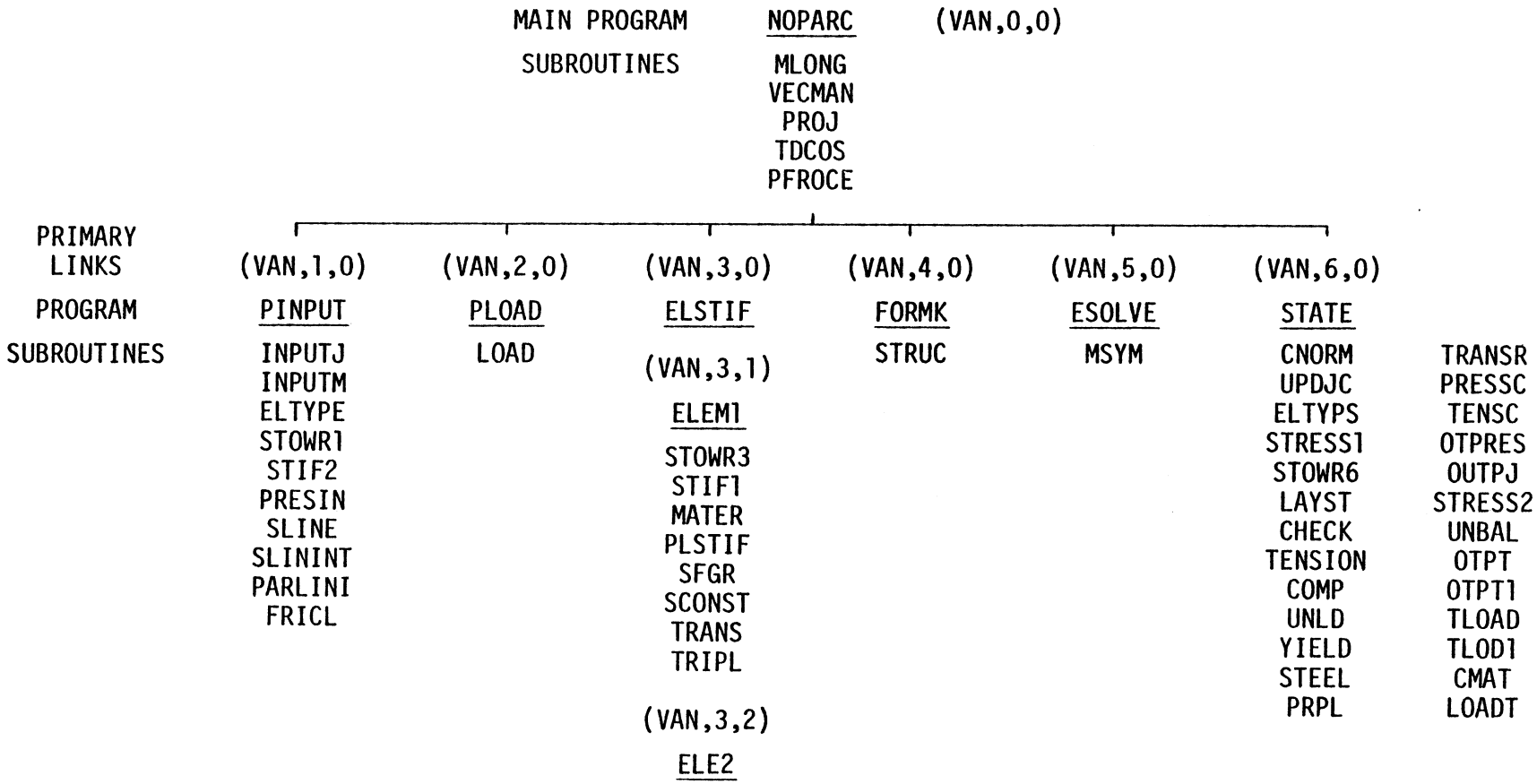

FIG. 5.11 COMPUTER PROGRAM NOPARC: OVERLAY STRUCTURE

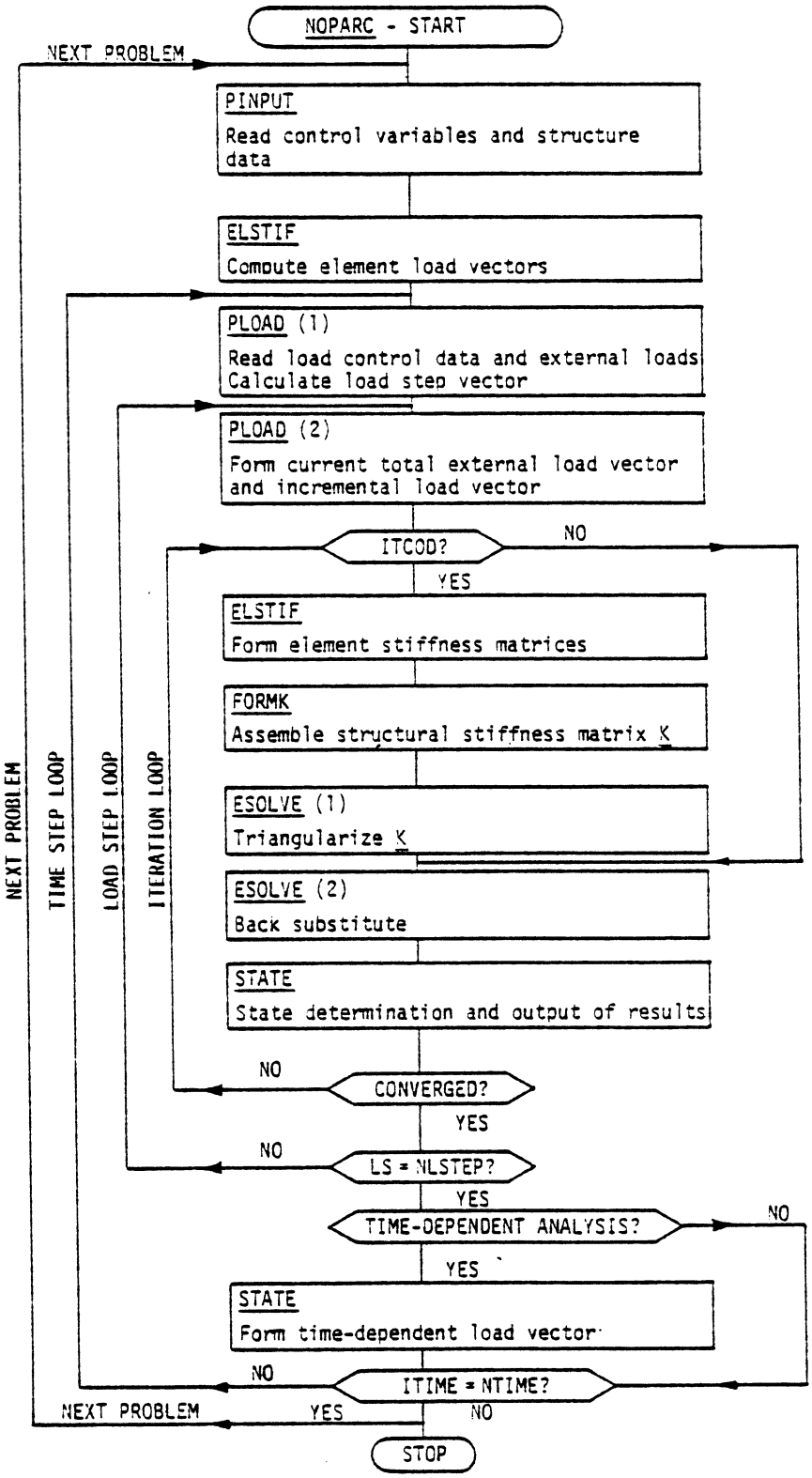

FIG. 5.12 PROGRAM FLOW DIAGRAM

6. NUMERICAL EXAMPLES

6.1 GENERAL REMARKS

A number of beams, columns and slabs have been analyzed with the computer program NOPARC described in section 5.9 for the following purposes:

1. To check the validity of the material models and analysis procedures used and developed in this study. This is accomplished by comparing the numerical results obtained with available theoretical and/or experimental data.

2. To demonstrate the applicability and capabilities of the analysis method developed in the present study to a variety of structures subjected to different load histories.

The examples are divided into three groups. The first group concerns examples for which linear elastic material properties are assumed and will be discussed in section 6.2. These examples serve to illustrate the accuracy and validity of the procedure adopted in this study to deal with the effects of geometric nonlinearities when large deflections are considered. The second group of examples, presented in section 6.3, deals with reinforced concrete beams and slabs for which material nonlinearities and in some instances also geometric nonlinearities must be considered in order to be able to predict the response of these structures at load levels where extensive cracking of the concrete has occurred. The third group, which will be discussed in section 6.4, consists of prestressed columns, beams and slabs which also exhibit pronounced nonlinear responses due to material and geometric nonlinearities. In all the examples, the reference plane is taken at mid-depth.

In section 6.5 the computer time needed for the solution of these examples and some related factors will be summarized.

6.2 LINEAR ELASTIC EXAMPLES

Three examples with linear elastic material properties are selected to illustrate the different types of geometric nonlinearities that can be handled using the approach employed in the present study. In the first example a cantilever subjected to an end moment only is bent into a circle to demonstrate that even very large deflections can be accommodated. The second example concerns the stiffening phenomenon due to in-plane tension forces, which has to be considered in axially restrained members when they undergo large out-of-plane deflections. For the third example an analysis of the buckling of a cantilever plate strip subjected to an eccentric axial force is carried out to demonstrate the applicability of the present method to the analysis of structures which exhibit softening under compressive loads.

6.2.1 Cantilever subjected to an end moment

A cantilever beam with dimensions and material properties as shown in Fig. 6.1 is subjected to an end moment. This results in the cantilever being bent into a circular arc and to bend it into a complete circle requires a moment:

$$M = 2\pi EI/\ell \ .$$

This end moment is applied in 20 equal steps and the resulting deformed shapes and deflection of the tip is shown in Fig. 6.1. The beam is modeled with 10 triangular elements and the cross section divided into 10 layers. The stiffness is re-formed for each iteration and to obtain convergence with a displacement tolerance of 0.001 in. requires an

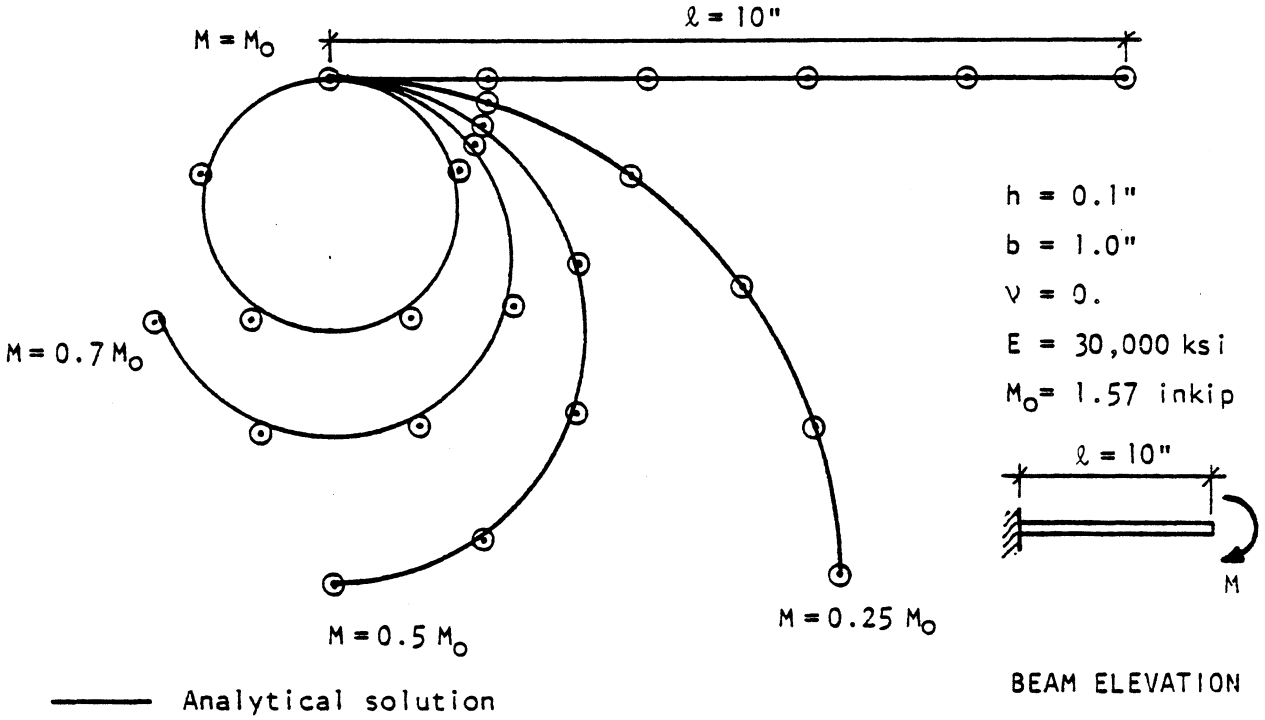

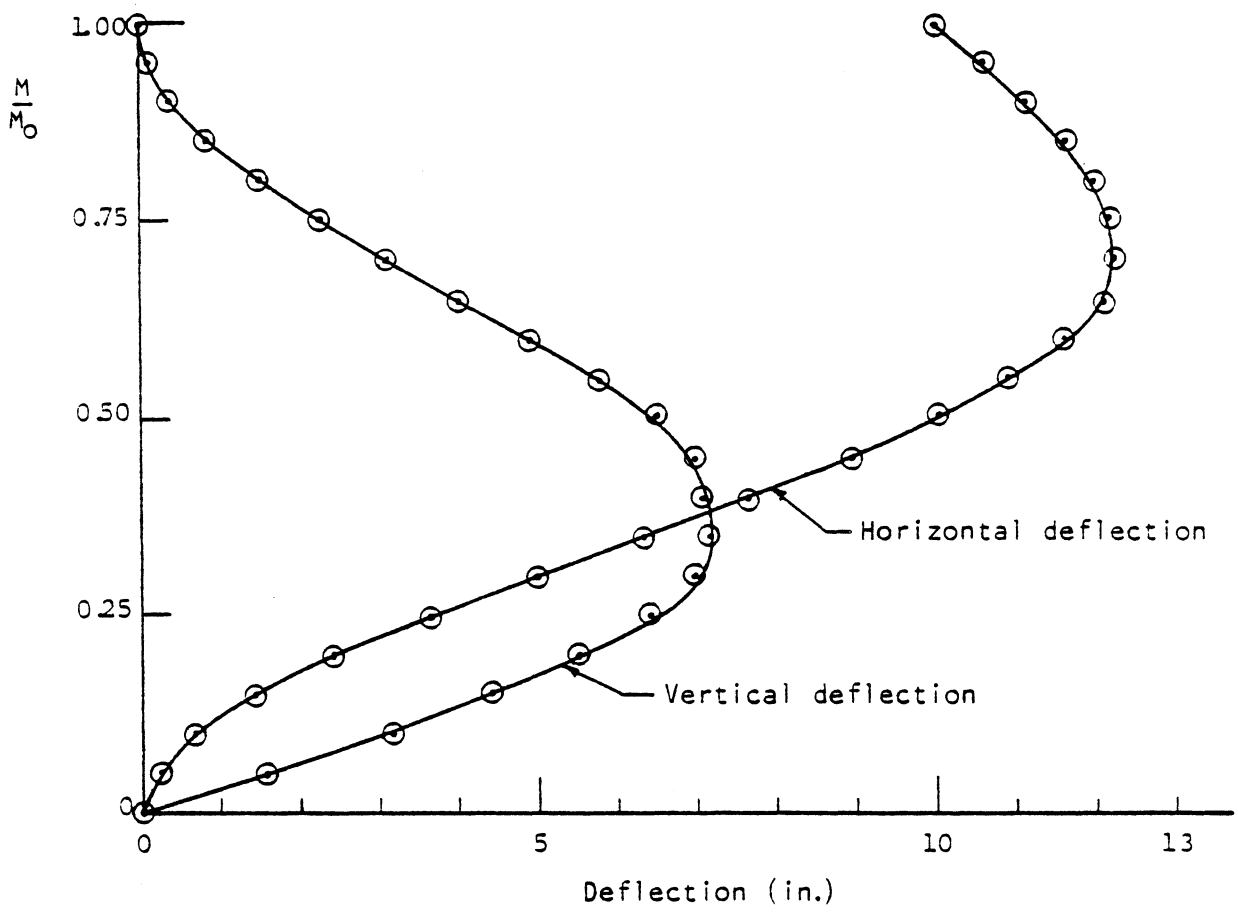

VERTICAL AND HORIZONTAL TIP DEFLECTIONS

FIG. 6.1 CANTILEVER SUBJECTED TO END MOMENT (Ex. 6.2.1).

average of 4 iterations per load step. The final position of the tip is accurate to within 0.1% -- a more stringent tolerance would result in better accuracy, but also require more iterations. Similar results for this problem were reported by Horrigmoe [113].

6.2.2 Simply supported square plate

A 16 in. square simply supported plate, 0.1 in. thick, is analyzed for a uniform load. Levy [124] solved the same problem by using a truncated trigonometric series approximation to solve the Von Karman plate equations. Due to symmetry a quarter of the plate is modeled with the finite element mesh shown in Fig. 6.3, while the cross section is divided into 10 equal layers. The edges are horizontally restrained.

The load is applied in the 6 steps indicated in Fig. 6.2, the stiffness re-formed for each iteration and convergence for a displacement tolerance of 0.001 in. obtained in an average of 3 iterations per load step. In Fig. 6.2 it can be seen that the center deflection obtained from the present finite element analysis shows excellent agreement with Levy's solution. The pronounced stiffening of the plate due to the development of tensile membrane forces should be noted. In Fig. 6.3 stresses obtained from both solutions are compared. The membrane stresses show good correspondence and so does σ_{xy} at the supported corner D. The agreement for the bending stress is within 7%. Murray [45], using an approach similar to that of the present study, and Bergan [114], employing shallow shell theory, solved the same problem using the FEM. They also reported similar good agreement for the membrane stresses, but agreement to within only about 10% for both σ_{xy} and the bending stresses. The results obtained in the present study therefore compare favorably with these earlier finite element solutions.

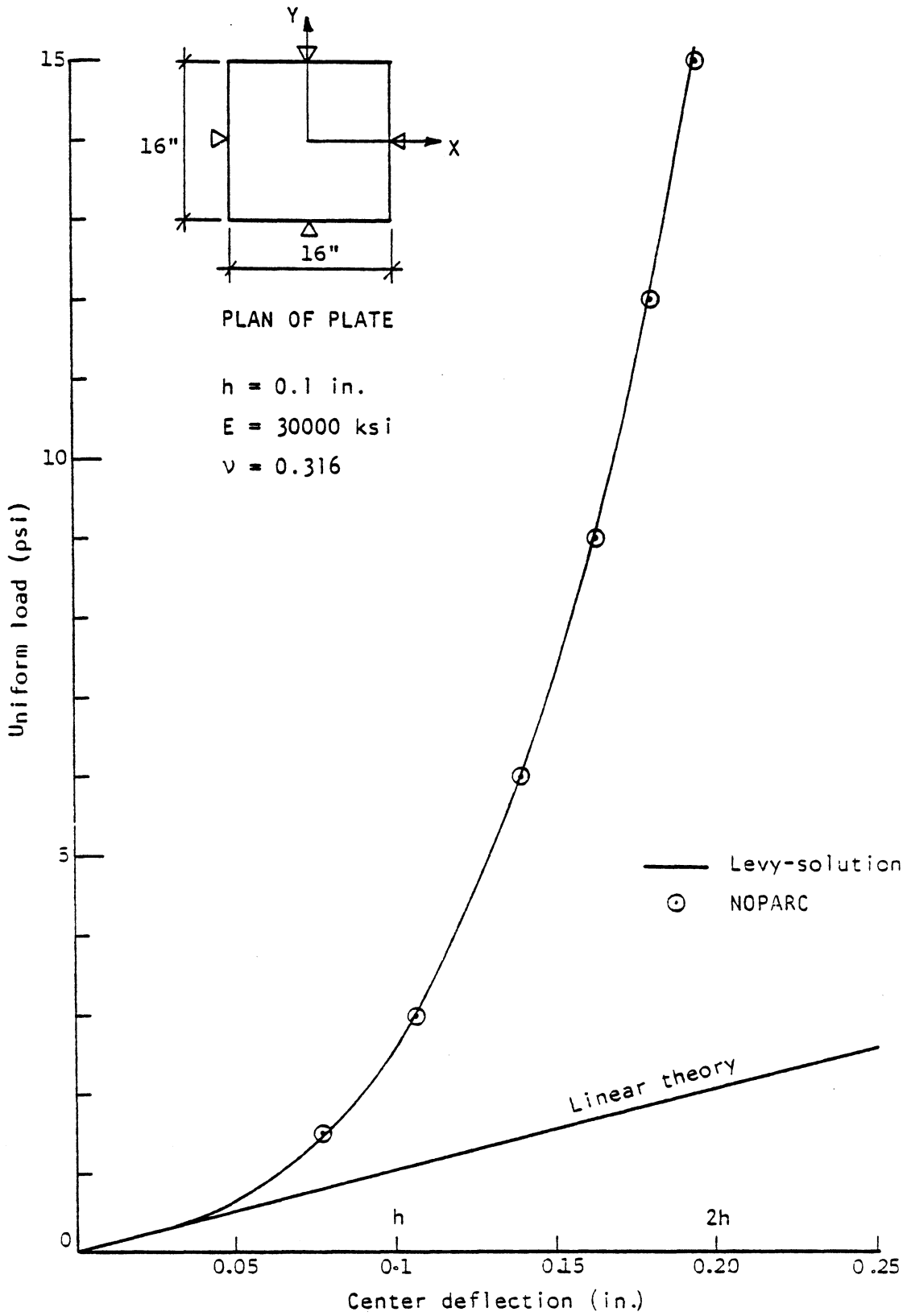

FIG. 6.2 SIMPLY SUPPORTED SQUARE PLATE UNDER UNIFORM LOAD (Ex. 6.2.2): CENTER DEFLECTION. (ALL EDGES ARE HORIZONTALLY RESTRAINED.)

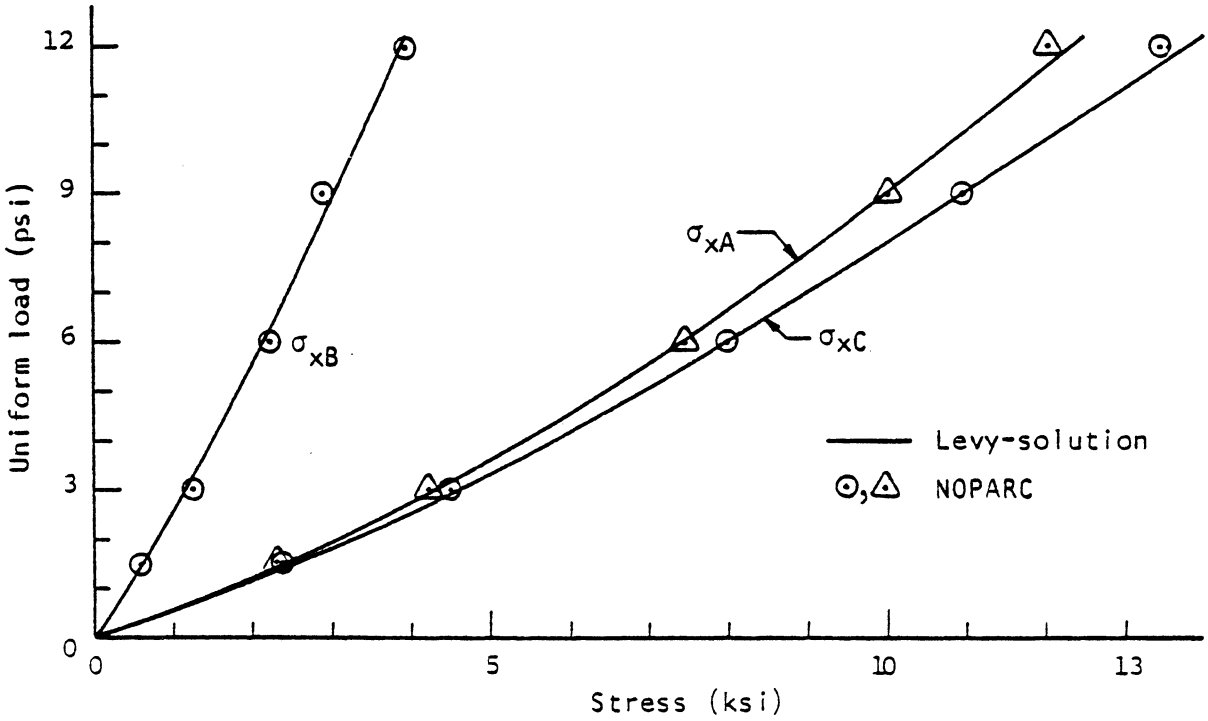

a. MEMBRANE STRESSES

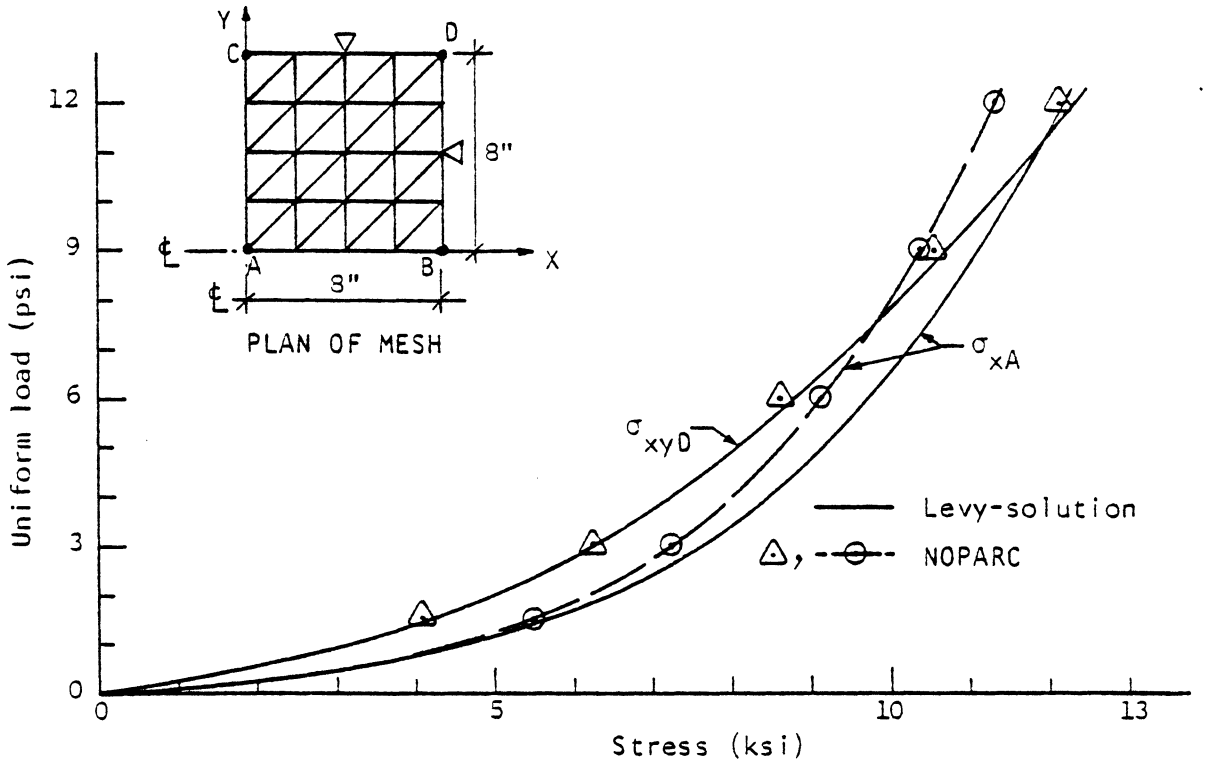

b. BENDING STRESSES

FIG. 6.3 SIMPLY SUPPORTED SQUARE PLATE UNDER UNIFORM LOAD (Ex. 6.2.2): STRESSES

6.2.3 Buckling of a cantilever plate strip

A section from a cantilever plate strip subjected to an axial compressive load and small end moment is analyzed. The plate strip is modeled with the finite element mesh shown in Fig. 6.4 and 10 equal layers are used for the cross section. The load is applied with an eccentricity of one tenth of the plate thickness to provide a small end moment to initiate transverse displacements which become large when the load approaches the critical load. This problem corresponds to the classical "elastica" column buckling problem and is an example of a structure that softens when geometric nonlinearities are taken into account.

The load is applied in small steps near the critical load to follow the load-deflection path more closely. The stiffness, with the geometric stiffness included, is re-formed for each iteration and with a displacement tolerance of 0.001 in. convergence is achieved in an average of 8 iterations per load step.

The load-deflection curves from the classical and finite element solutions are compared in Fig. 6.4 and good agreement can be observed.

6.3 REINFORCED CONCRETE EXAMPLES

Five reinforced concrete beams and slabs are selected for analysis. In the first example the behavior of an axially restrained beam is studied when different combinations of material and geometric nonlinearities are considered. The performance of the concrete model adopted in the present study is then checked through the analysis of a slab in the second example. The third example concerns the analysis of a simply supported slab where the effects of large deflections affect the solution significantly. In the fourth example a clamped reinforced concrete slab

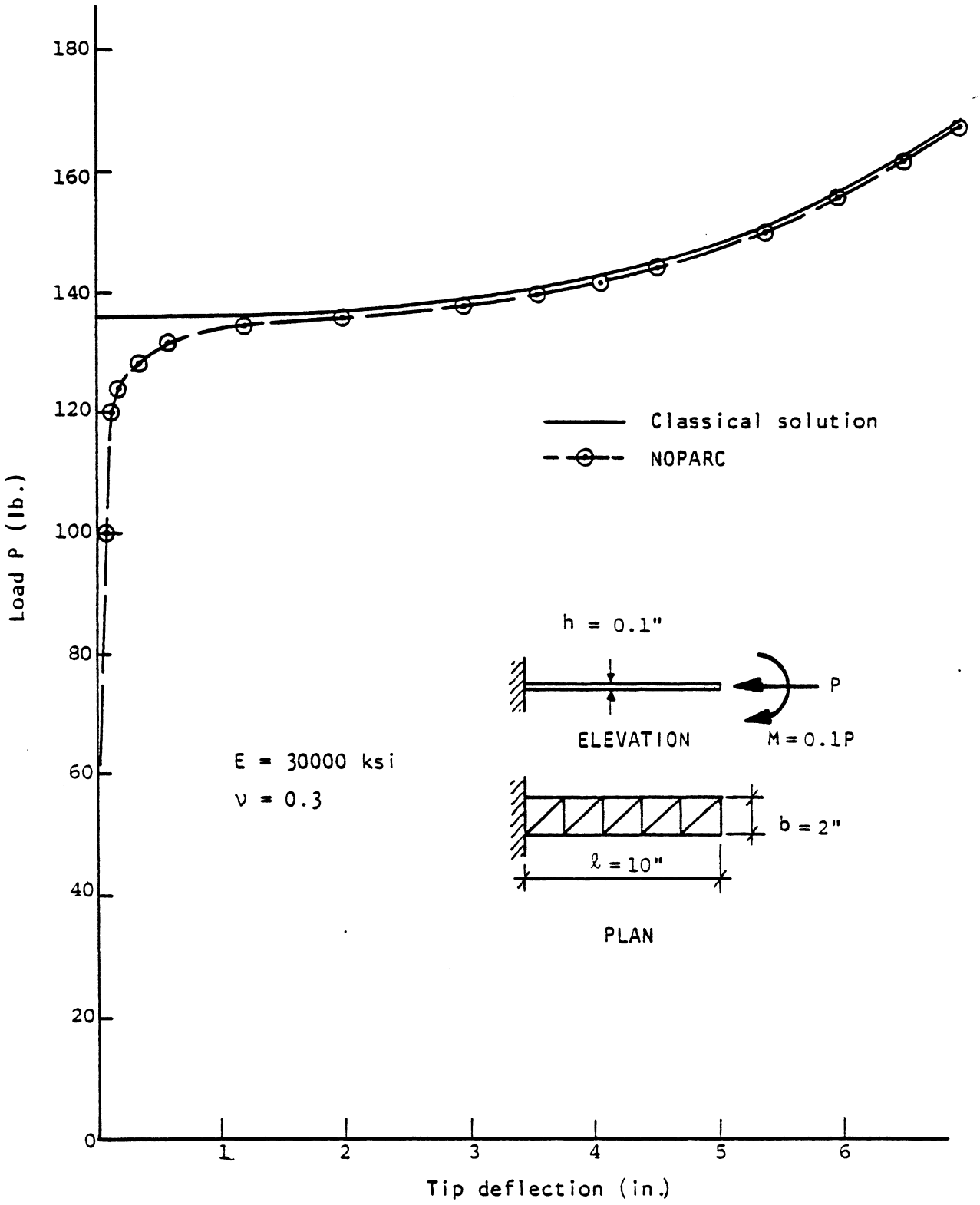

FIG. 6.4 BUCKLING OF CANTILEVER PLATE STRIP (Ex. 6.2.3)

which undergoes very large out-of-plane deflections is analyzed. The analysis procedure for time-dependent effects is demonstrated in the fifth example by analyzing a reinforced concrete beam subjected to temperature-dependent creep and shrinkage.

6.3.1 Reinforced concrete Timoshenko beam

A simply supported reinforced concrete beam, restrained axially and loaded uniformly, is analyzed to investigate the effects of both material and geometric nonlinearities for such a structure. The same example was studied by Kang [37]. In Fig. 6.5 the geometry of the beam is given and the material properties summarized. By utilizing symmetry, half of the beam is modeled with 10 triangular elements as shown. The cross section is divided into 10 concrete layers and one steel layer. To increase the ultimate load capacity of the cross section the compressive strength of the concrete and the yield strength of the reinforcing steel are arbitrarily increased to the values shown. The effect of tension stiffening after cracking of the concrete is ignored. The beam is analyzed up to a load $q = 150$ lb/in. in 9 load steps. A displacement tolerance of 0.005 in. resulted in convergence in the number of iterations per load step shown in Table 6.1.

The load-deflection curves for the midspan deflection are shown for 4 cases in Fig. 6.5. Case 1 represents linear elastic response. For case 2 only geometric nonlinearity is considered and a stiffening of the structure due to the development of membrane forces can be seen. Only the nonlinearity of the materials is considered for case 3. Beyond the cracking load the structure softens as the load increases due to additional cracking of the concrete and the gradual decrease of the modulus

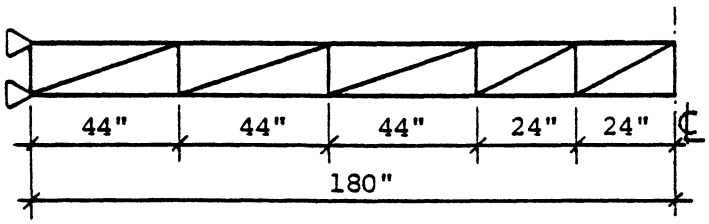

PLAN OF MESH

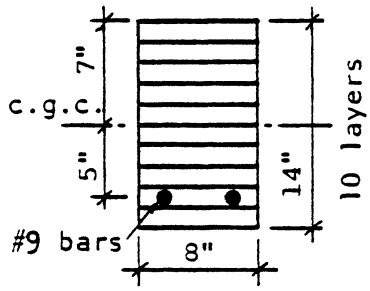

CROSS SECTION

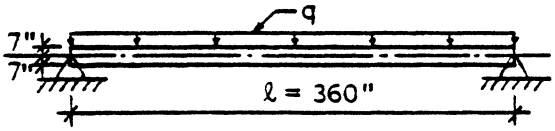

ELEVATION OF BEAM

E_s = 29000 ksi f_y = 120 ksi

E_{sh} = 346 ksi ε_{su} = 0.13

STEEL PROPERTIES

E_o = 3834 ksi

f'_c = 8000 psi

f'_t = 755 psi

ε_c = 0.004 in/in

ν = 0.

CONCRETE PROPERTIES

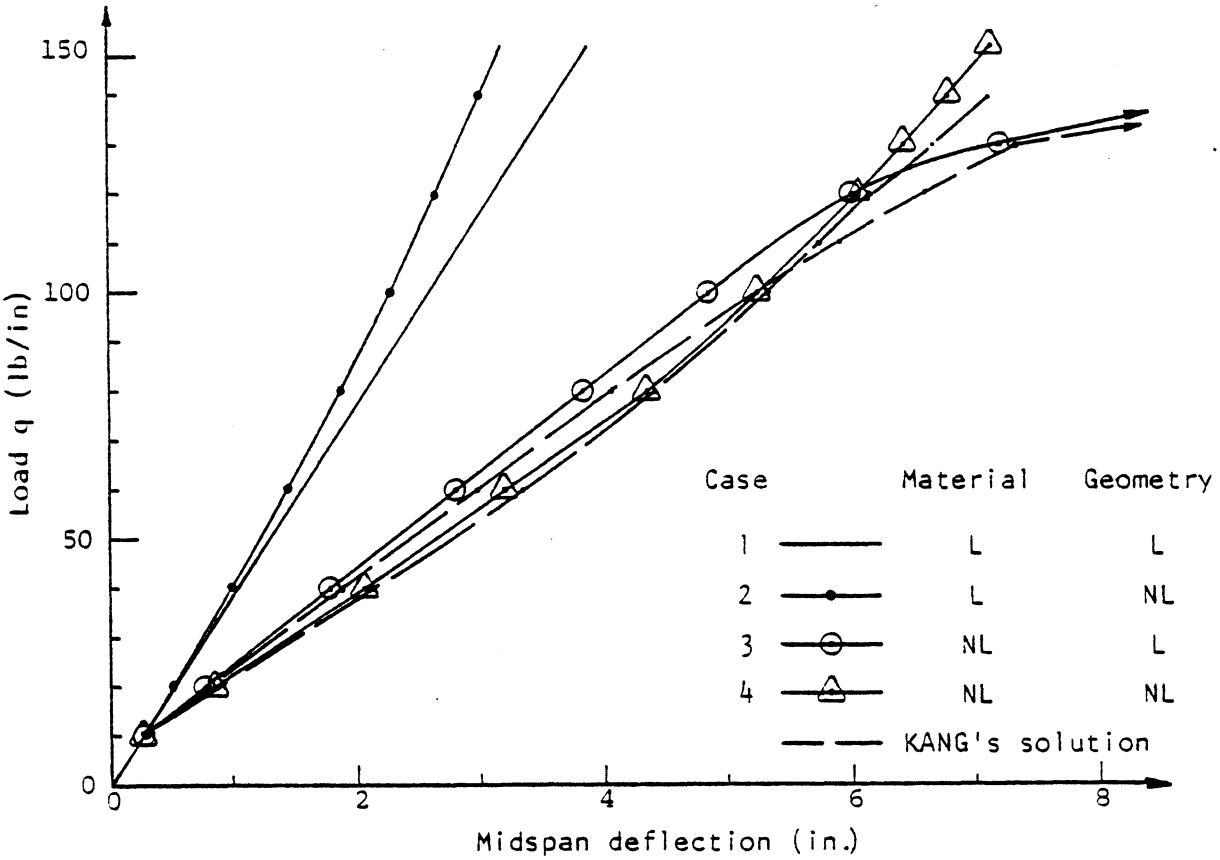

LOAD-DEFLECTION CURVE

FIG. 6.5. REINFORCED CONCRETE TIMOSHENKO BEAM UNDER UNIFORM LOAD (Ex. 6.3.1) (ENDS ARE HORIZONTALLY RESTRAINED)

of elasticity of the concrete up to failure of the concrete in compression. Both material and geometric nonlinearities are considered in case 4. Beyond the cracking load the structure softens even more than for case 3 -- this is attributed to the fact that the membrane forces that are developed cause additional cracking of the concrete and thus a greater decrease in stiffness of the cross section. However, at higher load levels the structure stiffens gradually. The tensile membrane force that is developed because of the large deflections relieves the compressive stress in the concrete and enables the structure to carry a higher load than that achieved in case 3.

The difference in the load-deflection curves obtained in the present study and those reported by Kang [37] is mainly due to the difference in the concrete models adopted. Kang used Hognestad's [72] stress-strain curve which has a linear variation of the modulus of elasticity and therefore results in a softer concrete model than the one employed in the present study. However, for case 3 both analyses show failure when the load is increased beyond 130 lb/in.

For case 3 the equilibrium equations are solved in the undeformed state. The bending moment at midspan is proportional to the applied load q and can be calculated in the usual manner since the effect of the axial force is neglected. In case 4, however, the equilibrium equations are solved in the deformed state and the effect of axial force P is included in calculating the bending moment. The bending moment M at midspan for this case can be calculated as:

$$M = qL^2/8 - P\delta$$

where

δ = transverse deflection

It can be noted that as the load q and the deflection increases, the portion of the moment resisted by the axial force also increases.

6.3.2 McNeice slab

An isotropically reinforced 36 in. square concrete slab, simply supported at the four corners, was tested by McNeice [10] and analyzed by various investigators [26,28,74]. The slab is 1.75 in. thick and divided into 10 equal layers. By taking advantage of symmetry a quarter of the slab is modeled by the finite element mesh shown in Fig. 6.6. The following material properties are used for the analysis:

Concrete:	Reinforcing Steel:
E_o = 4150 ksi	E_s = 29000 ksi
f'_c = 5500 psi	E_{sh} = 0
f'_t = 550 psi	f_y = 60 ksi
$\varepsilon_c = 2f'_c/E_o$	t_s = 0.0111 in.
ν = 0.15	ε_{su} = 0.1 in/in.

The slab is loaded by a concentrated load in the center which is applied in 4 load increments of 1 kip each. The second and third load increments are divided into 4 equal load steps each and the fourth into 6 load steps. With a displacement tolerance of 0.001 in. convergence is obtained in an average of 7.9 iterations per load step. The stiffness is re-formed at the beginning and subsequently after every six iterations in the load steps.

This example is used to check the concrete model and also to compare the two tension stiffening models incorporated in the present study. From the load-deflection curve for node A shown in Fig. 6.6 it can be

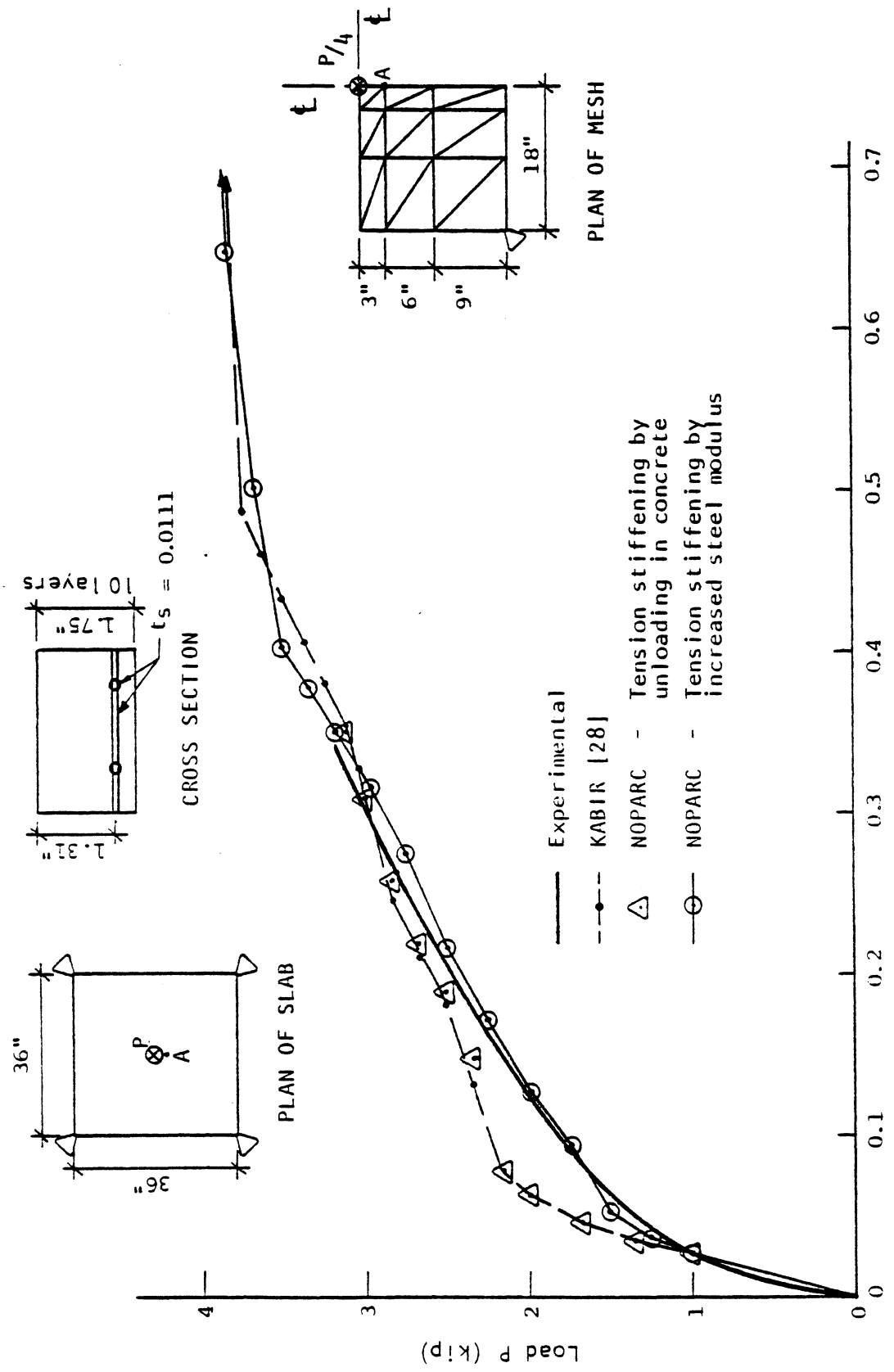

FIG. 6.6 McNEICE SLAB (Ex. 6.3.2): CORNER SUPPORTED SLAB UNDER CENTERPOINT LOAD. (NO HORIZONTAL RESTRAINT AT CORNERS)

observed that the tension stiffening model assuming unloading in the concrete results in the behavior of the slab being too stiff just after the initial cracking. The results from NOPARC for this tension stiffening model compare very well with those obtained by Kabir [28]. The analysis in which the tension stiffening model employing an increased steel modulus is used shows very good agreed with the experimental curve, similar to results reported by Gilbert and Warner [74].

6.3.3 Taylor slab

A series of simply supported, two-way square reinforced concrete slabs with varying thicknesses were tested by Taylor et al. [115]. They were interested in determining what the effect of variations in the arrangement of the reinforcement would be on the load-carrying capability of the slabs. One of these slabs with a thickness of 2 in. and spanning 6 ft. with a uniform spacing of the reinforcing in both directions was analyzed by Arneson et al. [30] and is also studied in the present investigation.

Due to symmetry a quarter of the slab is modeled by the finite element mesh shown in Fig. 6.7. The cross section is divided into 10 concrete layers and 2 orthogonal reinforcing steel layers of 3/16 in. diameter bars with the spacing as shown. The tension stiffening model using an increased modulus for the steel is used. The following material properties are used for the analysis:

Concrete:	Reinforcing Steel:
E_o = 4700 ksi	E_s = 30000 ksi
f'_c = 5940 psi	E_{sh} = 2000 ksi
f'_t = 550 psi	f_y = 54.5 ksi
ε_c = 0.0025 in/in.	ε_{su} = 0.1 in/in.
ν = 0.18	

The slab is subjected to a uniform pressure loading subdivided into the steps indicated in Fig. 6.7. One analysis is carried out taking only the material nonlinearity into account -- for this case the stiffness is re-formed at the beginning and after every 4 iterations in each load step. Another analysis for which both material and geometric nonlinearities are considered is also done. For this analysis the stiffness is re-formed after every 2 iterations in each load step. A displacement tolerance of 0.001 in. is used and the average number of iterations per load step is indicated in Table 6.1.

In Fig. 6.7 the load vs. center deflection curves obtained from the experiment, Arneson's analysis and the present analysis is shown. In both analytical cases the analysis neglecting the geometric nonlinearity indicates failure of the slab at a substantially lower load than recorded in the test. Both analyses including the geometric nonlinearity predict the failure load well.

When comparing the results from the present analysis and that of the experiment, the following can be noted. The load-deflection curve of the present analysis indicates larger deflections than recorded in the test just after the initial cracking (load levels 4-6 tons). This is considered to be caused by the fact that the corner of the slab is restrained

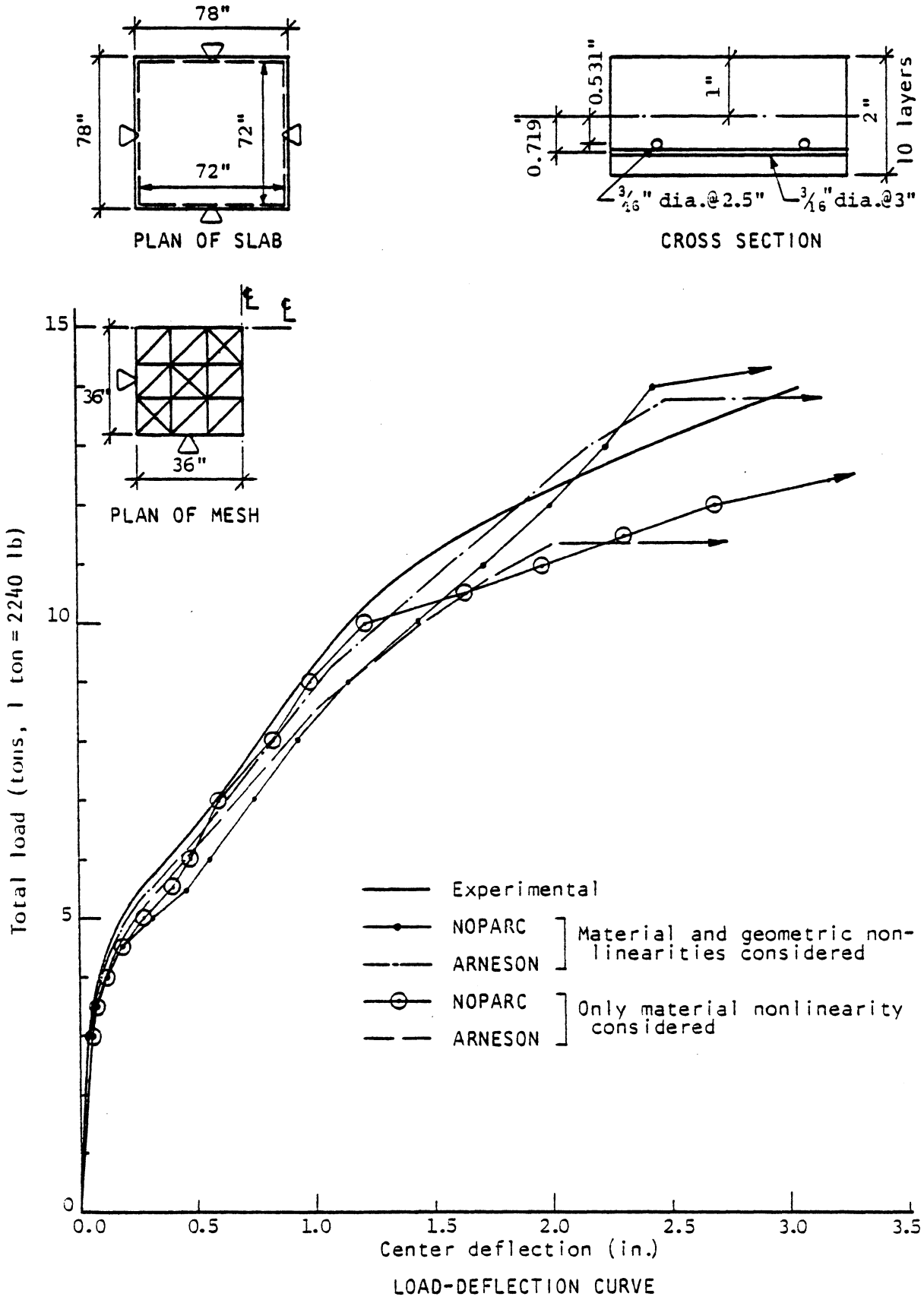

FIG. 6.7 TAYLOR SLAB (Ex. 6.3.3): SIMPLY SUPPORTED SLAB UNDER UNIFORM LOAD. (NO HORIZONTAL RESTRAINT AT EDGES)

in the finite element analysis, but was free to lift up in the test. In the analysis this reaction causes additional cracking of the unreinforced top surface near the corner of the slab which reduces the stiffness of the structure.

From the load-deflection curves obtained in the present study it can also be observed that when the effect of nonlinear geometry is included the behavior of the slab in the intermediate load ranges is softer than when it is ignored. This phenomenon is similar to what is observed in Ex. 6.3.1 and also deemed to be caused by the same mechanism indicated therein.

6.3.4 Black slab

A number of two-way, clamped reinforced concrete slabs were tested by Black [116] primarily to investigate the collapse of slabs with a high degree of edge restraint after large deflections have resulted in significant membrane action. Both static and and blast loads were considered. One of the slabs, 29 in. square and 0.89 in. thick and subjected to a static load is selected to be studied. The cross section is divided into 10 equal concrete layers and 2 to 4 reinforcing layers to model the steel layout shown in Fig. 6.8. Taking advantage of symmetry a quarter of the slab is modeled with the finite element mesh shown.

Very little information about the material properties is given. The concrete strength is assumed to be 4000 psi and the other concrete properties determined from the ACI formulae (section 3.2.4). Only the yield and ultimate strengths of the 0.08 in. diameter smooth reinforcing wire are given as 43.6 ksi and 73.5 ksi, respectively. The tension stiffening model using an increased modulus for the steel is used. The following material properties are also assumed.

E_s = 29000 ksi $\quad\quad$ ε_{su} = 0.11 in/in.

E_{sh} = 290 ksi $\quad\quad$ ν = 0.15

The slab is subjected to a uniform pressure loading subdivided into the steps indicated in Fig. 6.8. Both material and geometric nonlinearities are considered and the stiffness re-formed after every second iteration in each load step. A displacement tolerance of 0.001 in. is used and convergence is then obtained in an average of 15.5 iterations per load step.

Black [116] provides only the four pertinent points indicated on the average experimental load-deflection curve shown in Fig. 6.8. The initial ascending branch of the analytical curve agrees satisfactorily with the experimental curve, but due to the fact that handling of the snap-through type of behavior found here is not incorporated in the present computer program, the analytical solution will find an equilibrium configuration corresponding to a point on the secondary ascending branch of the load-deflection curve. For the point Q established at a load level of 16 psi the concrete in approximately 60 percent of the elements is completely cracked and/or crushed so that only the reinforcing steel present in these elements carry the load. To do any meaningful analysis of this part of the slab behavior detailed information about the stress-strain diagram of the reinforcing steel is needed -- the assumptions made for this analysis are obviously not quite correct. Since the reinforcing steel here becomes the dominant factor in the load-carrying ability of the slab a more sophisticated model for the reinforcing steel would also seem to be necessary to be able to obtain adequate results.

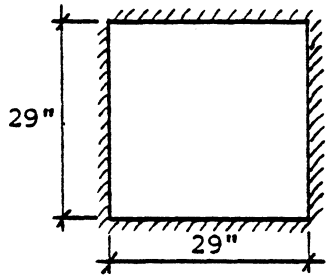

PLAN OF SLAB

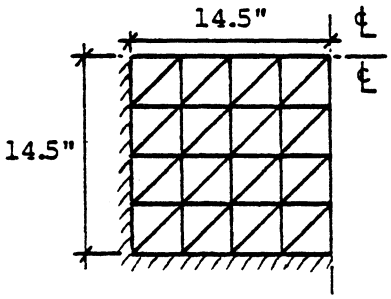

PLAN OF MESH

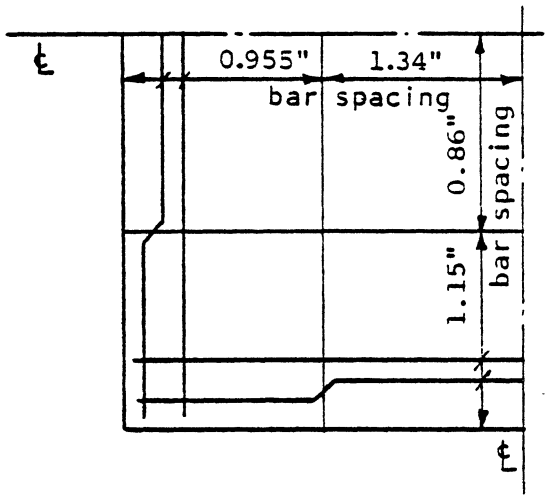

Notes: All bars are 0.08" dia wire.
Alternate bars are bent up.
Minimum cover 0.175".

REINFORCING STEEL LAYOUT

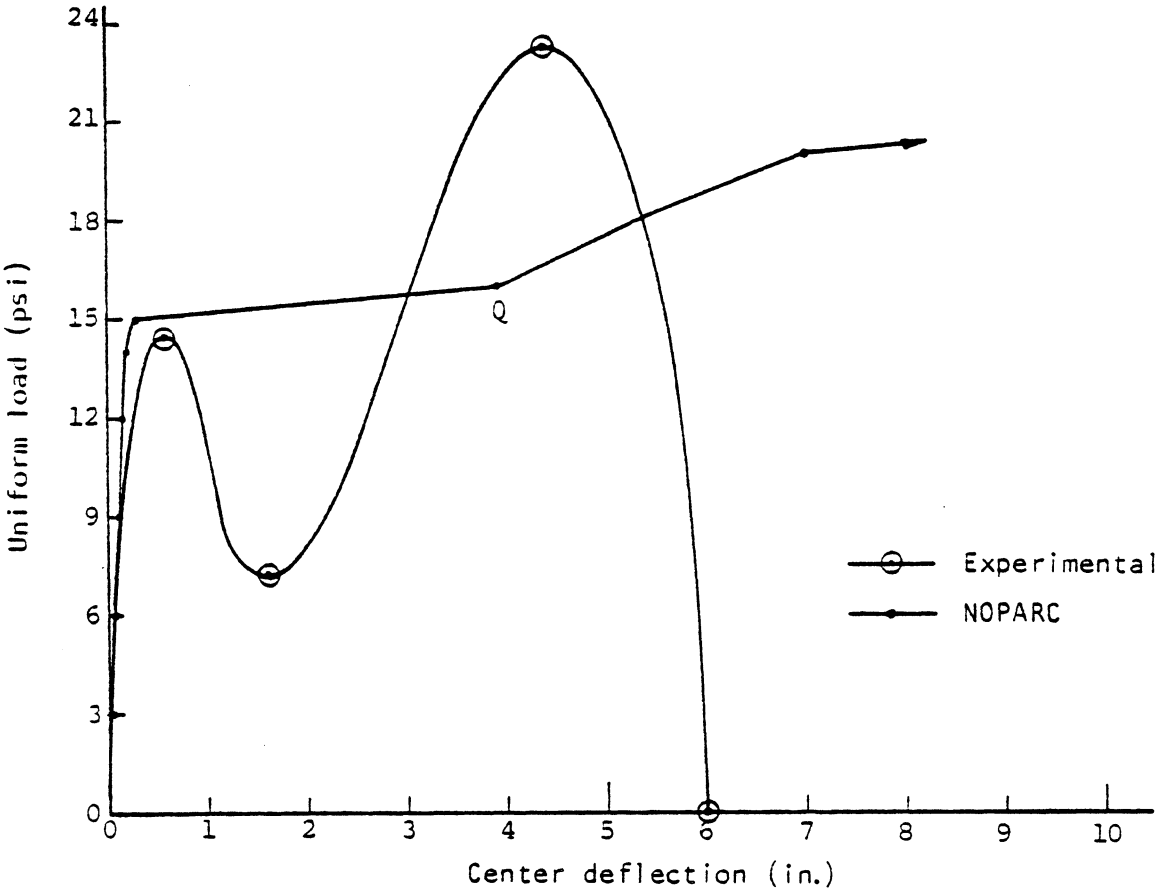

LOAD-DEFLECTION CURVE

FIG. 6.8 BLACK SLAB (Ex. 6.3.4): CLAMPED SLAB UNDER UNIFORM PRESSURE. (ALL EDGES HORIZONTALLY RESTRAINED)

Due to the lack of information, the high cost of an analysis and the simple model used for the reinforcing steel in this study, this example was not investigated further.

6.3.5 England-Ross beam

Many reinforced concrete structures like chimneys, floor slabs under boilers and nuclear containment vessels are subjected to thermal gradients. Due to the restraint of displacements in statically indeterminate structures or due to thermal gradients in thick members stresses develop in such structures. These stresses undergo changes because of the creep and shrinkage of concrete. However, creep and shrinkage of concrete is temperature-dependent as has been discussed in Chapter 3.

One of the earliest experimental and analytical studies of the effects of temperature-dependent creep and shrinkage was done by England and Ross [117]. They tested sealed and unsealed flexurally restrained reinforced concrete beams subjected to a linear thermal gradient. Creep and shrinkage curves for unreinforced concrete were obtained for different temperatures ranging from 68°F (20°C) to 284°F (140°C).

The unsealed beam, also analyzed by Kang [37], is selected to be studied. The beam ends are restrained against bending, but free to displace axially. The beam is modeled by 2 triangular elements and the cross section with 10 equal concrete layers and one layer of reinforcing steel as shown in Fig. 6.9. Tension stiffening in the concrete is ignored and the following material properties selected (properties not given are calculated from the ACI formulae, section 3.2.4):

Concrete:

$f'_c = 6250$ psi $\qquad\qquad \alpha = 6.722 \times 10^{-6}/°F$

$\nu = 0$

creep coefficients:

$\alpha_1 = 5.8 \times 10^{-7}$/psi $\qquad \tau_o = 10$ days

$\alpha_2 = 0.1 \times 10^{-7}$/psi $\qquad T_o = 176°F$ (80°C)

$\alpha_3 = 4.0 \times 10^{-7}$/psi

temperature shift function: $\phi(T) = e^{\psi(T)}$

$\psi(T) = -1.286 \times 10^{-4} T^2 + 0.0741 T - 8.0$

Reinforcing Steel:

$E_s = 30000$ ksi $\qquad f_y = 40$ ksi

$t_s = 0.0245$ in. $\qquad \alpha = 6.5 \times 10^{-6}/°F$

The α_i for the creep compliance function at other concrete ages are calculated using the ACI formulae as discussed in section 3.2.6. The curves for shrinkage at high temperatures obtained by England and Ross [117] are shown in Fig. 6.9.

The beam was cured for 10 days and then left unsealed at the laboratory temperature of 60.8°F (16°C). At 80 days after casting, the temperature gradient was applied by heating the top surface of the beam to 230°F (110°C) and the bottom surface to 149°F (65°C). The time-dependent analysis is carried out at the following 18 ages after casting: 20, 40, 60, 80, 81, 82, 83, 84, 85, 86, 88, 90, 94, 100, 110, 120, 135, 152. Only uniform shrinkage through the cross section can be accommodated in NOPARC and is therefore assumed. At 152 days after casting, the temperature gradient was removed and the beam allowed to return to laboratory temperature resulting in the steel stress change shown in Fig. 6.9.

The variation of steel stress with time for analysis 1, shown in Fig. 6.9, is obtained by using the shrinkage curve corresponding to the average temperature of 190°F. Analysis 2 is carried out by using the

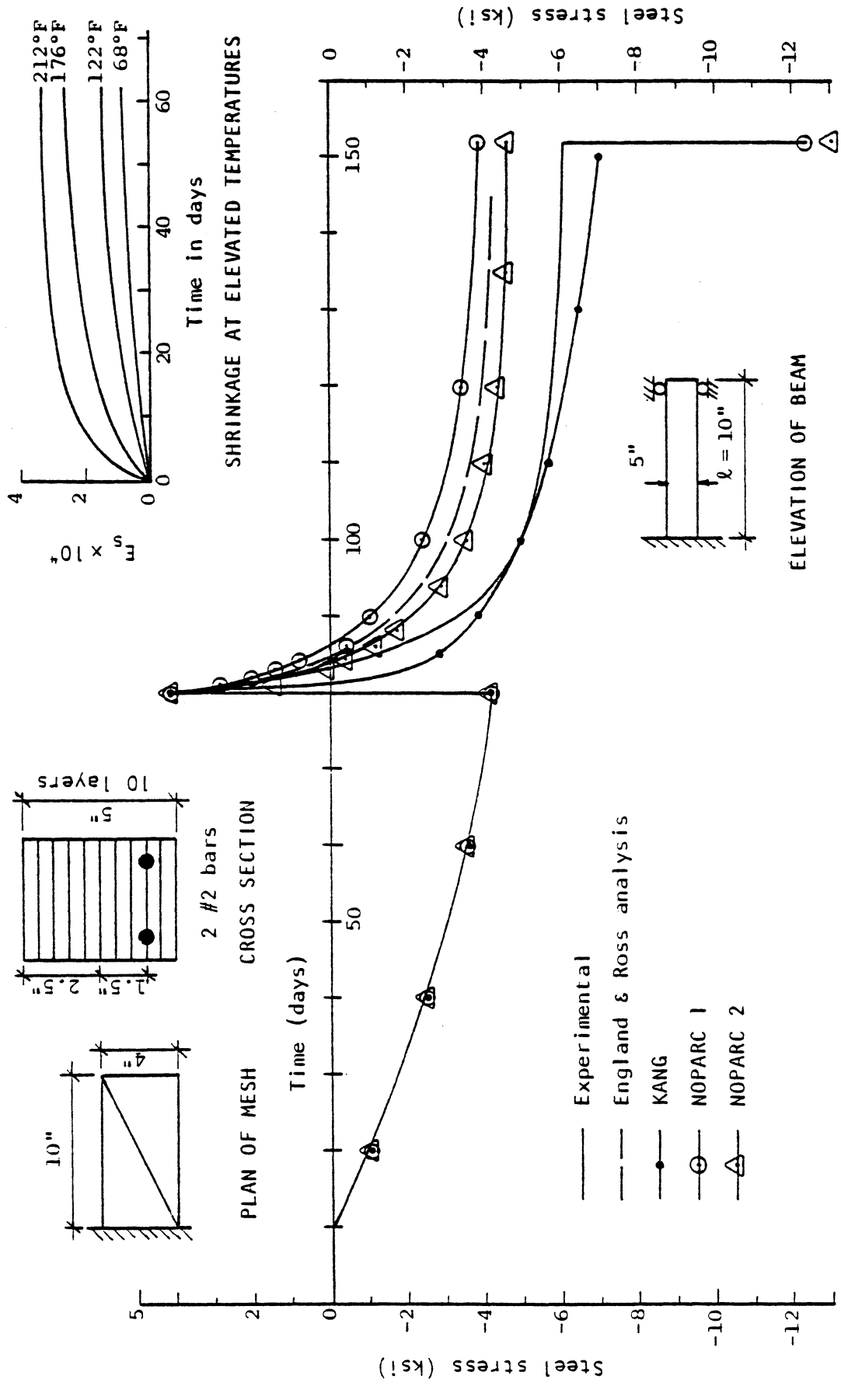

FIG. 6.9 ENGLAND-ROSS BEAM (Ex. 6.3.5).

shrinkage curve corresponding to a temperature of 212°F which is the average temperature for the uncracked layers after application of the temperature gradient. The temperature-dependent shrinkage of the concrete is therefore the dominant factor affecting the behavior of this beam. To obtain better correlation like that of Kang [37], differential shrinkage should be included in the analysis.

England and Ross [117] used a step-by-step method without considering creep recovery and the effect of aging on the specific creep to carry out their analysis.

6.4 PRESTRESSED CONCRETE EXAMPLES

To demonstrate the applicability of the method developed in the present study to the analysis of prestressed concrete structures, five columns, beams and slabs are selected to be studied. In the first example a pretensioned column subjected to an eccentric load is analyzed. The second example concerns the analysis of a bonded post-tensioned continuous beam. In the third example a plate strip with an unbonded tendon is studied, while the fourth example concerns the analysis of a simply supported slab prestressed with unbonded tendons. For the fifth example one panel of a slab system, simply supported on columns and stressed with unbonded tendons is analyzed for both short time and time-dependent behavior.

6.4.1 Aroni column

A series of eccentrically loaded pretensioned prestressed concrete columns were studied by Aroni [118,119] to investigate their behavior under different combinations of load eccentricity, slenderness and amount

of prestress. He also presented an analytical procedure to calculate the strength of such columns. One of the columns, designated $A_2$30c5, also studied by Kang [37], is analyzed to test the validity of the method used in the present study as applied to the nonlinear geometric analysis of a prestressed concrete member under compression.

The dimensions of the column are shown in Fig. 6.10. Due to symmetry one half of the column is modeled with 10 finite elements with the mesh shown, while the cross section is divided into 10 equal concrete layers. The column was axially pretensioned with four 0.198 in. diameter high tensile steel wires. The material properties used for the analysis are as follows:

Concrete:

E_o = 4940 ksi $\varepsilon_c = 2f'_c/E_o$

f'_c = 5585 psi ν = 0

f'_t = 558.5 psi

Prestressing steel:

P_o = 3435 lb/tendon A_s = 0.0308 in^2.

σ_1 = 146 ksi ε_1 = 0.004976

σ_2 = 196 ksi ε_2 = 0.00690

σ_3 = 218 ksi ε_3 = 0.00863

σ_4 = 240 ksi ε_4 = 0.030

σ_5 = 251 ksi ε_5 = 0.056

In the tests the prestress was transferred to the concrete at 14 days, the column cured under water up to 28 days after casting and the eccentric load then applied up to failure. The initial prestress force is not

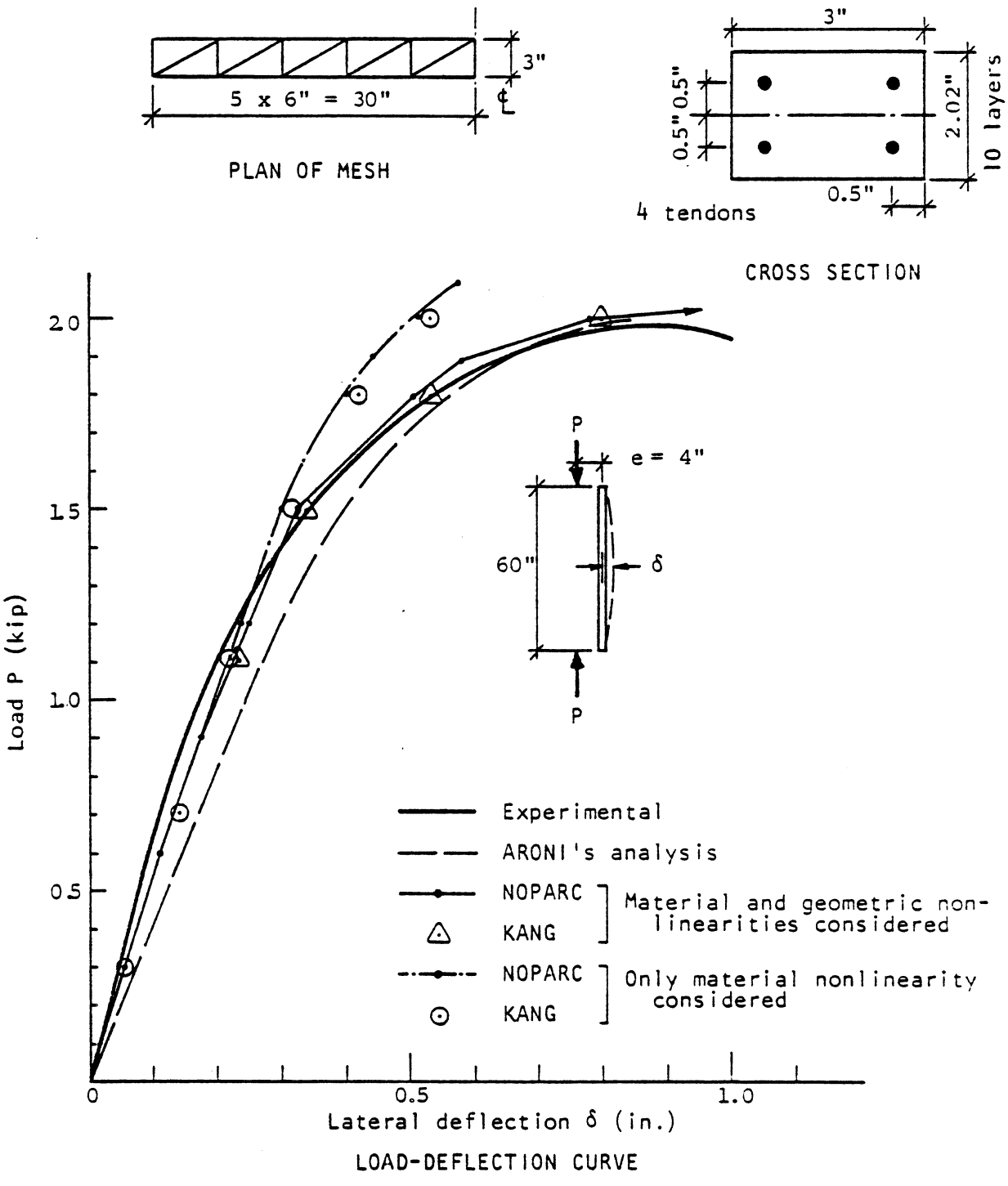

FIG. 6.10 ARONI PRETENSIONED COLUMN (Ex. 6.4.1).

specified in the references, but an initial compressive stress of 2267 psi in the concrete was recorded. The magnitude of the initial prestress force is therefore calculated to produce this concrete stress at transfer.

The eccentric load is applied as an axial load and an end moment in 6 steps up to 18 kips and then 3 more steps up to 21 kips. The stiffness (excluding the geometric stiffness) is re-formed for each iteration and with a displacement tolerance of 0.001 in. convergence is achieved in the average number of iterations per load step shown in Table 6.1.

To demonstrate the importance of the geometric nonlinearity in the behavior of this column, it is also analyzed taking only material nonlinearity into account. The load-deflection curves are shown in Fig. 6.10 and good agreement between the experimental results, the analysis of Aroni [118], that of Kang [37] and the present study can be observed. The significance of the geometric nonlinearity can be noted by the large difference in results obtained when it was not included. The difference between the results of Kang and that obtained in the present study is mainly due to the difference in concrete models used -- the concrete model of the present study being stiffer than the one employed by Kang (as was also noted and discussed for Ex. 6.3.1).

6.4.2 Lin continuous beam

Lin [120] tested four two-span continuous beams with a bonded post-tensioned tendon under static and repeated loads up to failure to determine their cracking and ultimate strengths. One beam subjected to a static load and reinforced with some additional mild steel bars in the regions of maximum positive and negative moments, is selected for study. This beam was also studied by Kang [37]. The dimensions of the beam are

shown in Fig. 6.11 and due to symmetry only one half of the beam is modeled with the finite element mesh shown. The cross section is divided into ten equal concrete layers and a layer of reinforcing steel consisting of two 0.55 in. diameter bars is included in the top of the beam in the region adjacent to the center support and in the bottom of the beam in the region of maximum positive moment. The single tendon, consisting of 32 - 0.198 in. diameter wires, has a concordant tendon profile made up of straight sections with maximum eccentricities of -1.97 in. under the load P and +3.46 in. at the center support. The tension stiffening model in which an increased modulus for the steel is used is employed. The material properties used for the analysis are given below and the ACI data are used for the time-dependent creep and shrinkage analysis (sections 3.2.6 and 3.2.7):

Concrete:

$\nu = 0$ $\quad$ $w = 155$ pcf

14 days:	28 days:
$E_o = 5300$ ksi	$E_o = 5500$ ksi
$f'_c = 5430$ psi	$f'_c = 6000$ psi
$f'_t = 700$ psi	$f'_t = 700$ psi
$\varepsilon_c = 0.002$ in/in.	$\varepsilon_c = 0.0022$ in/in.

Reinforcing Steel:

$E_s = 28400$ ksi	$A_s = 0.2376$ in^2.
$E_{sh} = 104$ ksi	$\varepsilon_{su} = 0.16$ in/in.
$f_y = 45.5$ ksi	

Prestressing Steel:

P_o = 145 kip	μ = 0.3/rad.
A_s = 0.965 in^2.	k = 0.00025/in.
anchor slip = 0.098 in.	c = 10 (relaxation)
σ_1 = 208.8 ksi	ε_1 = 0.0072
σ_2 = 227.8 ksi	ε_2 = 0.01
σ_3 = 244.4 ksi	ε_3 = 0.02
σ_4 = 250.0 ksi	ε_4 = 0.03
σ_5 = 256.0 ksi	ε_5 = 0.05

The stiffness is re-formed after each four iterations and convergence obtained in an average of 6.4 iterations per load step with a displacement tolerance of 0.001 in.

At 14 days after casting the prestress is applied with the indicated jacking force and the friction and anchor slip losses taken into account. A time-dependent analysis is then carried out up to age 28 days when the beam is loaded to failure by increasing the concentrated load P in the steps indicated in Fig. 6.11. Good agreement between the experimental load-deflection curve and that obtained in the present study, as well as the results reported by Kang [37], can be observed.

In Fig. 6.12a the end reaction obtained in the present study is shown to agree very well with the experimental values -- similar results were reported by Kang. The percentage increase in the force in the tendon in those elements closest to the maximum positive and negative moment regions obtained in the present study is compared to the values reported by Kang in Fig. 6.12b -- no experimental values are available. Good agreement can be observed -- differences can be ascribed to the fact that in this study the prestressing is applied in a different manner and the elongation of

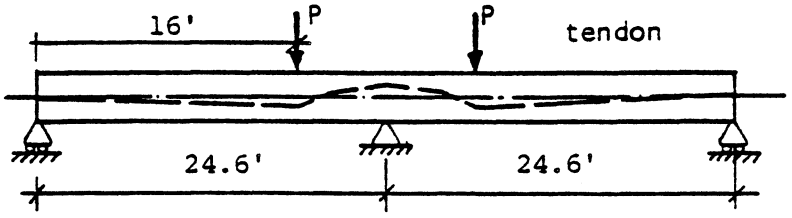

ELEVATION OF BEAM

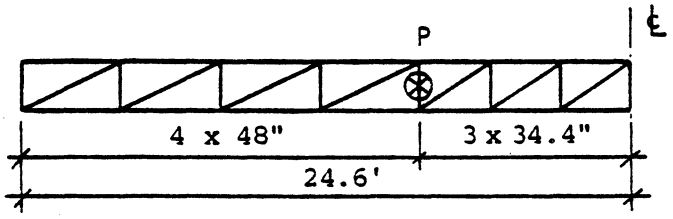

PLAN OF MESH

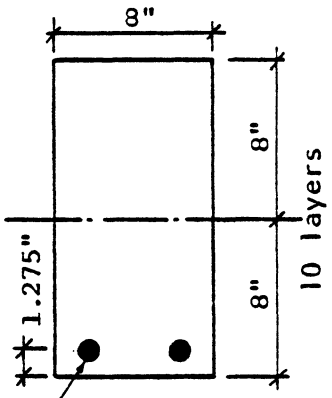

CROSS SECTION

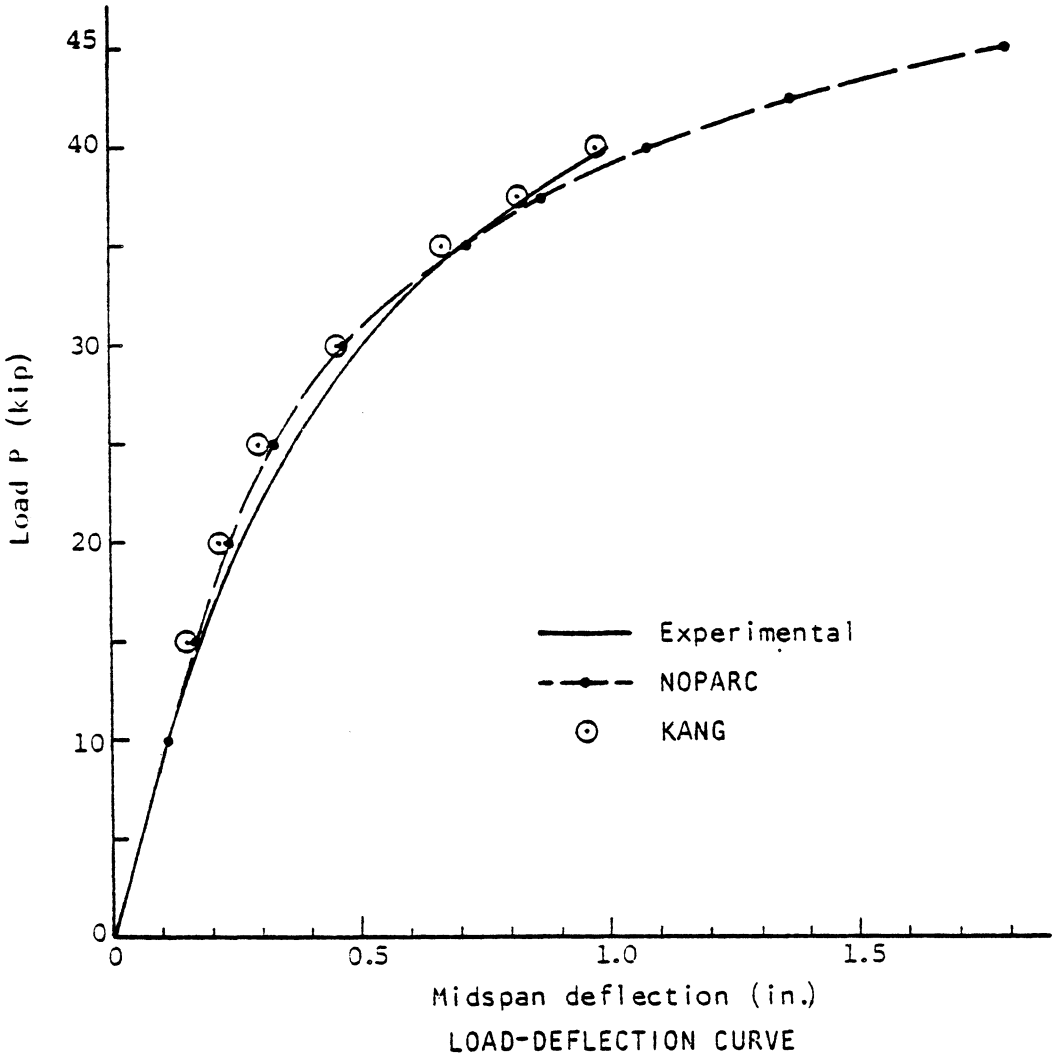

LOAD-DEFLECTION CURVE

FIG. 6.11 LIN CONTINUOUS PRESTRESSED BEAM (Ex. 6.4.2).

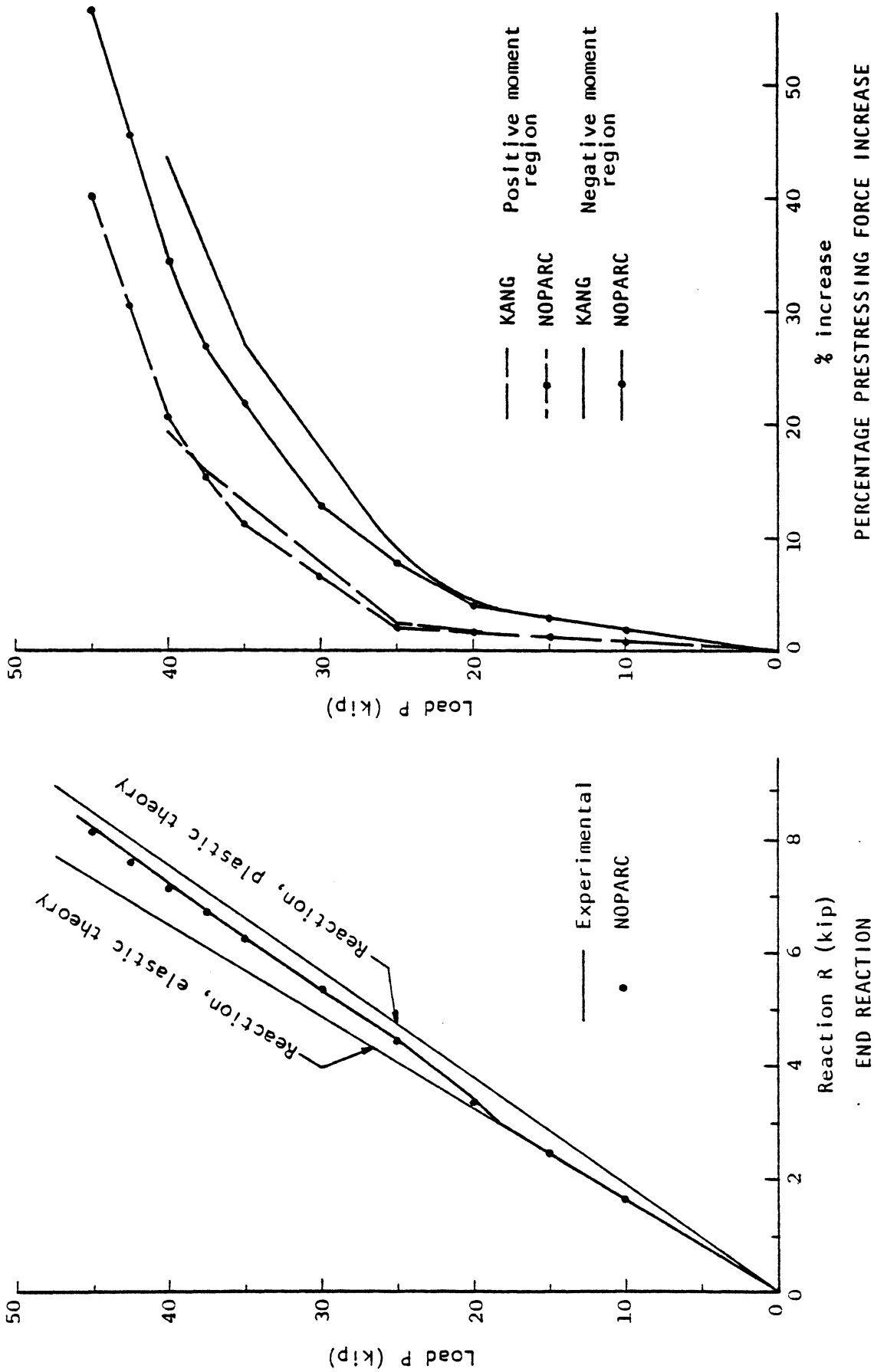

FIG. 6.12 LIN CONTINUOUS PRESTRESSED BEAM (Ex. 6.4.2).

the tendons also determined differently from the procedures used by Kang [37].

6.4.3 Ritz plate strip

Ritz et al. [121] tested five plate strips with unbonded post-tensioned tendons. An axial spring was used to study the behavior of these plate strips when membrane forces also become important. One of these plate strips (one with no axial spring, since the spring cannot be modeled in conjunction with prestressing) is selected for study.

Due to symmetry only half of the 141.72 in. span and 15.75 in. wide plate strip is modeled by the finite element mesh shown in Fig. 6.13b. The cross section of depth 7.86 in. is divided into 10 equal concrete layers and the small percentage of reinforcing steel is neglected. The single unbonded tendon has a parabolic profile with zero eccentricity at the end anchor and an eccentricity of -2.85 in. at the center of the span. The material properties used for the analysis are as follows:

Concrete:

E_o = 4560 ksi	ε_c = 0.002 in/in.
f'_c = 5000 psi	ν = 0
f'_t = 500 psi	w = 156 pcf.

Prestressing Steel:

P_o = 24.8 kip	μ = 0.1/rad.
A_s = 0.144 in^2.	k = 0.00004/in.
σ_1 = 216 ksi	ε_1 = 0.008
σ_2 = 233 ksi	ε_2 = 0.010
σ_3 = 241 ksi	ε_3 = 0.011

σ_4 = 249 ksi $\quad\quad$ ε_4 = 0.015

σ_5 = 256 ksi $\quad\quad$ ε_5 = 0.0266

The stiffness is re-formed each second iteration and convergence is obtained in an average of 5.6 iterations per load step with a displacement tolerance of 0.001 in.

In the first load step the prestressing and the dead load of the strip is applied and then the plate strip is loaded in further steps as shown in the load-deflection curve in Fig. 6.13b. In the test the deflection of the plate strip was 10.2 in. when the strip failed due to rupture of the tendon. The sustained load on the yield plateau of the load-deflection curve varied between 927 and 975 lb/in. The load-deflection curve obtained in the present study compares very well with the part of the experimental curve shown here. However, in the analysis the strip failed at a load of 900 lb/in. due to a hinge forming in the center of the span. At this stage the two center elements are cracked over their whole depth and this results in the structure collapsing.

In an actual structure cracking at a section causes additional stretching of all the other fibers that are in tension and thus the opening of a crack can be considered to be similar to a jacking operation on the tendon in the interior of the structure. This will tend to produce a higher stress in the interior parts of the tendon than at the anchors, since it is being stressed at the point where the cracking occurs and the anchors just act as dead anchors. This sequence of events is very difficult to model analytically, hence the assumption in this study that the stress variation for unbonded tendons remain the same as for the initial stressing operation. Due to large deflections the curvature of a tendon

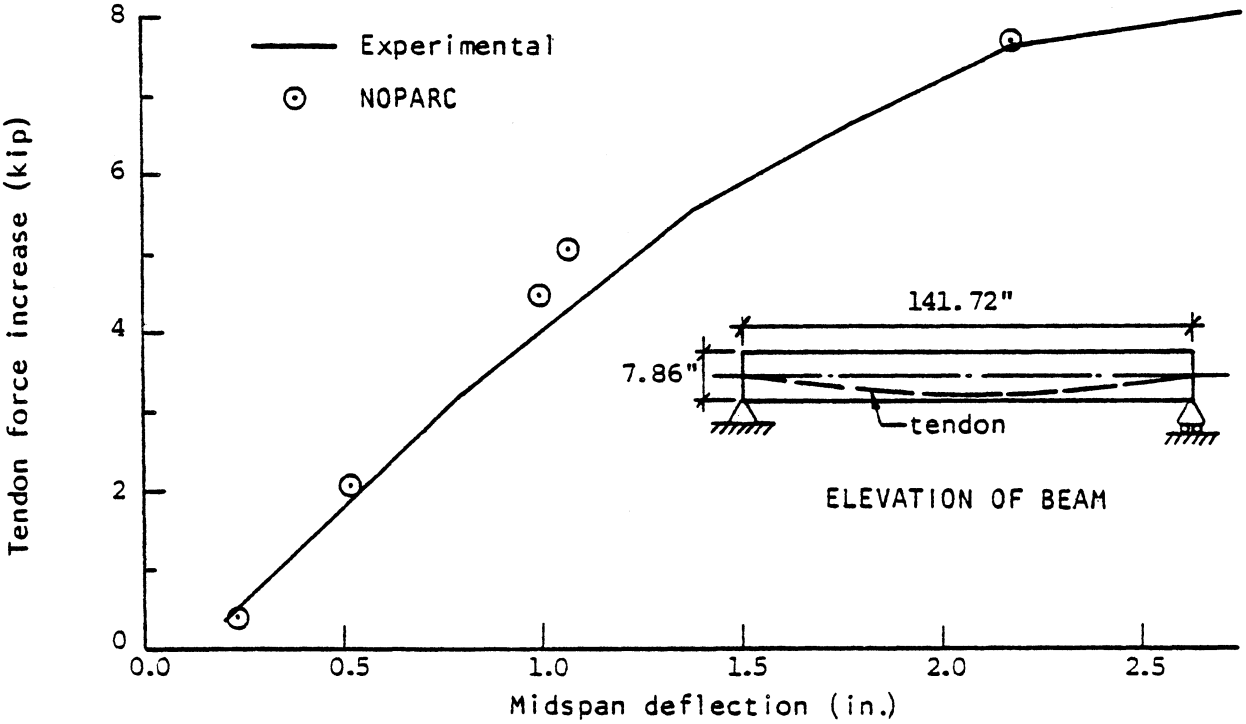

a. INCREASE IN PRESTRESSING TENDON FORCE

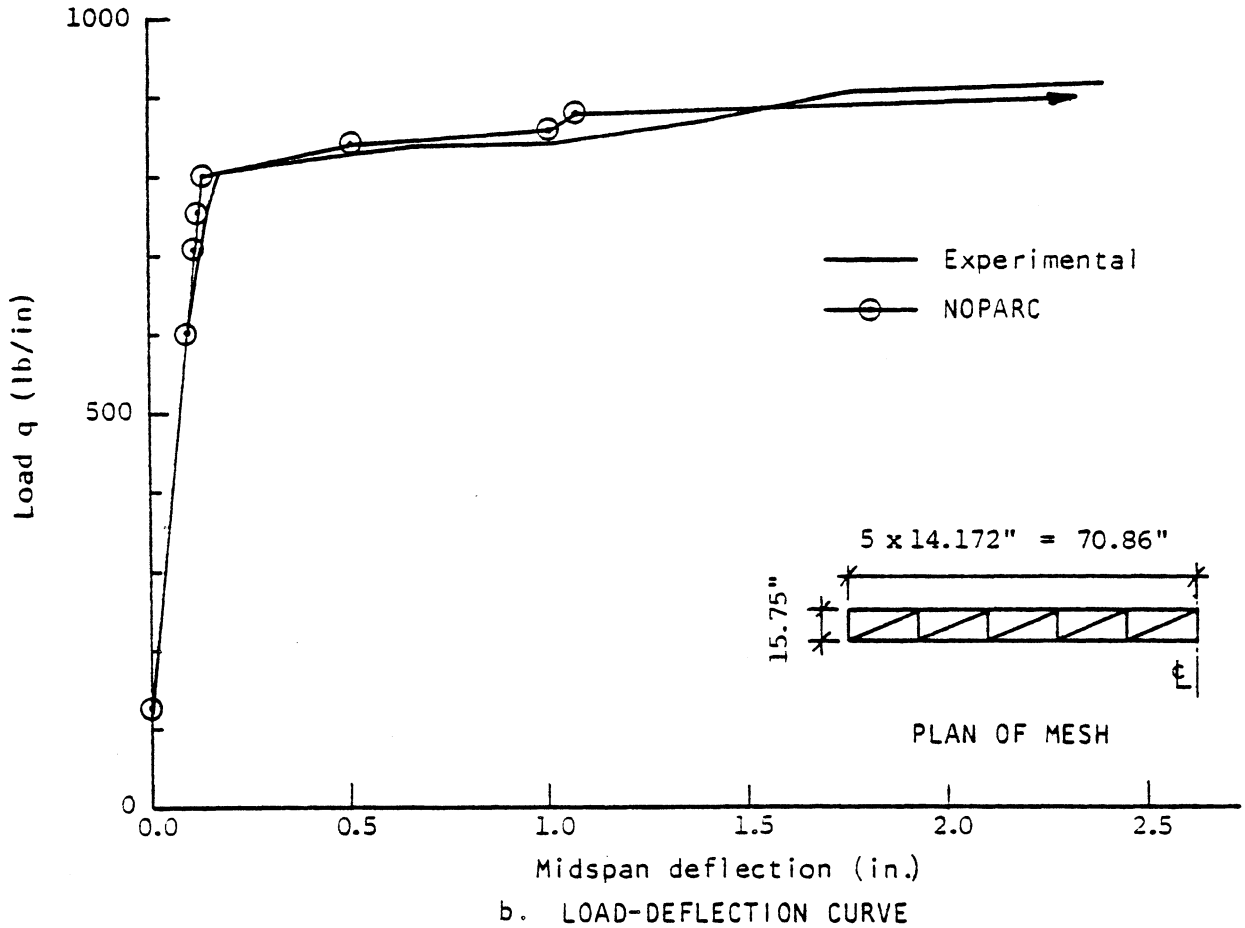

b. LOAD-DEFLECTION CURVE

FIG. 6.13 RITZ PRESTRESSED PLATE STRIP UNDER UNIFORM LOAD (Ex. 6.4.3)

also changes considerably and this will also increase the friction along the length of the tendon. These two factors will tend to cause higher tendon forces to be developed at cracks for a smaller tendon elongation. These two factors are considered to be the major reasons for the analytical failure of the plate strip at a lower load.

In Fig. 6.13a it can be seen that the increases in tendon force obtained from the present analysis compare well with the experimental curve.

6.4.4 Ritz simply supported slab

Ritz et al. [121] also tested a simply supported slab prestressed with unbonded post-tensioned tendons as a part of the same investigation mentioned in section 6.4.3. The slab is 141.72 in. square and 7.86 in. thick. Due to symmetry only one quarter of the slab is modeled with the finite element mesh shown in Fig. 6.14b. The cross section is divided into 10 equal concrete layers. The prestressing tendons have parabolic profiles with zero eccentricity at the outside edges and an eccentricity of 2.55 in. at their centers. The small amount of reinforcing steel used to form a beam around the slab perimeter is ignored. In the test a downward reaction at the slab corner was provided to simulate the usual assumption made in the analysis of simply supported plates. The material properties used for the analysis are as follows:

Concrete:

E_o = 4560 ksi $\qquad$ ε_c = 0.002 in/in.

f'_c = 5000 psi $\qquad$ ν = 0.18

f'_t = 500 psi $\qquad$ w = 156 pcf.

Prestressing Steel:

P_o = 24.56 kip	μ = 0.3/rad.
A_s = 0.144 in^2.	k = 0.0003/in.
σ_1 = 216 ksi	ε_1 = 0.008
σ_2 = 233 ksi	ε_2 = 0.010
σ_3 = 241 ksi	ε_3 = 0.011
σ_4 = 249 ksi	ε_4 = 0.015
σ_5 = 256 ksi	ε_5 = 0.0266

In the first load step the slab dead load and the prestressing are applied and the uniform load thereafter increased in steps as shown in Fig. 6.14b. From the load-deflection curve shown in this figure it can be seen that the behavior of the analytical model is considerably stiffer than that displayed by the test slab. In Fig. 6.14a the increases in the tendon forces obtained from the analysis are compared to the experimental values. It can be observed that the analytical values are slightly higher and that the force increases of all the tendons are roughly the same, while the experimental force increase of tendon 1 is considerably lower than that of the others.

The fact that these analytical tendon force increases of all the tendons are nearly the same is considered to be caused by the following phenomenon. The slab is relatively thick, the span to depth ratio being only 20, and the compressive strength of the concrete therefore does not control the ultimate load capacity -- the test slab failed due to rupture of the tendons. Due to cracking at the bottom of the slab the neutral axis moves upward and this causes arching. In this case the arching effects are most severe in the supported corner (where tendon 1 is located)

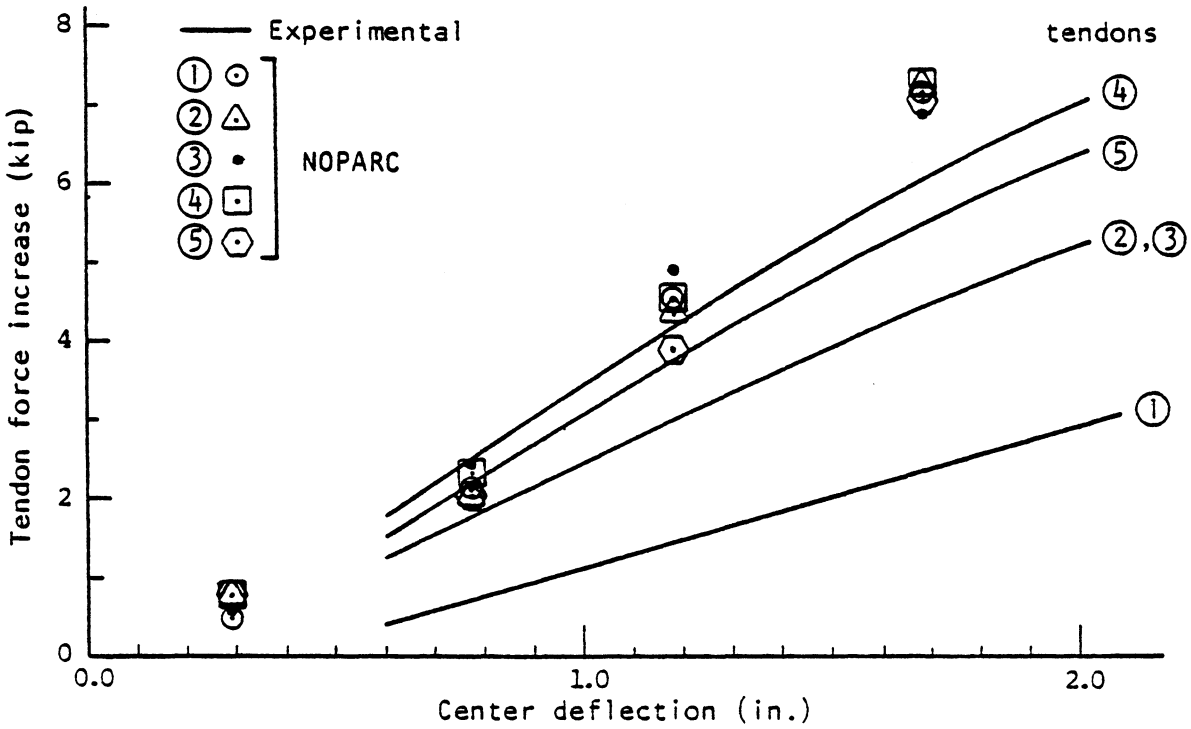

a. INCREASE IN PRESTRESSING TENDON FORCES

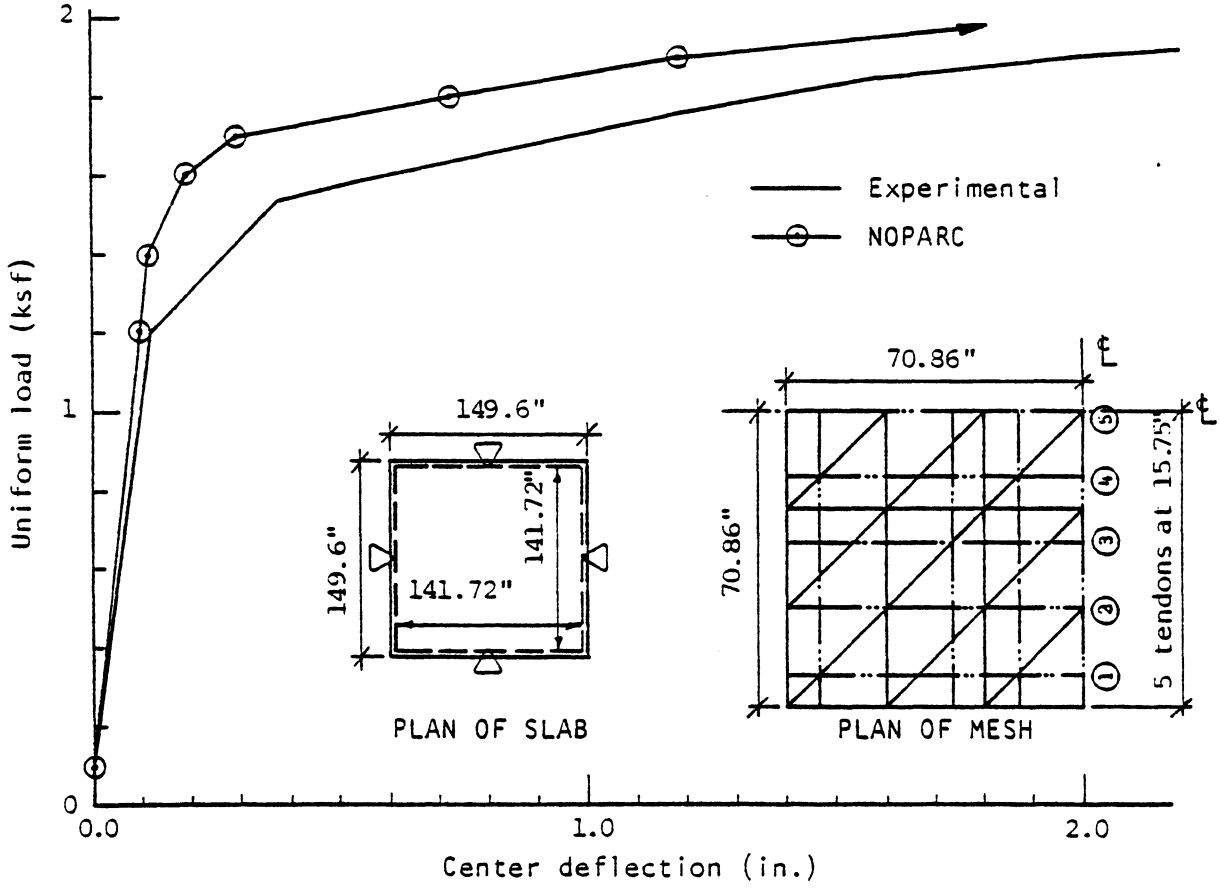

b. LOAD-DEFLECTION CURVE

FIG. 6.14 RITZ SIMPLY SUPPORTED PRESTRESSED SLAB UNDER UNIFORM LOAD (Ex. 6.3.4). (NO HORIZONTAL RESTRAINT AT EDGES)

and this causes tendon 1 to be stretched almost the same amount as tendons 4 or 5 are stretched by the effects of the out-of-plane displacements. This dominant arching action also explains why the analytical model is stiffer than the experimental slab.

6.4.5 Lin-Scordelis slab

A continuous two-way prestressed concrete slab, consisting of four panels supported on nine columns and stressed by 12 unbonded tendons in each direction, was tested by Lin, Scordelis and Itaya [122,123]. This was one of the first experimental studies undertaken to investigate the behavior of unbonded post-tensioned slabs. The slab is 3 in. thick with overall dimensions of 15 ft. square, resulting in 7 ft. center to center spans. Because of symmetry one of the panels, a quarter of the experimental slab, is modeled with the finite element mesh shown in Fig. 6.15. The cross section is divided into 10 equal concrete layers. The tendons have a spacing of 15 in. and the tendon profile is shown in Fig. 6.17a.

The test slab was stressed at 28 days after casting and loaded to failure 14 days afterwards. Two analyses are carried out to study the effect of the time-dependent factors on the behavior of the slab. For the first analysis the slab is stressed and loaded to failure at 28 days after casting. In the second analysis the slab is stressed at 14 days after casting and simultaneously loaded with the slab dead load only. At 42 days after casting the design live load of 80 psf. is added and kept on the slab up to 360 days after casting. At this age the slab is again loaded to failure. The time-dependent analysis is carried out at the days after casting indicated in Fig. 6.16 where the load history and variation of midpanel deflection with time is shown. The concrete

properties at the different ages are calculated from the 28 day values below by using the ACI formulae (section 3.2.4). For the calculation of the creep and shrinkage the ACI values presented in sections 3.2.7 and 3.2.6, respectively, are used.

Concrete (28 day properties):

E_o = 3650 ksi	ε_c = 0.002 in/in.
f'_c = 5450 psi	ν = 0.14
f'_t = 500 psi	w = 160 pcf.

Prestressing Steel:

P_o = 7.0 kip/tendon	μ = 0.4/rad.
A_s = 0.049 in^2.	k = 0.000167/in.
c = 10 (relaxation)	
σ_1 = 170.52 ksi	ε_1 = 0.0058
σ_2 = 220.0 ksi	ε_2 = 0.010
σ_3 = 240.0 ksi	ε_3 = 0.030
σ_4 = 253.0 ksi	ε_4 = 0.067

The stiffness is re-formed after each third iteration and convergence is achieved in the average number of iterations indicated in Table 6.1 with a displacement tolerance of 0.001 in.

A plot of uniform live load vs. midpanel deflection is shown in Fig. 6.15. The experimental values are the average of the values recorded at the centers of the four panels. Excellent agreement can be seen between the 28 day analytical curve and the experimental curve up to a live load level of 240 psf. The test slab developed very large cracks at a live load of 347 psf and deflections increased from 0.21 in. to 2.1 in.

at this point. The deflections of the analytical model keep on increasing in the load step above 320 psf in a way similar to the test slab. The test slab failed at a live load of 362 psf when the center column punched through the slab. The early failure of the analytical structure is also considered to be due to the fact that the real increase in the tendon forces in the interior of the slab caused by cracking is not incorporated in the present study as is discussed for Ex. 6.4.3.

The load-deflection curve for the loading to failure of the slab at 360 days after casting is also shown in Fig. 6.15. Due to the relaxation of the prestressing steel and the creep and shrinkage of the concrete the average loss of force in the tendons is 14.5% (see Fig. 6.17b) for the time period studied. Because of the reduction in the tendon forces it can be observed that larger deflections of the analytical slab are required at 360 days compared to those at 28 days to balance the applied load. The analytical model again fails at the same load level as in the 28 day analysis.

In Fig. 6.18 a plot of tendon force vs. midpanel deflection is shown for tendon 1, the one closest to the slab centerline, and for tendon 4, one in the interior of the slab. The recorded increases in the tendon forces for the test slab varied between 0.8 kip and 2.6 kip for the increase in live load from 0 to 356 psf and no particular distribution of these force increases could be noted.

The maximum analytical deflection of the slab after transfer is +0.026 in. upward for the 28 day analysis and +0.028 in. for the 360 day analysis. The latter value increases to +0.046 in. at 42 days and under the design live load this deflection changes from +0.011 in. to -0.007 in. indicating that the slab would stay almost flat under the design load.

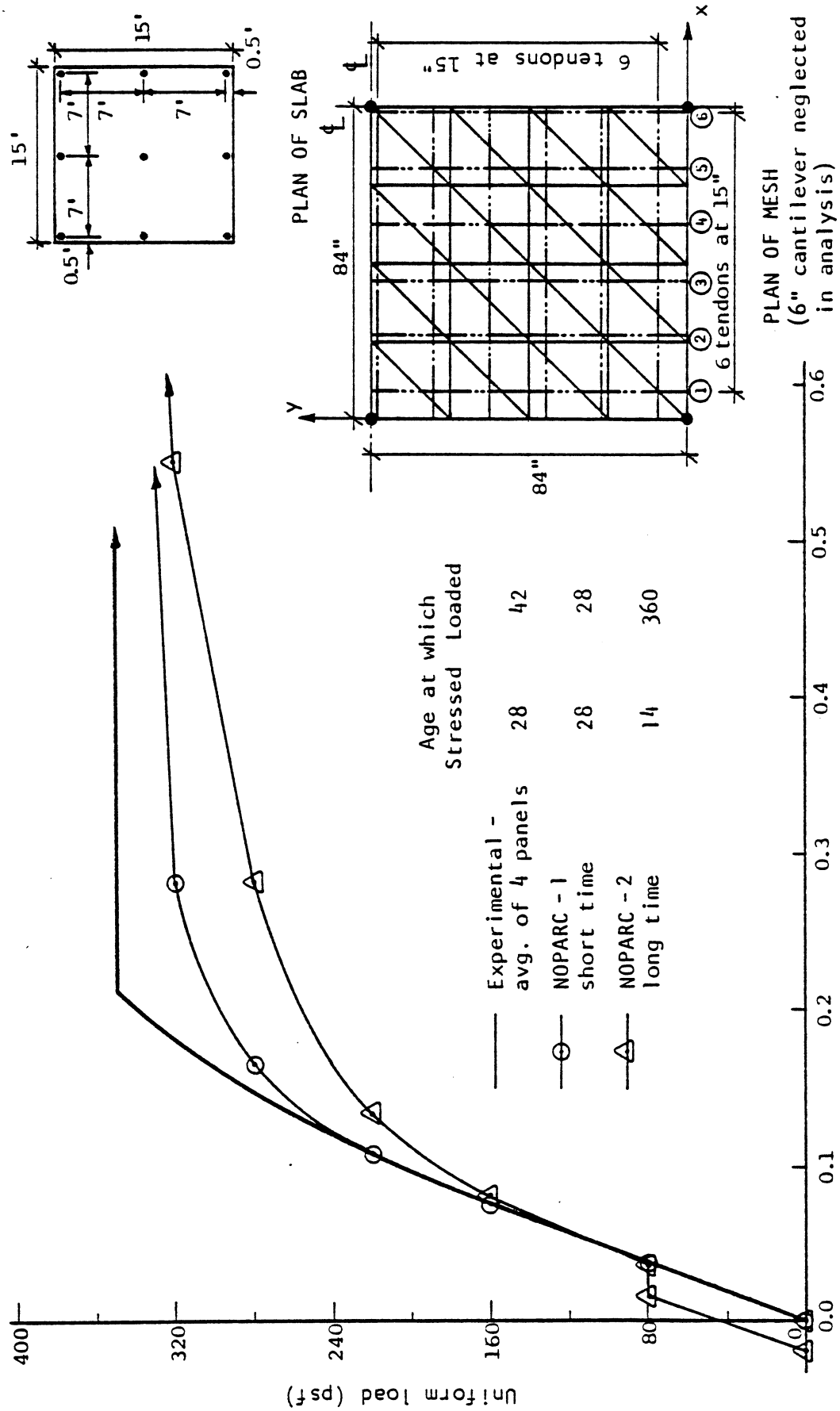

FIG. 6.15 LIN-SCORDELIS PRESTRESSED SLAB UNDER UNIFORM LOAD SLAB (Ex. 6.4.5).

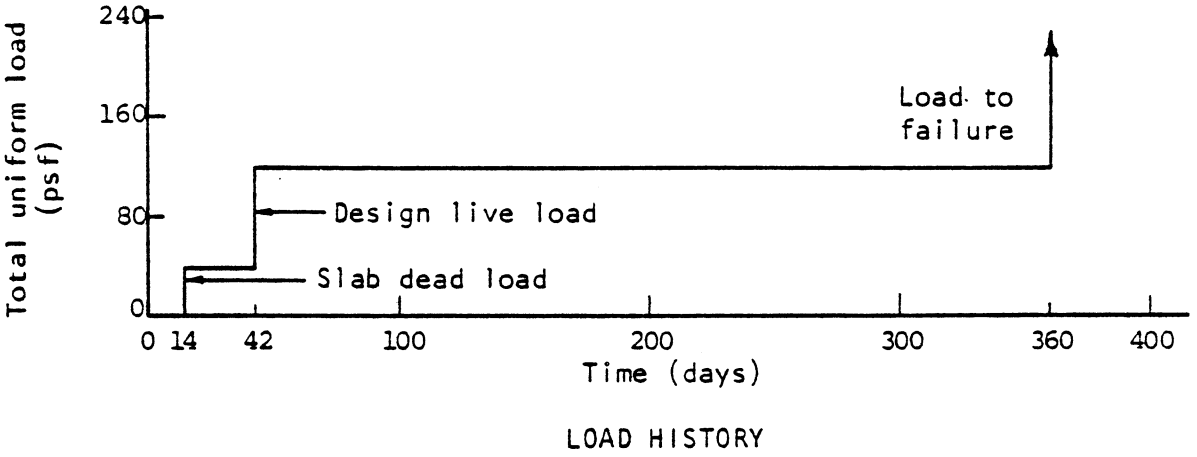

LOAD HISTORY

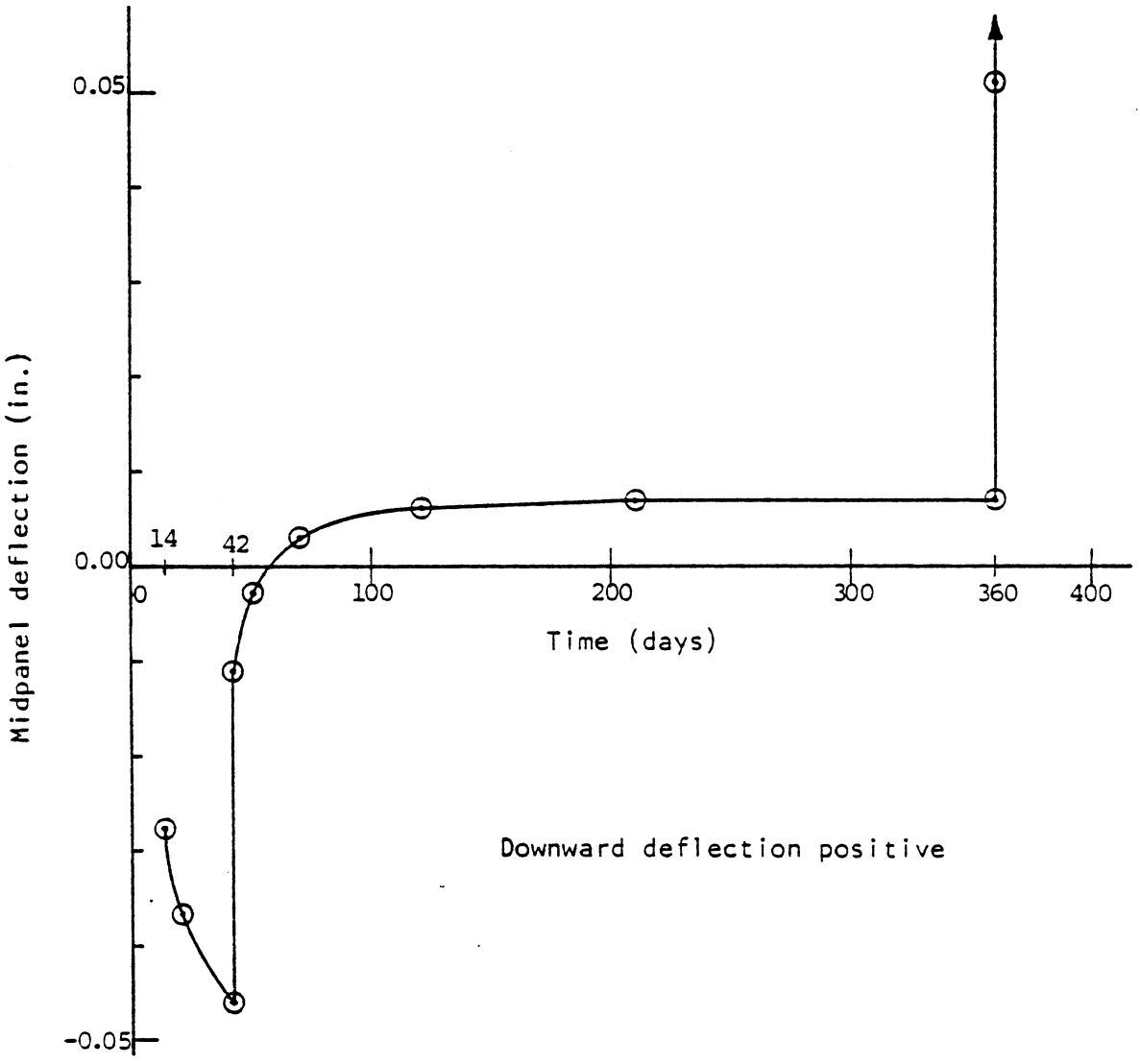

MIDPANEL DEFLECTION HISTORY

FIG. 6.16 LIN-SCORDELIS PRESTRESSED SLAB (Ex. 6.4.5): LOAD AND DEFLECTION HISTORY. (NOPARC ANALYTICAL SOLUTION ONLY)

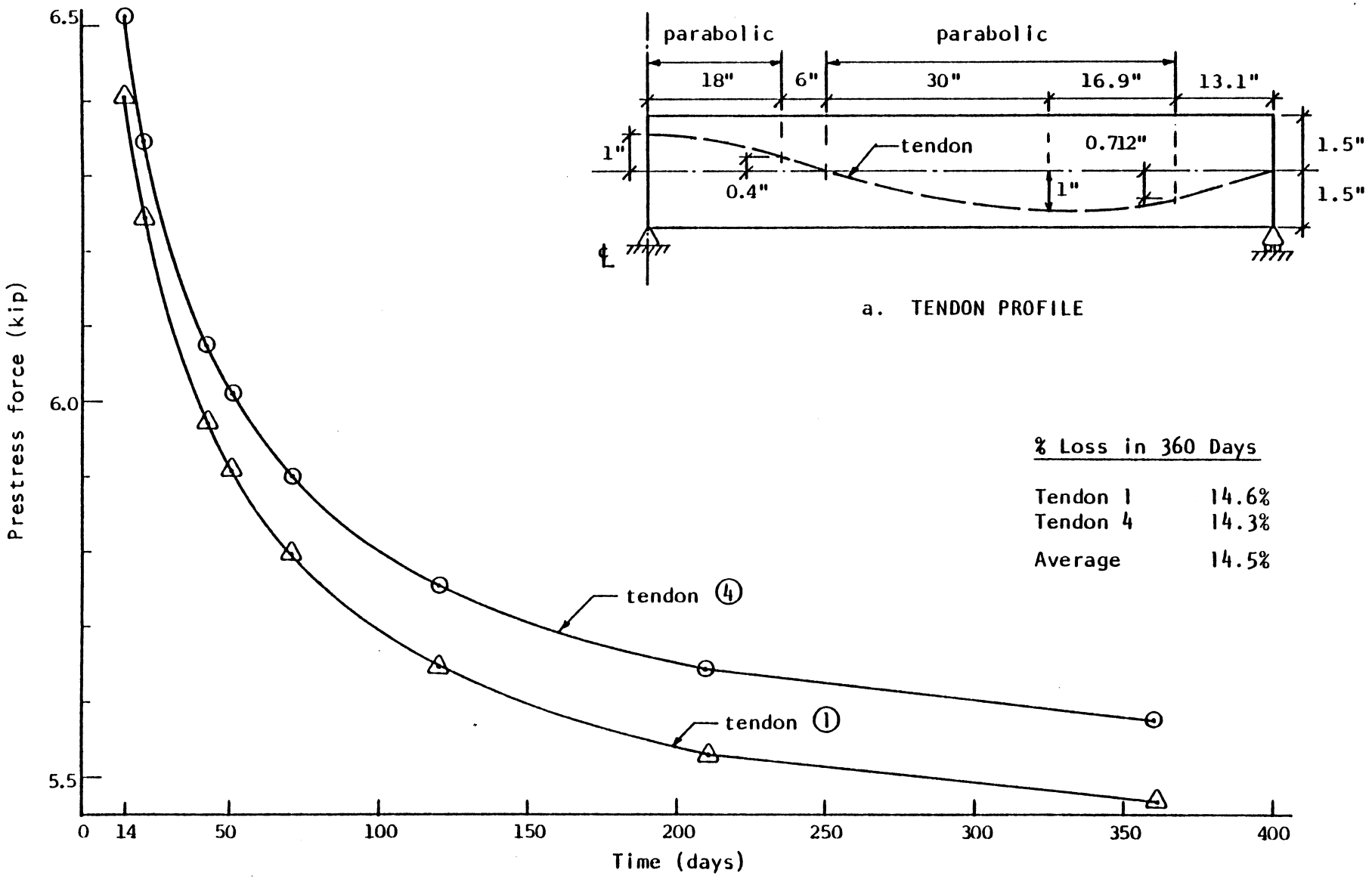

FIG. 6.17 LIN-SCORDELIS PRESTRESSED SLAB (Ex. 6.4.5).
(NOPARC ANALYTICAL SOLUTION ONLY)

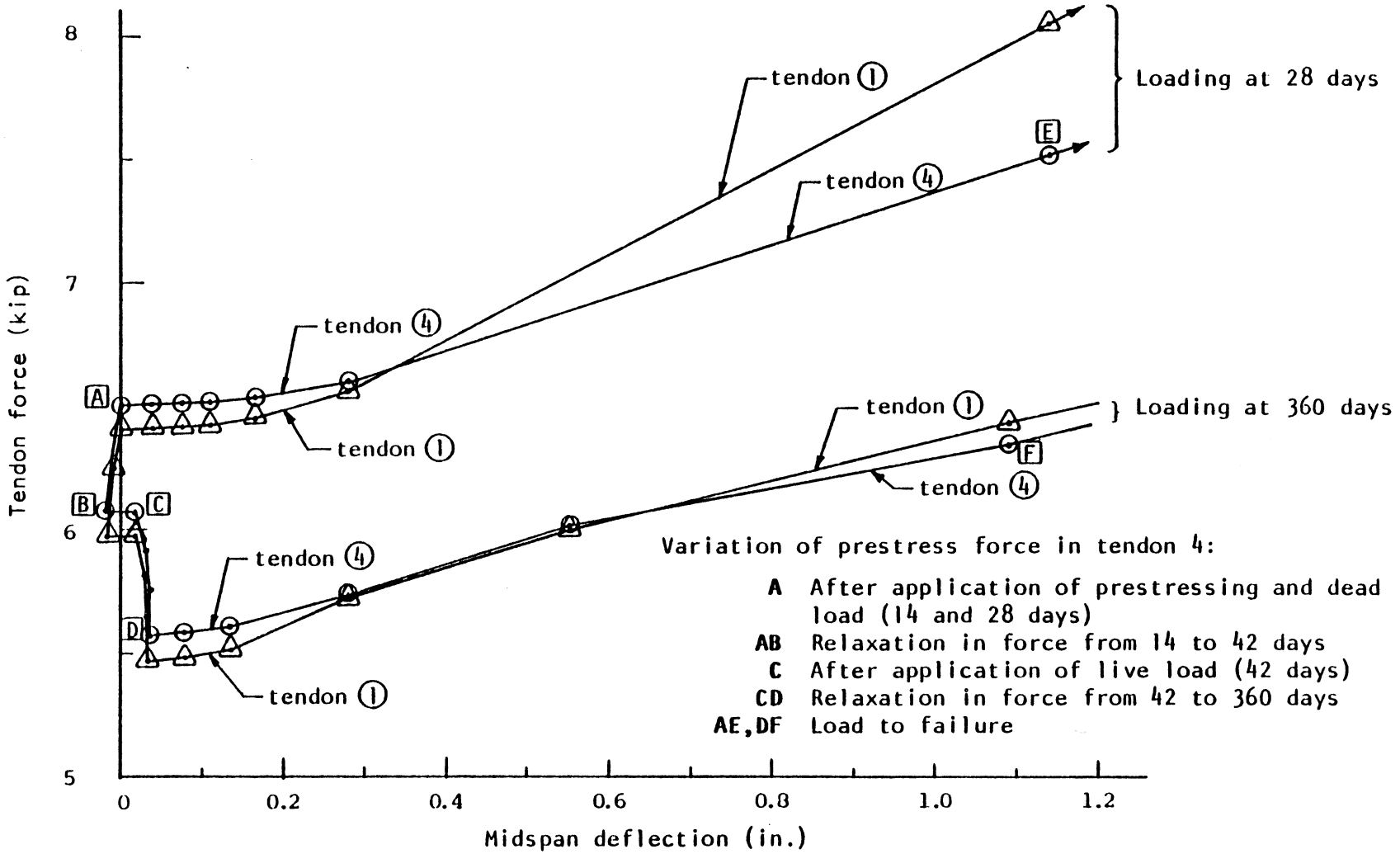

FIG. 6.18 LIN-SCORDELIS PRESTRESSED SLAB (Ex. 6.4.5): VARIATION OF PRESTRESS FORCE VS. MIDSPAN DEFLECTION. (NOPARC ANALYTICAL SOLUTION ONLY)

These values compare well with the maximum recorded deflection under dead load only of +0.052 in. upwards.

6.5 COMPUTER TIME

The examples presented in this chapter were run on the CDC 6400 computer of the University of California, Berkeley Computer Center. A binary version of the program NOPARC was used. The important parameters for each example together with the central processor, peripheral processor and effective times needed to run them are summarized in Table 6.1.

The numbers of joints and tendons are the main factors which determine the amount of central memory needed. The size of the structural stiffness matrix, the number of load steps, iterations per load step and how often the stiffness matrix is re-formed are the major factors determining the amount of central processor time consumed. The variables containing the data for the nonlinear material models and the time-dependent effects for each element are stored on slow-speed storage (tapes). The manipulation of this large amount of data is reflected in the peripheral processor time which for most examples contributes between one third and one half of the cost of the analysis.

Example No.	Time-Dependent Analysis	Nonlinear Material	Nonlinear Geometry	No. of Joints	No. of Elements	No. of Tendons	No. of Equations	Bandwidth	No. of Time Steps	Total No. of Load Steps	No. of Iterations Per Load Step	Central Processor Time (sec)	Peripheral Processor Time (sec)	Effective Time (sec)
6.2.2	NO	NO	YES	25	32	-	86	31	-	5	3.0	193	378	343
(2)	NO	NO	YES	12	10	-	30	12	-	10	2.4	84	84	127
6.3.1(3)	NO	YES	NO	12	10	-	30	12	-	9	4.1	104	113	165
(4)	NO	YES	YES	12	10	-	30	12	-	9	3.9	105	125	171
6.3.2	NO	YES	NO	16	18	-	63	23	-	15	7.9	432	578	708
6.3.3 a	NO	YES	NO	19	24	-	72	30	-	16	8.9	709	808	1105
b	NO	YES	YES	19	24	-	72	30	-	16	8.9	819	1090	1321
6.3.4	NO	YES	YES	25	32	-	64	28	-	10	15.5	936	989	1450
6.3.5	YES	YES	NO	4	2	-	4	4	18	20	2.3	39	96	91
6.4.1 a	NO	YES	NO	12	10	4	30	12	-	10	3.1	124	143	201
b	NO	YES	YES	12	10	4	30	12	-	10	5.5	152	161	238
6.4.2	YES	YES	NO	16	14	1	50	14	2	13	6.4	276	261	424
6.4.3	NO	YES	YES	12	10	1	30	12	-	9	5.6	148	186	241
6.4.4	NO	YES	YES	16	18	10	58	27	-	8	9.6	339	710	712
6.4.5 a	NO	YES	NO	25	32	12	101	33	-	7	7.0	431	730	841
b	YES	YES	NO	25	32	12	101	33	7	16	6.6	920	900	1510

TABLE 6.1 Summary of Important Parameters and Computer Time for The Examples Presented

7. SUMMARY AND CONCLUSIONS

7.1 SUMMARY

A numerical method of analysis, including material and geometric nonlinearities, has been developed to trace the quasi-static response of reinforced and prestressed concrete slabs and panels under short time and sustained load conditions. Time-dependent effects due to load history, temperature history, creep, shrinkage and aging of concrete and stress relaxation in the prestressing steel have been incorporated. The load-deflection and stress history of the above mentioned structures through the elastic, inelastic and ultimate ranges were traced. The collapse of these structures due to in-plane membrane plus bending effects was predicted considering local failures in steel and concrete along with the deterioration of the structural stiffness due to progressive cracking.

A finite element stiffness formulation, coupled with a time step integration scheme has been developed to analyze reinforced concrete systems. Within a time step, an incremental load procedure with an iterative approach to obtain an equilibrium position of the structure for each load increment, was adopted to trace the nonlinear behavior of such structures. All load changes were considered to occur at the beginning of a time step and the resultant state of stress was assumed to remain unchanged through the time step requiring that suitably small time steps should be chosen for the analysis.

An updated Lagrangian formulation has been employed to take the effects of changing structural geometry on the response of structures into account. The effect of initial stresses was incorporated by the inclusion of the geometric stiffness. By separating the rigid body displacements

from the true element deformation, problems where large displacements occur were analyzed, while the theory assuming small strains and rotations was still valid at the element level.

The reinforced concrete composite section was modeled as a layered system of concrete and equivalent smeared steel layers. Perfect bond was assumed to exist between the concrete and bonded steel layers. The layered system was capable of accounting for the effects of in-plane as well as flexural forces in a structural member. Kirchhoff's assumption of plane sections remaining plane was adopted to relate the displacements at various levels through the cross section depth and thus reduce each layer to a two-dimensional problem in which each layer was assumed to be in a state of plane stress. Variation of material properties through the depth of the member was then accommodated by allowing each layer to have different material properties according to its state of deformation. The nonlinear material behavior was taken into account by updating the material matrix of each concrete and steel layer. The stiffness of an element was then obtained by integrating the contribution of the concrete, the reinforcing steel and the bonded prestressing steel layers in the section.

Since each concrete layer was assumed to be in a state of plane stress, a nonlinear constitutive relationship, based on the available data from biaxial load tests, was selected. Tensile cracking at a limiting stress level, tension stiffening between cracks and the strain-softening phenomenon beyond the maximum compressive strength was incorporated. The effects of the stress history, temperature history, aging, creep and shrinkage were included in the long time deformations in the concrete layers. The steel reinforcement was represented by a bilinear, strain hardening model approximating the Bauschinger effect. The prestressing

steel was modeled by a multi-linear stress-strain relationship and the relaxation of stress over time was taken into account. The constitutive relations were based on the assumption of small strains and simple unloading paths for stress reversals were included.

An efficient procedure for the calculation of the effects of creep, which incluced all the important factors influencing creep and which has parameters that can be readily determined from experimental data, has been incorporated. The effects of stress history were accounted for by the application of the linear superposition method in the calculation of the creep strains. The influence of temperature variations on creep strains were incorporated by the time shift principle. These characterize concrete to be an aging visco-elastic thermorheologically simple material. Creep under a biaxial state of stress was represented by the introduction of the creep Poisson's ratio observed in a uniaxial, sustained load test. Variations of creep compliance due to the slump of the concrete mix, the size of a member, relative ambient humidity and high stress levels were considered on the basis of available experimental data. A shrinkage model, based on experimental observations and taking into account temperature and humidity changes, the slump of the concrete mix and the size of members, was also adopted.

Prestressed concrete slabs or panels having an arbitrary tendon layout with either pretensioned, or bonded or unbonded post-tensioned tendons can be analyzed. The tendon layout data can be specified and the loading due to prestressing and discretization of the tendons are then calculated in the computer program. Losses due to friction along the tendon, anchor slip and the deformation of the concrete were taken into account. The loads on the structure due to prestressing were calculated by using the

equivalent load concept. The state of strain and stress in unbonded tendons was determined with an iterative solution procedure.

Finally, calculations for the effects of short time and sustained loads were carried out for some typical examples using a computer program based on the above principles. Flat triangular shell elements were used and the examples include reinforced and prestressed concrete beams, columns and slabs. The numerical results were compared to available experimental and/or analytical data to check the applicability and validity of the method of analysis presented in this study.

7.2 CONCLUSIONS

1. It has been demonstrated that the numerical method of analysis developed in the present study can predict the response of reinforced and prestressed concrete beams and slabs subjected to both short time and sustained load conditions fairly accurately. Useful information about the behavior of such structures for different load histories can be obtained from the analysis.

2. The models adopted to represent the material properties are capable of simulating the dominant flexural and membrane behavior of reinforced and prestressed concrete beams, slabs and panels in the elastic, inelastic and ultimate ranges.

3. The time-dependent analysis procedure incorporated in the present method includes an efficient and comprehensive model for the creep of concrete in which either experimental or standard data can be used. Shrinkage and the effect of temperature on both creep and shrinkage of

concrete, as well as relaxation in prestressing steel are also taken into account.

4. The accuracy of the procedure adopted in this study to deal with geometric nonlinearity in planar structures has been demonstrated.

5. Prestressing tendons, with the accompanying interaction between the tendons and the concrete during loading of the structure, have been incorporated as an integral part of the slabs and panels analyzed.

7.3 RECOMMENDATIONS

1. The constitutive model adopted in this study to represent the behavior of concrete under a state of biaxial stress could be extended to include cyclic loading, unloading and reloading. The analysis of structures subjected to earthquake loadings, for example, would then be possible with the above model. Experimental studies, however, are needed to be able to check the validity of any proposed model regarding its representation of concrete behavior, not only under the above mentioned cyclic loadings, but also when subjected to non-monotonic and non-proportional loadings.

2. For the analysis of reinforced concrete slabs and panels under very large displacements, where the response of the structure is mainly determined by the behavior of the reinforcing steel in the strain hardening region, a better representation of the complete stress-strain curve of the reinforcing steel up to its ultimate strength, would be essential.

3. To analyze slab and beam systems more effectively a special reinforced concrete beam element which can be coupled to the shell element used in this study should be developed. The beam element should be capable of modeling beams which are concentric or eccentric with respect to the shell element representing the slabs or panels.

4. In the case of unbonded tendons further experimental and analytical studies are needed to determine the true variation of prestress force along the length of the tendon after cracking of the concrete due to the highly indeterminate nature of the friction forces after cracking.

5. Experimental data on the long-term behavior of reinforced and prestressed concrete slabs and panels, which are lacking at the present time, are needed to verify the results of the analytical procedures employed in the present study.

6. Possible future improvements to the computer program NOPARC, depending on its intended use, are suggested as follows.

   a) A restart option, whereby an analysis could be performed up to a certain stage and then later continued, would be useful.

   b) When only short time analyses are to be performed it would be advantageous, in terms of computer cost, to delete those subroutines and variables dealing with the time-dependent part of the analysis.

   c) The use of extended core storage instead of slow speed storage (tapes) could also be investigated.

REFERENCES

1. American Concrete Institute, "Building Code Requirements for Reinforced Concrete (ACI 318-77)," American Concrete Institute, Detroit, Michigan, 1977.

2. American Concrete Institute, "Commentary on Building Code Requirements for Reinforced Concrete (ACI 318-77)," American Concrete Institute, Detroit, Michigan, 1977.

3. Post-Tensioning Institute, "Design of Post-tensioned Slabs," Post-Tensioning Institute, Glenview, Illinois, 1977.

4. ACI-ASCE Committee 423, "Tentative Recommendations for Prestressed Concrete Flat Plates," ACI Journal, Vol. 71, No. 2, February 1974, pp. 61-71.

5. Lin, T. Y., Design of Prestressed Concrete Structures, Second Edition, Wiley, New York, 1963.

6. Scordelis, A. C., "Finite Element Analysis of Reinforced Concrete Structures," Proceedings of the Specialty Conference on Finite Element Methods in Civil Engineering, Montreal, June 1972.

7. Schnobrich, W. C., "Behavior of Reinforced Concrete Predicted by Finite Element Method," Proceedings of the Second National Symposium on Computerized Structural Analysis and Design, George Washington University, Washington, D. C., March 1976.

8. Wegner, R., "Finite Element Models for Reinforced Concrete," preprint, Proceedings of the U.S.-Germany Symposium on Formulations and Computational Methods in Finite Element Analysis, Massachusetts Institute of Technology, Cambridge, August 1976.

9. Scordelis, A. C., "Finite Element Modeling of Reinforced Concrete Structures," Seminar on the Finite Element Analysis of Reinforced Concrete Structures, University of Milan, June 1978, pp. 63-113.

10. Jofriet, J. C. and McNeice, G. M., "Finite Element Analysis of Reinforced Concrete Slabs," Journal of the Structural Division, ASCE, V. 97, No. ST3, March 1971.

11. Bell, J. C., "A Complete Analysis of Reinforced Concrete Slabs and Shells," Ph.D. Dissertation, Department of Civil Engineering, University of Canterbury, Christchurch, New Zealand, 1970.

12. Bell, J. C. and Elms, D., "Partially Cracked Finite Elements," Journal of the Structural Division, ASCE, Vol. 97, No. ST7, July 1971.

13. Scanlon, A., "Time Dependent Deflections of Reinforced Concrete Slabs," Ph.D. Dissertation, Department of Civil Engineering, University of Alberta, Edmonton, Canada, December 1971.

14. Scanlon, A. and Murray, D. W., "Time Dependent Reinforced Concrete Slab Deflections," Journal of the Structural Division, ASCE, Vol. 100, No. ST9, September 1974.

15. Dotroppe, J. C., Schnobrich, W. C., and Pecknold, D. A., "Layered Finite Element Procedure for Inelastic Analysis of Reinforced Concrete Slabs," IABSE Publication 33-11, 1973.

16. Berg, S., "Nonlinear Finite Element Analysis of Reinforced Concrete Plates," Report No. 73-1, Institutt for Statikk, Division of Structural Mechanics, University of Trondheim, Norway, February 1973.

17. Berg, S., Bergan, P. G., and Holand, I., "Nonlinear Finite Element Analysis of Reinforced Concrete Plates," Paper M3/5, 2nd International Conference on Structural Mechanics in Reactor Technology, Berlin, West Germany, September 1973.

18. Backlund, J., "Finite Element Analysis of Nonlinear Structures," Doctoral Thesis, Chalmers Technical University, Göteborg, Sweden, November 1973.

19. Schafer, H., Link, J., and Melhorn, G., "Zur Wirklichkeitsnahen Berechnung von Stahlbetonplatten Mit Der Finite Element Method," Beton and Stahlbetonbau, 11, 1975.

20. Wegner, R. and Duddeck, H., "Der Gerissenen Zustand Zweisetig Elagerter Platten unter Einzellasten - Nichtlineare Berechnung mit Finiten Elementen," Beton and Stahlbetonbau, 70, 1975.

21. Bashur, F. K. and Darwin, D., "Nonlinear Model for Reinforced Concrete Slabs," CRINC Report-SL-76-03, University of Kansas Center for Research, Inc., Lawrence, Kansas, December 1976.

22. Bashur, F. K. and Darwin, D., "Nonlinear Model for Reinforced Concrete Slabs," Journal of the Structural Division, ASCE, Vol. 104, No. ST1, January 1978, pp. 157-170.

23. Kristjansson, R., "Physikalisch und Geometrisce nichtlineare Berechnung von Stahlbetonplatten mit Hilfe Finiter Elemente," Dr.-Ing. Dissertation, University of Darmstadt, Darmstadt, West Germany, 1977.

24. Bell, J. C. and Elms, D. G., "A Finite Element Post Elastic Analysis of Reinforced Concrete Shells," Bulletin of the International Association for Shell and Spatial Structures, No. 54, April 1974.

25. Hand, F. R., Pecknold, D. A., and Schnobrich, W. C., "Nonlinear Layered Analysis of Reinforced Concrete Plates and Shells," Journal of the Structural Division, ASCE, V. 99, No. ST7, July 1973.

26. Lin, C. S., "Nonlinear Analysis of Reinforced Concrete Slabs and Shells," Ph.D. Dissertation, Division of Structural Engineering and Structural Mechanics, University of California, Berkeley, UC-SESM Report No. 73-7, April 1973.

27. Lin, C. S. and Scordelis, A. C., "Nonlinear Analysis of Reinforced Concrete Shells of General Form," Journal of the Structural Division, ASCE, V. 101, No. ST3, March 1975.

28. Kabir, A. F., "Nonlinear Analysis of Reinforced Concrete Panels, Slabs and Shells for Time Dependent Effects," Ph.D. Dissertation, Division of Structural Engineering and Structural Mechanics, University of California, Berkeley, UC-SESM Report No. 76-6, December 1976.

29. Müller, G., Kabir, A. F. and Scordelis, A. C., "Nonlinear Analysis of Reinforced Concrete Hyperbolic Paraboloid Shells," Proceedings, IASS Symposium on Nonlinear Behavior of Reinforced Concrete Spatial Structures," Darmstadt, West Germany, July 1978.

30. Arneson, A., Sorensen, S. I. and Bergan, P. G., "Nonlinear Analysis of Reinforced Concrete," International Conference on Engineering Application of the Finite Element Method, Oslo, May 1979.

31. Rashid, Y. R., "Ultimate Strength Analysis of Prestressed Concrete Pressure Vessels," Nuclear Engineering Design, V. 7, 1968.

32. Rashid, Y. R. and Rockenhauser, W., "Pressure Vessel Analysis by Finite Element Techniques," Conference on Prestressed Concrete Pressure Vessels, Institute of Civil Engineers, London, 1968.

33. Wahl, H. W. and Kasiba, R. J., "Design and Construction Aspects of Large Prestressed Concrete (PWR) Containment Vessels, ACI Journal, V. 66, No. 5, May 1969.

34. Zienkiewicz, O. C., Owen, D. R. J. and Phillips, D. W., "Finite Element Method in Analysis of Reinforced and Concrete Structures," Paper M1/1, 1st International Conference on Structural Mechanics in Reactor Technology, Berlin, West Germany, September 1971.

35. Argyris, J. H., Faust, G., Szimmat, J., Warnke, K. J. and Willam, K. J., Analysis of Prestressed Concrete Reactor Vessels," Paper H1/1, 2nd International Conference on Structural Mehcanics in Reactor Technology, Berlin, West Germany, September 1973.

36. Connor, J. J. and Sarne, Y., "Nonlinear Analysis of Prestressed Concrete Reactor Pressure Vessels," Paper H2/2, 3rd International Conference on Structural Mechanics in Reactor Technology, London, September 1975.

37. Kang, Y. J., "Nonlinear Geometric, Material and Time Dependent Analysis of Reinforced and Prestressed Concrete Frames," Ph.D. Dissertation, Division of Structural Engineering and Structural Mechanics, University of California, Berkeley, UC-SESM Report, No. 77-1, January 1977.

38. Youssef, A. A.-R., McCutcheon, J. O., Mufti, A. A. and Mirzra, M. S., "Inelastic Analysis of Plates and Slabs Using Finite Elements," Struc. Con. Ser. No. 71-1, McGill University, Montreal, March 1971.

39. American Concrete Institute, "Shear in Reinforced Concrete," ACI Special Publication SP-42, Detroit, 1974.

40. Hawkins, N. M. and Mitchell, D., "Progressive Collapse of Flat Plate Structures," ACI Journal, Vol. 76, No. 7, July 1979, pp. 775-808.

41. Fung, Y. C., Foundations of Solid Mechanics, Prentice-Hall, Englewood Cliffs, New Jersey, 1965.

42. Zienkiewicz, O. C., The Finite Element Method, third edition, McGraw-Hill, London, 1977.

43. Bathe, K. J., Ramm, E. and Wilson, E. L., "Finite Element Formulations for Large Displacement and Large Strain Analysis," Report No. UC-SESM 73-14, Department of Civil Engineering, University of California, Berkeley, September 1973.

44. Bathe, K. J., Ozdemir, H. and Wilson, E. L., "Static and Dynamic Geometric and Material Nonlinear Analysis," Report No. UC SESM 74-4, Department of Civil Engineering, University of California, Berkeley, February 1974.

45. Murray, D. W., "Large Deflection Analysis of Plates," Ph.D. Dissertation, Department of Civil Engineering, University of California, Berkeley, Report No. 67-44, September 1967.

46. Murray, D. W. and Wilson, E. L., "Finite Element Large Deflection Analysis of Plates," Journal of the Engineering Mechanics Division, ASCE, Vol. 95, No. EM1, February 1969, pp. 143-165.

47. Gallagher, R. H., Finite Element Analysis: Fundamentals, Prentice-Hall, Englewood Cliffs, New Jersey, 1975.

48. Hobbs, D. W. et al., "Design Stresses for Concrete Structures Subjected to Multi-axial Stresses," The Structural Engineer, Vol. 55, No. 4, April 1977, pp. 151-164.

49. Kupfer, H., Hilsdorf, H. K., and Rüsch, H., "Behavior of Concrete under Biaxial Stresses," ACI Journal, V. 66, No. 8, August 1969, pp. 656-666.

50. Scordelis, A. C., "General Report - Basic Problems," Proceedings, IASS Symposium on Nonlinear Behavior of Reinforced Concrete Spatial Structures, Darmstadt, West Germany, July 1978.

51. Aoyama, H. and Noguchi, H., "Mechanical Properties of Steel and Concrete under Load Cycles Idealizing Seismic Actions. Studies on Bond between Concrete and Steel: b) Concrete," AICAP-CEB Symposium, Rome, May 1979.

52. Nilson, A. H., "Nonlinear Analysis of Reinforced Concrete by the Finite Element Method," ACI Journal, V. 65, No. 9, September 1968.

53. Saenz, L. P., Discussion of "Equation for the Stress-Strain Curve of Concrete," by Desayi and Krishnan, ACI Journal, V. 61, No. 9, September 1964.

54. Franklin, H. A., :Nonlinear Analysis of Reinforced Concrete Frames and Panels," Ph.D. Dissertation, Division of Structural Engineering and Structural Mechanics, University of California, Berkeley, UC-SESM Report No. 70-5, March 1970.

55. Kupfer, H. B. and Gerstle, K. H., "Behavior of Concrete under Biaxial Stresses," Journal of the Engineering Mechanics Division, ASCE, V. 99, No. EM4, August 1973.

56. Romstad, K. M., Taylor, M. A., and Herrman, L. R., "Numerical Biaxial Characterization for Concrete," Journal of the Engineering Mechanics Division, ASCE, V. 100, No. EM5, October 1974.

57. Liu, T. C., Nilson, A. H., and Slate, F. O., "Stress-Strain Response and Fracture of Concrete in Uniaxial and Biaxial Compression," ACI Journal, V. 69, No. 5, May 1972.

58. Liu, T. C., Nilson, A. H. and Slate, F. O.,"Biaxial Stress-Strain Relations for Concrete," Journal of the Structural Division, ASCE, V. 98, No. ST5, May 1972.

59. Darwin, D. and Pecknold, D., "Inelastic Model for Cyclic Biaxial Loading of Reinforced Concrete," SRS No. 409, University of Illinois at Urbana-Champaign, Illinois, July 1974.

60. Darwin, D. and Pecknold, D., "Analysis of Reinforced Concrete Shear Panels under Cyclic Loading," Journal of the Structural Division, ASCE, V. 102, No. ST2, February 1976, pp. 355-369.

61. Darwin, D. and Pecknold, D. A., "Nonlinear Biaxial Stress-Strain Law for Concrete," Journal of the Engineering Mechanics Division, ASCE, Vol. 103, No. EM2, April 1977, pp. 229-241.

62. Chen, A. C. T. and Chen, W. F., "Constitutive Relations for Concrete," Journal of the Engineering Mechanics Division, ASCE, V. 101, No. EM4, August 1975.

63. Chen, A. C. T. and Chen, W. F., "Constitutive Equations and Punch Identification of Concrete," Journal of the Engineering Mechanics Division, ASCE, Vol. 101, No. EM6, December 1975.

64. Bazant, Z. P. and Bhat, P. D., "Endochronic Theory of Inelasticity and Failure of Concrete," Journal of the Engineering Mechanics Division, ASCE, Vol. 102, No. EM4, August 1976, pp. 701-722.

65. Bazant, Z. P., Bhat, P. D. and Shech, C. L., "Endochronic Theory for Structures," Structural Engineering Report No. 1976-12/259, Northwestern University, Evanston, Illinois, December 1976.

66. Valanis, K. C., "A Theory of Viscoplasticity without a Yield Surface," Archiwum Mechaniki Stossowanej (Archives of Mechanics, Warsaw), Vol. 23, 1971, pp. 517-551.

67. Noguchi, H., "Finite Element Nonlinear Analysis of Reinforced Concrete: Part 1: Stress-Strain Relationships of Concrete under Biaxial Stresses," Transaction of AIJ, No. 252, February 1977, pp. 1-11.

68. Nelissen, L. J. M., "Biaxial Testing of Normal Concrete," Heron, Delft, Vol. 18, No. 1, 1972.

69. Schnobrich, W. C., "Slab Problems," Seminar on the Finite Element Analysis of Reinforced Concrete Structures, University of Milan, June 1978, pp. 155-175.

70. Rajagopal, K. R., "Nonlinear Analysis of Reinforced Concrete Beams, Beam-columns and Slabs by Finite Elements," Ph.D. Dissertation, Iowa State University, Ames, Iowa, 1976.

71. ACI Committee 209, "Prediction of Creep, Shrinkage and Temperature Effects in Concrete Structures," Paper SP 27-3, ACI Special Publications SP-27, April 1970.

72. Hognestad, E., "A Study of Combined Bending and Axial Load in Reinforced Concrete Members," Bulletin Series No. 399, Bulletin No. 1, Engineering Experiment Station, University of Illinois, 1951.

73. Karsan, I. D. and Jirsa, J. O., "Behavior of Concrete under Compressive Loadings," Journal of the Structural Division, ASCE, V. 95, No. ST12, December 1969.

74. Gilbert, R. I. and Warner, R. F., "Nonlinear Analysis of Reinforced Concrete Slabs with Tension Stiffening," UNICIV Report No. R-167, University of New South Wales, Kensington, N.S.W., Australia, January 1977.

75. Branson, D. E. and Christiason, M. L., "Time-Dependent Concrete Properties Related to Design -- Strength and Elastic Properties, Creep and Shrinkage," Symposium on Creep, Shrinkage and Temperature Effects, ACI Special Publication SP-27, Detroit, 1971, pp. 257-277.

76. Freyssinet, E., "The Deformation of Concrete," Concrete Research, No. 8, 1951.

77. Vogt, F., "On the Flow and Extensibility of Concrete," Norges Tekniske Hoiskole, Norway, 1935.

78. Thomas, F. G., "Creep of Concrete under Load," International Association of Testing Materials, London Congress, April 1937.

79. Lynam, C. G., "Growth and Movement in Portland Cement Concrete," Oxford University Press, London, 1934.

80. Bresler, B. (ed.), Reinforced Concrete Engineering, Volume I, Wiley, New York, 1974.

81. Zienkiewicz, O. C. and Watson, M., "Some Creep Effects in Stress Analysis with Particular Reference to Concrete Pressure Vessels," Nuclear Engineering and Design, No. 4, 1966.

82. Volterra, V., "Sur les Equations Integro-Differentielles et Leurs Applications," Acta Mathematica, Stockholm, 1912.

83. Bazant, Z. P. and Wu, S. T., "Dirichlet Series Creep Function for Aging Concrete," ASCE Journal of the Engineering Mechanics Division, Vol. 99, No. EM2, Proc. Paper 9645, Apr. 1973, pp. 367-387.

84. Gopalakrishnan, K. S., Neville, A. M., and Ghali, A., "Creep Poisson's Ratio of Concrete under Multiaxial Compression," ACI Journal, V. 66, No. 12, December 1969.

85. Becker, J. and Bresler, B., "FIRES-RC, A Computer Program for the Fire Response of Structures -- Reinforced Concrete Frames," Report No. UCB FRG 74-3, Division of Structural Engineering and Structural Mechanics, University of California, Berkeley, July 1974.

86. Roll, F., "Long-time Creep-recovery of Highly Stressed Concrete Cylinders," Symposium on Creep of Concrete, ACI Special Publication SP-9, March 1964.

87. Mukaddam, M. A. and Bresler, B., "Behavior of Concrete under Variable Temperature and Loading," ACI Seminar on Concrete for Nuclear Reactors, SP-34, 1972.

88. King, I. P., "Finite Element Analysis of Two-dimensional Time Dependent Stress Problems," Report No. 65-1, Structures and Materials Research, University of California, Berkeley, 1965.

89. Ross, A. D., "Creep of Concrete under Variable Stress," ACI Journal, V. 64, No. 9, March 1958.

90. Selna, L. G., "Time-Dependent Behavior of Reinforced Concrete Structures," UC-SESM Report No. 67-19, University of California, Berkeley, 1967.

91. Philleo, R., "Some Physical Properties of Concrete at High Temperatures," ACI Journal, Vol. 54, April 1958.

92. Nilson, A. H., Design of Prestressed Concrete, Wiley, New York, 1978.

93. Huang, T., "Anchorage Take-up Loss in Post-Tensioned Members," PCI Journal, Vol. 14, No. 4, August 1969, pp. 30-35.

94. Magura, D. D., Sozen, M. A. and Siess, C. P., "A Study of Stress Relaxation in Prestressing Reinforcement," PCI Journal, Vol. 9, No. 2, April 1964.

95. Van Zyl, S. F., "Analysis of Curved Segmentally Erected Prestressed Concrete Box Girder Bridges," Ph.D. Dissertation, Division of Structural Engineering and Structural Mechanics, University of California, Berkeley, Report No. UC-SESM 78-2, January 1978.

96. Hernandez, H, D. and Gamble, W. L., "Time-Dependent Prestress Losses in Pretensioned Concrete Construction," Structural Research Series No. 417, Civil Engineering Studies, University of Illinois, Urbana, May 1975.

97. Ghali, A., Sisodiya, R. G. and Tadros, G. S., "Displacements and Losses in Multistage Prestressed Members," Journal of the Structural Division, ASCE, Vol. 100, No. ST11, November 1974, pp. 2307-2322.

98. CEB-FIP, "International Recommendations for the Calculation and Execution of Concrete Structures," Prague, Czechoslovakia, June 1970, Cement and Concrete Association, London.

99. Ashwell, D. G. and Gallagher, R. H. (Editors), Finite Elements for Thin Shells and Curved Members, Wiley, London, 1976.

100. Dovey, H. H., "Extension of Three-Dimensional Analysis to Shell Structures Using the Finite Element Idealization," Ph.D. Dissertation, Division of Structural Engineering and Structural Mechanics, University of California, Berkeley, Report No. UC-SESM 74-2, January 1974.

101. Kanoknukulchi, W., "A Simple and Efficient Finite Element for General Shell Analysis," Report No. UC-SESM 78-1, University of California, Berkeley, January 1978.

102. Hughes, T. J. R., Taylor, R. L. and Kanoknukuchai, W., "A Simple and Efficient Finite Element for Plate Bending," Int. J. Num. Meth. Engrg., Vol. 11, 1977, pp. 1529-1543.

103. Hughes, T. J. R., Cohen, M. and Haroun, M., "Reduced and Selective Integration Techniques in the Finite Element Analysis of Plates," to be published in Nuclear Engineering and Design.

104. Clough, R. W. and Felippa, C. A., "A Refined Quadrilateral Element for Analysis of Plate Bending," Proc. 2nd Conf. Matrix Meth. Struc. Mech., Wright Patterson AFB, Ohio, 1968.

105. Irons, B. M. and Razzaque, A., "Shape Function Formulations for Elements other than Displacement Models," Proc. Int. Conf. Variational Meth. Engrg., Southhampton, 1972, pp. 4/59-4/72.

106. Razzaque, A., "Program for Triangular Bending Elements with Derivative Smoothing," Int. J. Num. Meth. Engrg., Vol. 6, 1973, pp. 333-343.

107. Razzaque, A., Ph.D. Dissertation, University College of Swansea, 1973.

108. Clough, R. W. and Tocher, J. L., "Finite Element Stiffness Matrices for Analysis of Plate Bending," Proc. Conf. Matrix Meth. Struc. Mech., Wright-Patterson AFB, Ohio, 1965.

109. Bazeley, G. P., Cheung, Y. K., Irons, B. M. and Zienkiewicz, O. C., "Triangular Elements in Plate Bending -- Conforming and Nonconforming Solutions," Proc. Conf. Matrix Meth. Struc. Mech., Wright-Patterson AFB, Ohio, 1965.

110. Allwood, R. J. and Cornes, G. M. M., "A Polynomial Finite Element for Plate Bending Problems Using the Assumed Stress Approach," Int. J. Num. Meth. Engrg., Vol. 1, 1969, pp. 135-150.

111. Allman, D. J., "Triangular Finite Elements for Plate Bending with Constant and Linearly Varying Bending Moments," IUTAM Symp. High-Speed Comp. Elastic Struc., Liege, 1970.

112. Wilson, E. L., "Solid SAP -- A Static Analysis Program for Three Dimensional Solid Structures," UC-SESM Report No. 71-19, University of California, Berkeley, March 1972.

113. Horrigmoe, G., "Finite Element Instability Analysis of Free-Form Shells," Ph.D. Dissertation, University of Trondheim, Norway, 1977.

114. Bergan, P. G., "Nonlinear Analysis of Plates Considering Geometric and Material Effects," Ph.D. Dissertation, University of California, Berkeley, UC-SESM Report No. 71-7, April 1971.

115. Taylor, R., Maher, D. R. H. and Hayes, B., "Effect of the Arrangement of Reinforcement on the Behavior of Reinforced Concrete Slabs," Magazine of Concrete Research, Vol. 18, No. 55, June 1966, pp. 85-94.

116. Black, M. S., "Ultimate Strength Study of Two-way Concrete Slabs," Journal of the Structural Division, ASCE, Vol. 101, No. ST1, Jan. 1975, pp. 311-324.

117. England, G. L. and Ross, A. D., "Reinforced Concrete under Thermal Gradients," Magazine of Concrete Research, Vol. 14, No. 40, March 1962, pp. 5-12.

118. Aroni, S., "Slender Prestressed Concrete Columns," UC-SESM Report No. 67-10, Division of Structural Engineering and Structural Mechanics, University of California, Berkeley, 1967.

119. Aroni, S., "Slender Prestressed Concrete Columns," Journal of the Structural Division, ASCE, Vol. 94, No. ST4, April 1968.

120. Lin, T. Y., "Strength of Continuous Prestressed Concrete Beams under Static and Repeated Loads," ACI Journal, Vol. 26, No. 10, June 1955, pp. 1037-1059.

121. Ritz, P., Marti, P. and Thürlimann, B., "Versuche über das Biegeverhalten von Vorgespannten Platten ohne Verbund," Report No. 7305-1, Institut für Baustatik und Konstruktion, Zurich, June 1975.

122. Lin, T. Y., Scordelis, A. C. and Itaya, R., "Behavior of a Continuous Concrete Slab Prestressed in Two Directions," Report No. 100/5, Department of Civil Engineering, University of California, Berkeley, August 1958.

123. Scordelis, A. C., Lin, T. Y. and Itaya, R., "Behavior of a Continuous Slab Prestressed in Two Directions," ACI Journal, Vol. 56, No. 6, December 1959, pp. 441-459.

124. Levy, S., "Bending of Rectangular Plates with Large Deflections," NACA Technical note 846, 1942.

125. Mukaddam, M. A., "Behavior of Concrete under Variable Temperature and Loading," Interim Report to Oak Ridge National Laboratory, Reactor Division, Oak Ridge, Tennessee, 1969.

126. Arneson, A., "Analysis of Reinforced Concrete Shells Considering Material and Geometric Nonlinearities," Ph.D. Dissertation, Institutt for Statikk, Report No. 79-1, University of Trondheim, Norway, July 1979.

APPENDIX A.1

METHOD TO FIND LENGTH OVER WHICH ANCHOR SLIP TAKES PLACE

Referring to Eq. (4.1):

$$P = P_o\, e^{-(\mu\theta + kx)}$$

the curvature a of a parabolic curve is constant, thus θ can be written as follows:

$$\theta = ax$$

then

$$\mu\theta + kx = qx$$

where

$$q = \mu a + k \qquad (A.1)$$

Equation (4.1) then becomes:

$$P = P_o\, e^{-qx} \qquad (A.2)$$

Applying Eq. (A.2) in Fig. 3.2.a results in:

$$P_1 = P_o\, e^{-qL_a}$$

$$P_2 = P_1\, e^{-qL_a}$$

or

$$P_2 = P_o\, e^{-2qL_a} \qquad (A.3)$$

The average force loss ΔP over length L_a is approximately $(P_o - P_2)/2$, thus:

$$\Delta P = P_o\left(1 - e^{-2qL_a}\right)/2 \qquad (A.4)$$

From the elastic properties of the tendon ΔP can also be expressed as:

$$\Delta P = \frac{\Delta_s A_s E_s}{L_a} \tag{A.5}$$

By combining Eqs. (A.4) and (A.5) and rearranging Eq. (4.3) is obtained:

$$L_a = \frac{2\Delta_s A_s E_s}{P_o\left(1 - e^{-2qL_a}\right)}$$

Iteration with Newton's method

Equation (4.3) can also be written in the following way:

$$f(\ell) = \ell\left(1 - e^{-2q\ell}\right) - \frac{2\Delta_s A_s E_s}{P_o} = 0 \tag{A.6}$$

where

$$\ell = L_a$$

then

$$f'(\ell) = 1 - e^{-2q\ell} + 2q\ell e^{-2q\ell} \tag{A.7}$$

The iteration is to be performed as follows:

$$\ell_i = g\left(\ell_{i-1}\right) \tag{A.8}$$

For Newton's method $g(\ell)$ is obtained from:

$$g(\ell) = \ell - \frac{f(\ell)}{f'(\ell)} \tag{A.9}$$

Using Eqs. (A.6) and (A.7) and after simplification:

$$g(\ell) = \frac{\frac{2\Delta_s A_s E_s}{P_o} + 2q\ell^2 e^{-2q\ell}}{1 + e^{-2q\ell}(2q\ell - 1)} \qquad (A.10)$$

As an initial trial take:

$$\ell_o = 10 \frac{\Delta_s A_s E_s}{P_o} \qquad (A.11)$$

In the computer program the angle change is assumed to be linear over an element. Convergence to a tolerance of .001 should be obtained within about five iterations.

APPENDIX A.2

ELEMENT LOAD VECTOR DUE TO PRESTRESS

Refer to Fig. 4.3 and Eqs. (4.8). The distance between nodes I and K for i and between nodes J and K for j are as follows:

$$s_i = s_{iI} + s_{iK}$$

$$s_j = s_{jJ} + s_{jK}$$

Load vectors are then given by:

Nodes I and K for i :

F_x: $sP \cos\alpha \cos\phi$

F_y: $sP \cos\alpha \sin\phi$

F_z: $sP \sin\alpha$

M_x: $-sP \cos\alpha \sin\phi \, e_i$

M_y: $sP \cos\alpha \cos\phi \, e_i$

M_z: 0

For node I: $s = s_{iK}/s_i$

For node K: $s = s_{iI}/s_i$

Nodes J and K for j :

F_x: $-sP \cos\alpha \cos\phi$

F_y: $-sP \cos\alpha \sin\phi$

F_z: $-sP \sin\alpha$

M_x: $+sP \cos\alpha \sin\phi \, e_j$

M_y: $-sP \cos\alpha \cos\phi \, e_j$

M_z: 0

For node J: $s = s_{jK}/s_j$

For node K: $s = s_{jJ}/s_j$

APPENDIX B: COMPUTER PROGRAM NOPARC

UNIVERSITY OF CALIFORNIA
September 1979

Department of Civil Engineering
Faculty Investigator: A. C. Scordelis

COMPUTER PROGRAM FOR THE NONLINEAR MATERIAL, GEOMETRIC AND TIME-DEPENDENT ANALYSIS OF REINFORCED AND PRESTRESSED CONCRETE SLABS AND PANELS

IDENTIFICATION:

NOPARC: - NOnlinear analysis of Prestressed And Reinforced Concrete slabs and panels

Programmed by: J. van Greunen, University of California, Berkeley, 1979.

PURPOSE:

The computer program has been developed to trace the quasi-static response of reinforced and prestressed concrete slabs of arbitrary geometry and shear panels under instantaneous and sustained normal and in-plane load conditions. (Reinforced concrete shell-type structures can also be analyzed.) Time-dependent environmental phenomena such as creep and shrinkage effects are considered to trace the changes in the field variables of such structures in the elastic and inelastic regimes. The nonlinear effects due to the changing structural geometry under loads are also considered. Ultimate collapse loads are then predicted considering local failure in the steel and concrete along with the deterioration of structural stiffness due to progressive cracking.

DESCRIPTION:

A finite element tangent stiffness formulation, coupled with a time step integration scheme, is developed to analyze reinforced and prestressed concrete systems. Within a time step, an incremental load procedure, with an iterative approach to solve the equilibrium equations for each load increment, is adopted. The composite section of the two different materials is modeled as a layered system consisting of concrete and "equivalent smeared" reinforcing steel layers. Bonded prestressing tendons are also included as "equivalent smeared" layers. The stiffness properties of an element are then obtained by integrating the contributions from all the layers through the depth of the cross section.

The material behavior of concrete is characterized by a nonlinear constitutive relationship for a biaxial state of stress. This includes tensile cracking at a limiting stress level, tensile unloading after cracking and the strain softening of the concrete beyond its compressive strength. For the deformation of the concrete layers, the effects of stress history, partial creep recovery, aging and temperature variations are considered. These effects characterize concrete to be an aging, viscoelastic, thermorheologically simple material. Creep under a biaxial state of stress is represented by the introduction of Poisson's ratio. The reinforcing steel is represented by a bilinear, strain hardening model exhibiting the Bauschinger effect. The prestressing steel is characterized by a multilinear stress-strain relationship. An unloading path is also prescribed in the constitutive laws assumed for both steel and concrete.

For slabs and panels an arbitrary prestressing tendon layout can be specified. The loads due to prestressing and the tendon segments

associated with each element are calculated in the program. Pretensioned and bonded or unbonded post-tensioned tendons may be specified. During any time-dependent analysis the phenomenon of stress relaxation in the prestressing steel is taken into account.

The program is coded in FORTRAN IV and has been tested on the Berkeley Computer Center CDC 6400 computer. The program has an overlay structure and the blank common is dynamically dimensioned to match the requirements of the problem under consideration. This makes it possible to use the central memory capacity of the computer in an efficient manner.

RESTRICTIONS:

The number of nodal points, elements, prestressing tendons and time steps are restricted only by the available capacity of the computer. The restrictions placed on the number of material types, layer systems, etc. are given in the input instructions.

FORMAT OF INPUT DATA:

The input data is punched on cards in the fixed format indicated below. The sequential order of the input data must be strictly adhered to and consistent units must be used.

* Optional data. These cards must be omitted if not required. All other data are necessary.

(B1.2) The number refers to the card where a variable is defined.

B1. CONTROL CARDS

B1.1 TITLE CARD (12A6)

Col. 1-72 HED - Title of the problem to be printed with the output

B1.2 CONTROL CARD FOR ANALYSIS (11I5,15X,I10)

		Notes
Col. 1-5	NUMNP - number of nodes	
6-10	NELTYP - number of element types (maximum 9)	
11-15	NTIME - number of times or load increments for which an analysis is to be performed	(1.1)
16-20	ITCOD - iteration type code -1 = initial stiffness only 0 = constant stiffness iteration in the load steps N = reform the stiffness each N iterations	(1.2)
21-25	NGCOD - code for nonlinear geometry 0 = not considered 1 = included	
26-30	KGCOD - geometric stiffness code 0 = not considered 1 = included	
31-35	ICREEP - creep analysis code 0 = not considered 1 = included	
36-40	ISHRINK - shrinkage analysis code 0 = not considered 1 = included	
41-45	NORM - convergence norm code 0 = force norm 1 = displacement norm 2 = both force and displacement norms	(1.3)
46-50	KNORM - code to specify the type of convergence tolerances 0 = input absolute values 1 = input fractions	(1.4)

Notes

Col. 51-55 IPDIR - principal axes direction code (1.5)

0 = automatically calculated
1 = constrained to coincide with the element local axes

56-70 blank

71-80 MEML - central memory field length (default = 120 000_8) (1.6)

B1.3 CONTROL CARD FOR OUTPUT (5I5)

Col. 1-5 KOUT - output code (1.7)

0 = complete output at the end of the last iteration for each load step
1 = complete output after each iteration in each load step
2 = complete output only at the end of all load steps and iterations for the time or load increment

6-10 KDIS - code to output displacements in local coordinates

0 = NO
1 = YES

11-15 KCUR - code to output stress resultants

0 = NO
1 = YES

16-20 KSTN - code to output strains

0 = NO
1 = YES

21-25 KITER - code to output displacements and unbalanced forces

0 = only as specified by KOUT
1 = for each iteration

Notes:

1.1 For a short time analysis the total load to be applied to the structure can be divided into a number of load increments = NTIME. Each load increment can again be subdivided into a

number of equal load steps = NLSTEP (B8.1). For a time dependent analysis NTIME is the number of ages at which an analysis is desired. The number of time steps considered is (NTIME - 1).

1.2 The element and global stiffness matrices are reformed for the first iteration of each load step except when ITCOD = -1; in this case the initial stiffness is used for the whole analysis.

1.3 Two convergence norms are possible. When the force norm is specified (NORM = 0), the solution is deemed to have converged when the maximum component of the global unbalanced load vector is smaller than the tolerances specified. When the displacement norm is used (NORM = 1) it is assumed that convergence has been achieved when the maximum component of the displacement increment for an iteration is smaller than the tolerances specified. When both norms are used (NORM = 2), convergence is obtained only when both norms are satisfied.

1.4 The type of convergence tolerance (B2.1) is determined by KNORM. For KNORM = 0 the absolute values of the force or displacement convergence tolerances must be input. For KNORM = 1 a fraction must be specified. In the case of the force norm, convergence for a load step is then assumed when the maximum component of the global unbalanced load vector for an iteration is smaller than this fraction of the maximum component of the applied load step vector. For the displacement norm convergence is achieved when the displacement increment for an iteration is smaller than the specified fraction of the maximum

component of the displacement increment of the first iteration of the load step.

1.5 An option is provided to force the principal axes to coincide with the element local coordinate axes. This should only be necessary in the case of a structure with predominantly uniaxial behavior for which a time-dependent analysis is to be performed.

1.6 The central memory field length available depends on the computer. MEML therefore determines the size of the problem that can be analyzed.

1.7 The load increment is subdivided into load steps (see note 1.1). Iterations are then performed in each load step. The time-dependent load vector, representing the time-dependent effects for the time step (from the current time to the next time), is treated in the same way.

B2. CONVERGENCE CRITERIA

All convergence criteria refer to the global coordinate system. The tolerances and upper limits must be provided according to NORM (B1.2).

B2.1 CARD 1: CONVERGENCE TOLERANCES (4F10.0)

Absolute values or fractions must be specified as indicated in KNORM (B1.2).

			Notes
Col. 1-10	TOLER(1)	- force convergence	force norm
11-20	TOLER(2)	- moment convergence	force norm

Notes

Col. 21-30 TOLER(3) - displacment convergence
31-40 TOLER(4) - rotation convergence
} displacement norm

B2.2 CARD 2: UPPER LIMITS (4F10.0)

Col. 1-10 VMAX(1) - force
11-20 VMAX(2) - moment
} force norm (2.1)

21-30 VMAX(3) - displacement
31-40 VMAX(4) - rotation
} displacement norm (2.2)

Notes:

2.1 When the unbalanced forces or moments for an iteration exceed these upper limits, the solution is deemed to diverge and is therefore stopped.

2.2 The upper limits for the displacement norm is used in the following way: When a displacement increment exceeds these values, the whole vector of displacement increments is scaled back so that the absolute value of the maximum component equals the upper limit.

B3. DAYS CARD(S) (8F10.0)

DAYS(I), I = 1, NTIME (B1.2) - Ages in days after casting at which an analysis is required. Use as many cards as are needed. When time-dependent analysis is not performed blank cards can be used.

B4. NODAL COORDINATE CARDS (7I5,3F10.0,I5)

All boundary condition restraints and nodal coordinates refer to the global coordinate system, a right-hand Cartesian coordinate system, fixed in space and used to define the positions of all the nodes of the structure (Fig. B1).

			Notes
Col. 1-5	N - node number		(4.1)
6-10	ID(1,N) - translation in X-direction	boundary condition codes	(4.2)
11-15	ID(2,N) - translation in Y-direction		
16-20	ID(3,N) - translation in Z-direction		
21-25	ID(4,N) - rotation around X-axis		
26-30	ID(5,N) - rotation around Y-axis		
31-35	ID(6,N) - rotation around Z-axis		

Boundary condition code: 0 - node is free to displace in that direction
1 - node is fixed in that direction

Col. 36-45	X(N) - X-coordinate	
46-55	Y(N) - Y-coordinate	
56-65	Z(N) - Z-coordinate	
66-70	KN - generation parameter	(4.3)

Notes:

4.1 The nodes do not have to be in node-order sequence, but the node with the largest number must be the last card. The nodal data for a series of nodes can be generated through the use of KN - see Note 4.3.

4.2 The boundary condition codes are used to specify the boundary conditions in the global coordinate system for each node. Severe numerical difficulties may arise in the solution of the equilibrium equations if the stiffness associated with any global direction is zero or close to zero. These problems may be avoided by restraining the appropriate degrees of freedom (DOF) through use of the boundary condition codes. By restraining a DOF the equilibrium equation associated with that particular DOF is eliminated and thus prevents any instability in the solution of the equilibrium equations.

For the plane stress element, the translational DOF normal to the plane of the element and all three rotational DOF are not considered in the element stiffness formulation -- these DOF therefore have to be constrained.

For the plate bending element, the two in-plane translational DOF and the rotation about the normal to the plane of the element are not considered in the element stiffness formulation -- these DOF therefore have to be constrained. For geometric and/or material nonlinear analysis of slabs, however, the shell element should be used.

For the shell element, the rotation about the normal to the plane of the element is not considered in the stiffness formulation. For slabs this DOF must be constrained. For nearly co-planar shell elements, a fictitious rotational stiffness, about the normal to the shell surface at the node, can be provided by a boundary spring element. It is recommended that the value of the fictitious rotational stiffness

be taken as about 10% of the bending stiffness of the shell to avoid any ill-conditioning of the structural stiffness matrix as discussed in Chapter 5.4. (See Fig. B9.b.)

4.3 If cards are omitted, nodal data for a series of nodes is generated. KN, the mesh generation parameter on the last card of a mesh generation sequence, is the increment to be added to the previous nodal point number. The intermediate nodes are located at equal intervals along the straight line between the first and last node specified. The boundary condition codes for the generated nodes are set equal to that of the first node in the series (those of the last node remains as specified).

B5. MATERIAL PROPERTIES - CONCRETE, REINFORCING STEEL AND PRESTRESSING STEEL

B5.1 CONTROL CARD (5I5)

Col.	1-5	NUMCN - number of concrete types (max 4)
	6-10	NUMST - number of reinforcing steel types (max 4)
	11-15	NUMPT - number of prestressing steel types (max 5)
	16-20	NTCL - number of concrete layer systems (max 5)
	21-25	NTSL - number of reinforcing steel layer systems (max 9)

B5.2 CONCRETE MATERIAL PROPERTIES

NUMCN (B5.1) sets of cards are required

B5.2.1. CONCRETE CONTROL PARAMETERS (4I5,5F10.0)

Notes

Col. 1-5 I - concrete material number

6-10 JMT(I) - elastic material data code (5.1)
1 - input data (See B5.2.2.)
2 - use ACI formulae

11-15 JCR(I) - creep data code
1 - input data (See B5.2.3.)
2 - use ACI formulae

16-20 JSH(I) - shrinkage data code:
1 - input data (See B5.2.4.)
2 - use ACI formulae

21-30 FC28(I) - compressive strength f'_c at 28 days

31-40 CNU(I) - Poisson's ratio

41-50 RHO(I) - weight per unit volume (default = 0.087 lb/in^3 (150 lb/ft^3))

51-60 TSFAC - tension stiffening factor (5.2)

61-70 CSC(I) - cracked shear constant β

*B5.2.2. ELASTIC MATERIAL PROPERTIES (for t_1 = DAYS(1))(4F10.0)

Omit if JMT(I) = 2 .

Col. 1-10 EC(I) - initial modulus of elasticity $E_o(t_1)$

11-20 FCC(I) - compressive strength $f'_c(t_1)$

21-30 FTC(I) - tensile strength $f'_t(t_1)$

31-40 ECU(I) - strain at compressive strength $\varepsilon_c(t_1)$ (default: $\varepsilon_c = 2f'_c/\varepsilon_o$)

*B5.2.3. CREEP DATA CARDS

Notes

Omit if JCR(I) = 2, otherwise (5.3)

provide creep coefficients calculated from experimental curves. (See Chapter 3.2.7.)

(a) CONTROL PARAMETERS (2I5)

Col. 1-5 NAGE(I) - number of ages for which creep curves are provided (max 15)

6-10 NSER(I) - number of terms in the creep compliance series (max 3)

(b) CONCRETE AGES (8F10.0)

SAGE(I,J),J=1,NAGE(I) - ages for which creep curves are provided - 2 cards if necessary

(c) AGE SCALE FACTORS α_i (3E15.6)

ACI(I,J),J=1,NSER(I) - age scale factors for creep compliance function (NAGE(I) cards)

(d) CREEP EXPONENTIAL FACTORS λ_i (3F10.0)

W1(I,J),J=1,NSER(I) - creep exponential factors for compliance series

(e) COEFFICIENTS OF TEMPERATURE SHIFT FUNCTION $\phi(T)$ (4F10.0)

W2(I,J),J=1,4 - coefficients c_i for polynomial function $\psi(T)$ (5.3)

*B5.2.4. SHRINKAGE DATA CARDS (8F10.0)

Omit if JSH(I) = 2 . (B5.2.1)

*B5.2.4. SHRINKAGE DATA CARDS (8F10.0) (cont'd)

TEPSS(I,N),N=1,NTIME (B1.2) - total shrinkage strains (negative) at the days when the analysis is required (as many cards as are needed)

B5.2.5. CONCRETE GENERAL PARAMETERS (5F10.0)

Col. 1-10 SHRU(I) - ultimate shrinkage strain (default = -800×10^{-6})

11-20 SLUMP(I) - slump in inches (default = 2.7 in.)

21-30 SIZE(I) - minimum dimension of member in inches (default = 6.0 in.)

31-40 RH(I) - percentage relative ambient humidity (default = 40.%)

41-50 CTEMP(I) - coefficient of thermal expansion (default = $5.5 \times 10^{-6}/°F$)

Notes:

5.1 If the ACI formulae are used, all units should be pounds and inches. If the elastic material data is input, the same information is needed for all the ages at which analyses are required -- see B8.

5.2 Two tension stiffening models are available in the program as discussed in Chapter 3.2.5:

a) Increased steel modulus:

TSFAC = 0 - the model using an increased modulus for the reinforcing steel. (See B5.3.2 to input the parameters.)

b) Unloading in the concrete:

TSFAC = 1 - no tension stiffening

TSFAC > 1 - a linear unloading slope for the concrete after cracking is assumed with TSFAC determining the ultimate tensile strain as shown in Fig. B2.

5.3 In cases where experimental creep data is available, it is possible to calculate the necessary coefficients of the creep compliance function.

$$C(\tau,t-\tau,T) = \sum_{i=1}^{m} \alpha_i(\tau) \left[1 - e^{-\lambda_i \phi(T)(t-\tau)}\right]$$

and $$\phi(T) = e^{\psi(T)} .$$

The method is explained in detail in Chapter 3.2.7.e and can be summarized as follows: Select m and λ_i, $i = 1, m$ on a trial basis and select a reference temperature T_o. Calculate α_i, $i = 1, m$ for the ages desired by the least squares method. The temperature shift function $\phi(T) = e^{\psi(T)}$ is constructed by calculating the coefficients of the polynomial function $\psi(T)$. The calculation of these coefficients λ_i, α_i and c_i, needed for input into this program, must be performed using other available programs.

*B5.3. REINFORCING STEEL

Notes

Omit if NUMST = 0 (B5.1).

B5.3.1. CARD 1: MATERIAL PROPERTIES (I5,4F10.0) (5.5)

NUMST (B5.1) cards are required.

B5.3.1. CARD 1: MATERIAL PROPERTIES (cont'd)

Col. 5-10 N - reinforcing steel material number

6-15 ES(N) - modulus of elasticity E_s

16-25 FYS(N) - yield stress f_y

26-35 ESTAR(N) - modulus for strain-hardening

36-45 ESU(N) - ultimate strain ε_{su}

*B5.3.2. CARD 2: PARAMETERS FOR TENSION STIFFENING (12F5.0)

If TSFAC = 0 (B5.2.1, note 5.2), this card must be included. Omit this card if TSFAC ≠ 0 .

Col. 1-30 TSF(I),I=1,6 - factors by which the reinforcing steel stiffness is increased (defaults shown in Fig. B3).

31-60 ETS(I),I=1,6 - multiples of the concrete cracking strain at which factors TSF change value (defaults shown in Fig. B3).

If the default values are desired use a blank card.

*B5.4. PRESTRESSING STEEL

Omit if NUMPT = 0, NUMPT (B5.1) sets of cards are required.

B5.4.1. CARD 1 (2I5,4F10.0,I5)

Notes

Col. 1-5 I - prestressing steel material number (5.5)

6-10 KBON(I) - bond code: (5.4)

0 - post-tensioned unbonded
1 - post-tensioned bonded
2 - pretensioned

B5.4.1. CARD 1 (cont'd)

Col. 11-20 TAR(I) - tendon area

21-30 CKW(I) - wobble friction coefficient

31-40 CQQ(I) - curvature friction coefficient

41-50 FY1(I) - 0.1% offset yield stress

51-60 CR(I) - relaxation coefficient (default = 10)

61-65 IP - number of points on the stress-strain curve, maximum of 5 with the origin excluded and also not input

B5.4.2. CARDS 2 (8F10.0/2F10.0) 2 cards

(PSF(I,J),PSE(I,J),J=1,IP - pairs of stress and strain values

B5.5. CONCRETE LAYER SYSTEM CARDS

NTCL (B5.1) sets of cards are required.

B5.5.1. CONTROL CARD (2I5)

Col. 1-5 L - concrete layer system number

6-10 NCLAY(L) - number of concrete layers (max 10)

B5.5.2. LAYER BOUNDARY COORDINATES (8F10.0)

ZC(J,L),J=NCLAY(L)+1 - $\bar{z}$-coordinates of layer boundaries (see Fig. B4) - two cards if necessary

*B5.6. REINFORCING STEEL LAYER SYSTEM CARDS

Omit if NTSL = 0, NTSL (B5.1) sets of cards are required.

B5.6.1. CONTROL CARD (3I5)

Col. 1-5 L - reinforcing steel layer system number

6-10 NSLAY(L) - number of steel layers (max 4)

11-15 IANG(L) - angle index: (See Fig. B5.)
0 - local coordinate system
1 - global coordinate system

B5.6.2. LAYER DATA (2I5,3F10.0)

NSLAY(L) cards are required.

Col. 1-5 J - layer number

6-10 MTN(J,L) - material type number

11-20 ZS(J,L) - $\bar{z}$-coordinate to center of layer (See Fig. B4.)

21-30 PS(J,L) - smeared thickness

31-40 ALPH(J,L) - angle in degrees defining the direction of the reinforcing bars (See Fig. B5.)

Notes:

5.4 Only tendons with the same bond code may be used in a given problem.

5.5 For reinforcing and prestressing steel a coefficient of thermal expansion of $6.5 \times 10^{-6}/°F$ is always assumed.

B6. ELEMENT CARDS (NELTYP sets of cards) (B1.2)

B6.1. ELEMENT TYPE 1: TRIANGULAR ELEMENTS

For the flat triangular element three options are available: (1) modeling plane stress behavior by use of the constant strain triangle (CST); (2) modeling plate bending behavior by use of the 9-DOF Irons-Razzaque triangular plate

B6.1. ELEMENT TYPE 1: TRIANGULAR ELEMENTS (cont'd)

bending element; and (3) modeling the behavior of shell-type structures, where loads are carried by both in-plane and bending action, by a combination of the above mentioned two elements to form a shell element. For geometric and material nonlinear analysis of slabs the shell element should be used.

The element cross-section is modeled as a layered system consisting of concrete (Fig. B4) and "equivalent smeared" reinforcing and prestressing steel layers. Variation of the material properties through the depth of the cross-section is accommodated by assuming that the strain and stress state determines the properties of the material of each layer.

If the CST is used for plane stress analysis, the material properties must be symmetric about the middepth reference surface of the element. Usually, only one layer should be used in such a case.

The DOF associated with the above mentioned elements are illustrated in Fig. B7.

B6.1.1. CONTROL CARD (4I5)

Col. 1-5	NPAR(IEL,1)	- element type number -1
6-10	NPAR(IEL,2)	- number of elements of type 1
11-15	NPAR(IEL,3)	- element type option: 0 - shell element 1 - membrane element 2 - plate bending element

B6.1.1. CONTROL CARD (cont'd)

		Notes
Col. 16-20	NPAR(IEL,4) - loading option 0 - consistent loads 1 - tributary loads	(6.1)

B6.1.2. GRAVITY LOAD CARD (3F10.0)

Col. 1-10	GM(1) - gravity load multiplier in global X-direction	(6.2)
11-20	GM(2) - gravity load multiplier in global Y-direction	
21-30	GM(3) - gravity load multiplier in global Z-direction	

B6.1.3. ELEMENT CARDS (8I5,F5.0,I5,5F6.0)

Col. 1-5	MM - element number	
6-10	NODE(1) - node I	(6.3)
11-15	NODE(2) - node J	
16-20	NODE(3) - node K	
21-25	MC - concrete material property number	
26-30	NCL - concrete layer system number	
31-35	NSL - steel layer system number	
36-40	LOCO - local coordinate system code 0 - defined by nodes I and J 1 - defined by specifying α 2 - defined by specifying γ	(6.4)
41-45	ANLO - angle α or γ in degrees	(6.4)

B6.1.3. ELEMENT CARDS (cont'd)

			Notes
Col. 46-50	KN	- element generation parameter	(6.5)
51-56	PN	- uniform distributed load normal to surface per unit area	
57-62	PT(1)	- uniform distributed load in the global X-direction per unit area of the YZ-plane	
63-68	PT(2)	- uniform distributed load in the global Y-direction per unit area of the XZ-plane	
69-74	PT(3)	- uniform distributed load in the global Z-direction per unit area of the SY-plane	
75-80	TEMPS	- element temperature (default 68°F)	

Notes:

6.1 For consistent loading the element nodal loads are calculated from Eq. (2.27). When tributary loads are specified, only nodal forces are generated at the element level - element nodal moments are taken to be zero.

6.2 The gravity loads are calculated in the global directions to be equal to the unit weight of the concrete multiplied by the corresponding gravity load multiplier.

6.3 Nodes I, J and K are always specified in counterclockwise order about the local $\bar{z}$-axis (Fig. B6).

6.4 The local coordinate system code and the angles α and γ are indicated in Fig. B8. The local coordinate system $\bar{x}\bar{y}\bar{z}$ is also a right-hand Cartesian coordinate system. The plane of the triangle is also the $\bar{x}\bar{y}$-plane with $\bar{z}$ perpendicular to the plane of the element. In Fig. B8 $\bar{x}'$ and $\bar{y}'$ are the projections of $\bar{x}$ and $\bar{y}$ on the global XY-plane. Three options may be used to define the orientation of the local coordinate system:

LOCO = 0: $\bar{x}$ coincides with side IJ and ANLO is left blank.

LOCO = 1: $\bar{x}$ is defined by specifying ANLO = α (in XY-plane).

LOCO = 2: $\bar{y}$ is defined by specifying ANLO = γ (in XY-plane).

6.5 Element cards must be in element number sequence. If cards are omitted, element data will be generated. The element generation parameter KN is specified on the last card in the sequence (only the element number and KN are needed on this card). The increment for the element number is one. The corresponding increment for the element nodes is KN, i.e. $I_{i+1} = I_i + KN$, etc. The material properties, layer systems, definition of the local coordinate system, distributed loads and element temperature of the generated elements are the same as that of the first element in the series.

B6.2. ELEMENT TYPE 2: BOUNDARY ELEMENT

B6.2.1. CONTROL CARD (2I5)

Col. 1-5 NPAR(IEL,1) - element type number - 2

B6.2.1. CONTROL CARD (cont'd)

		Notes
Col. 6-10	NPAR(IEL,2) - number of boundary elements	

B6.2.2. ELEMENT CARDS (8I5, 2F10.0, E10.0)

		Notes
Col. 1-5	N- node to which element is attached	
6-10	I - node I	
11-15	J - node J	(6.6)
16-20	K - node K	(6.6)
21-25	L - node L	(6.6)
26-30	KD - code for translation	(6.7)
31-35	KR - code for rotation	(6.8)
36-40	KN - element generation parameter	(6.9)
41-50	SD - specified translation along the element axis	
51-60	SR - specified rotation about the element axis	
61-70	TRACE - stiffness for translation or rotation (default = 10^{10})	(6.10)

Nodes defining the direction of the boundary element, Fig. B9

Notes:

6.6 The direction of the boundary element at node N can be specified in either of two ways (Fig. B9):

a) A second node I defines the positive direction $\underset{\sim}{n}$ of the element from node I to node N. (Leave J,K,L blank.)

b) Four nodes I, J, K and L specify the positive direction of the element as the normal $\underset{\sim}{n}$ to the plane defined by the two vectors $\underset{\sim}{a}$ and $\underset{\sim}{b}$ in Fig. B9a.

The positive direction of the boundary element corresponds to the direction of $\underset{\sim}{n}$. Nodes I, J, K and L are used only to define the direction of the element, and if convenient may be any nodes used to define the structure. "Artificial nodes", with all their DOF restrained, may also be used for this purpose.

The positive directions of the internal forces in the boundary element and their corresponding reactions acting on node N are shown in Fig. B9 c) and d).

6.7 The code for translation KD is used in the following way:

KD = 0: Node N is free to translate and the translational stiffness of the boundary element is set to zero.

KD = 1: The translation SD and stiffness TRACE are used in the following way. A load P = TRACE * SD is applied at node N according to the sign of SD. If TRACE is much greater than the stiffness of the structure at node N without the boundary element, then the net effect is to produce a displacement very nearly equal to SD at node N. This feature can be used to find the reactions at supports by setting SD = 0 and a high value for TRACE.

6.8 The code for rotation KR, the specified rotation SR and TRACE may be used in a fashion similar to that described for the translation in note 6.7 above.

6.9 The element generation parameter KN can be used when a series of nodes are such that all have identical boundary elements attached. The direction, all specified displacements or rotations and stiffness of these boundary elements should be the same and the series of nodes must form an arithmetic sequence, i.e., N, N+KN, N+2KN, etc. In such cases only the first and last nodes of the series need to be input -- KN is specified on the last card of the series.

6.10 The boundary elements are assumed to be linear elastic throughout any analysis with a constant translational or rotational stiffness equal to TRACE .

*B7. PRESTRESSING TENDON DATA

Omit if NUMPT = 0 . (B5.1)

B7.1. CONTROL CARD (4I5)

Col. 1-5 NTEN - number of tendons

6-10 MAXE - maximum number of elements crossed by a tendon

10-15 MAXI - maximum number of inflexion points per tendon. (The tendon ends are always considered to be inflexion points.)

16-20 MAXT - maximum number of tendon segments in any element

B7.2. TENDON DATA (slab and panel tendons)

A set of four types of cards are needed to describe the position, profile and jacking force for each tendon. Tendons must be in numerical sequence and generation is possible.

B7.2.1. CARD 1: Tendon card (14I5)

			Notes
Col.	1-5	N - tendon number	
	6-10	ITD(1,N) - tendon code: 0 - slab tendon in elements 1 - slab tendon on nodes 2 - panel tendon	(7.1)
	11-15	ITD(2,N) - jacking code: 0 - jacking from one end or both ends 1 - jacking symmetrical	(7.2)
	16-20	ITD(3,N) - tendon material number	
	21-25	ITD(4,N) - number of elements this tendon crosses	
	26-30	ITD(5,N) - number of inflexion points for this tendon	
	31-35	ITD(6,N) - node a } nodes between which the	(7.3)
	36-40	ITD(7,N) - node b } tendon starts	
	41-45	ITD(8,N) - node y } nodes between which the	
	46-50	ITD(9,N) - node z } tendon ends	
	51-55	K - node generation parameter	(7.4)
	56-60	KE - element generation parameter	
	61-65	KI - inflexion point generation code 0 - no generation 1 - inflexion points are to be generated	
	66-70	KM - number of tendons to be generated (excluding the first in the series)	

B7.2.2. CARD 2: Jacking force data (3F10.0)

Col.	1-10	TJF(1,N) - anchor slip

B7.2.2. CARD 2: Jacking force data (cont'd) — Notes

Col. 11-20 TFJ(2,N) - jacking force at start of tendon (7.2)

21-30 TJF(3,N) - jacking force at end of tendon

B7.2.3. CARDS 3: Element numbers (16I5)

IMT(I,N),I = ITD(4,N) (B7.2.1)

The numbers of the sequence of elements crossed by the tendon from start to end -- as many cards as are needed. (7.5)

B7.2.4. CARDS 4: Inflexion point data (6F10.0)

One card for each inflexion point (7.6)

(TIP(J,I,N),I=1,6),J=1,ITD(5,N) (B7.2.1)

a) Slab tendons: (ITD(1,N) = 0 or 1 on card B7.2.1)

Col. 1-10 X-coordinate } global coordinates of the tendon at this inflexion point (7.7)

11-20 Y-coordinate }

21-30 Tendon eccentricity at this point

31-40 Type of curve to be fitted from this point: (7.8)

0. - straight
1. - parabolic

41-50 Distance from this point to any other point Q on the tendon before the next inflexion point (Fig. B11).

51-60 Tendon eccentricity at point Q

B7.2.4. CARDS 4: Inflexion point data (cont'd)

Notes

b) Panel tendons: (ITD(1,N) = 2 on card B7.2.1)

Col.	1-10	X-coordinate	global coordinates of the tendon at this inflexion point	(7.7)
	11-20	Y-coordinate		
	21-30	blank		
	31-40	type of curve to be fitted from this point: 0. - straight 1. - parabolic		(7.8)
	41-50	X-coordinate	global coordinates of any other point Q on the tendon before the next inflexion point (Fig. B11).	(7.9)
	51-60	Y-coordinate		

Notes:

7.1 Slab tendons are straight in plan (of the slab) and vary in position through the depth of the slab in a plane perpendicular to the plane of the slab. (See Fig. B11a,b.) Panel tendons lie at the middepth of the slab and may have a curvature in plan. (See Fig. B11c.)

7.2 Jacking forces can be specified at only one or both ends of a tendon. Symmetrical jacking means that the same jacking force is applied at both ends of the tendon simultaneously and that both the structure and the tendon are symmetric -- the jacking force at the start of the tendon is specified.

7.3 Tendons start and end only on element boundaries. The tendon start should be the tendon end closest to the origin of the

global coordinate system -- this is used in the program to define the orientation of the loads due to prestressing on the structure. For slab tendons on the nodes, nodes b and z (B7.2.1) should be left blank. (See Fig. B11.)

7.4 Generation of tendons: A series of tendons can be generated by use of the parameters K, KE, KI and KM as follows:

a) The tendon number is increased by 1, KM times.

b) The tendon code, jacking code, tendon material number, the number of elements crossed, the number of inflexion points, the anchor slip and jacking forces of the generated tendons are the same as for the first tendon in the series.

c) The numbers of the nodes a, b, y and z (B7.2.1) are incremented by K . (For generation of a tendon starting and ending between the same nodes, K = 0 .)

d) The numbers of the elements crossed by the generated tendons are increased by KE . If KE is left blank, the sequence of element numbers must be input for each tendon, i.e. cards 3 must be input for each tendon generated.

e) If KI = 1 the set of inflexion point data for the first, and immediately following, that for the last tendon in the series must be input. The X- and Y-coordinates of the inflexion points of the generated tendons are obtained by linear interpolation between the first and last set of inflexion points. The tendon eccentricities, type of curve and distance to point Q of the generated inflexion points

are the same as that of the first set of inflexion points. If KI = 0 or blank, a set of inflexion points for each tendon (cards 4) must be input in sequence.

7.5 For slab tendons on nodes the sequence of elements on either side of the nodes can be specified. In the case of bonded tendons, the stiffness of the tendon is then added to the stiffness of these elements.

7.6 Straight tendons may have harp points, but tendons with parabolic profiles are assumed to be smooth continuous curves. No concentrated angle changes are taken into account at inflexion points between parabolic sections or parabolic and straight sections.

7.7 Tendon first and last inflexion points are the start and end of the tendon and must lie on element boundaries. Slab tendons are assumed to be straight in plan between their first and last inflexion points -- See Fig. B11.

7.8 For straight tendons and also for the last inflexion point, columns 31-60 may be left blank.

7.9 For a parabolic tendon profile a zero tendon slope at an inflexion point may be specified by letting point Q coincide with that inflexion point -- See Fig. B11d (inflexion point IP3 and point Q_2).

B8. LOADING CARDS

Notes

A set of cards for each of the NTIME (B1.2) times or load increments are required.

B8.1. LOAD CONTROL CARD (3I5,5F5.0,4I5)

Col. 1-5 NLSTEP - number of load steps

6-10 NITER - maximum number of iterations allowed per load step

11-15 NLJ - number of loaded nodes

16-20 PDL - fraction of dead load

21-25 PDSL - fraction of distributed surface loads

26-30 PSPL - fraction of spring loads (from boundary elements)

31-35 PPSL - fraction of the prestressing load (8.1)

36-40 PALF - fraction of elastic deformation at transfer which causes a loss of prestress (8.2)

41-45 NSTIM - number of load steps for time-dependent analysis (8.3)

46-50 NITERT - maximum number of iterations allowed per load step for time-dependent analysis

51-55 ITC - ITCOD - the iteration type code (B1.2) (8.4)

56-60 NTE - number of elements with temperature changes

*B8.2. CONCENTRATED NODAL LOADS (I5,6F10.0)

Omit if NLJ = 0, NLJ cards needed. All concentrated loads refer to the global coordinate system.

Col. 1-5 N - node number

6-15 RB(1) - load in X-direction

*B8.2. CONCENTRATED NODAL LOADS (cont'd)

Col. 16-25 RB(2) - load in Y-direction

26-35 RB(3) - load in Z-direction

36-45 RB(4) - moment about X-axis

46-55 RB(5) - moment about Y-axis

56-65 RB(6) - moment about Z-axis

*B8.3. CONCRETE PROPERTIES AT NEW TIME t (4F10.0)

This card is only needed when doing time-dependent analysis (i.e. NSTIM > 0) and if JMT(I) = 1 (B5.2.1), i.e. when elastic material data for the concrete is input. I = 1, NUMCN (B5.1) cards are required.

Col. 1-10 EC(I) - modulus of elasticity $E_o(t)$

11-20 FCC(I) - compressive strength $f'_c(t)$

21-30 FTC(I) - tensile strength $f'_t(t)$

31-40 ECU(I) - strain at compressive strength $_c(t)$
(default: $\varepsilon_c = 2f'_c/E_o$)

*B8.4. ELEMENT TEMPERATURE CARDS (2I5,2F10.0) Notes

Omit if NTE = 0, NTE (B8.1) cards required unless generation is used.

Col. 1-5 NE - element number

6-10 NEZ - element number of the last element of the series that are to be generated (8.5)

11-20 TEMR - new temperature at the element reference level (°F)

21-30 TEMG - temperature gradient over element depth (°F/length)
positive for top warmer than bottom

*B8.4. ELEMENT TEMPERATURE CARDS (cont'd)

Only if there is no temperature change for the last element, end the element temperature cards with a blank card.

Notes:

8.1 It is assumed that there is only one prestressing operation and that it forms part of the first loads that are applied to a structure, i.e. PPSL = 1.0 must be specified on only the first load control card and NLSTEP = 1 must also be specified.

8.2 The application of the prestressing causes an elastic deformation of the structure at transfer. PALF can be used to consider this effect as discussed in Chapter 4.2.4. For PALF = 1.0 the tendons will be shortened by this elastic deformation and the tendon forces reduced accordingly. For PALF = 0. the initial tendon forces are those calculated from the information supplied and the elastic deformation of the structure at transfer is ignored. To model a case somewhere between these two extremes an appropriate value $0 \leqslant \text{PALF} \leqslant 1.$ can be selected. This effect is only considered at transfer, i.e. at the time when the loads due to prestressing are applied.

8.3 The analysis for time-dependent effects is carried out from the current time to the next time, i.e. from time t_i to time t_{i+1}. Therefore NSTIM and NITERT for time step Δt_i $(= t_{i+1} - t_i)$ must be specified on the load control card for time t_i.

8.4 The iteration type code as specified on the structure control card (B1.2) can be changed at each time. Leave blank if no change is desired.

8.5 When a series of elements have the same new temperature at the reference level,and temperature gradient through the element thickness, generation is possible. The element number is incremented by 1 from element NE up to element NEZ .

B9. NEXT PROBLEM

Data cards B1-B8 are repeated for the next problem or terminate the deck with two blank cards.

DESCRIPTION OF OUTPUT

The output consists of the following two parts:

Echo of input

The complete input data for the problem is printed with appropriate labels to facilitate the detection of punching errors and to have a record of the problem statement.

Results

The results are also labeled and the form will depend on what is specified on the output control card B1.3. A complete output of all possible results at the end of an iteration would consist of the following:

1. Problem title, time or load increment, load step and iteration numbers.

2. The total applied external nodal forces in the global coordinate system.

3. The global unbalanced nodal forces in the global coordinate system.

4. The total global displacements.

5. The following results for each triangular element:

   a. Nodal displacements in local coordinates (if KDIS = 1)

   b. For each of the three integration points the following:

      (i) Integration point global coordinates and angle ANLO (B6.1.3)

      (ii) Stresses in the local and principal directions, angles between the principal and the local and global axes and material state and stress reversal codes for each concrete layer. (See note 3.)

      (iii) Stress and material state code for the reinforcing steel layers. (See note 4.)

      (iv) Total strains in the local coordinates for each concrete and reinforcing steel layer (if KSTN = 1).

      (v) When a time-dependent analysis is perfomed, the total creep and shrinkage strains (if KSTN = 1, ICREEP = 1, ISHRINK = 1 (B1.2))

   c. For each prestressing tendon segment in an element the tendon number, the bond code, the current tendon force and the material state code.

   d. The moment resultants in the local coordinate system with the global coordinates for each integration point and the membrane stress resultants at the center of the element.

6. The extensional and rotational stresses in the boundary elements.

Notes:

1. Tensile stresses are positive and compressive stresses are negative.

2. An explanation of the meaning of the material state and stress reversal codes are printed at the start of the triangular element results.

3. The concrete layer stresses are output in the local coordinate system with the positive direction defined in Fig. B10. For the principal stresses it is assumed that $\sigma_1 > \sigma_2$. The principal axes in the local coordinate system is defined by the angle α (Fig. B10), while its projection on the global XY-plane is defined by α' (Fig. B10). The first crack will be perpendicular to principal direction 1 while the second will be in this principal direction.

4. The steel layer stresses is in the direction of the reinforcing bars.

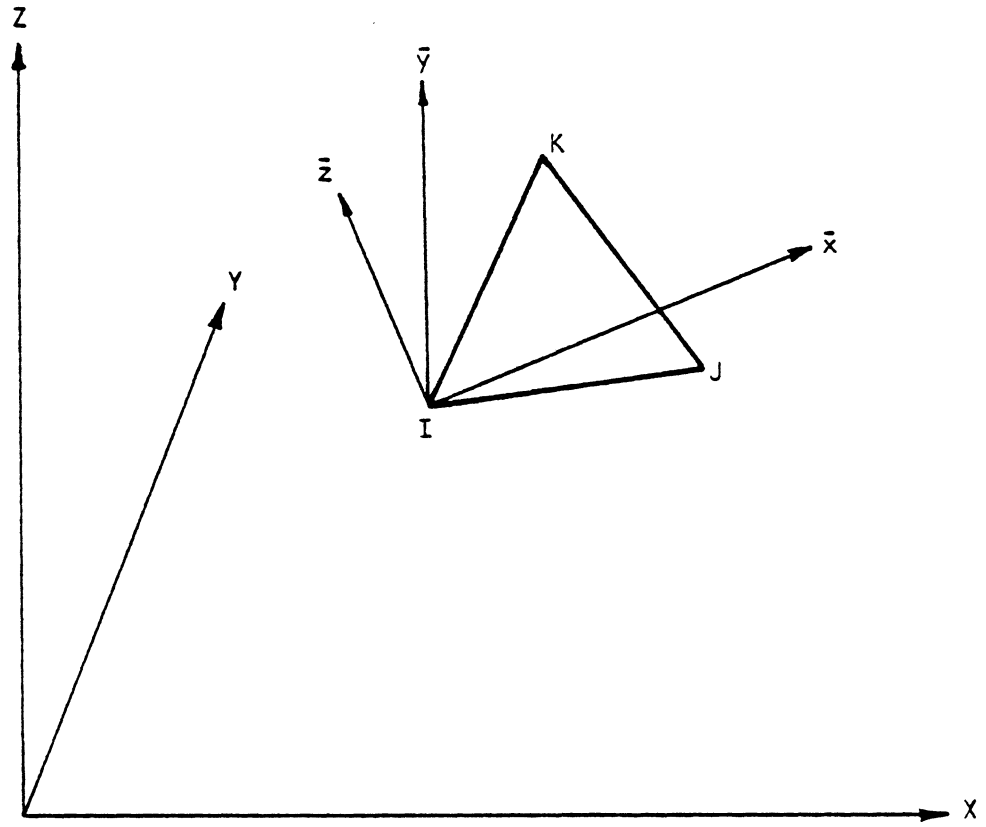

X Y Z = Global coordinate system, follows right-hand rule.

$\bar{x}$ $\bar{y}$ $\bar{z}$ = Local element coordinate system, follows right-hand rule such that $\bar{z}$ is perpendicular to the plane of the element IJK. $\bar{x}$ and $\bar{y}$ define the plane of the element IJK.

FIG. B1 GLOBAL AND LOCAL ELEMENT COORDINATE SYSTEMS

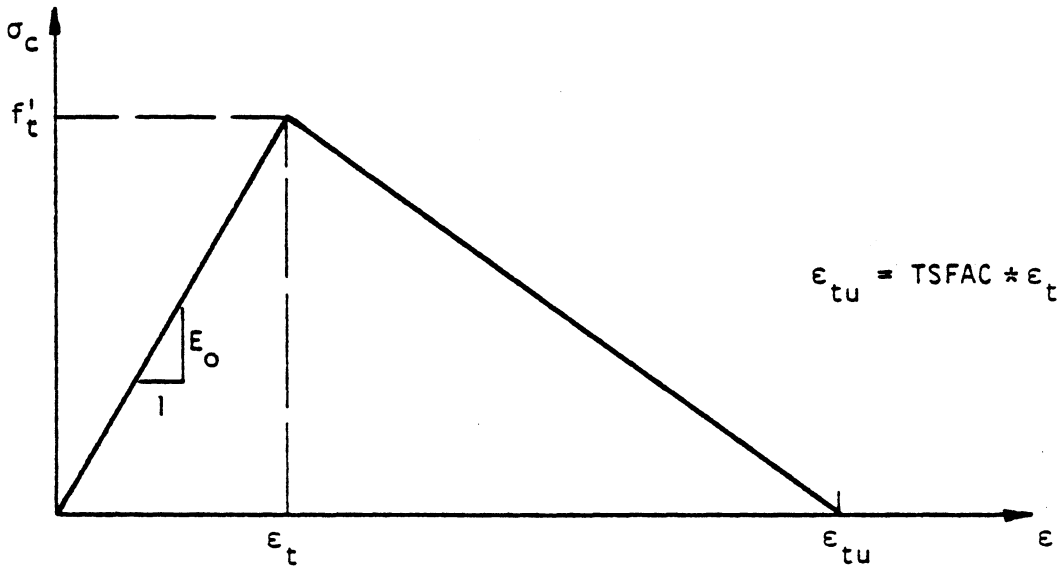

FIG. B2 TENSION STIFFENING MODEL (b)

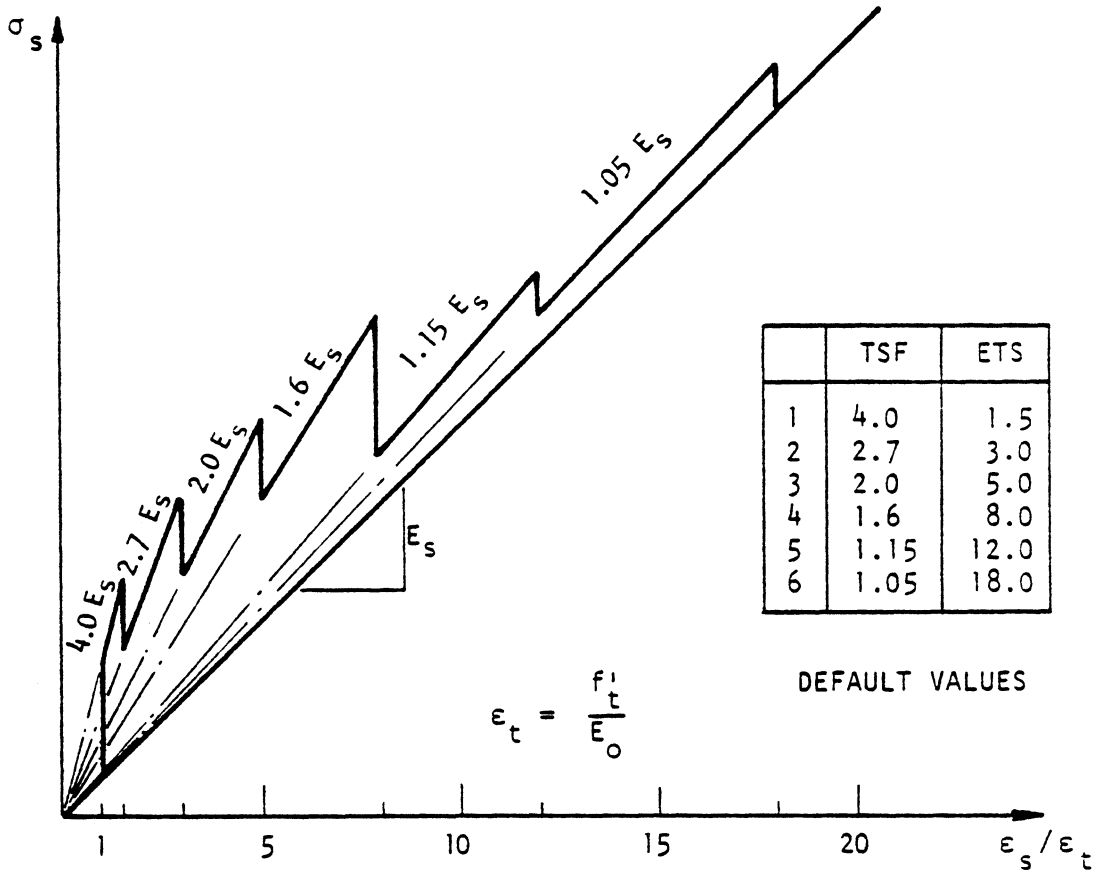

	TSF	ETS
1	4.0	1.5
2	2.7	3.0
3	2.0	5.0
4	1.6	8.0
5	1.15	12.0
6	1.05	18.0

DEFAULT VALUES

FIG. B3 TENSION STIFFENING : MODIFIED STEEL STRESS-STRAIN DIAGRAM FOR MODEL (a)

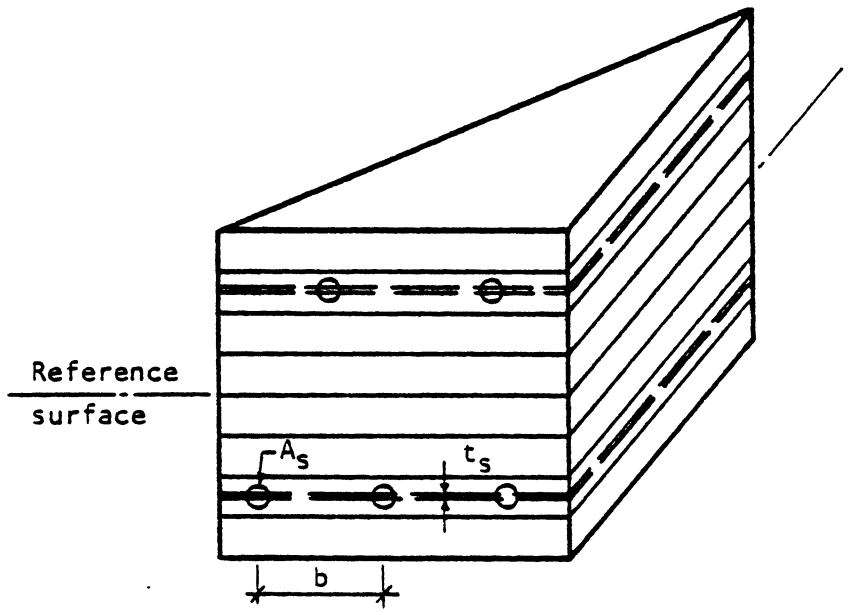

CONCRETE AND "EQUIVALENT SMEARED" STEEL LAYERS

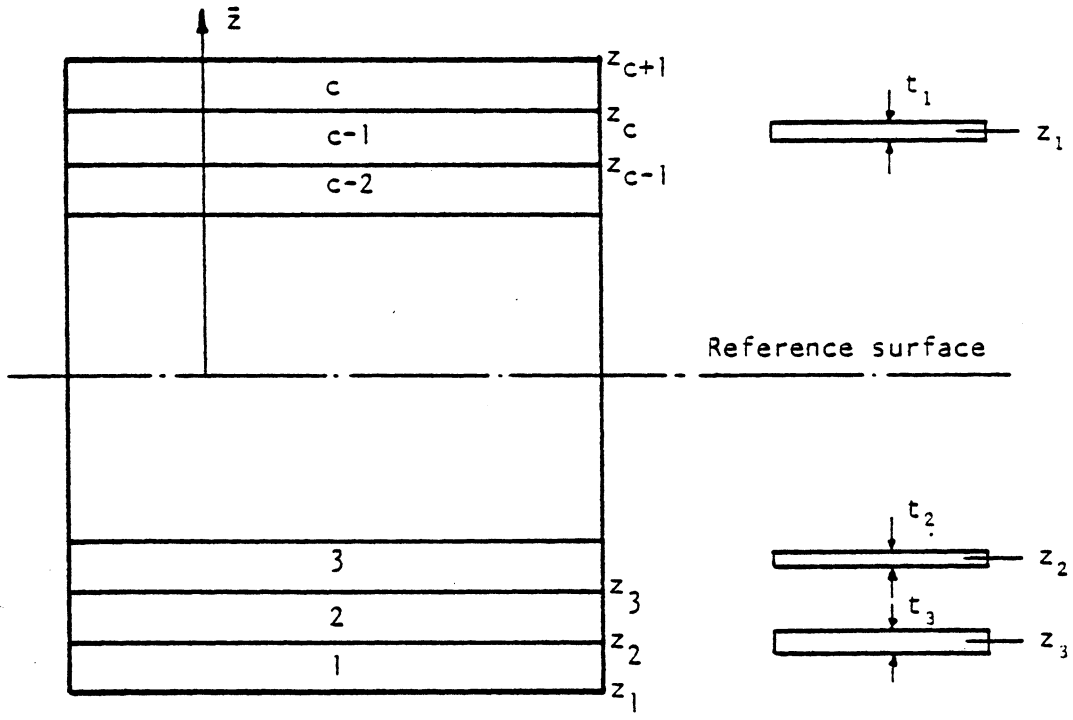

CONCRETE LAYERS STEEL LAYERS

FIG. B4 LAYER SYSTEM OF A TRIANGULAR ELEMENT

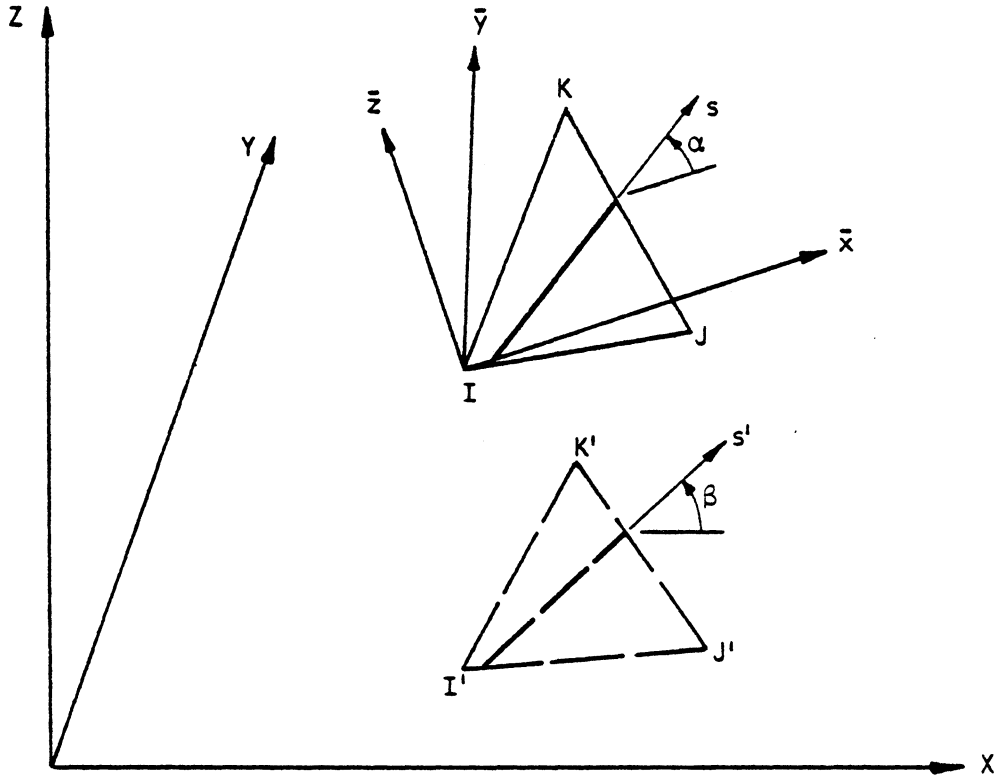

XYZ = Global coordinate system
$\bar{x}\bar{y}\bar{z}$ = Local element coordinate system ($\bar{z} \perp \Delta IJK$)
s = Direction of reinforcing bar in the plane of ΔIJK
s' = Projection of s-axis on global XY plane
α = Angle from $\bar{x}$ to s
β = Angle from X to s'

FIG. B5 DIRECTION OF THE REINFORCING BARS IN A TRIANGULAR ELEMENT

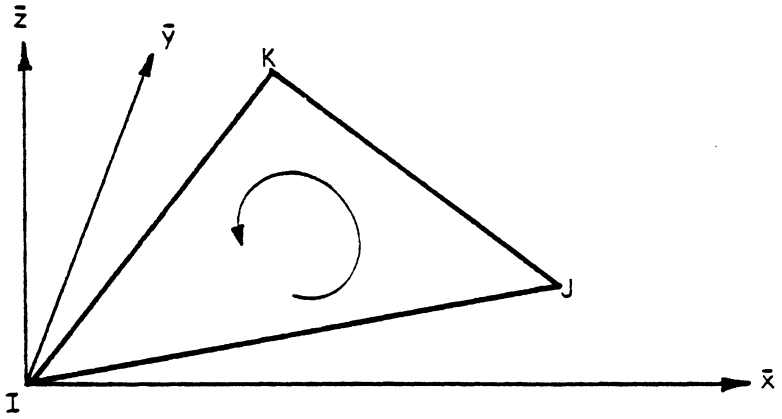

FIG. B6 NODE LAYOUT OF A TRIANGULAR ELEMENT

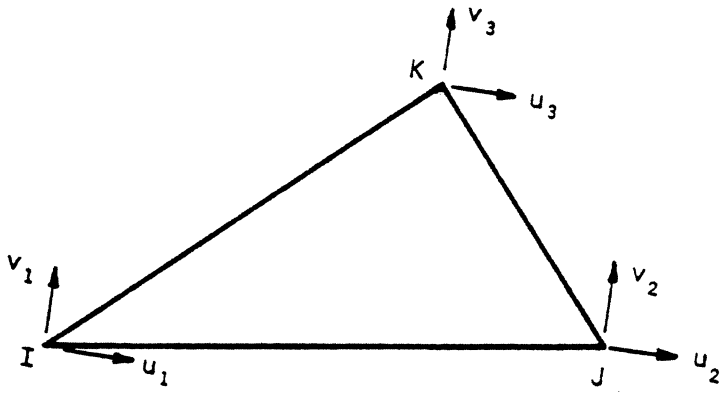

a. MEMBRANE ELEMENT (CST)

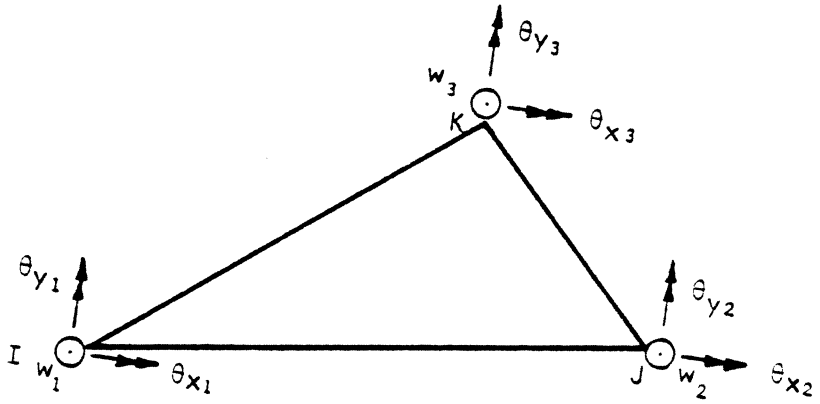

b. PLATE BENDING ELEMENT (IRONS-RAZZAQUE)

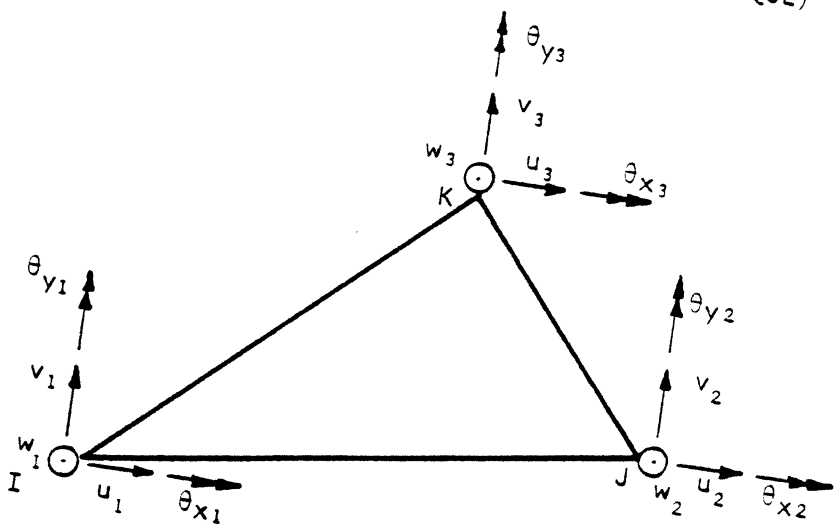

c. SHELL ELEMENT (CST + IRONS-RAZZAQUE)

FIG. B7 GLOBAL AND LOCAL ELEMENT COORDINATE SYSTEMS

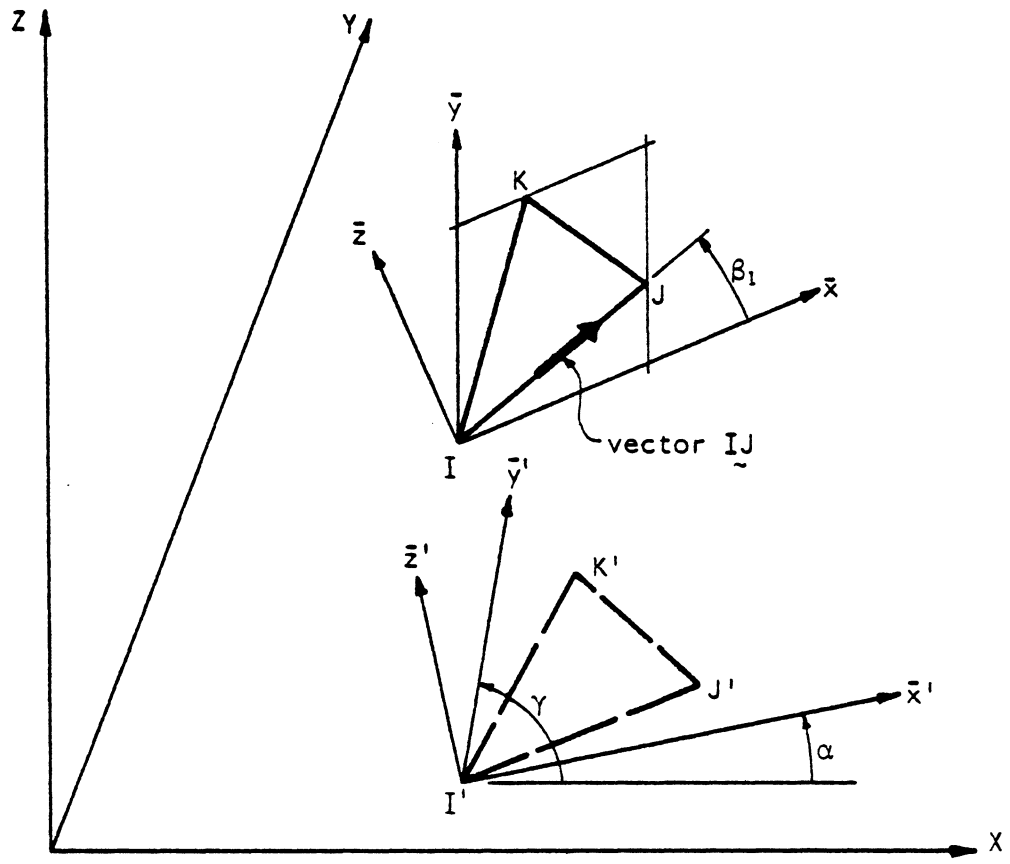

XYZ = Global coordinate system

$\bar{x}\bar{y}\bar{z}$ = Local element coordinate system

ΔIJK = Element with nodes IJK

ΔI'J'K' = ΔIJK projected on global XY plane

$\bar{x}'\bar{y}'\bar{z}'$ = Projection of $\bar{x}\bar{y}\bar{z}$ on XY plane

CASE 1 : LOCO = 0 $\bar{x}$ coincides with $\underset{\sim}{IJ}$

CASE 2 : LOCO = 1 $\bar{x}$ is defined by specifying α

CASE 3 : LOCO = 2 $\bar{y}$ is defined by specifying γ

FIG. B8 DEFINITION OF LOCAL ELEMENT COORDINATE SYSTEM

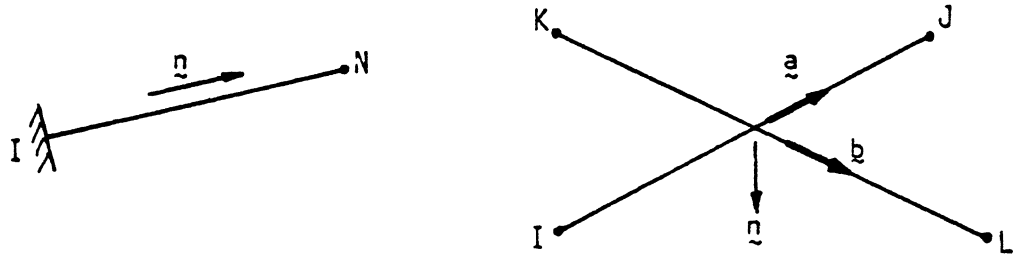

a. POSITIVE DIRECTIONS OF THE BOUNDARY ELEMENT

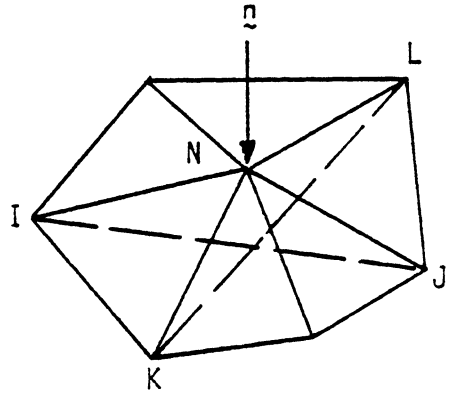

b. ROTATIONAL RESTRAINT ABOUT THE SURFACE NORMAL OF A THIN SHELL

c. POSITIVE FORCES ON BOUNDARY ELEMENT

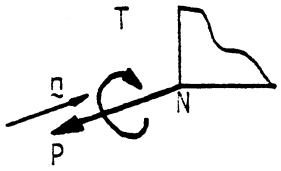

d. POSITIVE REACTIONS AT NODE N

FIG. B9 BOUNDARY ELEMENT

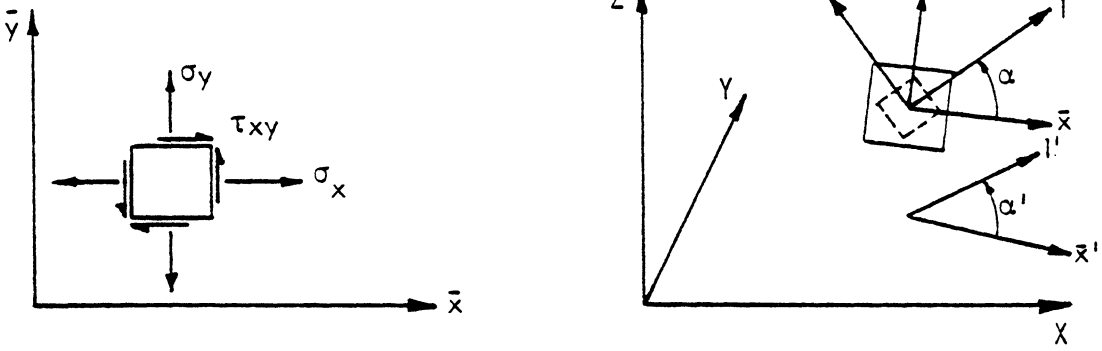

FIG. B10 SIGN CONVENTION FOR STRESS OUTPUT

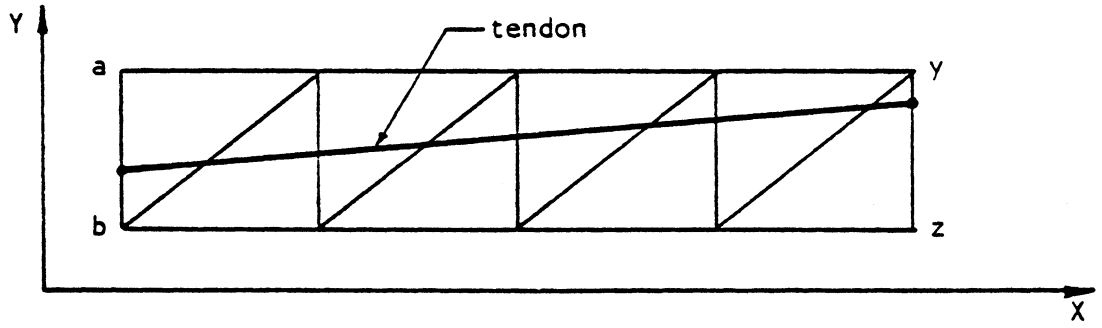

a. SLAB TENDON IN ELEMENTS (ITD(1,N) = 0)

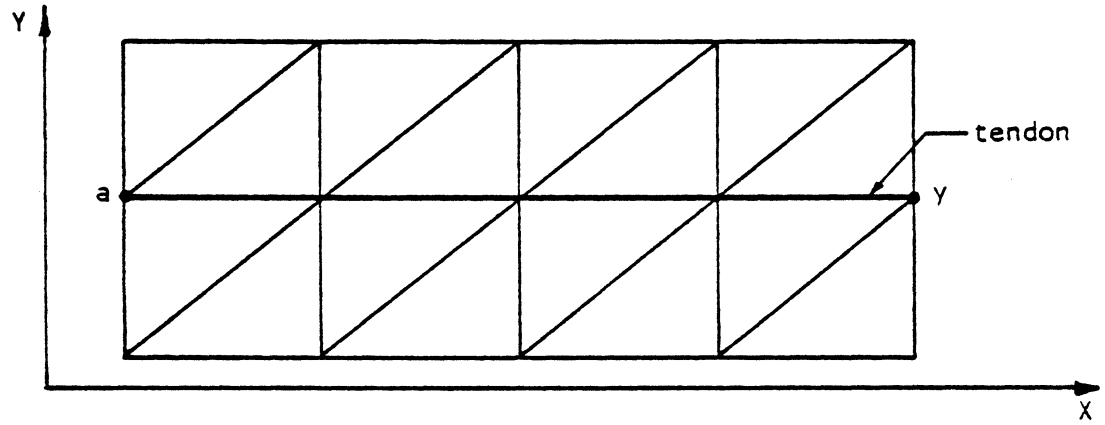

b. SLAB TENDON ON NODES (ITD(1,N) = 1)

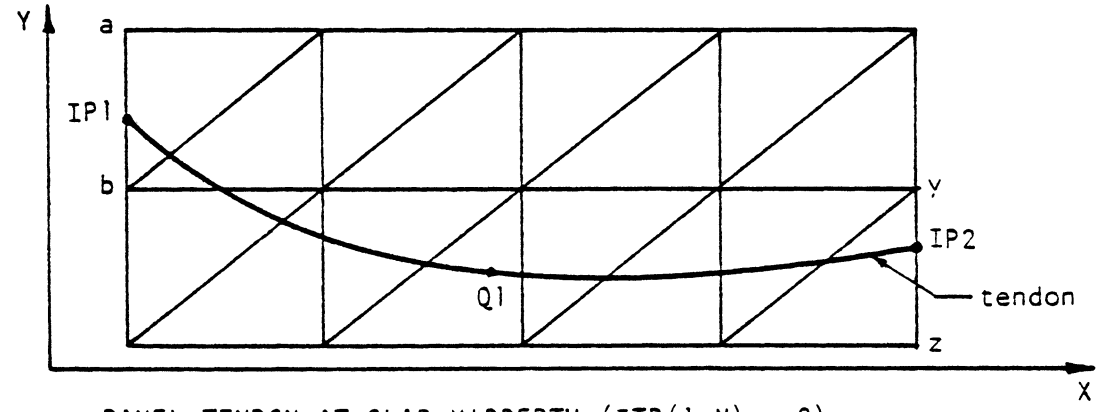

c. PANEL TENDON AT SLAB MIDDEPTH (ITD(1,N) = 2)

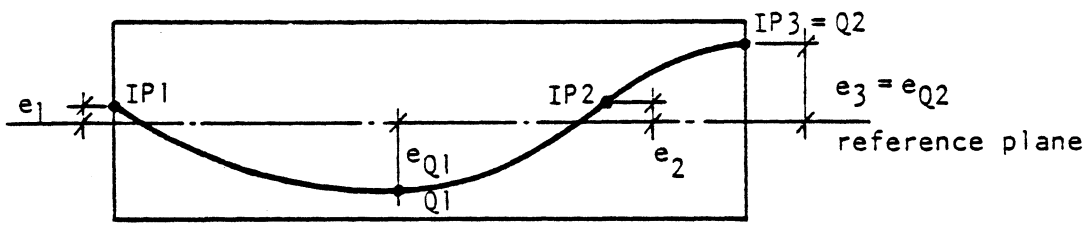

d. ELEVATION SHOWING TYPICAL TENDON PROFILE

FIG. B11 PRESTRESSING TENDON LAYOUTS